CNS Inflammasome Activation and Pyroptosis in Multiple Sclerosis and Experimental Autoimmune Encephalomyelitis

by

Brienne Alexandra Furfaro McKenzie

A thesis submitted in partial fulfillment of the requirements for the degree of

Doctor of Philosophy

in

IMMUNOLOGY

Department of Medical Microbiology and Immunology

University of Alberta

Abstract

Multiple sclerosis (MS) is a progressive and incurable demyelinating disease of the central nervous system (CNS). The neuropathogenesis of MS and its prototypic animal model, experimental autoimmune encephalomyelitis (EAE), is defined by persistent neuroinflammation, involving the activation of microglia (the resident macrophages of the CNS), as well as infiltrating T lymphocytes, B lymphocytes, and monocyte-derived macrophages. Inflammasomes are multi-protein cytosolic complexes that mediate the maturation and release of proinflammatory cytokines (IL-1β and IL-18); they participate in the pathogenesis of EAE, notably in the activation and recruitment of CNS-infiltrating immune cells. Inflammasomes also initiate a form of lytic programmed cell death termed pyroptosis ("fiery death"), driven by the pore-forming executioner protein, gasdermin D (GSDMD). Neither the presence of GSDMD within CNS-resident cells nor the contribution of pyroptosis to MS or EAE has been investigated to date.

In this thesis, inflammasome activation and GSDMD-mediated pyroptosis were demonstrated in both myeloid cells (microglia/macrophages) and in myelin-forming oligodendrocytes (ODCs) in the CNS during MS and EAE. Inflammasome activation and pyroptosis occurred in human microglia *in vitro* after exposure to MS-relevant inflammatory stimuli. GSDMD inhibition by siRNA and caspase-1 inhibition by VX-765 suppressed pyroptosis in human microglia. VX-765 treatment of EAE animals reduced expression of inflammasome- and pyroptosis-associated proteins in the CNS, prevented axonal injury, and improved neurobehavioral performance. Thus, this thesis provided

evidence for GSDMD-mediated pyroptosis in multiple glial cell types as a previously unrecognized mechanism contributing to inflammatory demyelination.

Recent evidence has suggested that subcellular changes, including nuclear condensation, pyroptotic body formation, and mitochondrial dysfunction, precede GSDMD-mediated cell lysis during pyroptosis. These observations are reminiscent of changes observed during apoptosis, which prompted the investigation of apoptotic executioner caspase-3/7 as potential drivers of pyroptosis. This thesis provided the first evidence that human microglia undergoing pyroptosis activate caspase-3/7 downstream of inflammasome activation, which is prevented by caspase-1 inhibition. Specific substrates of caspase-3/7 were cleaved during pyroptosis in the nucleus (DFF45, PARP) and the cytoplasm (ROCK1). The siRNA-mediated suppression of caspase-3/7 interrupted pyroptosis, inhibited nuclear disintegration, reduced pyroptotic body formation, prevented plasma membrane rupture, and diminished proteolytic cleavage of caspase-3/7 substrates. Using human microglia as a model system, these findings reveal a previously undiscovered role for caspase-3/7 as executioners of GSDMD-mediated pyroptosis.

This thesis offers a novel perspective on inflammatory demyelination in the CNS by identifying a previously unrecognized molecular pathway that perpetuates cell death and neuroinflammation in MS and EAE. In addition, a clinically relevant therapeutic strategy for MS that targets this pathway is proposed. Lastly, the first demonstration of a functional role for caspase-3/7 in driving GSDMD-mediated pyroptosis is provided,

which challenges the use of cleaved caspase-3/7 and their substrates as universal biomarkers for apoptosis. These findings represent a substantial conceptual advance in our understanding of the molecular mechanisms underlying pyroptosis.

Preface

Sections of this thesis (Chapters 3 and 4) have been published:

McKenzie, BA, Mamik MK, Saito LB, Boghozian R, Monaco MC, Major EO, Lu JQ, Branton WG, Power C. (2018) Caspase-1 inhibition prevents glial inflammasome activation and pyroptosis in models of multiple sclerosis. *PNAS*. 115 (26): E6065-E6074.

I designed and performed experiments, interpreted data and wrote the draft of the manuscript. Dr. Christopher Power was the supervisory author, designed experiments, interpreted data, and edited the manuscript. The remaining authors designed and performed experiments.

Sections of this thesis (Chapters 4 and 5) have been submitted:

McKenzie, BA, Fernandes J, Doan M, Branton WG, Power C. (2019). Caspase-3/7 drive pyroptosis in human microglia. *Submitted*.

I designed and performed experiments, interpreted data and wrote the draft of the manuscript. Dr. Christopher Power was the supervisory author, designed experiments, interpreted data, and edited the manuscript. The remaining authors designed and performed experiments.

All experiments in this thesis were performed by Brienne McKenzie with the following exceptions. Human autopsy tissue immunofluorescence [Figure 3.2, 5.15A-C] was performed and quantified with the assistance of technician William Branton. The EAE time course experiment [Figure 3.3] was performed by post-doctoral fellow Dr. Stacey Reinke, with molecular analysis [Figure 3.3, 3.4] performed by Brienne McKenzie. Bielchowsky silver stain [Figure 3.10E-G] was performed by NACTRC personnel, imaged and quantified by Brienne McKenzie. Select western blots and quantification [Figure

5.3B, 5.9B-C, 5.11A-C, and 5.13H-I] were performed by Jason Fernandes, a technician in the Power lab, using lysates provided by Brienne McKenzie. GSDMD-deficient THP-1 cells were provided by Dr. Vijay Rathinam, University of Connecticut. All experiments were performed under the supervision of Dr. Christopher Power.

The use of human tissues was approved (Pro0002291, Pro00027660) by the University of Alberta Human Research Ethics Board (Biomedical) and written informed consent was received for all samples. All animal experiments were performed according to the Canadian Council on Animal Care and University of Alberta Health Sciences Animal Care and Use Committee guidelines (AUP#00000317).

Acknowledgements

I would like to thank my supervisor, Dr. Christopher Power, for his mentorship, guidance, and insightful scientific feedback over the past several years. His excitement for scientific inquiry is truly contagious. As a physician, Dr. Power brought a wealth of clinical expertise that ensured our research never lost sight of the patients whom we ultimately serve. To that end, I would like to express my gratitude to the Multiple Sclerosis Society of Canada for their dedication to scientific research and unwavering advocacy on behalf of patients and researchers alike. The opportunities to interact with patients, caregivers, and other people whose lives have been touched by MS are unparalleled. Their funding support for this research project has been instrumental. I am also grateful to the Canadian Institutes of Health Research (CIHR) and Alberta Innovates Health Solutions (AIHS) for funding my doctoral studies. To my committee members, Dr. Maya Shmulevitz and Dr. Troy Baldwin, your mentorship, scientific insights, and steadfast support over the years are deeply appreciated. I have taken the lessons learned from you to heart and will strive to uphold those standards of scientific rigour in all of my future endeavours. To our MMI graduate coordinators, Dr. Kevin Kane and Dr. Edan Foley, thank you for your steadfast support over the years and for your tireless dedication to the wellbeing and success of the graduate students in our program.

I would also like to express my thanks to the members of the Power lab past and present, without whom much of this work would not have been possible. Manmeet, I am eternally grateful for your friendship, advice, and brilliant sense of adventure; from

Edmonton to Jerusalem, it has been a privilege to share these experiences with you. Will, Matt, and Jason, thank you for the unwavering support, friendship, good humour, and excellent scientific discussions over the years. To all of my co-authors, especially Leina, thank you for your diligence, technical expertise, and thoughtful contributions to these manuscripts.

To those who have supported me along the way, including Sarah, Shawn, Andrew, Steph, Lina, and Ninad, thank you for the years of encouragement, support, wisdom, and enduring friendship. To my parents Brian and Teri, my sister Sierra, my parents-in-law Jill and Allister, and my beloved husband Mark, words cannot express my gratitude for your boundless support, patience, love, and wisdom on this journey.

Table of Contents

List of Tables

CHAPTER II

CHAPTER III

List of Figures

CHAPTER I

Chapter III

CHAPTER IV

Chapter V

List of Abbreviations

AD	Alzheimer's disease
AICD	Activation induced cell death
AIM	Absent in melanoma
ALR	AIM2-like receptor
ALS	Amyotrophic lateral sclerosis
AP-1	Activator protein 1
APC	Antigen presenting cell
ASC	Apoptosis-associated speck-like protein containing a CARD
BAM	Border-associated macrophages
BBB	Blood brain barrier
BBI	Blood brain interface
CAPS	Cryopyrin-associated periodic syndrome
CARD	Caspase-activation and recruitment domain
CIS	Clinically isolated syndrome
CNS	Central nervous system
CSF	Cerebral spinal fluid
DAM	Disease-associated macrophages
DAMP	Damage-associated molecular pattern
DC	Dendritic cells
DFF45	DNA fragmentation factor 45
DMT	Disease-modifying therapy
EAE	Experimental autoimmune encephalomyelitis
ECM	Extracellular matrix
FCAS	Familial cold auto-inflammatory syndrome
GBM	Glioblastoma multiforme
GFP	Green fluorescent protein
GSDMD	Gasdermin D
HD	Huntington's disease
HMGB1	High-mobility group protein B1
HSP	Heat shock protein
IAP	Inhibitors of apoptosis
IFN	Interferon
IL-1β	Interleukin-1β
iNOS	Inducible nitric oxide synthase
IP	Intraperitoneal
IRAK	Interleukin-1 receptor-activated protein kinase
IRF	Interferon regulatory factor
LDH	Lactate dehydrogenase
LPS	Lipopolysaccharide
MCP1	Monocyte chemoattractant protein 1
MDM	Monocyte-derived macrophages
MHC	Major histocompatibility complex
MLC	Myosin light chain
MOG	Myelin oligodendrocyte glycoprotein
MS	Multiple sclerosis
mtROS	Mitochondrial reactive oxygen species
MWS	Muckle-Wells syndrome

MYD88	Myeloid differentiation primary response gene 88
NAIP	Neuronal apoptosis inhibitory protein
NAWM	Normal-appearing white matter
NCCD	Nomenclature Committee on Cell Death
NEK	NIMA-related protein kinase
NF-kB	Nuclear factor kappa-light-chain-enhance of activated B cells
NK	Natural killer
NLR	NOD-like receptor
NOMID	Neonatal-onset multisystem inflammatory disorder
ODC	Oligodendrocyte
OPC	Oligodendrocyte precursor cell
PAM	Proliferation-associated macrophages
PAMP	Pathogen-associated molecular pattern
PARP	Poly-ADP ribose polymerase
PBMCs	Peripheral blood mononuclear cells
PCD	Programmed cell death
PD	Parksinson's disease
PI	Propidium iodide
PPMS	Primary progressive multiple sclerosis
PRR	Pattern recognition receptor
PS	Phosphatidylserine
PTX	Pertussis toxin
PYD	Pyrin domain
RLR	RIGI-like receptor
RNS	Reactive nitrogen species
ROS	Reactive oxygen species
RRMS	Relapsing-remitting multiple sclerosis
SDTF	Signal dependent transcription factor
SPMS	Secondary progressive multiple sclerosis
STAT	Signal transducers and activators of transcription
TBI	Traumatic brain injury
TLR	Toll-like receptor
TNFα	Tumour necrosis factor α
TUNEL	Terminal deoxynucleotidyl transferase dUTP nick end labeling

CHAPTER I: INTRODUCTION

I.I. Inflammation and Immunity in the Central Nervous System

The central nervous system (CNS), consisting of the brain and spinal cord, was historically considered *immune privileged*, based upon observations that circulating lymphocytes were excluded from the CNS parenchyma by a selectively permeable blood-brain barrier (BBB), and that rejection of foreign tissue from the CNS was delayed compared to the periphery[1-3]. Combined with the lack of professional antigen-presenting cells (APCs) in the CNS parenchyma, and relatively low expression of major histocompatibility complex (MHC)-I and II molecules, these observations shaped the enduring concept that the CNS was exempt from peripheral immunosurveillance[1-3].

However, a more nuanced understanding of CNS immunity has since developed[4]. A substantial repertoire of immune cells is found within specific CNS compartments, participating in immunosurveillance and mediating the immune response to antigen in the parenchyma under pathological conditions[3,5]. A network of meningeal lymphatics was also recently re-identified[6,7], providing a novel mechanism for exposure of peripheral APCs to CNS antigen[8]. The major mediators of the innate immune response within the CNS parenchyma are tissue-resident macrophages known as microglia[5]. Upon activation, these cells engage major cytokine/chemokine signaling networks, permeabilize the BBB, and recruit immune cells from the periphery and the border compartments of the CNS[2,4,5]. Rather than the immune-privileged site originally conceptualized, the CNS is subject to constant immune surveillance, and is capable of mounting a formidable immune response upon infection or injury. Thus, immune

privilege is relative, not absolute, and breaks down with age, inflammation, or injury[9]. Given the delicate nature of CNS tissue and the post-mitotic state of many of its cells, these immune responses are carefully orchestrated to prevent neurotoxicity[8].

1.1.1. Major Immune Compartments of the CNS

High-dimensional cytometry studies have assessed the CNS immune cell repertoire at homeostasis, demonstrating that the majority of CNS-resident leukocytes are microglia, followed by border-associated macrophages (BAMs) from the choroid plexus/meninges/perivascular space, with sizeable populations of neutrophils, dendritic cells (DCs), and monocytes, as well as both B and T lymphocytes[10,11]. In order to regulate CNS-immune interactions, the CNS is anatomically compartmentalized, and most non-microglial immune cells are confined to the border regions (choroid plexus, meninges, and perivascular space). Such regions harbour diverse populations of immune cells at homeostasis, but their access to the parenchyma is restricted, with microglia constituting over 98% of parenchymal immune cells at homeostasis[11]. Nonetheless, immune cells at the border regions of the CNS profoundly influence the parenchyma, through soluble factors, BBB modulation, interaction with infiltrating cells from the periphery, and direct entry into the parenchyma during neuroinflammation[11].

Three major routes of entry into the CNS parenchyma exist for circulating immune cells [Figure 1.1]: (i) through selectively permeable structures, such as the choroid plexus (ii) through the perivascular space surrounding meningeal venules, and (iii) across post-capillary venules and directly into the CNS parenchyma[5]. These regions are

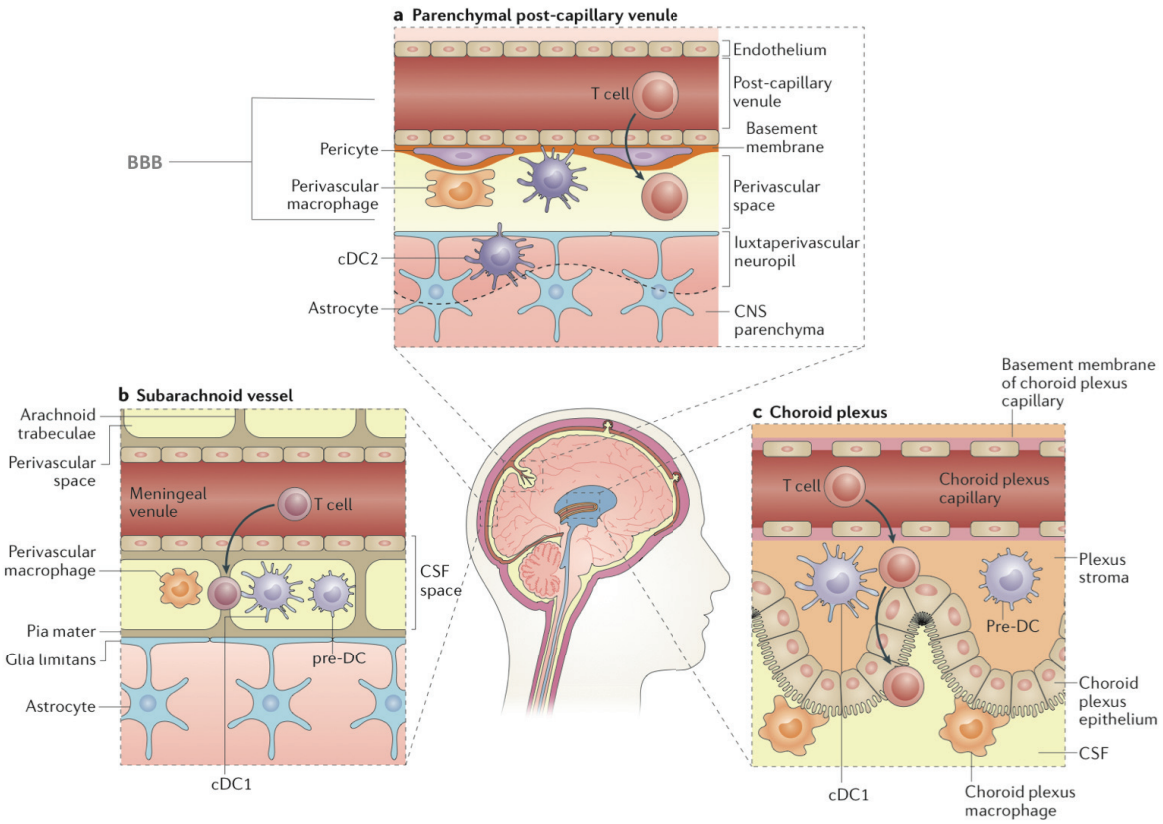

Figure 1.1: ***The three main ports of entry for infiltrating immune cells into the CNS are characterized by unique anatomical substructures and immune populations***

(A) Parenchymal post-capillary venules are surrounded by the perivascular space, containing several populations of antigen presenting cells, including perivascular macrophages and dendritic cells (DCs). Circulating immune cells (e.g. T cells) must cross the blood-brain barrier (BBB), including the tight junctions of post-capillary venule endothelium, the basement membrane, the perivascular space, and the glial limitans formed by astrocytic endfeet prior to entering the parenchyma. (B) Meningeal blood vessels are located in the subarachnoid space, above the pia mater, and are likewise surrounded by a perivascular space containing perivascular macrophages, DCs, and pre-DCs (as well as other cell types, not shown) under homeostatic conditions. (C) The architecture of the choroid plexus vasculature is substantially different than the subarachnoid vessels and the parenchymal post-capillary venules. The endothelium of the choroid plexus capillary does not contain tight junctions, facilitating extravasion of circulating immune cells. The stroma of the choroid plexus contains pre-DCs and DCs, while a population of choroid plexus macrophages lines the choroid plexus epithelium that secretes CSF. Circulating immune cells can enter the CSF by crossing the choroid plexus epithelium.

Adapted from: Korn T, and Kallies A. (2017). T cell responses in the central nervous system. *Nature Reviews Immunology*. 17(3), 179-194. Springer Nature License Copy Number: 4535660615295

characterized by unique anatomical substructures and harbour distinct local immune repertoires [Figure 1.1].

1.1.1.1 Meninges

The meninges are located immediately under the skull and consist of three layers (the dura mater, pia mater, and arachnoid membrane) that enclose the brain parenchyma. The subarachnoid space, which contains the main arterial branches of the CNS, is located between the arachnoid membrane and pia matter [Figure 1.1B]. From here, capillary beds extend deep into the brain parenchyma, surrounded by a perivascular space, within which various immune populations reside[2]. Meningeal macrophages are particularly important in CNS immunity, and like microglia are derived from erythromyeloid precursors during embryogenesis[12]. Along with choroid plexus macrophages, they constitute a population of distinct BAMs with important roles in CNS immunosurveillance[10]. The meninges also contain an abundance of DCs and pre-DCs that are capable of antigen presentation and activation of naïve T $CD4^+$ lymphocytes[5,10]. According to mass cytometry studies of the murine brain at homeostasis, the meningeal repertoire of $CD45^{high}$ immune cells also includes significant proportions of $CD4^+$ and $CD8^+$ T lymphocytes, B lymphocytes, Gr-1^+ myeloid cells (e.g. neutrophils), DCs, monocytes/macrophages, and a small population of natural killer (NK) cells[11]. During neuroinflammation, the immune repertoire of the meninges expands dramatically, which can lead to immune cell infiltration of the parenchyma across the pial membrane[4]. Recent studies have also characterized lymphatic vessels in the meninges as a possible route by which CNS antigen can exit into the periphery, highlighting the role of the meninges in the dynamic interplay between the CNS and the periphery[7].

1.1.1.2 Blood-Brain Barrier and Perivascular Space

The BBB [Figure 1.1A] is a selectively restrictive structure that encloses the brain's vasculature and regulates the passage of ions, molecules, and cells from the circulation into the CNS[13,14]. It consists of a network of highly polarized endothelial cells, bound by tight junctions, which functionally exclude ~98% of antibodies and small molecules at homeostasis[2]. The endothelial cells and associated pericytes are surrounded by a double basement membrane comprised of extracellular matrix (ECM) components. The perivascular space surrounds the vasculature and supports a significant population of immune cells, including perivascular macrophages[15]. Between the perivascular space and the brain parenchyma is a layer of astrocytes endfeet known as the glial limitans[14].

The BBB excludes peripheral immune cells under homeostatic conditions and limits infiltration during inflammation compared to peripheral tissue[9]. In one classical experiment, lipopolysaccharide (LPS) injected into the brain parenchyma caused infiltration of monocytes/neutrophils that was vastly reduced compared to the skin; however, when LPS was injected into the ventricles, which do not have a BBB, recruitment was comparable to the skin, illustrating the importance of the BBB in modulating the infiltration of peripheral immune cells[16]. Under pathological conditions, migration across the BBB is mediated by the activation of endothelial cells and astrocytes, leading to an up-regulation of adhesion molecules, a reduction in tight junction integrity, and the formation of transendothelial cell channels that facilitate the passage of peripheral leukocytes[2]. Disruption of the BBB is a key feature of many neurological disorders, including multiples sclerosis (MS), Alzheimer's disease (AD),

Parkinson's disease (PD), stroke, traumatic brain injury (TBI) and others[13]. It is worth noting that the concept of the "blood-brain interface" (BBI) has recently been proposed to replace the BBB, as it more accurately encapsulates the dynamic, relative, and regulated nature of this structure[17].

1.1.1.3 Choroid Plexus and the Cerebrospinal Fluid

Cerebral spinal fluid (CSF) is produced by filtering blood to produce a low-protein fluid for circulation around the CNS[4]. It is released into the ventricles by secretory epithelial cells in the choroid plexus [Figure 1.1C][2]. Choroid plexus vasculature lacks tight junctions and expresses an array of adhesion molecules at baseline[4,5], positioning the choroid plexus as one of the major entry points into the CNS[2,5]. Proinflammatory cytokines [such as interleukin (IL)-1β and tumour necrosis factor (TNF)-α] and chemokines up-regulate adhesion molecule expression to increase immune cell infiltration into the CNS[4]. Choroid plexus macrophages constitute an important population in CNS immunity, although unlike microglia and perivascular/meningeal macrophages, these cells are replenished in part by bone marrow-derived cells, highlighting the choroid plexus as a key point of interaction between the peripheral circulation and the CNS[12]. Other immune cell types in the choroid plexus include $CD4^+$ and $CD8^+$ lymphocytes, B lymphocytes, and NK cells[11]. The CSF itself has a low absolute cell count (1000-3000 cells/mL in humans at homeostasis), and its immune repertoire differs significantly from the blood, highlighting the selective concentration of specific cells within the CSF[2,4,5]. Almost 80% of the immune cells in the CSF are T cells[5], with DCs constituting a significant proportion of the remaining cells[5]. Changes in the

concentration and composition of the CSF's immune cell repertoire is a hallmark of neuroinflammation[4].

1.1.2 Immune Surveillance of the CNS Parenchyma

1.1.2.1 Microglia: Sentinels of the CNS

Although multiple CNS cell types [including neurons, astrocytes, and oligodendrocytes (ODCs)] have the capacity to detect and respond to danger, microglia are the primary immune sentinels of the CNS parenchyma, representing 5-12% of the total cells in the CNS[18,19]. Microglia are yolk-sac-derived, arising from erythromyeloid precursors in mice on embryonic day 7.5 (E7.5), and entering the CNS early in embryogenesis (E9.5), before the closure of the BBB around E13.5[12,18,20]. They actively modulate the development of other cell types, including the proliferation, survival, and differentiation of ODC progenitors and neural precursor cells, outgrowth of axons, maturation of synapses, and branching of vasculature[18]. Interestingly, proinflammatory mediators such as IL-18 are abundantly expressed in microglia early in development but are down-regulated in adulthood[21]. Such observations have been born out by large-scale transcription studies: subsets of microglia within the developing brain, called "proliferation-associated macrophages" (PAMs), resemble highly proinflammatory disease-associated macrophages (DAMs), with higher metabolic rates and enhanced phagocytic activity compared to homeostatic microglia[20]. However, as microglia undergo maturation, thought to be complete by P14 in mice[22], they adopt the classical immunosurveillance expression profiles of adult homeostatic microglia[20].

Adult microglial self-renewal is independent of blood monocytes and hematopoietic stem cells under physiological conditions[23-25]. Detailed life cycle analysis of human microglia was recently performed by integrating atmospheric ^{14}C information to retrospectively birth date microglia from human autopsy donors, revealing an average age of 4.2 years, with some microglia persisting up to 20 years[26]. Under physiological conditions, microglia are locally maintained through a tightly regulated combination of proliferation and apoptosis[27], and the population can be rapidly reconstituted from surviving microglia following ablation by either genetic[28] or pharmacological[29] means. Fate-mapping studies also demonstrated that while microglial self-renewal is stochastic at homeostasis, clonal expansion occurs under pathological conditions[30].

1.1.2.2 Immune Surveillance by Homeostatic Microglia

Homeostatic microglia have stable, non-motile cell bodies but highly motile and elongated processes, that continually patrol the brain parenchyma for disruptions in homeostasis[31]. Each microglial cell occupies its own niche, and it is estimated that the entire extracellular space of the CNS parenchyma is surveyed by one or more microglial processes every few hours[32]. Recent studies have characterized a constitutively expressed microglial "sensome" consisting of 100 unique surface receptors that are poised to detect changes within the local microenvironment[33]. These included pattern recognition receptors (25%), chemokine receptors (10%), cytokine receptors (10%), and Fc receptors (7%), among others[33]. Several sensome genes, including *Tmem119*, *Trem2*, and *Cx3cr1*, were enriched in microglia compared to other tissue macrophages[33].

Many groups have focused on delineating homeostatic gene signatures for both human and mouse microglia during immune surveillance. At least seven studies have agreed upon a core set of genes that are consistently enriched in (though not exclusive to) murine microglial populations at homeostasis, compared to other CNS cells, other tissue-resident macrophages, and monocytes[34]. These genes include *Sall1, Hexb, Fcrls, Gpr43, Cx3cr1, Tmem119, Trem2, P2ry12, Mertk, Pros1,* and *SiglecH*[34]. Reasonably high concordance (>50%) is observed when human microglia transcriptomics datasets are compared to mouse studies[34].

1.1.3 The Call to Arms: Microglial Activation in the Damaged CNS

1.1.3.1 Danger, Damage, and the Hidden Self

Homeostatic microglia constantly patrol for signs of infection [indicated by pathogen-associated molecular patterns (PAMPs)] or danger [indicated by endogenous damage-associated molecular patterns (DAMPs)]. The notion that endogenously derived "self" molecules can initiate an inflammatory response in the absence of pathogens was postulated in Polly Matzinger's "danger theory" and has since become a pillar of innate immunity[35]. According to this paradigm, endogenous intracellular molecules (i.e. the "hidden self") are released in large quantities upon cellular injury or death, acting in a paracrine manner to propagate inflammation. Detection of extracellular DAMPs can also activate cell death programs, including apoptosis, necroptosis, and pyroptosis, perpetuating the inflammatory cascade[36].

1.1.3.2 The Nature of Damage-Associated Molecular Patterns in the CNS

DAMPs in the CNS include proteins [e.g. high-mobility group protein B1 (HMGB1), heat shock proteins (HSPs), IL-33, Il1α] as well as nucleic acids and their derivatives (e.g. mitochondrial DNA, extracellular ATP)[1]. Of these, extracellular ATP is one of the best-characterized DAMPs in the CNS[1,5]. Several cell death modalities, including apoptosis, pyroptosis, necroptosis, and necrosis, can cause ATP release, albeit with differing kinetics and at differing concentrations[36]. Extracellular ATP binds the P2X7 receptor (P2X7R), a ligand-gated ion channel widely expressed in the CNS whose activation leads to ion flux and inflammasome activation[36]. Microglia respond to P2X7R ligation by producing cytokines (e.g. Il-1β, IL-18) and chemokines (e.g. CCL3), which accentuate the local immune response. Importantly, extracellular ATP can also initiate multiple cell death modalities (including apoptosis and pyroptosis), highlighting an important link between inflammation and tissue damage[1,36]. Extracellular ATP is thought to contribute to the pathogenesis of MS and its animal model, experimental autoimmune encephalomyelitis (EAE) through P2X7R ligation. P2X7R is up-regulated in myeloid cells in the CNS of MS patients[37] and gain-of-function mutations in P2X7R are associated with increased risk of MS[38]; likewise, P2X7R deficiency and pharmacological inhibition of P2X7R are both protective in EAE[39,40].

1.1.3.3 Detecting Danger: Pattern Recognition Receptors

Several classes of PRRs are responsible for detecting danger signals, including (i) Toll-like receptors (TLRs) (ii) NOD-like receptors (NLRs) (iii) RIGI-like receptors (RLRs), and (iv) AIM2-like receptors (ALRs)[1,36]. TLRs are transmembrane glycoproteins found on both intracellular and extracellular membranes, where they initiate a signaling

response through TRIF and Myd88. By contrast, NLRs and ALRs are cytoplasmic and signal through the inflammasome. RLRs are cytoplasmic sensors of RNA. Each class of PRRs can detect an array of molecules, and individual PRRs can detect multiple PAMPs and DAMPs [e.g. TLR4 can detect lipopolysaccharide (LPS), endogenous HMGB1, HSPs, heparin sulphate, and S100 proteins among others][36,41]. Through a series of intracellular adapter molecules, the sensory inputs from the PRRs are integrated and translated into a proinflammatory effector response. Depending upon the PRR pathway engaged, different transcriptional networks can be activated by signal-dependent transcription factors (SDTFs), including those of the nuclear factor kappa-light-chain-enhancer of activated B cells (NF-κB), activator protein 1 (AP-1), interferon regulatory factor (IRF), and signal transducers and activators of transcription (STAT) families[42].

1.1.3.4 Profiles of Microglial Activation

Microglial activation was originally conceptualized using the M1/M2 macrophage polarization paradigm, in which M1 classically-activated microglia were neurotoxic and proinflammatory, while M2 alternatively-activated microglia were involved in resolution of inflammation[43-46]. This dichotomy is now considered overly simplistic in the era of single cell RNA sequencing and high-dimensional flow cytometry[1,47-49]. Based upon transcript and surface marker expression data, a spectrum of different activation signatures have been observed in neurodegenerative and neuroinflammatory conditions, including AD[50,51], Huntington's disease (HD)[52], ALS[52], aging[53], and MS[12,52,53]. Different microglial profiles have been shown to emerge over time or concurrently within a single disease state, highlighting temporal and regional heterogeneity in microglial phenotypes[12,49,54]. Much as there is evidence for a core gene signature

associated with homeostatic microglia, there is also evidence for a core gene signature in disease-associated microglia ("DAM signature"). This includes inflammatory molecules such as *Apoe*, *Itgax*, *CCl2*, *Clec7a*, and *Axl*) and down-regulation of homeostatic microglial genes (including *P2ry12*, *Tmem119*, *Csf1r*, *Hexb*, *Mertk*, *Cx3cr1*)[12]. Although the specific disease signature varies, the microglial activation phenotype includes several common features, including enhanced proliferation, release of cytokines, chemokines, and other inflammatory mediators, enhanced phagocytosis, and increased antigen presentation capacity[12].

1.1.3.5 Secretory Profiles of Activated Microglia

The microglial secretome is a crucial feature of CNS inflammation, responsible for propagation of inflammation, recruitment of peripheral cells, and activation of the BBB. Depending upon the nature of the stimulus, the inflammatory response is typically coordinated by the NF-κB, JAK/STAT, JNK, ERK1/2 and p38 signaling pathways[12]. Activation of these pathways results in the production of an array of proinflammatory cytokines, including IL-1β, IL-6, TNFα, IL-18, Il-12, and Il-23[12], some of which are neurotoxic in high concentrations[55]. Chemokines such as CCL2-5, CCL7, CCL12, and CCL22, as well as reactive oxygen/nitrogen species (ROS/RNS), are also secreted from activated microglia[12]. The specific combination of inflammatory mediators released varies substantially between individual microglia, and recent high-throughput single-cell approaches are beginning to shed light upon these differences[52,54].

1.1.4 Calling for Back-up: Peripheral Immune Cell Trafficking into the CNS

Under homeostatic conditions, the expression profile of adhesion molecules on the CNS endothelium is exquisitely adapted to prevent extravasation of leukocytes into the CNS[5]. Expression of cell adhesion molecules on the CNS endothelium is only 10% of that on other organs, and adhesion of rolling leukocytes to the endothelium is comparably reduced[5]. Nonetheless, danger signals from the CNS activate the CNS endothelium, increase expression of adhesion molecules, and facilitate the extravasation of leukocytes[2,5]. Antagonism of adhesion molecules is an effective strategy for mitigating CNS inflammation, as demonstrated with the blocking antibody natalizumab, which blocks $\alpha_4\beta_1$-integrin and is approved for use in MS[56].

1.1.4.1 Monocyte-derived Macrophages

Blood-derived monocytes have different transcriptional profiles than CNS-resident macrophage and microglia populations, but upon entering the CNS, monocytes undergo differentiation into mDCs or macrophages that bear notable similarities in their surface marker expression profiles to microglia[12,34,52]. Microglial depletion studies have demonstrated that MDMs can migrate into the CNS to replenish the microglial niche, but these cells still retain a unique signature that differentiates them from yolk-sac-derived microglia[57]. Although recruitment of peripheral monocytes into CNS in response to infectious stimuli is less profound than in other organs such as the skin (injection of LPS into the CNS parenchyma required a 100-fold higher dose to obtain the same level of monocyte recruitment[9]), monocytes represent one of the major infiltrating cell types during CNS injury, infection, and autoimmunity. Interestingly, purely neurodegenerative

diseases such as HD and ALS do not show monocyte migration into the brain[52]. In injury models, recruitment of monocytes is substantial, occurring within one day post-injury[1]. Once in the CNS, MDMs can have both detrimental and protective effects. MDMs promote wound healing, re-vascularization, phagocytosis, and debris clearance, but can also release the excitotoxic neurotransmitter glutamate, along with neurotoxic cytokines and ROS[1]. In many models of neuroinflammation, including EAE, depletion of monocytes is neuroprotective[52].

1.1.4.2 T Lymphocytes

T lymphocytes mainly persist in the border regions of the CNS (meninges and choroid plexus) and can be recruited into the CNS parenchyma during injury, infection, or autoimmunity, albeit with generally slower kinetics than monocytes, potentially due to the necessity for antigen-dependent activation prior to tissue invasion[1,8]. Although the choroid plexus, meninges, and perivascular space have all been postulated as major routes for T lymphocyte entry into the CNS, one recent EAE study highlighted the leptomeningeal vessels as the main site of T cell extravasation[58]. Accordingly, T cells recruited from the periphery migrated out of the leptomeningeal vessels before being successfully re-activated by antigen-presenting perivascular macrophages, licensing the T lymphocytes to acquire effector functions and migrate deep into the parenchyma[58]. Other MHCII-expressing cells, including microglia, astrocytes, neutrophils, B cells, perivascular DCs, and BAMs, are thought to play a role in antigen presentation and T cell reactivation, but their respective roles may prove to be stimuli- and anatomical niche-dependent[8]. Likewise, the chemokines responsible for T cell recruitment are likely

context-dependent; however, CCL4, CCL5, CCL20, CXCL1, and CXCL2 have all been proposed to play a role in recruitment of encephalogenic T lymphocytes[2].

1.1.4.3 Other Cell Types

Neutrophils are short-lived granulocytes recruited to the CNS in response to injury or infection[1] and evidence has emerged for a role for neutrophils in models of stroke[59], AD[60] and MS[61]. Circulating populations of neutrophils within the meninges and choroid plexus[10,11] highlight a potentially important role in CNS inflammation. Mast cells, best known for their role in allergic responses, also accumulate in various CNS compartments during neuroinflammation[62]. DCs reside in the border regions of the CNS but are excluded from the parenchyma under homeostatic conditions[10,11]. They are recruited into the perivascular space and parenchyma during inflammation, where they are loaded with CNS antigen; these cells appear to accumulate locally and mediate *in situ* antigen presentation to T cells[9]. B cell germinal centers can also be found in the meninges/choroid plexus and produce CNS-specific antibodies. B cells can migrate into the parenchyma in MS/EAE, but less is known about their role in other CNS pathologies[63].

I.II. Inflammasome Structure and Function

Discovered in 2002, inflammasomes are cytosolic, multi-protein platforms for activating the caspase-1 family of proteases[64]. They are cross-linked molecular scaffolds, maintained through protein: protein interactions between conserved domains[65]. Assembly of the inflammasome provides a platform for cleavage and activation of diverse caspase-1 family substrates, including cytokines (IL-1β and IL-18) and the

executioner protein gasdermin D (GSDMD), which drives inflammasome-dependent programmed cell death known as *pyroptosis* ("fiery death")[66].

1.2.1 Components of the Inflammasome

The prototypical inflammasome includes four components: (i) a sensor protein (ii) a non-enzymatic scaffolding protein (iii) an inflammatory caspase, and (iv) substrates of the inflammatory caspase that interact transiently with the complex [Figure 1.2]. Following transcriptional up-regulation of inflammasome components in response to a priming signal (Signal 1), the assembly of the inflammasome protein complex is triggered when sensor proteins detect their ligand (Signal 2) and rapidly oligomerize[67]. This nucleates the inflammasome and triggers polymerization of the scaffolding protein, apoptosis-associated speck-like protein containing a CARD (ASC), a bipartite protein comprised of an N-terminal pyrin domain (PYD) and a C-terminal caspase-activation and recruitment (CARD) domain[66,67]. Cross-linked filaments of ASC recruit proinflammatory caspases, which are retained in the complex through homotypic interactions between CARD domains of ASC and caspase molecules. Caspase molecules in close contact undergo proximity-induced auto-activation, enabling them to acquire proteolytic activity and cleave their substrates (e.g. Il-1β and IL-18). Certain inflammasomes (such as the NLRC4 inflammasome) can form without ASC, due to the presence of a CARD protein domain on the sensor protein that enables direct interaction with the inflammatory caspases[67]. An overview of the domains mediating homotypic protein-protein interactions within the inflammasome is provided in [Figure 1.3]. Particularly large filamentous structures known as ASC specks can also form,

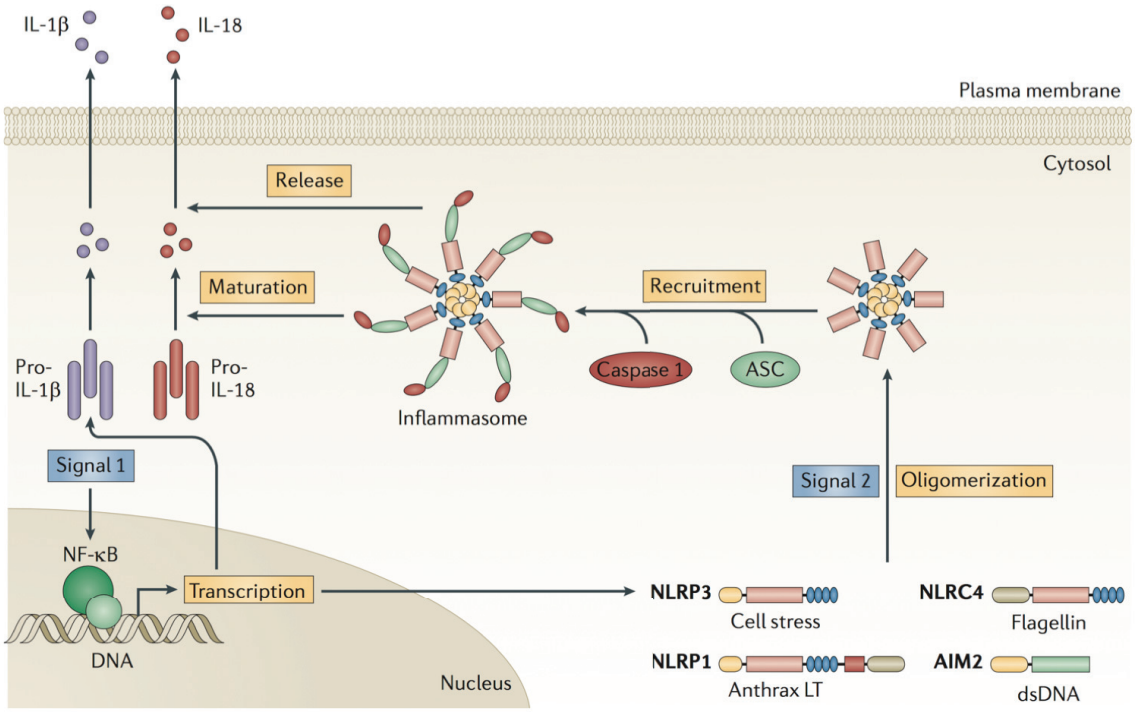

Figure 1.2: ***Formation of the inflammasome complex***

Following exposure to individual pathogens or host-derived insults, a number of cytosolic sensors (e.g NOD-, LRR- and pyrin domain-containing 1 (NLRP1), NLRP3, NOD-, LRR- and CARD-containing 4 (NLRC4) and absent in melanoma 2 (AIM2)) are capable of forming inflammasomes that mediate common downstream events. A priming stimulus (Signal 1), acting through the nuclear factor-κB (NF-κB) pathway, often precedes assembly of the inflammasome complex in order to up-regulate the transcript levels of pro-interleukin-1β (pro-IL-1β) and NLRP3. Upon ligand sensing or enzymatic activation within the cytosol (Signal 2), the cytosolic sensors oligomerize to form an activation platform for caspase-1. For most complexes, recruitment of caspase 1 also requires the adaptor protein, ASC (apoptosis-associated speck-like protein containing a CARD). Through its protease activity, caspase-1 regulates the maturation and release of IL-1β and IL-18. For some inflammasome complexes, the direct activating stimulus is known, but for other complexes (i.e. NLRP3), activation has been associated with a range of physiological stressors, including ion fluxes, endosomal rupture, reactive oxygen species or mitochondrial dysfunction. dsDNA, double-stranded DNA; LT, lethal toxin.

Adapted from: Walsh J, Muruve D, and Power C. (2014). Inflammasomes in the CNS. *Nature Reviews Neuroscience*. 15(2), 84-97. Springer Nature License Copy Number: 4535661035848

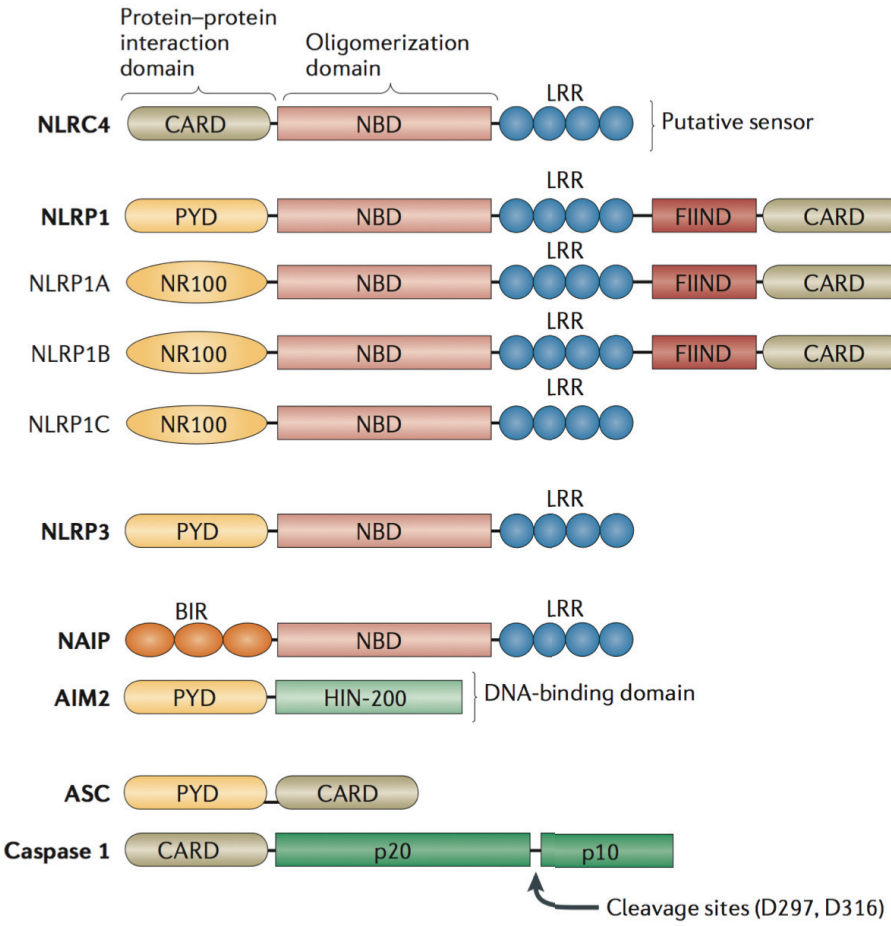

Figure 1.3: ***Domain structures of major inflammasome components***

Inflammasome assembly is mediated by homotypic interactions between protein domains. The NLR family of proteins contain a putative sensory component formed by the C-terminal leucine-rich repeat (LRR). Oligomerization of the NLRs is mediated by their nucleotide-binding domains (NBD). Protein-protein interactions between the NLRs and the scaffolding protein ASC are mediated by the N-terminal pyrin domain (PYD). The caspase activation and recruitment (CARD) domain of ASC facilitates protein-protein interactions with the CARD domain of caspase-1. NLRP1 and NLRC4 sensor proteins can also interact directly with caspase-1 through their respective CARD domains. Murine NLRP1A-C contain an NR100 domain which has no known homologue in humans. AIM2's HIN-200 domain serves to detect and bind to DNA directly while its PYD mediates interactions with ASC.

Adapted from: Walsh J, Muruve D, and Power C. (2014). Inflammasomes in the CNS. *Nature Reviews Neuroscience*. 15(2), 84-97.
Springer Nature License Copy Number: 4535661035848

representing large inflammasome aggregates that can be released extracellularly and have a variety of physiological effects[68].

1.2.2 The Inflammatory Caspases

1.2.2.1 A Brief Overview of the Caspase Family

Caspases are a family of cysteine-aspartic acid proteases that can cleave an array of different protein substrates based upon stringent specificity for a tetrapeptide motif. Caspase family members have been broadly classified as either apoptotic (caspase-3, 6, 7, 8, 9, 10) or inflammatory (caspase-1, 4, 5, 11, 12), based upon phylogenetic analysis[69,70]. Amongst the apoptotic caspases, caspase-8/9/10 are considered "initiator caspases", because they directly cleave and activate the "effector caspases" (-3/6/7), which execute apoptosis[70]. All caspases are assembled from highly conserved domains, including a p20 and p10 domain, in combination with a prodomain of differing length and composition[71]. Caspases are typically present in an inactive precursor form and attain proteolytic function once they are cleaved and activated. Activation can occur in two ways: (i) through direct proteolytic cleavage by upstream caspases, or (ii) through a dimerization-induced auto-cleavage event facilitated by a multi-protein signaling platform[36]. The effector caspases (3,6,7) are activated according to the first paradigm, whereby initiator caspases provide the activating cleavage event. By contrast, the initiator caspases (8,9,10) tend to be activated by proximity-induced auto-activation, which is facilitated by a larger signaling platform, such as the apoptosome or the inflammasome[36]. Altogether, over 1500 caspase substrates have been identified[72], with the number of substrates cleaved by an individual caspase ranging from several targets (e.g. caspase-4, -5, -9) to several hundred (e.g. caspase-1, -3, -6, -7, -8)[72].

1.2.2.2 Caspase-1 Family Proteases

In humans, the caspase-1 subfamily consists of caspase-1, 4, and 5, and in mice caspase-1 and -11, all of which can form inflammasomes. Functionally, murine caspase-11 is considered a homologue of human caspase-4/5 and shares 59% and 54% amino acid sequence homology respectively[71]. In humans, caspase-4 and -5 share significant (77% identical) sequence homology, and it has been speculated that gene duplication of an ancestral caspase-11-like gene ultimately gave rise to caspase-4/5[71]. In addition to the p20 and p10 domains shared by all caspases, the caspase-1 family also shares an N-terminus CARD domain that facilitates inflammasome formation[69].

Active caspase-1 is a highly transient species, with a half-life of only 9 minutes, compared to 8hr for caspase-3 and 11hr for caspase-7[73]. It was recently demonstrated that clustering of caspase-1 in the inflammasome leads to the generation of a transient p33/p10 species, which is responsible for most substrate cleavage events[74]. Cleavage of the CARD domain from the p33 fragment generates a p20/p10 species that rapidly dissociates from the inflammasome and loses its activity[74].

The substrate profile of caspase-1 has been extensively characterized. Depending upon the stimulus, the experimental conditions (cell-free versus *in vitro*), the nature of the protein substrate (natural versus synthetic), and the concentration of caspase-1 (cell-free only), different caspase-1 substrate profiles have been generated, with over 100 substrates identified in total[75-77]. In addition to GSDMD and the well-characterized cytokines (Il-1β and IL-18), substrates also include a number of cell death proteins,

notably the apoptotic executioner caspases-3 and -7[75,78-80]. Although it has been speculated that activation of apoptotic caspases in concert with other caspase-1 substrates might mediate pyroptosis[75], this idea was largely, and arguably prematurely, sidelined with the discovery of GSDMD as the primary executioner of cell lysis during pyroptosis[81,82].

1.2.2.3 Non-canonical versus Canonical Inflammasomes

Inflammasome activation generally follows one of two paradigms, depending upon which caspase is engaged[36]. *Canonical inflammasome activation* engages caspase-1, which has a high affinity for GSDMD and the inflammasome-associated cytokines (IL-1β and IL-18). Canonical inflammasome activation can cause cytokine release, pyroptosis, or both[36]. A lack of IL-1β or IL-18 release does not rule out canonical inflammasome activation, however, as these substrates are not present in all cell types and are not mechanistically required for canonical inflammasome activation. *Non-canonical inflammasome activation*, by contrast, involves the engagement of caspase-4/11 either directly by LPS or downstream of TLR4[83]. However, caspase-4/11 has a more restricted substrate profile, with a lower affinity for Il-1β and IL-18[83]. As such, non-canonical inflammasomes will often drive pyroptosis without cytokine release[83].

1.2.3 Inflammasome-Associated Cytokines

1.2.3.1 IL-1β

IL-1β is a potent inflammatory signaling molecule, with diverse autocrine, paracrine, and systemic functions. When released into the circulation, IL-1β serves as an endogenous pyrogen to induce fever and pain hypersensitivity[84]. IL-1β is expressed at

low levels in CNS tissue and is detectable in the CSF at homeostasis[85]. Rapid and profound transcriptional up-regulation of IL-1β can be triggered by a multitude of stimuli, including LPS, hypoxia, TNFα, IL-18, and IL-1β itself[86]. Unlike many cytokines, IL-1β is translated on non-membrane-associated polyribosomes in the cytoplasm rather than in association with the ER/Golgi[87]. Following translation, IL-1β interacts with inflammasome complexes where it undergoes proteolysis to form the bioactive cytokine. IL-1β lacks a signal sequence, and unconventional (Golgi-independent) secretion of IL-1β has been widely observed[86]. Several pathways have been proposed to explain how IL-1β exits the cell, including secretory vesicles, exosomes, and cell membrane rupture[86,87], with caspase-1 and GSDMD being strongly implicated in this process[88]. The intersection between IL-1β secretion and GSDMD is discussed more fully in Section IV. Extracellular IL-1β is detected by the receptor IL-1R1, found on virtually all hematopoietic and non-hematopoietic cells[86,89]. The receptor antagonist, IL-1RA, also binds the receptor competitively without inducing downstream signaling, and serves as a means of regulating the Il1β signaling pathway. The co-receptor, Il-1 receptor accessory protein (IL-1RAcP) is also required for signal transduction. Expression levels of these proteins, in addition to IL-1β itself, can be regulated in order to modulate the IL-1 signaling pathway[89]. Following ligation of the IL-1R1 by IL-1β, the accessory protein is recruited, leading to the recruitment of the adapter proteins, myeloid differentiation primary response gene 88 (MYD88) and interleukin-1 receptor–activated protein kinase (IRAK4). Through a series of signaling intermediates (IRAK1/2/4, TRAF6, and TAK1), this pathway activates several transcription factors,

including NF-κB and AP-1, up-regulating several hundred genes involved in innate immunity[89]. IL-1-responsive genes include chemokines, cytokines, and proinflammatory molecules, such as IL-6, IL-8, MCP1, and COX2, as well as IL1β itself[89]. The release of neurotoxic cytokines such as IL-6, TNFα, and IL-1β itself downstream of IL-1β represents one important mechanism linking inflammasome activation and neurodegeneration[90].

1.2.3.2 IL-18

IL-18 is an important proinflammatory cytokine with non-redundant functions compared to IL-1β, and forms a crucial link between the innate and adaptive immune systems. It is a potent inducer of interferon gamma (IFN-γ) in Th1 cells (in combination with IL-12 or IL-15), and potentiates the activity of NK and $CD8^+$ T lymphocytes[21,86]. IL-18 tends to be constitutively expressed as pro-IL-18, which is cleaved and activated by the inflammasome. Extracellular Il-18 binds to the heterodimeric receptor composed of IL-18Rα/β. Like IL-1β, IL-18 has several negative regulators, most notably the IL-18 binding protein (IL-18BP), which binds with high affinity to active extracellular IL-18, blocking its interaction with its cognate receptor. Ligation of the IL-18 receptor by IL-18 signals through the MyD88 adapter protein to up-regulate NF-κB-associated genes[21].

1.2.4 Pattern Recognition Receptors in the Inflammasome

Inflammasome-associated PRRs are activated either by direct engagement of their ligand (e.g. AIM2), or indirectly through disruptions of cellular homeostasis (e.g. NLRP3)[66]. Like ASC and caspase-1, conserved protein domains are found on sensor proteins in different combinations [Figure 1.3], including PYD domains (to facilitate

protein: protein interactions with ASC), leucine-rich repeats [(LRRs), putatively for ligand binding], CARD domains (to facilitate protein: protein interactions with caspase-1), and nucleotide-binding domains [(NBD), to facilitate oligomerization].

1.2.4.1 NLRP1 Inflammasome

NLRP1 was the first inflammasome identified and has proved particularly enigmatic, in part due to its unique structure and activation mechanism, and in part due to notable differences between human and mouse NLRP1[91,92]. NLRP1 in both mice and humans contains a unique C-terminal function-to-find domain (FIIND) whose function is still being elucidated. Furthermore, NLRP1 contains a CARD domain, which should allow it to interact with caspase-1 independently of ASC; nonetheless, ASC appears to be required for optimal NLRP1 inflammasome function[92]. NLRP1 is activated by specific proteases, including anthrax lethal factor, which liberate a 4kDa fragment from the N-terminus of NLRP1 through mechanisms that are still under investigation[91,93].

1.2.4.2 NLRP3 Inflammasome

The NLRP3 inflammasome has a tripartite structure, containing an N-terminal PYRIN domain, a nucleotide-binding-and-oligomerization NACHT domain (mediating ATP binding and hydrolysis), and a C-terminal LRR domain. Mutations in the region of the NACHT domain containing the ATPase activity inactivate NLRP3[94]. NLRP3 detects a diverse range of stimuli, including viruses, bacteria, and perturbations to cellular homeostasis, though the mechanism of activation is debated (described below)[91].

1.2.4.3 NLRC4 Inflammasome

NLRC4 detects bacterial components, including flagellin and components of the Gram-negative type III and IV secretion systems[91,92]. NLRC4 acts in concert with members of the neuronal apoptosis inhibitory protein (NAIP) family, which are direct sensors of bacterial ligands. NAIP1, 2, 5, and 6 each detect a specific bacterial ligand and subsequently bind NLRC4 to activate the inflammasome[91,92].

1.2.4.4 AIM2 Inflammasome

AIM2 detects double-stranded DNA, either pathogen or host-derived, through its C-terminal HIN200 domain[91]. AIM2 is thought to be maintained in an auto-inhibitory conformation whereby the interaction between the PYD and HIN200 domains is lifted upon DNA binding to enable inflammasome formation[92].

1.2.4.5 Pyrin Inflammasome

Pyrin detects changes to intracellular homeostasis mediated by bacterial toxins such as *C. difficile* toxin B and pertussis toxin (PTX). At homeostasis, pyrin is kept constitutively inactive by a pathway that senses the phosphorylation state of Rho-GTPases. Toxin-induced perturbation of the phosphorylation stage of this pathway leads to the removal of inhibitory signals and activation of the pyrin inflammasome[95].

1.2.4.6 Other Inflammasome Sensors

Various other NLR family members form inflammasomes, including NLRP2, NLRP6, NLRC5, and NLRP12, and these await more extensive characterization[65,92].

1.2.5 The NLRP3 Inflammasome In Depth

The NLRP3 inflammasome can be triggered by a variety of DAMPs and PAMPs, including cholesterol crystals, pore-forming toxins, ionophores, extracellular ATP, mitochondrial damage, ER stress, viruses, bacteria, and other stressors. This led to the characterization of NLRP3 as a sensor of homeostatic disruption rather than a single ligand[91,94]. The NLRP3 inflammasome has been repeatedly implicated in different models of neuroinflammation, but a unifying mechanism of activation remains elusive.

1.2.5.1 Priming the NLRP3 Inflammasome

In myeloid cells, NLRP3 and Il-1β are typically maintained at low levels under homeostatic conditions, inhibiting spontaneous inflammasome formation[94,96]. Thus, a priming step is often required to induce transcription and translation of these proteins to a degree that kinetically favours inflammasome formation[97]. Priming occurs through ligation of a TLR or cytokine receptor to generate an NF-κB-mediated up-regulation of inflammasome-associated genes[96]. NLRP3 is retained in an auto-inhibited conformation by post-translational modifications until an activating stimulus triggers inflammasome assembly[94]. Overexpression of NRLP3 removes the need for the priming step[94,97]. Although priming with LPS is the most common experimental approach, TNFα and IL-1β can also prime the NLRP3 inflammasome[96]. IL-1β is thus both a consequence and effector of inflammasome activation, highlighting autocrine and paracrine IL-1β signaling as a means to propagate inflammasome activation[98]. Importantly, pre-existing pools of IL-1β and IL-18 do exist in many cell types, and these can be processed independently of transcription in under 15 minutes[99].

1.2.5.2 Unifying Mechanisms for NLRP3 Activation

To date, debate remains about whether a single unifying mechanism underlies the response to different NLRP3 activators. Conserved binding partners for NLRP3 have been elusive, with the exception of NIMA-related protein kinase 7 (NEK7), which mediates NLPR3 inflammasome activation in mouse myeloid cells downstream of ion flux and ROS generation[100-102]. Caspase-8 activation has also been shown upstream of NLRP3 in several mouse and human inflammasome activation paradigms, although this was not recapitulated in nigericin-treated human myeloid cells[94,103].

Mechanism 1: Ion Flux

Amongst the earliest NLRP3 inflammasome activators identified were (i) ionophores, bacterial pathogenesis factors that permeabilize the plasma membrane to enable K^+ efflux (such as nigericin) [Figure 1.4], and (ii) endogenous extracellular ligands that open K^+-permeable channels in the plasma membrane (such as extracellular ATP) [Figure 1.4][94]. K^+ flux precedes NLRP3 inflammasome activation for virtually all stimuli tested, and NLRP3 inflammasome activation can be selectively blocked by concentrated extracellular K^+; likewise, suppressing intracellular K^+ is sufficient to activate the NLRP3 inflammasome, and spontaneous inflammasome assembly can be triggered in a cell-free system with low K^+ levels[104,105]. This body of data has supported the concept that K^+ flux is necessary and sufficient for NLRP3 activation, though the mechanism by which NLRP3 detects K^+ efflux is unknown. Ca^{2+} signaling, mediated largely by the endoplasmic reticulum (ER) as a major reservoir for intracellular Ca^{2+}, has also been suggested as a trigger for NLRP3 inflammasome activation[96]. Common NLRP3 activators including ATP and nigericin mobilize intracellular Ca^{2+}, inhibition of which blocks

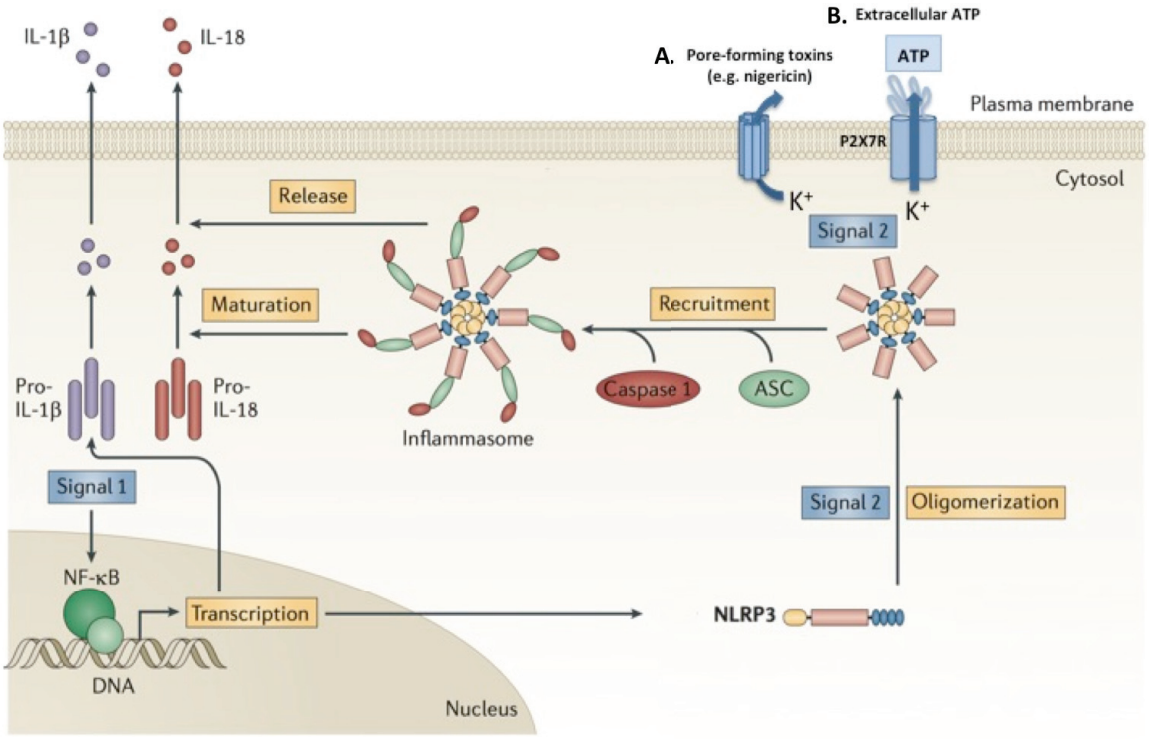

Figure 1.4: *K⁺ efflux as a mechanism for NLRP3 inflammasome activation by ATP*

K⁺ efflux has been proposed as a unifying mechanism underlying NLRP3 inflammasome activation in response to a diverse array of stimuli. (A) Nigericin is a pore-forming toxin that permits rapid K⁺ efflux out of the cell. (B) Extracellular ATP is detected by the P2X7 receptor (P2X7R) transmembrane channel, which upon ligand binding, opens a K⁺-permeable channel to allow ion efflux from the cell. K⁺ efflux is sensed by NLRP3 through a yet-unknown mechanism, acting as a Signal 2 to trigger the oligomerization of NLRP3 with ASC and caspase-1 to form the inflammasome complex.

Adapted from: Walsh J, Muruve D, and Power C. (2014). Inflammasomes in the CNS. *Nature Reviews Neuroscience*. 15(2), 84-97. Springer Nature License Copy Number: 4535661035848

NLRP3 but not AIM2 or NLRC4 activation[96]. Nonetheless, others have found Ca^{2+} signaling to be dispensable[96]. Along with the challenge of uncoupling Ca^{2+} and K^+ flux physiologically, these findings have ensured that the role of Ca^{2+} signaling remains controversial[96].

Mechanism 2: Mitochondrial Danger Signals

Mitochondria are central integrators of homeostatic information, and many NLRP3 activators trigger disruptions in homeostasis that are readily detected by mitochondria[94,96]. It has been suggested the release of ROS (mtROS) from mitochondria is upstream of NLRP3 inflammasome activation[96]. However, cytosolic mitochondrial DNA and externalization of mitochondrial cardiolipid have also been proposed as unifying factors upstream of NLRP3[94]. NLRP3 itself has been shown to localize to the mitochondria through interactions with MAVS, lending credence to this hypothesis[106].

Mechanism 3: Lysosomal Disruption

NLRP3 activation is a common downstream result of phagocytosis of crystals (e.g. cholesterol crystals) or proteinaceous aggregates (e.g. amyloid beta). The process of lysosomal damage leads to intracellular release of cathepsins upstream of NLRP3 activation in several activation paradigms[94]. Cathepsin release appears to be amplified by extracellular release of ATP and efflux of intracellular K^+ through a currently undefined mechanism, which serves to augment the NLRP3 activation process[94].

1.2.6 Inflammasomopathies

Clinically, gain-of-function mutations in inflammasome components cause hereditary autoinflammatory disorders, such as cryopyrin-associated periodic syndrome

(CAPS)[107]. CAPS includes a spectrum of pathologies, including Muckle-Wells syndrome (MWS), familial cold auto-inflammatory syndrome (FCAS), and neonatal-onset multisystem inflammatory disorder (NOMID), all caused by gain-of-function mutations in *NLRP3*[107]. To date, over 200 mutations in the *NLRP3* gene have been associated with CAPS[94]. When such mutations are expressed in murine models, the outcome is profound systemic inflammation[108]. In humans, these activating mutations cause spontaneous NLRP3 inflammasome assembly in the absence of pathogenic stimuli, which drives tissue and systemic inflammation[107]. These disorders present with a variety of symptoms, including fever and tissue-specific inflammation[94,107,109]. Depending upon the cohort, between 40-92% of CAPS patients report neurological symptoms[110]. Likewise, activating mutations in *NLRC4*, *NLRP1*, and *MEFV* (encoding pyrin) can cause a spectrum of autoinflammatory diseases of varying severity[107,109]. Mouse models of these inflammasomopathies have provided a useful platform for dissecting the contribution of cytokines versus pyroptosis in the context of constitutive inflammasome activation. One group compared double- and triple-transgenic mice harbouring CAPS-associated activating *NLRP3* mutations in combination with either *IL1R1* or *IL18R* deletions. Interestingly, spontaneous cell death persisted in the mice with deficient IL-1β and IL-18 signaling, suggesting a cytokine-independent role for pyroptosis in CAPS[108]. Likewise, GSDMD knock-out in NOMID mice is highly protective[111].

1.2.7 Inflammasome Inhibitors

1.2.7.1 Inhibitors of the IL-1β Signaling Axis

Therapies targeting the IL-1β signaling axis are widely used and well-tolerated for several conditions, including CAPS, rheumatoid arthritis, gout, and Type 2 diabetes.

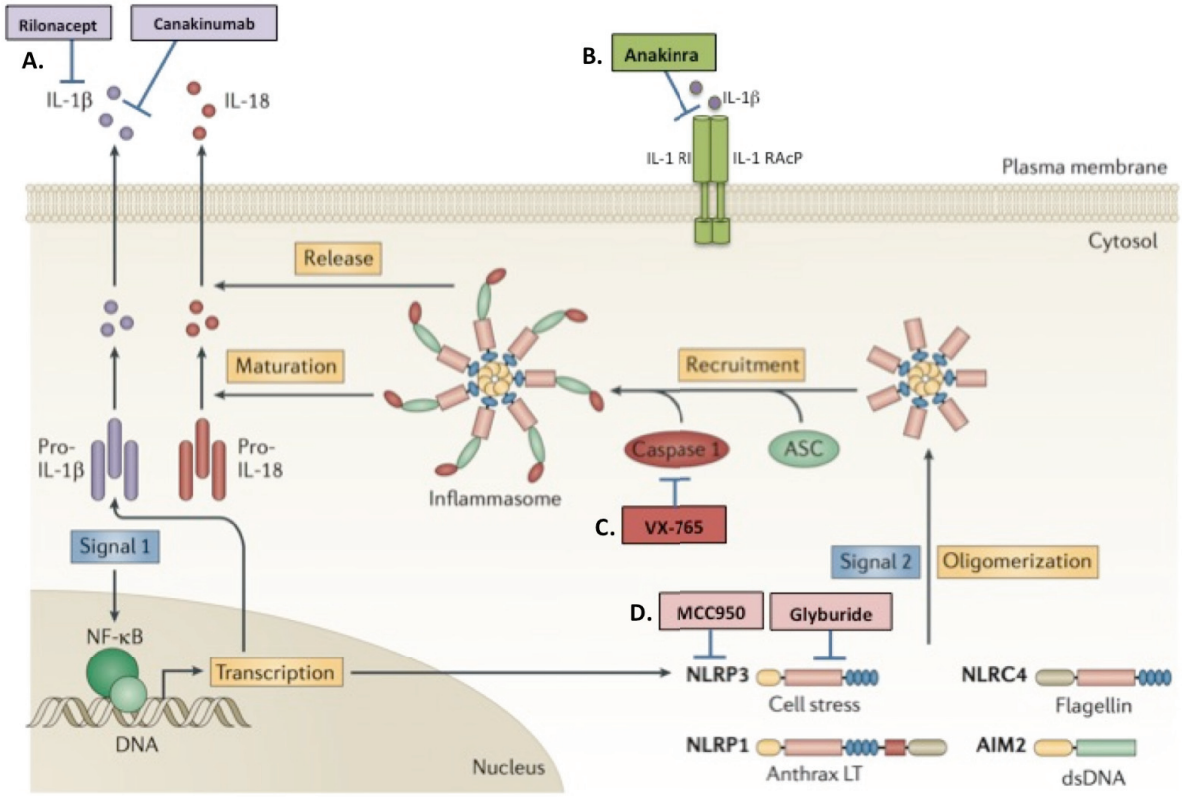

Figure 1.5: ***Strategies for blocking inflammasome activation***

Different approaches for blocking the inflammasome have been tested, including: (A) inhibiting extracellular IL-1β signaling directly (Rilonacept, Canakinumab), (B) inhibiting the IL-1 receptor (Anakinra), (C) inhibiting caspase-1 (VX-765), and (D) inhibiting the NLRP3 inflammasome (MCC950, Glyburide), although the mechanism of NLRP3 inflammasome inhibition has not yet been directly established.

Adapted from: Walsh J, Muruve D, and Power C. (2014). Inflammasomes in the CNS. *Nature Reviews Neuroscience*. 15(2), 84-97. Springer Nature License Copy Number: 4535661035848

Several IL-1β-targeting agents are FDA-approved [Figure 1.5], including: (i) anakinra, a recombinant IL-1 receptor antagonist (ii) rilonacept, a soluble version of the decoy receptor, and (iii) canakinumab, a blocking antibody against IL-1β[98]. Anakinra and canakinumab are effective treatments for CAPS, highlighting a role for IL-1β in its pathology[94]. However, because these compounds target only inflammasome-associated cytokines, other caspase-1 substrates may still drive pathology, as highlighted by the limited efficacy of IL-1β inhibitors in resolving all CAPS-associated symptoms[91].

1.2.7.2 Inhibitors of Proinflammatory Caspases

VX-765 and its related compounds are peptidomimetics, which are metabolized into more potent forms *in vivo* by plasma and liver esterases[94]. VX-765 inhibits caspase-1 [Figure 1.5], reduces IL-1β and IL-18 release[112], and has been widely used for *in vitro* and *in vivo* studies, ranging from neurological conditions (epilepsy, depression, anxiety, multiple system atrophy, PD and AD models)[113-118] to heart disease and HIV[119,120]. VX-765 reached phase II clinical trials as a novel therapeutic for epilepsy and psoriasis with no major side effects[94] although markers of liver toxicity were observed which led to discontinuation of the trials. VX-765 crosses the BBB and reaches bioactive concentrations in the CNS following intraperitoneal (IP) administration[113,118].

1.2.7.3 NLRP3 Inflammasome Inhibitors

The most well-characterized NLRP3 inflammasome inhibitor is the diarylsulfonylurea compound CP-456,733, (CRID/ MCC950) [Figure 1.5][94]. It is highly specific for NLRP3, with no known efficacy against other inflammasomes or signaling pathways tested, but its target (i.e. NLRP3 itself or an upstream molecule) is unknown[94]. This compound was

tested in Phase II clinical trials for use in rheumatoid arthritis but was subsequently discontinued due to elevated serum liver enzymes[94]. Glyburide is a sulfonylurea-based compound that has also been shown to inhibit NLRP3 inflammasome activation by nigericin, ATP, and other stimuli, although the precise mechanism is unknown. It is clinically used for Type 2 diabetes, where it inhibits ATP-sensitive K^+ channels; however, its inhibitory effect on the NRLP3 inflammasome does not seem to be derived from this mechanism, and thus its mechanism of action remains elusive[121].

I. III. Inflammasome Activation in the Central Nervous System

1.3.1 CNS Inflammasomes during Homeostasis

Inflammasome components are expressed constitutively in the CNS, where they serve a variety of functions under homeostatic conditions[92,122]. IL-1β and IL-18 play a role in learning and memory, feeding, sleep regulation, and sensory functions, as well as sickness behaviours[21,122]. IL-18 protein is detectable in healthy neurons, microglia, and astrocytes, while the IL-18R subunits are broadly distributed throughout the CNS[21]. The IL-1β receptor is also expressed within the healthy CNS[122,123]. Human transcriptomics studies investigating homeostatic microglial signatures revealed that microglia RNA expression profiles are highly enriched for inflammasome genes compared to whole parietal cortex[34].

1.3.2 Expression of Inflammasome Components by Cell Type

1.3.2.1 Neurons

Despite well-documented neurotoxic effects of IL-1β at high concentrations, neurons express caspase-1 and can secrete IL-1β under pathological conditions[92]. The most well-

studied inflammasomes in mouse, rat, and human neurons are the NLRP1, NLRP3, and AIM2 inflammasomes, with NLRC4 also detected[92,122,124].

1.3.2.2 Oligodendrocytes

Prior to this thesis and others in the Power lab, inflammasome activation in ODCs has not been investigated. However, some historic precedent for the activation of proinflammatory caspases in ODCs exists, as caspase-1/11 have been observed in ODCs during EAE prior to the discovery of inflammasomes[125], and caspase-11 has been shown to activate caspase-3 in ODCs under hypoxic conditions[126].

1.3.2.3 Astrocytes

The most well-characterized astrocyte inflammasomes are the NLRP3 and NLRP2 inflammasomes. While NLRP3 inflammasome activation is quite common in different CNS cell types, the NLRP2 inflammasome has only been well characterized in astrocytes, in which it is activated by ATP in a pannexin1-dependent manner[127]. NLRC4 expression has also been observed in astrocytes[124]. IL-1β release from astrocytes is well-documented in mouse but it is less consistently observed in human astrocytes[128], and, due to the presence of these cells in the glial limitans of the BBB, may influence BBB permeability[129].

1.3.2.4 Microglia

Microglia constitutively express inflammasome components under homeostatic conditions, which are highly up-regulated during inflammation. The NLRP1, NLRP3, and NLRC4 inflammasomes have been particularly well-studied in microglia[122].

1.3.3 Conserved Mechanisms Linking Inflammasomes and Neurodegeneration

Neurodegeneration is the widespread tissue destruction that occurs during neurological disease, and secondarily to neurological injury, as a result of axonal loss and cell death in the CNS. Many mechanisms contribute to neurodegeneration, including Wallerian (distal to injury) and retrograde (proximal to injury) degeneration of injured axons, demyelination, excitotoxicity, and programmed cell death[90]. Inflammasome-associated neurodegeneration may occur through several mechanisms, including: (i) death of neurons or glia by pyroptosis (ii) release of neurotoxic inflammasome-associated cytokines from microglia or other cells, (iii) activation of neurotoxic astrocytes, and (iv) release of secondary neurotoxic inflammatory mediators/cytokines (e.g. NOS, IL-6, TNFα) and DAMPS (e.g. ATP, HMGB1) from activated or dying cells, which can perpetuate the inflammatory cascade and lead to programmed cell death[36]. Direct cytokine neurotoxicity is well-documented: both IL-1β and other inflammatory mediators downstream of IL-1β (e.g. NOS, TNFα, Il-6) can mediate neurotoxicity[130-133], although cytokines can exert beneficial effects in some circumstances[90]. IL-1β also inhibits glutamate re-uptake by astrocytes, allowing synaptic glutamate accumulation and promoting glutamate excitotoxicity[134]. Interestingly, IL-1β release in peripheral (non-CNS) tissue is accompanied by a 100-1000-fold higher release of the IL-1RA, and this antagonist quickly shuts down IL-1β signaling; however, this response is muted in the CNS and studies in epilepsy have shown that IL-1RA release is modest and delayed compared to the periphery[134]. This delayed feedback mechanism may allow a pathogenic window for cytokine neurotoxicity in the brain. As inflammatory signaling

hubs in the CNS, inflammasomes are key mediators in the interplay between inflammation and cell death in the CNS[135].

1.3.4 Inflammasomes in Neurological Injury and Disease

1.3.4.1 Alzheimer's Disease

Substantial evidence supports a role for the inflammasome in AD, a form of dementia whose pathology involves intracellular and extracellular plaque formation, neurofibrillary tangles, inflammation, and neuronal loss[136]. Microglial-derived proinflammatory cytokines are believed to play a pathogenic role in AD, with IL-1β and IL-18 exacerbating the disease[21]. IL-18 has been detected in microglia, astrocytes, and neurons in AD brains, and tends to co-localize with amyloid-β (Aβ) plaques and tau[21]. Likewise, IL-1β is consistently expressed in the brains of AD patients, particularly in microglia and astrocytes, and is also detectable in the CSF[122], while NLRP1 has been detected in neurons from AD patients[137]. *Ex vivo*, oligomeric fibrils of Aβ are known to induce ASC- and NLRP3-dependent IL-1β release from both astrocytes and microglia[124], as well as NLRP1-dependent IL-1β release from neurons[138]. Inhibition of NLRP3 is protective in mouse models of AD, causing reduced microglial activation, IL-1β release, and memory loss[139-141]. Similarly, NLRP3 knock-out mice experienced almost complete protection from memory loss, accompanied by an anti-inflammatory microglial profile[139]. A rather unique pathogenic role for inflammasomes in AD concerns the role of extracellular ASC in plaque formation. Aβ has been detected bound to fibrillar ASC specks in brain lysates from both AD animal models and human AD patients, suggesting a role for ASC in seeding Aβ plaques[142].

1.3.4.2 Parkinson's Disease

PD is characterized by a loss of dopaminergic neurons, accumulation of α-synuclein protein aggregates, and chronic neuroinflammation. Inflammasome components including NLRP3, caspase-1, and ASC accumulate in the substantia nigra in both PD patients and in mouse models of the disease[143]. Recent studies have shown a role for microglial NLRP3 inflammasome activation in α-synuclein pathology and demonstrated that MCC950 ameliorated motor deficits and rescued degeneration of dopaminergic neurons[143]. Interestingly, although protein aggregates of α-synuclein are a known NLRP3 inflammasome activator, neuronal degeneration also triggers the NLRP3 inflammasome in the absence of α-synuclein aggregates, highlighting additional neuronal DAMPs driving inflammasome activation[143]. Interestingly, microglia-specific expression of a constitutively active NRLP3 mutant using a $Cx3Cr1Cre^{ER}$ system caused an exacerbation of motor deficits and neuronal loss in an MPTP model of PD[144].

1.3.4.3 Epilepsy

Multiple studies have suggested a role for IL-1β, NLRP3, NLRP1, and caspase-1 in epileptic seizure models[114,118], which formed the basis of clinical trials of VX-765 in epilepsy[145,146]. Inflammasome-driven pathogenicity arises through several mechanisms. IL-1β lowered the threshold for provoking seizure-like discharges in a brain slice model of temporal lobe epilepsy, contributing to hyperexcitability[147]. Furthermore, inflammasomes may mediate seizure-evoked neuronal cell death, either directly (e.g. pyroptosis), through cytokine neurotoxicity, or enhanced glutamate excitotoxicity[134]. Recent work has also examined the phenotypic and transcriptional profiles of microglia

of temporal lobe epilepsy patients; this revealed a local, transient phenotype of highly activated microglia that released IL-1β and other cytokines, and identified NLRP3 as a major regulatory hub of this seizure-induced phenotype[148].

1.3.4.4 Traumatic Brain and Spinal Cord Injury

Traumatic injury in the CNS involves two stages: (i) the initial injury, leading to necrotic cell death and widespread release of DAMPs into the CNS[135], and (ii) the secondary neuroinflammatory cascade, involving astrocyte and microglial activation, oxidative stress, loss of BBB integrity, and release of ROS/RNS, cytokines, and chemokines[135]. Multiple inflammasomes, including NLRP1, NLRP3, NLRC4, and AIM2, have been implicated in TBI and SCI, highlighting the diverse nature of danger signals resulting from tissue damage[122]. Elevated levels of ASC, NLRP1, and caspase-1 are detectable in CSF following brain injury[149]. NLRP3 KO mice have improved outcomes, and pharmacological NLRP3 inhibition is protective[150]. Neuronal AIM2 inflammasomes are activated following injury, driving IL-1β release and pyroptosis; neurons co-cultured with CSF from TBI patients increase AIM2 expression and caspase-1 activation[151].

1.3.4.5 Glioma

Gliomas are CNS tumours of astrocytic origin, which can be classified into four grades (I-IV) based upon severity. NLRP3, IL-1β, caspase-1, and ASC expression all positively correlate with tumour grade[152]. Glioblastoma multiforme (GBM; Grade IV) is a highly invasive brain tumour characterized by a profound macrophage/microglial infiltration. Although GBM cell lines U87 and U251 secrete abundant IL-1β in response to various stimuli, primary human astrocytes do not release IL-1β as readily, despite synthesizing

IL-1β transcript[153]. The NLRP3 inflammasome has also been implicated in GBM pathogenesis, where dsDNA, K^+ flux, and ATP have been proposed to activate macrophage/microglial inflammasomes[122]. Microglia-derived IL-1β is thought to activate STAT3, an important transcription factor driving tumour proliferation[153]. Over-expression of NLRP3 promotes migration, proliferation, and invasion, potentially though the AKT pathway[152].

1.3.5 Outstanding Questions and Limitations

Although mechanisms of inflammasome activation appear to be largely conserved in the CNS compared to the periphery, several key differences may be observed. For instance, inflammasome-associated cytokines are expressed constitutively at low levels in the CNS, and single cell transcriptomics studies have verified that microglia express IL-1β transcript during homeostasis[34]. This differs from monocyte- and bone marrow-derived macrophages, which have informed the majority of the inflammasome literature and in which transcriptional up-regulation of IL-1β (i.e. priming) is essential for inflammasome activation[94]. These pre-existing pools of IL-1β allow for a more rapid response to danger than if synthesized *de novo*. Likewise, microglia produce lower levels of inflammasome-associated cytokines compared to their peripheral counterparts[154] and have more sustained IL-1β release[155]. Such observations suggest that CNS inflammasomes are subject to a unique regulatory framework, and thus mechanisms of inflammasome activation and regulation in peripheral cells must be extrapolated to the CNS with caution. Recent analyses have identified the paucity of human CNS inflammasome data, which presents a major limitation in the field due to emerging inconsistencies between

human and mouse inflammasomes[109]. Such inconsistencies may limit the translation potential of research findings, unless primary human cells and clinical data are also prioritized within the field.

I.IV. Pyroptosis: Inflammasome-dependent Cell Death

1.4.1 Overview of Programmed Cell Death

The Nomenclature Committee on Cell Death (NCCD) issues recommendations to delineate the different types of programmed cell death (PCD), of which twelve have been identified as of 2018[156]. PCD is unique from necrosis, which occurs under extreme physical circumstances, is instantaneous and catastrophic, and cannot be delayed, prevented, or accelerated through pharmacological or genetic interventions[156]. For the purposes of this thesis, several relevant types of PCD are highlighted below, derived from the NCCD 2018 report[156].

1.4.2 Types of Programmed Cell Death

1.4.2.1 Apoptosis

Apoptosis is an "immunologically quiet" form of cell death, mediated principally by the executioner caspases-3/7, which compartmentalizes cellular components into discreet membrane-bound bodies that are removed from the local microenvironment through phagocytosis. Apoptosis may be classified as either intrinsic or extrinsic apoptosis, depending upon the molecular events precipitating executioner caspase activation. *Extrinsic apoptosis* is defined as "a specific variant of cell death initiated by perturbations of the extracellular microenvironment detected by plasma membrane receptors, propagated by caspase-8, and precipitated by executioner caspases, mainly

caspase-3"[156]. Well-studied triggers include the interaction of extracellular ligands (such as TNFα and Fas) with their cognate death receptors on the plasma membrane (TNFR1 and FasL respectively). Ligation of death receptors recruits intracellular adapter molecules such as TNF receptor type 1-associated death domain (TRADD) and Fas-associated protein with death domain (FADD), along with the initiator caspase-8, which in turn cleaves and activates caspase-3/6/7. *Intrinsic apoptosis* is defined as "a type of cell death initiated by perturbations of the extracellular or intracellular microenvironment, demarcated by mitochondrial outer membrane permeabilization, and precipitated by the executioner caspases, mainly caspase-3"[156]. Well-studied triggers include DNA damage, oxidative stress, ER stress, ion imbalance, and others. These intracellular stresses culminate in the release of pro-apoptotic factors such as SMAC/Diablo and cytochrome C from the mitochondria. These factors ultimately lead to the activation of caspase-9, which cleaves and activates the executioner caspases-3/7. These execute a catalytic program of systematic cellular demolition involving widespread proteolysis, with hundreds of unique protein substrates undergoing cleavage. In most cell types, a single cleavage event during apoptosis does not drive cell death, but rather synthetic lethality is achieved through widespread proteolysis[72]. The morphological and molecular features of apoptosis have been extensively reviewed and are highlighted below[157-159].

Features of Apoptosis: Nuclear Condensation and DNA Fragmentation

Apoptosis involves nuclear condensation, nuclear envelope disintegration, chromatin condensation, and DNA fragmentation, all of which are mediated directly or indirectly by substrates of caspase-3/7. For example, DFF45 is a constitutively active inhibitor of

DFF40, an endonuclease that fragments DNA during apoptosis. Upon caspase-3/7-mediated proteolysis, DFF45 is inactivated, releasing its inhibitory function on DFF40. Poly-ADP ribose polymerase (PARP) is another nuclear caspase-3/7 substrate whose cleavage is a well-validated biomarker of apoptosis. DNA fragmentation causes apoptotic cells to stain positive for terminal deoxynucleotidyl transferase dUTP nick end labeling (TUNEL), a widely used (but non-specific) biomarker for apoptosis.

Features of Apoptosis: Cytoskeleton Changes

Caspase-3/7 are also responsible for dismantling the cytoskeleton through proteolysis of cytoskeletal constituents, including myosins, tubulins, keratins, and nuclear lamins. These cleavage events contribute to rounding and retraction of cell processes during apoptosis. The caspase-3/7 substrate Rho-associated protein kinase 1 (ROCK1) is an important mediator of cytoskeletal changes. This kinase becomes constitutively activated upon removal of the C-terminus by apoptotic caspases, leading to the phosphorylation of myosin light chain (MLC) and contraction of actin bundles.

Features of Apoptosis: Membrane Structures

Apoptosis involves unique membrane features, such as the flipping of phosphatidylserine (PS) to the outer leaflet of the plasma membrane, which serves to recruit phagocytes and is a popular biomarker for apoptosis. The formation of *membrane blebs* or *apoptotic bodies* along the plasma membrane is also an iconic feature of apoptosis, tightly controlled by caspase-3-mediated actin-myosin cytoskeletal rearrangements. Phosphorylation of MLC by caspase-3-activated ROCK1 leads to actomyosin contraction, which helps to locally separate the plasma membrane from the

cytoskeleton. Membrane blebs are loaded with degraded cellular components in a ROCK-1-dependent manner, before budding off to form membrane-bound vesicles that are easily phagocytosed[158]. In some hematopoietic lineage cells, apoptotic bodies appear as apoptopodia or "beads-on-a-string"[158]. Membrane-bound, debris-loaded blebs ("beads") are attached to the cell by a long tether ("string"), which may extend up to eight times the length of the cell[158]. These have been historically considered unique morphological features of apoptosis.

Features of Apoptosis: Transcription and Translational Repression

Many transcription factors, including NF-κB p65, are cleaved and inactivated by caspase-3 during apoptosis. Ribosomal proteins such as p70S6K are also cleaved and inactivated. Although the reasons for shutting down transcription and translation in apoptosis are unclear, it may serve to prevent viral hijacking of cellular machinery.

1.4.2.2 Secondary Necrosis

The term "secondary necrosis" has been widely applied to refer to end-stage apoptosis in which apoptotic cells that have not been phagocytosed lose plasma membrane integrity and release proinflammatory cellular contents. However, recent research has suggested that the "secondary necrosis" nomenclature is less apt than originally thought, due to the involvement of the pore-forming executioner protein GSDME (DFNA5) in the loss of membrane integrity[160]. This suggests that – according to the NCCD definition – secondary necrosis may constitute a form of pyroptosis instead.

1.4.2.3 Pyroptosis

The NCCD operationally defines pyroptosis as "a type of cell death that critically depends on the formation of plasma membrane pores by members of the gasdermin protein family, often (but not always) as a consequence of inflammatory caspase activation". Juxtaposing this definition against that proposed in 2012 of pyroptosis as "a caspase-1-dependent cell death subroutine that is associated with the generation of pyrogenic mediators such as IL-1β and IL-18"[161] highlights the rapid conceptual advancement of this field in recent years. The updated definition highlights several salient points: (i) gasdermin family members serve as the executioners of pyroptosis (ii) caspase-1 and caspase-4/5/11 are the principal activators of pyroptosis, but other caspases can be involved, and (iii) IL-1β and IL-18 release is often associated with pyroptosis but is neither necessary nor sufficient for pyroptosis to occur. Pyroptosis ("fiery death") is highly proinflammatory and culminates in a membrane rupture event.

1.4.3 Pyroptosis: GSDMD-Dependent Cell Lysis

Unlike apoptosis, which is required in non-inflammatory cell death situations such as CNS development and cell turnover at homeostasis, pyroptosis is lytic, profoundly inflammatory, and has been implicated in bacterial, viral, and fungal infection control[162]. Although dysregulated pyroptosis has been implicated in a variety of inflammatory diseases, including autoimmunity and sepsis, other physiological roles for pyroptosis may remain to be discovered.

1.4.3.1 Discovery of GSDMD

GSDMD was identified downstream of LPS-induced inflammasome engagement independently by two groups using high-throughput screens. One group performed a CRISPR/Cas9 genome-wide screen, while the other group performed a N-ethyl-N-nitrosourea mutagenesis screen, to identify genes that rescued pyroptosis in mouse macrophages[81,82]. In these ground-breaking studies, GSDMD was identified and validated as the crucial executioner of pyroptosis in both human and mouse cells, in response to both canonical and non-canonical inflammasome activation[81,82]. The pore-forming capacity of the active N-terminal of GSDMD was subsequently confirmed in several elegant studies, while an autoinhibitory role for the GSDMD C-terminal was also proposed[163-167]. Other members of the gasdermin family have recently been characterized, the majority of which share a two-domain structure, a high degree of homology in their N-terminal domains, and pore-forming capacity, suggesting functional similarities to GSDMD[168]. A caspase-3-gasdermin E (GSDME) axis has recently been identified, with particular relevance to cancer cells[169-172]. Nonetheless, GSDMD has been most well-characterized and will be the focus of the remainder of this section.

1.4.3.2 Auto-inhibitory Structure of GSDMD

Human GSDMD contains a 242 AA N-terminal domain with pore-forming activity, a 199 AA C-terminal domain with repressor activity, and a 43 AA linker domain, which contains a caspase-1/4 cleavage site after AA275[168]. GSDMD's two-domain structure underlies an autoinhibitory mechanism whereby the C-terminal domain constitutively interacts with and represses the N-terminal domain, preventing it from acquiring pore-forming activity [Figure 1.6]; mutation of the residues responsible for inter-domain

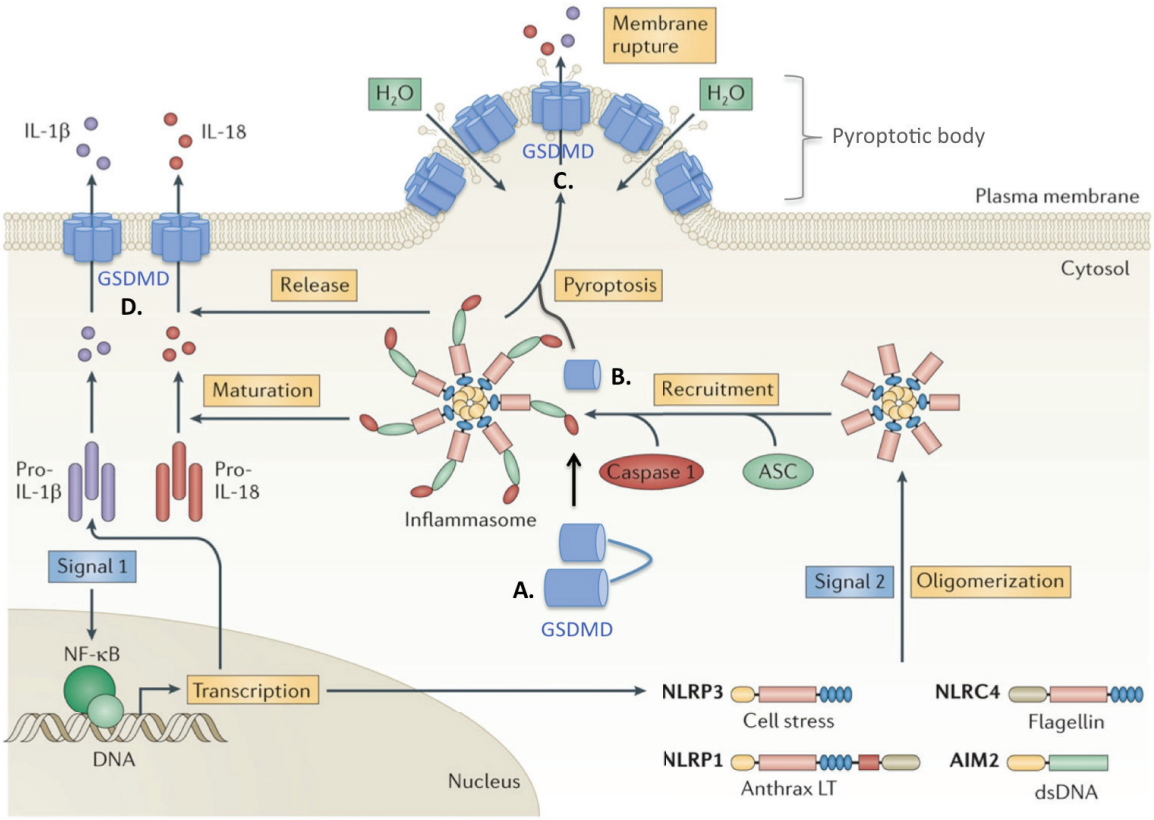

Figure 1.6: ***Mechanism of GSDMD activation in pyroptosis***

(A) GSDMD exists in an auto-inhibitory conformation at homeostasis, in which the inhibitory C-terminal domain retains the pore-forming N-terminal domain in an inactive state. (B) Upon processing by the inflammasome, the GSDMD N-terminal is released and translocates to the cell membrane, where it oligomerizes to form pores. (C) Pore formation disrupts local osmotic gradients, causing localized swelling and the formation of membrane protrusions called pyroptotic bodies, which rupture to release cellular contents. (D) Prior to membrane rupture, small molecules including IL-1β and IL-18 are released through GSDMD pores in the membrane. GSDMD pores are now believed to be a major mechanism by which these cytokines are unconventionally secreted, either prior to or in the absence of pyroptosis.

Adapted from: Walsh J, Muruve D, and Power C. (2014). Inflammasomes in the CNS. *Nature Reviews Neuroscience*. 15(2), 84-97. Springer Nature License Copy Number: 4535661035848

binding release the inhibitory effect on the N-terminal and enhance pyroptosis[173]. Once activated by caspase-1/4, the autoinhibitory action of the GSDMD C-terminus is relieved, releasing a highly active p30 N-terminal fragment. Over-expression of the N-GSDMD fragment is sufficient to activate pyroptosis[81,82]. N-GSDMD displays the highest affinity for cardiolipin and phosphatidylinositol phosphate PIP_1 and PIP_2, with a lower affinity for PIP_3 and phosphatidylserine (PS)[168]. PIP_1 and PIP_2 are restricted primarily to the inner leaflet of the plasma membrane, where lipid binding triggers the oligomerization of N-GSDMD, forming pores in the plasma membrane[163,164]. The pores disrupt local osmotic potential, leading to swelling, membrane rupture, and lysis, rapidly dissipating cellular contents into the extracellular environment [Figure 1.6, 1.7]. The affinity of N-GSDMD for lipids enriched on the inner membrane and not the outer membrane means that neighbouring cells are protected from its cytotoxic effects[164,174]. This also suggests that N-GSDMD may target membranes that have a lipid composition similar to the inner leaflet of the plasma membrane, including vacuoles and the ER[168]. Cardiolipin, the other major target of N-GSDMD, is found on the inner mitochondrial membrane, suggesting the intriguing possibility that pore formation might occur in the mitochondria[168]. Cardiolipin is also found on bacteria, and extra-cellular N-GSDMD has bactericidal properties *in vitro*[164].

1.4.3.3 Properties of GSDMD Pores

Using atomic force and electron microscopy, several groups have visualized the formation of oligomeric N-GSDMD pores within minutes of GSDMD cleavage[163-166]. The composition of the N-GSDMD pore has varied, with 16-24 monomers assembled into a pore, and an inner pore diameter ranging from 10-20nm[163-166]. GSDMD pores are

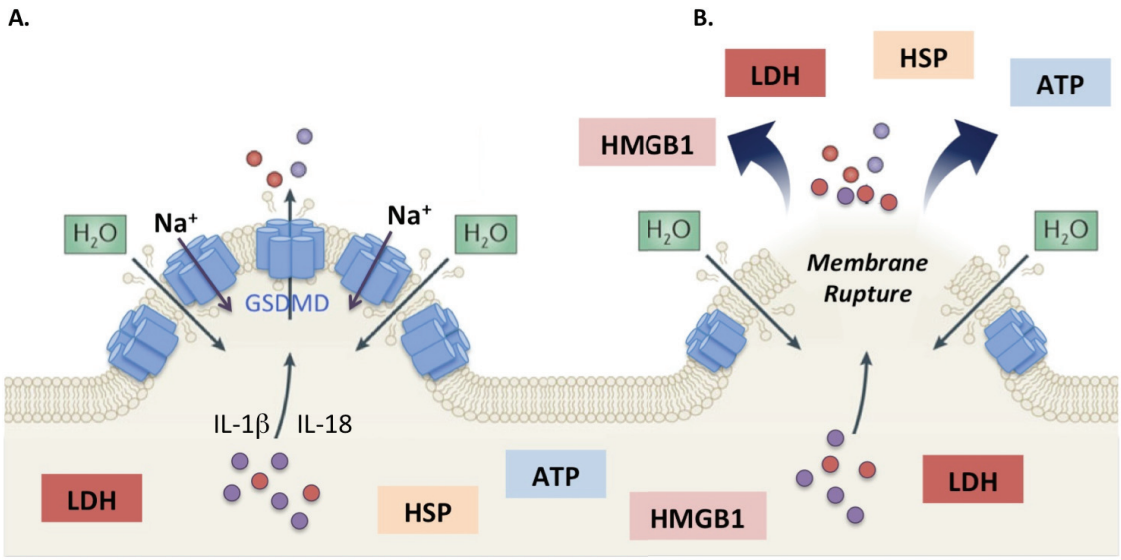

Figure 1.7: ***Properties of GSDMD pores and pyroptotic bodies***

(A) Pyroptotic bodies are localized regions of cell membrane swelling that result from osmotic disruptions induced by GSDMD pore formation. Upon pore formation, Na^+ (which is highly concentrated in the extracellular environment) is drawn into the cell in the direction of its electrochemical gradient, which in turn draws water into the cell and causes localized swelling. At this stage, cytokines (IL-1β, IL-18) may be released through GSDMD pores but large molecules such as lactate dehydrogenase (LDH) are retained inside the cell. (B) If the osmotic pressure exceeds the compensatory mechanisms of the cell, the plasma membrane ruptures catastrophically and irreversibly. This releases cytokines (IL-1β, IL18), large cytoplasmic proteins (LDH), and a variety of intracellular DAMPs (e.g. ATP, HSPs, HMGB1) into the extracellular environment, perpetuating the cycle of inflammation.

permeable to ions and small molecules (10nm or smaller), including water, cytokines, propidium iodide (PI), and GFP, but not large molecules like lactate dehydrogenase (LDH); thus, release of intracellular LDH into the supernatant is often used as a marker for membrane rupture during pyroptosis [Figure 1.7][168]. Extracellular glycine can prevent plasma membrane rupture, an informative strategy to assess if a given molecule requires membrane rupture (e.g. LDH) or passes freely through GSDMD pores (e.g. PI)[168]. Pharmacological approaches in which the pore-forming capacity of GSDMD is blocked are under development as novel therapies to prevent pyroptosis[175,176].

1.4.3.4 Membrane Features During Pyroptosis

While GSDMD is diffusely expressed in macrophages exposed to a priming stimulus (e.g. LPS) alone, addition of nigericin has been shown to cause a distinctive enrichment of GSDMD immunoreactivity at the plasma membrane early in pyroptosis[167]. The formation of small membrane protrusions of the same size as apoptotic bodies (1-5 μm in diameter), dubbed "pyroptotic bodies", has also been observed using scanning electron microscopy[167]. In the later stages of pyroptosis, the cell membrane ruptures, leaving a relatively intact nucleus and diffuse GSDMD-immunopositive cellular debris[167]. Live cell imaging has recapitulated these findings, demonstrating that diffuse cytoplasmic GSDMD immunoreactivity gives way to localized aggregates at the plasma membrane within 15 minutes of nigericin exposure, and this plasma membrane localization corresponds to the appearance of bleb-like membrane protrusions (i.e. pyroptotic bodies)[177]. Likewise, *S. typhimurium* and other NLRC4 inflammasome activators trigger pyroptotic body formation, and these can be seen bursting to release cellular contents using time lapse confocal microscopy[178]. It has been proposed that

pyroptotic bodies form when the local osmotic changes caused by membrane permeability exceed the cell's compensatory mechanisms, causing the plasma membrane to separate from the cortical cytoskeleton to form fluid-filled balloons [Figure 1.7][168]. The putatively passive nature of this mechanism remains to be verified. Regardless of the mechanism of pyroptotic body formation, the rupture of these structures is catastrophic and irreversible. Interestingly, however, the corpses of pyroptotic cells can still have a purpose following cell death; it was recently shown that pyroptotic corpses can trap intracellular bacteria due to the presence of "pore-induced traps" that prevent release of bacteria into the extracellular milieu[178].

1.4.3.5 Cytokine Release and Pyroptosis

Although inflammasome-associated cytokines (i.e. IL-1β, IL-18) and executioner proteins (i.e. GSDMD) are activated on the same molecular platform, it was initially unclear whether cytokine release required GSDMD[168]. To this end, two salient questions have been extensively investigated: (i) does cytokine release require the GSDMD-mediated terminal membrane rupture event in pyroptosis, and (ii) if not, what is the mechanism of cytokine release and does it require GSDMD pore formation? To address this, several studies recently demonstrated IL-1β secretion from living cells, highlighting that membrane rupture is not a requirement for cytokine release[41,179,180]. Detailed characterization of the GSDMD pore (10-15nm diameter) offered a logical conduit by which IL-1β (4.5nm diameter) and IL-18 (5.0nm diameter) might escape the cell[168] and indeed GSDMD deficiency has been known to ameliorate IL-1β secretion[181]. Several elegant studies have subsequently verified IL-1β secretion through plasma

membrane GSDMD pores in mouse and human systems[180,182,183]. Not surprisingly, both GSDMD-independent and dependent secretion mechanisms can be observed in the same system, with GSDMD often being required for optimal magnitude and efficiency of cytokine release[179,182]. Mechanisms of Il-1β release independent of GSDMD pores include slow vesicular release of IL-1β[179] and a novel mechanism of IL-1β release involving PIP_2-dependent translocation of active IL-1β to membrane ruffles[182].

1.4.3.6 Non-lethal Cytokine Release Versus Cell Death

It is currently believed that pyroptosis occurs when GSDMD pores disrupt the ion gradient across the cell membrane, leading localized swelling, formation of pyroptotic bodies, and subsequent membrane rupture[168]. However, since GSDMD pores are also an important part of cytokine secretion from living cells, what mechanisms prevent pyroptosis following formation of GSDMD pores in the membrane during cytokine secretion? Several non-exclusive options may be considered:

Option I: *GSDMD pores for cytokine secretion are transient.*

This option would suggest that GSDMD pores are removed from the membrane prior to pyroptotic body formation, and is consistent with the recent discovery of an endosomal sorting complex required for transport (ESCRT)-dependent membrane repair process downstream of GSDMD activation[184]. In this study, ESCRT machinery removed GSDMD pores through shedding of $GSDMD^+$ ectosomes.

Option II: *GSDMD⁺ pyroptotic body formation requires densely clustered GSDMD pores.* This option would suggest a threshold effect, whereby GSDMD pores may exist in lower numbers or be more sparsely distributed under conditions of non-lethal cytokine secretion, but may cluster to cause pyroptotic body formation and membrane rupture during pyroptosis. This would imply either a negative feedback regulatory mechanism at the synthesis/activation step of GSDMD to prevent pyroptosis, or a selective mechanism for clustering GSDMD pores in the membrane to activate pyroptosis.

Option III: *Additional cell death pathways facilitate GSDMD-dependent pyroptosis.* Given that caspase-1 can activate over a hundred different substrates in addition to GSDMD, including executioner proteins such as caspases-3/7[75], it reasonable to question whether GSDMD is the only substrate involved in pyroptosis. The presence or absence of additional inflammasome-activated cell death signaling pathways could thus provide a checkpoint between cytokine release and pyroptosis.

1.4.3.7 Alternative Processing of GSDMD

The past year has resulted in several interesting and hypothesis-generating studies concerning the cleavage of GSDMD at different sites with diverging biological effects. Caspase-8, which is traditionally considered an initiator caspase for apoptosis, was shown to cleave and activate GSDMD, triggering a re-evaluation of the definition of pyroptosis as dependent upon the proinflammatory caspases[185]. Furthermore, caspase-3 was shown to cleave and inactivate GSDMD, generating a non-bioactive p43 N-terminal fragment in response to certain apoptotic stimuli[79]. Certain viruses encode

proteases that recapitulate this GSDMD-inactivating cleavage event, thus rendering the cell resistant to pyroptosis in response to viral infection[186]. These studies suggest a physiologically important role for the selective inactivation of GSDMD under conditions where proinflammatory cell death is not favourable.

1.4.3.8 GSDMD-Inflammasome Feedback Loops

Recent research has also highlighted examples of GSDMD activation upstream of inflammasome engagement. For instance, GSDMD-deficient BMDMs showed compromised caspase-1 activation compared to WT cells in response to AIM2 activators, such as poly(dA:dT), CMV infection, and *Francisella novicida* infection[187]. Other groups have suggested a role for activated GSDMD in the generation of mitochondrial ROS upstream of the NLRP3 inflammasome, based on an enrichment of GSDMD at the mitochondria in a non-canonical Shiga toxin/LPS system[188]. Such studies suggest a mechanism linking non-canonical inflammasome-mediated GSDMD activation to canonical inflammasome activation through the generation of intracellular DAMPs.

1.4.3.9 Subcellular Features of Pyroptosis

The hypothesis that pyroptosis is more nuanced than simply GSDMD-mediated membrane rupture – and that both GSDMD-dependent and –independent subcellular events may contribute to pyroptosis prior to a terminal lytic event - is just emerging. Additional intracellular functions of GSDMD have been proposed due to its enrichment in organelles such as the mitochondria during pyroptosis[188]. Likewise, given that caspase-1 can activate over a hundred different substrates in addition to GSDMD[75], such substrates might also serve as mediators of the subcellular changes associated with

pyroptosis. Based upon detailed kinetic assessments of cell viability, organelle function, and cell membrane permeability, several groups have illustrated profound intracellular disruption prior to membrane lysis[189,190]. For instance, one group demonstrated caspase-1-dependent mitochondrial depolarization and cytochrome C release downstream of NLRP3 and AIM2 inflammasomes[191], though not all groups recapitulate these results[192]. Using live-cell confocal microscopy, the mitochondrial network has been shown to fragment during pyroptosis downstream of NLRP1 and NLRC4 inflammasome-activating stimuli[189]. Likewise, mitochondrial depolarization, like that seen during intrinsic apoptosis, was shown to occur consistently ~20 minutes prior to membrane rupture in response to both canonical and non-canonical stimuli[189]. Subsequent experiments with GSDMD-deficient macrophages transfected with LPS suggested a requirement for GSDMD in mitochondrial depolarization[189]. The authors also utilized live-cell confocal microscopy to confirm previous reports of nuclear rounding and condensation in late-stage pyroptosis, concomitant with membrane rupture[189]. Chromatin condensation and DNA damage/fragmentation have been previously observed in pyroptosis[36,193] but thus far these features are not attributable to GSDMD and not functionally required for pyroptosis[193]. They are, however, consistent with alternative signaling pathways being activated concurrently with GSDMD within pyroptotic cells. Collectively, these intracellular changes illustrate a level of nuance to pyroptosis beyond simply GSDMD-mediated plasma membrane lysis. This idea is supported by additional studies demonstrating that cell death and plasma membrane lysis are in fact separable events[190]. In one study, the authors demonstrated that mitochondrial depolarization and loss of cell motility are concomitant with plasma

membrane permeability (indicative of GSDMD pore formation) but prior to membrane lysis (indicated by LDH release), and dependent upon GSDMD[190]. Collectively, these results point to both GSDMD-dependent and GSDMD-independent intracellular changes during pyroptosis.

1.4.4 Crosstalk between Pyroptosis and Apoptosis

It is becoming increasingly apparent that crosstalk exists between pyroptotic and apoptotic signaling pathways. As mentioned above, apoptotic stimuli can trigger caspase-3-mediated inactivation of GSDMD through the generation of a truncated N-terminal with no pore-forming ability[79]. Conversely, pyroptotic stimuli can induce caspase-1-dependent apoptosis in the absence of GSDMD[79,190] or non-caspase-1-dependent apoptosis in the absence of caspase-1[194]. Most significantly to this thesis, caspase-1 has been shown to function upstream of executioner caspase activation and can mediate cleavage of caspase-3 and -7 either directly through proteolysis or indirectly through activation of upstream activator caspases[75,78-80]. In some systems, but not all[78], caspase-1-mediated cleavage of the executioner caspases is only unmasked in GSDMD-deficient conditions[181]. PARP, the prototypic marker of caspase-3/7 activation in apoptosis, is also cleaved during pyroptosis downstream of executioner caspases[79,195], although GSDMD deficiency increases PARP cleavage and presumably promotes an apoptotic cell death program[79]. Some groups have attributed PARP cleavage in pyroptosis to a subset of apoptotic cells[79], but this conclusion is often drawn in the absence of supporting data at the single-cell level. Other groups have demonstrated PARP cleavage following non-lethal LPS treatment downstream of caspase-7 and inflammasome activation, in which system cleaved PARP enhances

transcription of a subset of NF-κB-dependent genes[196]. PARP1-deficient macrophages may be partially protected from pyroptosis, though the mechanism is unknown[195]. In response to NLRP1-, NLRP3-, and AIM2-activating stimuli, capsase-1 can also cleave and activate Bid, a pro-apoptotic protein whose primary function is to initiate mitochondrial outer membrane permeabilization (MOMP) and cytochrome C release that ultimately triggers activation of caspase-3/7[189,191].

Interestingly, common mechanisms are involved in negatively regulating both apoptosis and pyroptosis. For instance, the anti-apoptotic protein Bcl-2 has been shown to inhibit both the NLRP1 and NLRP3 inflammasomes, and to inhibit caspase-1-dependent cell death pathways[75]. Bcl-XL, another anti-apoptotic protein, has been shown to interact with NLRP1 and the inhibitors of apoptosis (IAPs) have been shown to regulate caspase-1 activity; some, including XIAP, are substrates of caspase-1[92].

Importantly, many markers for apoptosis are shared with pyroptosis, including Annexin-V staining[189,193], TUNEL staining[193], and PARP cleavage[79]. Widely used double-staining paradigms identify early apoptotic cells by virtue of being Annexin-V^+ and PI^-. However, this population is also found in pyroptotic cells following either NLRP1 or NLRC4 inflammasome activation, and thus the utility of this and other markers of apoptosis must be carefully examined[189].

1.4.5 Areas of Ongoing Study

With the discovery of GSDMD only four years ago, many outstanding questions remain, and several important areas of investigation are highlighted here:

(I) The ability to modulate pyroptosis through alternative cleavage of GSDMD has just been appreciated, and is likely to have widespread implications in the fields of infectious disease (wherein pathogens can modulate cell death pathways) and cancer biology (wherein dysregulation of cell death pathways is a hallmark of transformation).

(II) Shared morphological and molecular features between apoptosis and pyroptosis (e.g. membrane blebs, DNA fragmentation, PARP cleavage) speak to a more complex program of cellular changes in pyroptosis than explained by GSDMD alone, and should be further examined. Standardized biomarkers also need to be established to distinguish between the two cell death modalities, as non-specific markers (e.g. TUNEL, Annexin-V, PARP cleavage) are still widely used to indicate apoptosis.

(III) The molecular mechanisms governing cell fate (i.e. non-lethal cytokine secretion versus pyroptosis) are largely unknown. Likewise, the subcellular events prior to membrane rupture, both GSDMD-dependent and GSDMD-independent, are poorly characterized; although executioner caspases-3/7 have been shown to be activated downstream of inflammasome activation, their function remains elusive.

(IV) It is not yet known whether the mechanisms of pyroptosis observed to date are conserved between stimuli, between species, between cell types, and between cancer versus primary cell models. Given that cancer cells have profoundly dysregulated cell death pathways, and that interspecies differences have been well-documented in the

inflammasome literature, investigation of pyroptosis in primary, non-transformed human cell lines should be a priority to ensure the relevance of current findings.

I.V. Pyroptosis in the Central Nervous System

Prior to this thesis, no studies had examined GSDMD-dependent pyroptosis in the CNS *in vivo* or in CNS cells *in vitro,* and our understanding of the mechanisms driving GSDMD-mediated pyroptosis were inferred entirely from studies of peripheral myeloid populations. Nonetheless, inflammasome-mediated cell death has been studied in multiple CNS disease models. In the absence of a unique pyroptosis marker, many of the original studies used a two-step strategy to infer pyroptosis in the CNS: (i) cell-specific expression of inflammasome components was demonstrated in the CNS using animal models or clinical samples, and (ii) exposure of the relevant cells types to disease-relevant stimuli *ex vivo* to showed that cell death (and usually cytokine release) occured in response to disease-associated stimuli. Studies that relied upon knock-out of inflammasome components to infer pyroptosis were and continue to be confounded by the fact that inflammasome activation can also drive neurodegeneration through non-pyroptotic mechanisms. With the discovery of GSDMD, the gold standard for demonstrating pyroptosis in neurological disease is now to demonstrate the up-regulation and (if possible) cleavage of GSDMD in a cell-type-specific manner in the diseased CNS *in vivo*, and recapitulate GSDMD-mediated cell death in the relevant cell types in response to disease-relevant stimuli *ex vivo*.

1.5.1 Pyroptosis in Microglia

Pyroptosis of human and mouse microglia in response to infectious stimuli, *including L. pneumophila, S. aureus, M. tuberculosis*, and cytomegalovirus, has been reported by multiple groups[92,122]. However, the ability of microglia to undergo pyroptosis during sterile inflammation is largely unknown. In one model of ballistic penetrating traumatic brain injury (PTBI), the authors detected GSDMD in the brain lysates from PTBI animals[197]. Using ASC as a surrogate for pyroptosis, the authors demonstrated that while neurons were immunopositive for ASC for a 24hr window, ASC-positive microglia were detected up to 12 weeks post-injury, leading to the conclusion that microglia were the most likely cell types to undergo inflammasome activation and pyroptosis[197]. However, co-expression of GSDMD with microglial markers was not performed and neuronal pyroptosis was not ruled out. A more recent study by the same authors demonstrated that both infiltrating leukocytes and resident microglia showed increased caspase-1 activation following injury, and that $CD11b^+$ cells (which includes both populations) undergo pyroptosis (defined by LIVE/DEAD staining and caspase-1 FAM-FLICA signal); pyroptosis in this $CD11b^+$ population was reduced with administration of an anti-ASC blocking antibody[198]. Other recent studies have demonstrated microglial inflammasome activation and pyroptosis *in vitro* in response to ischemic conditions and in the brain following ischemic stroke[199]. Interestingly, the authors observed caspase-3 activation in addition to the activation and cleavage of pyroptosis-associated proteins (caspase-1, Il-1β, etc.) and interpreted this to mean that a subset of cells was undergoing apoptosis instead. However, in the absence of single-cell analysis (e.g. by

confocal microscopy or flow cytometry), it is difficult to know whether these indeed represent two separate populations of cells, or whether individual cells express markers for both apoptosis and pyroptosis. In another study examining cerebral venous thrombosis, the authors demonstrated that activated $CD68^+$ microglia were immunopositive for inflammasome components (NLRP3, IL-1β) and stained positive for TUNEL[200]. Nonetheless, the presence of GSDMD was not demonstrated in either study.

Interestingly, microglial pyroptosis may have been identified prior to the discovery of inflammasomes. Researchers observed the phenomenon of "activation- induced cell death" (AICD) downstream of high-dose LPS, and identified this microglial cytotoxicity as a unique type of apoptosis, based upon the expression of double-stranded DNA breaks, cell surface PS expression, and caspase-3 activation[201]. However, as described above and will be explored in this thesis, such biomarkers are shared with pyroptosis, and thus such studies may represent the earliest accounts of microglial pyroptosis. The observation of microglial AICD has been confirmed both *in vitro* and *in vivo*, in response to multiple exposure paradigms including LPS + IFNγ[202] and IFNγ alone[203], highlighting a mechanistic role for iNOS[204,205] and a caspase-11/caspase-1/caspase-3 signaling axis in this phenomenon[205]. Other groups identified a population of PI^+ cleaved-$caspase\text{-}3^+$ microglia *in vitro* following IFNγ exposure and concluded based upon the high PI signal (and subsequent TUNEL staining) that these were mitotic cells undergoing an apoptotic AICD program[206]; the authors also identified a population of highly $TUNEL^+$ microglia in the spinal cord during EAE and postulated this as an example of AICD in neuroinflammation. Although these may represent early indications of microglial

pyroptosis, the current defining feature of pyroptosis is involvement of GSDMD (or related gasdermin family members) and prior to this thesis, no group had examined this requirement in microglial cell death.

1.5.2 Pyroptosis in Neurons

Substantial interest has emerged in neuronal pyroptosis as a pathogenic mechanism of neurodegeneration in various diseases. In humans with medial temporal lobe epilepsy and in the amygdala kindling-induced seizure rat model of epilepsy, profound neuronal loss is observed, which is associated with caspase-1 and NLRP1 immunoreactivity in neurons[207]. Neuronal loss is partially rescued when NRLP1 or caspase-1 are inhibited via *in vivo* siRNA infusion[207]. Interestingly, the AIM2 inflammasome has also been implicated in neuronal pyroptosis during TBI, during which widespread necrotic cell death releases copious amounts of cell-free DNA in the CSF, which may serve as a ligand for AIM2[151]. Neuronal pyroptosis is also of particular interest in AD. Amyloid-β can induce NLRP1-dependent, caspase-1-dependent pyroptosis in neurons *in vitro*, and inhibition of either NLRP1 or caspase-1 in AD transgenic models reduces neuronal cell death[138]. Many of these observations await further validation regarding the role of GSDMD in these animal models.

1.5.3 Pyroptosis in CNS Endothelial Cells

Recent work has demonstrated that brain microvascular endothelial cells can undergo inflammasome activation and pyroptosis following TBI, suggesting a novel mechanism by which the BBB is disrupted following injury[208]. NLRP1, NLRC4, NLRP3, and AIM2 were all found to be up-regulated in CNS endothelial cells following injury.

1.5.4 Pyroptosis in Astrocytes

A limited number of studies have identified pyroptosis in astrocytes compared to other cell types. Rat astrocytes can undergo pyroptosis *in vitro*, which is inhibited by the caspase-1 inhibitor VX-765[209]. Furthermore, a proportion of mouse astrocytes in culture undergo pyroptosis *in vitro* in response to ATP, LPS, or ethanol exposure, as measured by LDH release in association with IL-1β/IL-18 release[210].

1.5.5 Pyroptosis in ODCs

Pyroptosis has not been documented in ODC-lineage cells. However, early reports prior to the discovery of inflammasomes or pyroptosis have implicated inflammatory caspases in what was often deemed to be a unique form of apoptosis[125,211].

1.5.6 Outstanding Questions

As the field advances, it will be critical to isolate the role of proinflammatory cytokines from the role of pyroptosis in neuroinflammation and neurodegeneration. Given the overlapping role of GSDMD in cytokine release and cell death, this will be a formidable barrier to overcome. While inflammasome-associated cytokines certainly play a role in neurotoxicity, pyroptosis as a direct mechanism of neurodegeneration merits thorough examination. Targeting pyroptosis may represent a viable neuroprotective strategy in diseases with a profound neuroinflammation and neurodegeneration, such as MS.

I.VI. Pathogenesis of Multiple Sclerosis

1.6.1 Clinical Overview

Multiple sclerosis is a chronic inflammatory neurodegenerative disease of the CNS that affects approximately 2.5 million people worldwide[12]. The disease has a higher prevalence in women and tends to present in young adults[212]. Clinical features include a spectrum of neurological signs from sensorimotor disturbances to fatigue and neurocognitive deficits. The etiology of MS is unknown, but is thought to involve infiltration of autoreactive lymphocytes into the CNS, which drives local inflammation, demyelination, and a progressive neurodegenerative pathology[213].

1.6.1.1 Diagnosis, Disease Course, and Progression

Diagnosis of MS is based upon several features, including the distinctive clinical course (often relapsing/remitting), the presence of IgG oligoclonal bands in the CSF (often targeting ubiquitous intracellular antigens), and radiological evidence of lesions based on T2-weighted MRI. Prior to a diagnosis of MS, some patients present with clinically isolated syndrome (CIS), in which a single clinical event is combined with radiological evidence for lesion formation. The majority of patients (~85%) present with an initial disease course that is relapsing-remitting (RRMS), with intermittent relapses interspersed with periods of remission[214]. However, in the majority of patients (~70%), the disease transitions into a secondary progressive stage (SPMS; median time to conversion of 19 years). A subset of patients (15%) present with primary progressive MS (PPMS), which is characterized by an unrelenting clinical progression rather than relapse-remission[214].

1.6.2 Disease-Modifying Therapies

Virtually all disease modifying therapies (DMTs) available are immunomodulatory or immunosuppressive in nature. Currently approved immunotherapies tend to be effective in RRMS but only one (ocrelizumab) is approved for use in PPMS. The first DMT was IFNβ, FDA-approved in 1993 for treatment of RRMS. Its mechanism is pleiotropic, with effects ranging from production of anti-inflammatory cytokines (IL-10, IL-4), to suppression of proinflammatory cytokines (IFNγ, TNFα). Fingolimod, the first oral DMT, binds S1P receptors on lymphocytes, which sequesters them in the lymphatic tissue and prevents migration into the CNS[215]. Natalizumab is a potent humanized monoclonal antibody targeting the adhesion molecule, VLA-4 (α4β1-integrin), which prevents lymphocyte migration across the BBB[214,215]. Although highly effective, natalizumab is a third-line therapy due to the risk of progressive multifocal leukoencephalopathy (PML) as a result of viral infection of the CNS[214,215]. Alemtuzumab is a humanized antibody targeting CD52, concurrently ablating multiple lymphocyte cell populations and leading to long-lasting immune suppression[214,215]. Although highly effective, alemtuzumab has a sobering side effect profile, with adverse effects ranging from viral infections to secondary autoimmune disorders. Ocrelizumab, rituximab, and ofatumumab deplete B cells, through recognition of the B-lymphocyte marker CD20, and have also proven effective[214,215]. However, although ocrelizumab is approved for PPMS, such therapies only slow disease progression, and none are considered curative.

1.6.3 Neuropathological Features of MS

1.6.3.1 Overall Pathology and Progression

MS is characterized by extensive demyelination, loss of axons, infiltration of macrophages and CNS-reactive T cells, as well as local innate immune activation [Figure 1.8][213]. The early (relapsing/remitting) stage of the disease is characterized by localized demyelinating plaques, predominantly but not exclusively in the white matter (composed primarily of myelinated axon tracts), with clinical relapses appearing to correspond with waves of infiltrating autoreactive T lymphocytes. By contrast, the progressive stage of the disease is neurodegenerative in nature, including white matter injury, cortical demyelination, and tissue atrophy in both the white and grey matter (consisting primarily of neuronal cell bodies) in both the brain and spinal cord[212].

White matter lesions predominate in heavily myelinated areas, such as the optic nerve, periventricular and subcortical white matter, and the spinal cord, while cortical lesions are associated with profound inflammation in the meninges, suggesting that meningeal immune infiltration may initiate cortical lesions[213,214]. Immunosuppressive drugs lose their efficacy when patients enter the progressive stage of MS, highlighting the different disease mechanisms driving pathology at different stages[213]. The hypothesis that innate immune activation is particularly important in SPMS and PPMS has gained substantial traction in recent years[215,216]. In particular, it has been suggested that inflammation is compartmentalized in the CNS as the disease progresses, becoming uncoupled from the systemic immune response[215]. Neurodegeneration thus results from unrelenting

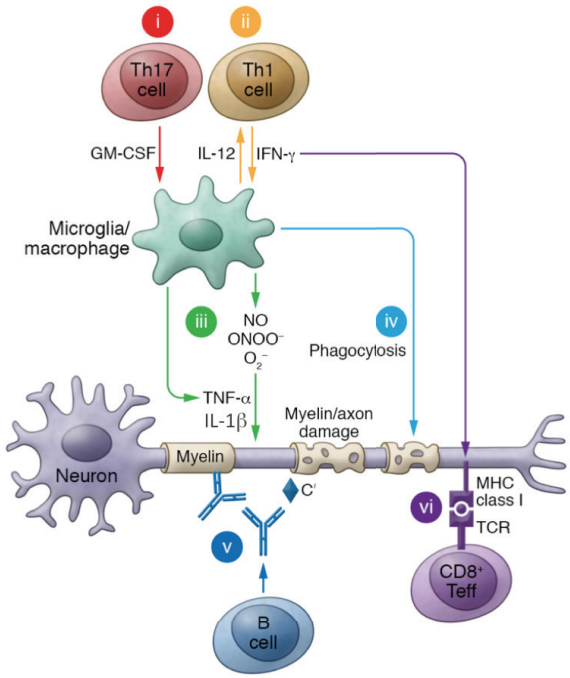

Figure 1.8: ***Mechanisms of immune-mediated attack on axons and myelin***

During MS and EAE, axonal damage and demyelination are mediated by a multi-pronged inflammatory response within the CNS, including (i) $CD4^+$ Th17 cells, which produce GM-CSF to activate macrophages and microglia; (ii) $CD4^+$ Th1 cells which produce IFNγ; (iii-iv) microglia/ macrophages that produce a variety of potentially neurotoxic proinflammatory mediators, including IL-1β, TNFα, and reactive oxygen/nitrogen species (ROS/RNS), and phagocytose myelin debris. (v) B cells produce antibodies that bind to myelin sheaths and may promote complement-mediated damage, while $CD8^+$ T cells (vi) can potentially produce a cytotoxic T cell response following IFNγ-induced up-regulation of MHC Class I by CNS-resident cells.

Adapted from: Chitnis, T and Weiner HL. (2017). CNS inflammation and neurodegeneration. *Journal of Clinical Investigation*. 127 (10), 3577-87. Copyright license number: 4536661229698

smoldering inflammation within an already vulnerable CNS.

1.6.3.2 Updated Classification of MS Lesions: Microglia/macrophages

The prominence of microglia/macrophages in the pathophysiology of MS has been highlighted by the recent update of lesion classification, in which microglial content and distribution is a defining feature in staging lesions[217]. Active lesions display massive microglia/macrophages infiltration throughout the lesion, while inactive lesions lack cellular infiltrates and are fully demyelinated. Mixed active/inactive lesions typically have a ring of microglia/macrophages along the border of the lesion with a hypocellular center. Both active and mixed active/inactive can be subdivided into either demyelinating or post-demyelinating based upon whether or not myelin destruction has ceased, with the presence of myelin components within phagocytotic microglia/macrophages being considered indicative of ongoing myelin destruction[217]. The white matter surrounding the lesion is known as "normal-appearing white matter" (NAWM), although this tissue is not truly normal and contains cellular infiltrates that are not found in healthy tissue[212].

1.6.4 Cellular Features of Active MS Lesions

1.6.4.1 Demyelination

Demyelination is the defining feature of MS lesions, which is believed to be caused by the destruction of myelin-producing ODCs [Figure 1.8]. Remyelination can occur but is sporadic and incomplete, even in the presence of $NG2^+$ ODC precursor cells[215]. The specific factors inhibiting remyelination are an area of current investigation.

1.6.4.2 Axonal Loss

Axonal loss is observed in demyelinating lesions, affecting 30-80% of axons within a lesion[215]. Using confocal microscopy, it has been demonstrated that there are over 11,000 transected axons/mm^2 in active lesions, compared to less than 1 transected axon/mm^2 in control WM[218,219]. Axonal loss correlates with permanent neurological deficits in the later stages of MS, apparent as 'black holes' on brain MRI [213,220].

1.6.4.3 T and B Cell Infiltration

In the initial stages of lesion formation, infiltration of proinflammatory microglia is accompanied by a wave of CD8$^+$ T cells, supporting the hypothesis that initial demyelinating events may be autoimmune in nature[213]. Several studies have demonstrated that CD8$^+$ T cells predominate over CD4$^+$ T cells in both cortical and white matter lesions, as well as in NAWM[221]. CD4$^+$ T cells accumulate more profoundly in the perivascular spaces and in the meninges, where B cells can also be found[213]. Single-cell analyses and high-throughput sequencing have both been performed to characterize the T cell receptor (TCR) repertoire expressed by lesion-infiltrating and CSF T cell populations; such studies have demonstrated that both populations are oligoclonal, a phenomenon that indicates shared antigen specificity within the population[221-223]. Attempts to identify a triggering antigen have been largely unsuccessful[224]. Nonetheless, CD8$^+$ T cells have been proposed to play a role in axonal transection and have been shown to correlate with axonal injury[224]. CD8$^+$ T cells produce a number of potentially harmful molecules, including granzyme B, perforin, IFNγ, IL-17, and even glutamate, providing an additional mechanism for their cytotoxicity[90,224]. T_H1 and T_H17 CD4$^+$ T cells have known pathogenic mechanisms in MS, releasing cytokines such as TNFα, IFNγ

and IL-17 into the proinflammatory milieu, increasing extravasion across the BBB, and recruiting monocytes into the CNS[90].

B cells, plasmablasts, and plasma cells accumulate in lesions, meninges, and CSF during MS, and it has been suggested that glial cells contribute to the trophic support of B cells[63,215]. Like T cells, ample evidence exists for the clonal expansion of B cell populations in the CSF and blood, but a single target antigen remains elusive[63]. B cells have multiple potential pathogenic effector mechanisms, including release of proinflammatory cytokines and CNS-specific auto-antibodies that can activate the complement cascade and target cells for destruction[63]. B cells and plasma cells in the meninges and CSF seem to be associated with disease activity and clinical outcome[215]. The clinical efficacy of B cell-specific therapies suggests that these cells play a pathogenic role in MS, the mechanism of which remains to be fully elucidated.

1.6.4.4 Microglia/Macrophage Activation

Recent studies have combined histological analysis and micro-dissection of MS lesions to delineate the gene signatures of microglia/macrophages recruited to lesion sites. Active lesions have been shown to contain approximately triple the number of microglia/macrophages than NAWM or NWM from non-MS controls[225]. $TMEM119^{+}$ microglia were shown to predominate early in lesion formation, while $TMEM119^{-}$ monocyte-derived cells increased with lesion maturity[225]. Homeostatic microglial gene signatures were lost in areas of active demyelination, while markers of phagocytosis, oxidative injury, antigen presentation, and T cell stimulation were unregulated, indicating a highly proinflammatory phenotype[225]. The clinical relevance of microglial

activation is highlighted by recent clinical trials using minocycline, which dampens microglial activation[226], to prevent transition from CIS to MS[227].

1.6.5 Additional Molecular Mediators of Neuronal and ODC Injury in MS

1.6.5.1 Mitochondrial Damage and Oxidative Stress

Recent studies have indicated a growing role for mitochondrial dysfunction in MS, which can exacerbate tissue destruction through either energy failure, induction of apoptosis, or increased release of ROS[213]. Energy failure is thought to underlie destruction of axons with low mitochondrial content, and to undermine the ability of ODC progenitors to differentiate into mature ODCs and facilitate remyelination[213]. Several proinflammatory mediators released from dysfunctional mitochondria, including ROS and RNS, can cause oxidative injury during inflammatory demyelination. One recent study demonstrated that oxidized forms of both lipids and DNA were prevalent in apoptotic ODCs in MS lesions[228]. Furthermore, oxidized phospholipids accumulated in disrupted myelin sheaths and axons[228]. Microglia and macrophages associated with MS lesions express high levels of inducible nitric oxide synthase (iNOS) and NADPH oxidase, major sources of RNS/ROS respectively[213].

1.6.5.2 Mechanisms of Programmed Cell Death in MS

Apoptosis has traditionally been considered a major driver of ODC cell death in MS. In fact, it has been observed that early lesions consist almost exclusively of apoptotic ODCs and activated microglia, with few infiltrating lymphocytes[229,230]. Transgenic animal models of ODC apoptosis have validated that this phenomenon is sufficient to cause rapid demyelination[231]. Necroptosis has also been recently identified as a mechanism of

cell death in MS based upon the presence of the hallmark mediators of necroptosis (e.g. MLKL, RIPK1, RIPK3) in cortical lesions[232].

I.VII. Inflammasome Activation in MS and its Animal Models

1.7.1 Experimental Autoimmune Encephalomyelitis

EAE is a common model for MS pathogenesis that recapitulates key autoimmune and neuroinflammatory components of MS. EAE can be (i) active, involving immunization of the animal with adjuvant and self-antigen (e.g. a myelin-derived peptide) to generate an encephalitogenic auto-reactive T cell response, (ii) passive, which involves the transfer of auto-reactive T lymphocytes to a recipient animal to generate encephalopathy or (iii) genetic, in which transgenic mice express a myelin-specific TCR (e.g. 2D2 mice)[233].

1.7.1.1 C57Bl/6 MOG_{35-55} EAE

The most common type of EAE is induced on a C57Bl/6 mouse background, using Complete Freud's Adjuvant (CFA) in combination with murine myelin oligodendrocyte glycoprotein (MOG_{35-55})[233,234]. In this system, pertussis toxin (PTX) is administered as a co-adjuvant to achieve full disease. In the few days post-induction, MOG-specific $CD4^+$ T lymphocytes are primed and differentiated in the secondary lymphoid organs of the periphery. These cells eventually traffic across the BBB, where they re-encounter their cognate antigen (MOG_{35-55}), which may be presented by MHC II-expressing APCs in both the meninges (e.g. meningeal macrophages, DCs) and in the CNS parenchyma (e.g. microglia). This re-activation of $CD4^+$ T cells results in the release of pathogenic effector molecules, including cytokines and chemokines, which culminate in activation of CNS-resident microglia, infiltration of peripheral leukocytes (e.g. T cells, monocytes), and the

formation of demyelinating plaques, all key features of MS pathology[233,234]. In the MOG_{35-55} model EAE, the neurobehavioural presentation involves temporary ascending paralysis, beginning with tail, then hind limbs, then forelimbs[233].

1.7.1.2 Role of Microglia/Macrophages in EAE

Significant heterogeneity has been observed in microglia/macrophage phenotypes in EAE, both temporally and regionally[54]. One recent report utilized single-cell transcriptome analysis to identify four different disease-associated microglial sub-groups in the CNS parenchyma in EAE, with differing levels of proliferation-associated and inflammation-associated genes[235]. Recent reports have demonstrated that neuroinflammation in EAE is dominated by pSTAT3-expressing monocyte-derived cells in the active stage, but NF-κB-expressing microglia in the chronic progressive phase[52]. Although monocytes are detected in the CNS prior to onset of neurobehavioural symptoms and persist through peak disease, transition into the chronic stage of EAE is associated with a disappearance of monocytes from the CNS while activated microglia persist[52]. The same study confirmed earlier reports that blocking monocyte infiltration either at induction or following disease onset attenuates EAE[52]. Other groups have used myeloablation in parabiosis models to demonstrate that infiltrating monocytes contribute profoundly to the pathology of EAE; unlike microglia, these recruited cells did not return to quiescence but rather "vanished" from the CNS during remission[236]. Recent studies using single-cell profiling have confirmed that the infiltrating monocyte population expands rapidly until peak disease, but these cells decline in numbers during the chronic phase and fail to engraft permanently in the CNS[235]; accumulation of these cells in close proximity to the meninges and within the perivascular space suggested

these sites as routes of entry for infiltrating monocytes. The same study also demonstrated that microglia, perivascular macrophages, and meningeal macrophages proliferate during disease, with microglia demonstrating the most dramatic and rapid expansion[235]. Despite these observations, macrophage/microglia cell death has also been documented in EAE models, although this has often been attributed to apoptosis based upon TUNEL staining, a biomarker now known to be non-specific[206,235,237]. When analyzed at the single-cell level, both meningeal macrophages and microglia were shown to be TUNEL-positive during the chronic phase of EAE[235].

1.7.2 Cuprizone Neurotoxin Model

Cuprizone, a copper-chelation-based model that leads to loss of ODCs in the corpus callosum and other regions, is a chronic demyelination model[238]. It lacks an autoimmune component but is associated with local inflammation, astrogliosis, and microglial activation. It can also be useful for studying remyelination, as the cessation of cuprizone administration leads to spontaneous remyelination.

1.7.3 Inflammasomes in MS/EAE: Existing Evidence and Outstanding Questions

As described above, inflammasome-associated neurodegeneration may be propagated through several mechanisms, including: (i) pyroptosis of neuronal and glial cells (ii) release of neurotoxic inflammasome-associated cytokines (Il-1β and IL-18), and (iii) release of secondary neurotoxic inflammatory mediators/cytokines (e.g. IL-6, TNFα) from IL-1β/IL-18-activated cells that perpetuate neuroinflammation and neurotoxicity. The contribution of peripheral immune populations during MS/EAE suggests several other potential mechanisms by which inflammasomes and their associated cytokines

might drive pathology, including the compromise of BBB integrity and the associated migration of immune cells into the CNS.

1.7.3.1 Evidence from Clinical Studies

Multiple studies have confirmed that IL-18, IL-1β, NLRP3, and caspase-1 expression is elevated in the serum, CSF, and PBMCs of MS patients compared to controls, with levels of IL-1β in the CSF correlating to both the number and volume of cortical lesions, as well as the severity of disease course[239-243]. Various inflammasome components, including caspase-1 and IL-1β, are present in myeloid cells in demyelinating lesions and in microglia nodules of NAWM[244,245]. Serum levels of ASC and caspase-1 have also been proposed as candidate biomarkers for MS[246].

1.7.3.2 Evidence from Genetic Knock-out Studies

In EAE, deficiency of IL-1β[247-249], IL-18[222], NLRP3[250,251], ASC[248], pyrin[252], caspase-11[125], and caspase-1[222] have been associated with a reduction in neuroinflammation and disease severity by various groups, although not all studies recapitulate the identical phenotypes. These studies have dissected multiple mechanisms by which inflammasomes contribute to disease processes, illustrating a multifactorial pathogenic role for inflammasome activation in EAE. In addition to the known neurotoxic properties of inflammasome-associated cytokines at high concentrations, they are also important in facilitating the T cell responses that are critical to the development of EAE. IL-1β has a well-established role in promoting differentiation of naive $CD4^+$ T lymphocytes into T_H17 cells, while IL-18 (originally called IFNγ-inducing factor) participates in establishing the T_H1 response, both of which are strongly implicated in

EAE pathology[135,253]. NLRP3 has been shown to play a role in the migration of T cells into the CNS[250,254] and the signaling cascade initiated by the pyrin inflammasome facilitates leukocyte adhesion and crawling in CNS vasculature downstream of enzymatically active pertussis toxin[252]. A deficiency in inflammasome signaling is associated with reduced infiltration of APCs, monocytes, and T cells into the CNS during EAE, all of which have known contributions to EAE pathology[249,254]. Mechanistically, the release of IL-1β by monocytes has been shown to drive the release of GM-CSF by CNS endothelial cells; this promotes conversion of monocytes into APCs, and the subsequent interaction of these cells with pathogenic $CD4^+$ T cells in the CNS mediates neurotoxicity[247,249]. This body of literature is complemented by knock-out studies in the cuprizone model of demyelination, which lacks an autoimmune component and thus may be used to evaluate the impact on inflammasome activation during demyelination independently of infiltrating immune cells. In this model, NLRP3, IL-18, and caspase-1 knock-out mice (but not IL-1β knock-out mice) have reduced demyelination and gliosis[251]. Collectively, these studies indicate a pathological role for inflammasome activation in inflammatory demyelination.

1.7.3.3 Evidence from Pharmacological Intervention Studies

Pharmacological intervention studies have consistently supported the pathogenic role for inflammasomes in EAE. For instance, the NLRP3 inflammasome inhibitor, MCC950, reduced IL-1β production and attenuated EAE severity[255]. Likewise, many groups have shown that the exogenous recombinant IL-1R antagonist is protective in rodent EAE models[256,257]. Interestingly, NLRP3-independent EAE can also be induced in the context

of aggressive immunization[258,259]. IFNβ does not retain its therapeutic efficacy in this context, suggesting that inflammasome modulation is an important mechanism by which IFNβ improves outcomes in MS/EAE; this is consistent with clinical data showing that IFNβ down-regulates IL-1β and IL-18[260] and that only patients who have high NLRP3 and IL-1β expression respond well to IFNβ therapy[135].

1.7.3.4 Limitations of Existing Studies and Outstanding Questions

While existing studies have made excellent progress in understanding the mechanisms by which inflammasomes contribute to the priming, activation, and chemotaxis of infiltrating immune cell populations, the question of whether pyroptosis occurs in CNS-resident cells during inflammatory demyelination remains unaddressed. Since the discovery of GSDMD as the executioner of pyroptosis, no studies have examined whether it is present in MS/EAE. Given the pathogenic contribution of pyroptosis to other neurological conditions, and the smoldering inflammatory milieu in the CNS during MS/EAE, the role for pyroptosis in the pathogenesis of inflammatory demyelination seems worthy of investigation. Although GSDMD inhibitors are in their infancy, caspase-1 inhibitors that act directly upstream of GSDMD are readily available. Caspase-1 represents an excellent therapeutic target in MS/EAE because it is highly conserved across different types of inflammasomes, and its inhibition concurrently blocks cytokine maturation and pyroptosis. Few studies have assessed the viability of this approach. Thus, within this thesis, I seek to address the outstanding questions of whether pyroptosis occurs in the CNS during MS/EAE, and whether this pathway can be targeted pharmacologically through inhibition of caspase-1.

I. VIII. Thesis Objectives

This thesis is divided into three objectives.

OBJECTIVE I:

To evaluate the evidence for CNS inflammasome activation and pyroptosis in MS and EAE and determine whether caspase-1 modulation affected neuroinflammation and neurobehavioural outcomes using the EAE model

Hypothesis I: Inflammasome activation and pyroptosis occur in the CNS during MS and EAE, which can be modulated with VX-765.

Within this objective, we first established evidence for CNS inflammasome activation and pyroptosis in white matter of MS patients. We then delineated the inflammasome profile within the CNS over time during EAE, validated the presence of pyroptosis in multiple cell types, and demonstrated that inhibition of inflammasome activation and pyroptosis improves outcomes in EAE.

OBJECTIVE II:

To characterize primary human microglial pyroptosis ex vivo using well-characterized and disease-relevant NLRP3 inflammasome activating stimuli and to validate a clinically relevant inhibitor of caspase-1 in this system

Hypothesis II: Human microglia undergo inflammasome activation and pyroptosis in response to MS-relevant stimuli *in vitro* in a GSDMD- and caspase-1 dependent manner.

Within this objective, we established primary human microglia as a model for both inflammasome activation and GSDMD-dependent pyroptosis and developed a classification paradigm for profiling the molecular and morphological features of pyroptosis using semi-quantitative confocal microscopy. We also validated VX-765 as a modulator of inflammasome activation and pyroptosis.

OBJECTIVE III:

To interrogate whether a functional role exists for apoptotic caspase-3/7 in pyroptosis using human microglia as a model system.

Hypothesis III: Apoptotic caspase-3/7 drive GSDMD-dependent pyroptosis.

Within this objective, we provided proof-of-principle that cleaved apoptotic caspase-3 was co-expressed with pyroptotic marker GSDMD in myeloid cells in MS lesions. We demonstrated that caspase-3/7 are cleaved and activated during GSDMD-driven pyroptosis downstream of caspase-1 in human microglia. We further demonstrated that inhibition of caspase-3/7 with siRNA inhibits pyroptosis, reduces membrane permeability, and prevents nuclear disintegration. Lastly, we demonstrate that specific caspase-3/7 substrates are cleaved in multiple compartments of the cell during pyroptosis, which is rescued by caspase-3/7 inhibition.

CHAPTER II: METHODS

II.I. Ethics Statements

2.1.1 Research ethics statements

The use of autopsied brain tissues was approved (Pro0002291) by the University of Alberta Human Research Ethics Board (Biomedical) and written informed consent was received for all samples. Frontal white matter including demyelinating lesions and normal appearing white matter from MS patients and other disease controls (non-MS) were examined. Human fetal tissues were obtained from 15-20-week aborted fetuses that were collected with the written informed consent of the donor (Pro00027660), approved by the University of Alberta Human Research Ethics Board (Biomedical). All animals were housed and monitored on a regular schedule, and experiments were performed according to the Canadian Council on Animal Care and University of Alberta Health Sciences Animal Care and Use Committee guidelines.

II.II. *In Vitro* Experiments

2.2.1 Primary cell cultures

Primary fetal human microglia were isolated based on differential culture conditions, as previously described[261,262]. Fetal brain tissues from 17-20 week fetuses were dissected, meninges were removed, and a single cell suspension was prepared through enzymatic digestion for 60 min with 2.5% trypsin and 0.2 mg/ml DNAse I, followed by titration through a 70-µm cell strainer. Cells were washed twice with fresh medium and plated in T-75 flasks. Cultures were maintained in MEM supplemented with 10% FBS, 2mM L-glutamine, 1mM sodium pyruvate, 1X MEM nonessential amino acids, 0.1% dextrose, 100 U/ml penicillin, 100 µg/ml streptomycin, 0.5 µg/ml amphotericin B, and 20µg/ml

gentamicin. For microglial cells, mixed cultures were maintained for 1-2 weeks, at which point astrocytes and neurons formed an adherent cell layer with microglia loosely attached or free floating in the medium. Cultures were gently rocked for 20 min to re-suspend the weakly adhering microglia in medium, which were then decanted, washed and plated. Purity of cultures was verified by immunofluorescence as previously reported by our group[263].

2.2.2 Induction of pyroptosis and apoptosis *in vitro*

Microglia were plated in 6-well (Western blot, caspase-3 cell lysate ELISA, PCR), 8-well (immunofluorescence) or 96-well (DAPI, LDH assay, cytokine ELISAs) plates for 24hr prior to treatment. Cells were exposed to nigericin (5μM; InvivoGen cat# tlrl-nig), nigericin plus VX-765 (50μM, 4hr pre-treatment; InvivoGen cat# inh-vx765-1), ATP-γ-S [100 μM, adenosine 5′-O-(3-thiotriphosphate), a thiophosphorylated phosphatase-resistant form of ATP; Sigma-Aldrich #11162306001], ATP plus VX-765 (as above), staurosporine (5μM; Abcam #ab120056) staurosporine plus VX-765 (as above), or solvent control for 4hr unless otherwise indicated. Supernatants were harvested and stored at -80°C.

2.2.3 siRNA knockdowns

Microglia were plated as described above for 24hr prior to transfection. Cells were transfected with 30nM of non-targeting universal negative control siRNA (Integrated DNA Technologies TriFECTa RNAi Kit) or a cocktail of three pre-designed commercially available GSDMD/GSDME/caspase-3/caspase-7-targeting Dicer-Substrate siRNAs (10nM each), in combination with PrecisionFectin Transfection Reagent (Precision Bio

Laboratories, Edmonton, Canada SKU #TF071-500) according to manufacturer's instructions. Cells were permitted to recover for 24hr, and then exposed to nigericin, ATP, or solvent control for 24hr unless otherwise indicated.

Table 2.1: siRNA Sequences Utilized

Target	Sequence
Caspase-3 siRNA 1	5' rGrArC rGrCrU rArCrU rUrUrU rCrArU rGrCrArGrUrU rUrCrU rUrUrG rCrArU rGrArA rArArG
Caspase-3 siRNA 2	5' rGrGrA rArUrU rGrArU rGrCrG rUrGrA rUrGrUrUrU rArGrA rArArC rArUrC rArCrG rCrArU
Caspase-3 siRNA 3	5' rUrCrU rGrUrU rGrArA rGrUrUrUrArC RArArU rUrCrC rUrUrU rGrArU rUrGrU rArArA rCrUrU
Caspase-7 siRNA 1	5' rGrArA rArUrU rGrArC rUrUrArCrArU rArGrA rUrUrU rArUrC rArUrC rUrArUrGrUrA rArGrU
Caspase-7 siRNA 2	5' rGrGrG rCrArA rArUrG rCrArU rCrArU rArArU rGrUrUrGrUrUrUrArUrUrArUrGrArU rGrCrA
Caspase-7 siRNA 3	5' rGrUrU rUrUrG rArCrG rUrGrA rUrUrG rUrCrUrUrCrArUrUrA rUrArG rArCrArArUrC rArCrG
GSDME siRNA 1	5' rGrArU rGrArU rGrGrA rGrUrA rUrCrUrGrArU rCrUrU
GSDME siRNA 2	5' rGrCrG rGrUrC rCrUrA rUrUrU rGrArU rGrArU rGrArA
GSDMD siRNA 1	5' rCrArArCrCrUrGrUrCrUrArUrCrArArGrGrArCrArGrGrArUr GrUrCrCrUrUrGrArUrArGrA
GSDMD siRNA 2	5' rArCrUrCrUrGrArCrUrUrGrGrArCrGrUrCrCrArArGrArGrArArGrGr ArCrGrUrCrCrArA
GSDMD siRNA 3	5' rCrArArUrArArArGrGrUrGrGrCrArUrArCrGrUrUrUrCrCrUrCrGr UrArUrGrCrCrArCrC

2.2.4 Western blot analysis

Immunoblot analysis of tissue and cell lysates was performed as described previously [263,264]. Following protein extraction using RIPA buffer, samples were quantified using a DC Protein Assay Kit (Bio-Rad; cat# 5000112), then treated with Laemmli buffer (Bio-Rad; Cat#161-0747) and incubated at 95°C for 8 minutes. Samples were loaded onto 4-20% Precast SDS-PAGE gels (Bio-Rad; Cat# 456-1094) and run for 65-75 minutes at 100-120V. Following electrophoresis, gels were transferred onto 0.2μm nitrocellulose (Bio-Rad; cat# 1620112) membranes using a BioRad Mini Trans-Blot Wet Transfer system for 45-55 minutes at 0.12A. To prevent protein loss during successive wash steps, membranes were immersed in 0.4% paraformaldehyde for 30 minutes, followed by rinses in PBS. Membranes were blocked for 1 hour with Odyssey Blocking Buffer (LICOR; cat#927-40000), followed by overnight incubation at room temperature with primary antibody. Membranes were then washed 3x5 minutes with PBS-T (1x PBS-0.05% Tween-20), and incubated with HRP-conjugated secondary antibody (Jackson ImmunoResearch) for 1 hour, followed by 3x5 minute washes. Membranes were developed with ECL reagent (Thermo Scientific; cat#32132), and imaged using an ImageQuant LAS4000 Biomolecular Imager (GE Life Sciences). Band intensity was quantified using ImageStudioLite and normalized to β-actin.

Table 2.2: Antibodies Utilized

	Protein of Interest	Product Information	In Vitro IF	Tissue IF	Tissue IHC	Western blot
Cell Markers	Iba-1	Wako 019-19741	NA	1:500	1:500	NA
	MHC-II	Dako M0775	NA	1:500	1:500	NA
	GSTpi	Abcam ab53943	NA	1:500	NA	NA
	GFAP	Dako GA524	NA	1:500	NA	NA
	Neurofilament	Abcam ab4680	NA	1:500	NA	NA
Inflammasome Associated Proteins	GSDMD	Sigma WH0079792M1 (3F12-1B2)	1:200	1:200	1:200	1:500
	IL-1β	SCB sc7884	1:200	NA	1:200	NA
	Caspase-1	SCB Sc-514	1:200	1:200	1:100	NA
Apoptosis Associated Proteins	Total Caspase-3	R&D AF-605-NA	1:200	NA	NA	NA
	Cleaved Caspase-3	CST 9661	1:200	NA	NA	1:200
	Cleaved Caspase-7	CST 9491	1:200	NA	NA	1:200
	Cleaved PARP1	CST 9541	1:200	NA	NA	1:250
	Cleaved ROCK1	Novus NB100-56596	1:200	NA	NA	NA
	Cleaved DFF45	CST 9731	1:200	NA	NA	NA

2.2.5 LDH assay

LDH activity in cell supernatants was assessed using the LDH-Cytotoxicity Assay Kit II (Abcam, ab65393) according to manufacturer's instructions. Briefly, microglia were plated in 96-well plates and cultured as indicated above for 24hr before transfection or treatment. Supernatants were harvested and stored at -80°C prior to use.

2.2.6 FAM-FLICA caspase assay

Microglia were plated as above (96-well plate, 24hrs) for analysis by microplate reader and as below (8-well plate, 24hrs) for analysis by confocal microscopy. Cells were treated with nigericin, ATP, staurosporine, or solvent control as indicated and caspase-1 (Immunochemistry Technologies, #97) or caspase-3/7 (ImmunoChemistry Technologies, #93) assessed according to manufacturer's instructions.

2.2.7 Cytokine ELISAs

IL-1β assays were performed using the Human IL-1β DuoSet ELISA kit (R&D Systems, DY201) according to manufacturer's instructions. IL-18 assays were performed using the ThermoFisher IL-18 Human Instant ELISA kit (BMS267INST) as described previously[261,263].

2.2.8 Caspase-3 cell lysate ELISA

Microglia were plated in 6-well plates and exposed to pyroptotic or apoptotic stimuli as indicated. Triplicate wells were harvested and pooled and lysates analyzed using the Human Active Caspase-3 Ser29 ELISA Kit (Abcam, ab181418) according to manufacturer's instructions.

2.2.9 Polymerase chain reaction (PCR)

1μg of total RNA was used for first-strand cDNA using Superscript II reverse transcriptase (Invitrogen, Carlsbad CA, USA) and with random hexamer primers (Roche). Specific genes were quantified by real-time reverse transcriptase PCR (RT-PCR) using i-Cycler IQ5 system (Bio-Rad, Mississauga, ON, Canada). Semi-quantitative PCR analysis was performed by monitoring the increase of fluorescence of the SYBR Green dye (iQ™ SYBR Green Supermix Bio-Rad) on the Bio-Rad detection system as previously reported[265], normalized to housekeeping gene expression (*GAPDH* for human samples and *hprt* for mouse samples), and expressed as relative fold change (RFC) compared to untreated cells, non-MS controls, or CFA control mice as appropriate.

Table 2.3: Human Primer Sequences Utilized

Gene Name	*Species*	*Sequence*
NLRP3	human	5'-GAT CTT CGC TGC GAT CAA CAG-3' 5'-CGT GCA TTA TCT GAA CCC CAC-3'
CASP1	human	5'-TCC AAT AAT GGA CAA GTC AAG CC-3' 5'-GCT GTA CCC CAG ATT TTG TAG CA-3'
IL1B	human	5'-CCA AAG AAG AAG ATG GAA AAG C-3' 5'-GGT GCT GAT GTA CCA GTT GGG-3'
IL18	human	5'- TCT TCA TTG ACC AAG GAA ATC GG-3' 5'-TCC GGG GTG CAT TAT CTC TAC-3'
ASC	human	5'-GCC TGC ACT TTA TAG ACC AGC-3' 5'-GCT TCC GCA TCT TGC TTG G-3'
AIM2	human	5'-TCA AGC TGA AAT GAG TCC TGC-3' 5'-CAC GTT GCT TTG CGA CAT CA-3'
NLRP1	human	5'-ATT CCA GTT TGT GCG AAT CCA-3' 5'-GTT CCT TGG GGA GTA TTT CCA G-3'
NLRP2	human	5'-ATG CAC CGA ATG GAT CTG TC-3' 5'-CGT TCT TTC CGT GTT ATC CC-3'
MEFV	human	5'-GGC TAA GAC AGT GCC T-3' 5'-GGT AAG CGG TTT CTG C-3'
CASP4	human	5'-CAA GAG AAG CAA CGT ATG GCA-3' 5'-AGG CAG ATG GTC AAA CTC TGT A-3'
NLRC4	human	5'-TGC ATC ATT GAA GGG GAA TCT G-3' 5'-GAT TGT GCC AGG TAT ATC CAG G-3'
GSDMD	human	5'-TGTGTCAACCTGTCTATCAAGG-3' 5'-GATCTTTGCCTGTCCTGGG-3'
GAPDH	human	5'-AGC CTT CTC CAT GGT GGT GAA GAC-3' 5'-CGG AGT CAA CGG ATT TGG TCG -3'

Table 2.4: Mouse Primer Sequences Utilized

Gene Name	*Species*	*Sequence*
nlrp3	mouse	5'-ATT ACC CGC CCG AGA AAG G-3' 5'-TCG CAG CAA AGA TCC ACA CAG-3'
casp1	mouse	5'-ACA AGG CAC GGG ACC TAT G-3' 5'-TCC CAG TCA GTC CTG GAA ATG-3'
il1b	mouse	5'-GCA ACT GTT CCT GAA CTC AAC T-3' 5'-ATC TTT TGG GGT CCG TCA ACT-3'
il18	mouse	5'-ACT TTG GCC GAC TTC ACT GT-3' 5'-GGG TTC ACT GGC ACT TTG AT-3'
asc	mouse	5'-CTT GTC AGG GGA TGA ACT CAA AA-3' 5'-GCC ATA CGA CTC CAG ATA GTA GC-3'
aim2	mouse	5'-GTC ACC AGT TCC TCA GTT GTG -3' 5'- CAC CTC CAT TGT CCC TGT TTT AT-3'
nlrp1a	mouse	5'-ACA GAC ATG GAC CTC ATG GTG GTT-3' 5'-CAA CTC CTC CAG GTT TCT GGC TAA C-3'
nlrp6	mouse	5'-TCT TTT GCT TGC CCT TCT GT-3' 5'-AGC CCA AAG TCC CTC TGA AT-3
nlrp2	mouse	5'-CAT GCC AAC ACT TCC TCC TT-3' 5'-ACG GTC CAC TTT CTG TTT GG-3'
mefv	mouse	5'-CCC TAC TGG ATG AGA TGA TTG AAG AAC-3' 5'-TCC AAC AGC TCA GAG GCA GAC AT-3'
casp11	mouse	5'-AGA GGG CAT GGA GTC AGA GA-3' 5'-GCC ATG AGA CAT TAG CAC CA-3'
nlrc4	mouse	5'-AAT TCA GAT GGG CAG ACA GG-3' 5'-TCA CCT GAA GCT CCA CCT CT-3'
cd3e	mouse	5'-GAT GCA GTC GGG CAC TCA CT-3' 5'-CAT TAC CAT CTT GCC CCC AA-3'
tnfa	mouse	5'-CAT CTT CTC AAA ATT CGA GTG ACA A-3' 5'-TGG GAG TAG ACA AGG TAC AAC CC-3'
f480	mouse	5'-GCT GTG AGA TTG TGG AAG CA-3' 5'-AGT TTG CCA TCC GGT TAC AG-3'
ifng	mouse	5'-GCA TTC ATG AGT ATT GCC AAG-3' 5'-GGT GGA CCA CTC GGA TGA-3'
gsdmd	mouse	5' GCA GAC AAA GGA GGA AGT GC 3' 5' ATA AAG CTC CAG GCA GCG TA 3'
hprt	mouse	5'-AGC CTA AGA TGA GCG CAA GT-3' 5'-TTA CTA GGC AGA TGG CCA CA-3'

2.2.10 Cell culture immunofluorescence

Detection of cellular proteins was performed using immunofluorescence as described previously[263]. Cells were cultured on 180μm thick polymer coverslip 8 well plates (μ-Slide ibiTreat plates #80826) and treated as appropriate. After 24hr, cells were fixed using 4% paraformaldehyde. Cells were permeablized using 0.1% Triton in PBS, blocked using Odyssey blocking buffer, and incubated with primary antibody overnight at 4°C. Primary antibody binding was detected using AlexaFluor 488 goat anti-mouse IgG (Abcam 1:500); AlexaFluor 647 goat anti-rabbit IgG (1:500); or AlexaFluor 568 rabbit anti-goat IgG (Abcam, 1:500). Cells were stained with DAPI and mounted using Prolong™ Gold antifade reagent (Invitrogen, #P36934). Slides were imaged using a Wave FX spinning disc confocal microscope (Zeiss) with Volocity 6.3 acquisition and analysis software (Perkin Elmer), and basic contrast enhancement performed using automatic black-point calculation. Composite z-stack images included 15-20 XY planes over a total vertical distance of 4-6 μm using the Improvision Focus Drive. All cells were imaged using a 40X oil immersion objective lens unless otherwise indicated and quantification was performed on a single XY plane per field of view.

2.2.11 Cell culture immunofluorescence quantification

For quantification purposes, adjacent fields of view were imaged at 40X and analyzed using Volocity 6.3 acquisition and analysis software. The intensity of each fluorescent channel was quantified by highlighting each individual cell or nucleus to form a region of interest (ROI) and recording the mean fluorescent intensity (MFI) and area (μm^2) for

each ROI. Cross-sectional area of the nucleus and the cell were also recorded. *In vitro* images were taken on a single plane and no contrast enhancement or other modifications were performed on images prior to analysis. Background MFI values from a blank portion of the slide were subtracted from total MFI values for every field of view.

To categorize cells as immunopositive for proteins of interest, the threshold MFI for "immunopositive" was set at 3X background MFI and cells categorized accordingly. Classification of cells into the stages of pyroptosis was performed manually using the criteria indicated: STAGE 0: "Intact" (adherent cell, elongated processes, baseline GSDMD expression); STAGE 1: "Rounding" (rounded cell, loss of processes, increased GSDMD expression throughout the cell); STAGE 2: "Ring of fire" (translocation of GSDMD to cell membrane, no pyroptotic bodies); STAGE 3: "Pyroptotic bodies" (formation of one or more discreet $GSDMD^+$ membrane blebs); STAGE 4: "Lysis" (membrane rupture, nucleus intact); and STAGE 5: "Ghost cells" (nucleus disintegrated, diffuse residual $GSDMD^+$ cell debris). MFI was not measured for Stage 5 cells due to the diffuse nature of the cell debris. Cells that were excessively saturated in one or more channels and cells with more than one nuclei were excluded. Slides were imaged using a Wave FX spinning disc confocal microscope (Zeiss) with Volocity 6.3 acquisition and analysis software (Perkin Elmer).

II.III. *In Vivo* Experiments

2.3.1 Tissue immunofluorescence

As described previously[264], tissue slides were de-paraffinized by incubation for 1hr at 60°C followed by one 10min and two 5min incubations in toluene baths through decreasing concentrations of ethanol to distilled water. Antigen retrieval was performed by boiling in 10mM sodium citrate (pH 6.0). Slides were blocked with HHFH buffer [1.0 mM HEPES buffer, 2% (v/v) horse serum, 5% (v/v) FBS, 0.1% (w/v) sodium azide in Hank's balanced salt solution (HBSS)] for 4hr. Slides were incubated with primary antibodies at 4°C overnight. Primary antibody was removed by PBS washes (5 min x3) and slides incubated for 3min in 0.22mm filtered 1% (w/v) Sudan black in 70% ethanol and washed three times in PBS. Slides were incubated in 1:500 fluorescent secondary antibodies for 2hr, washed three times in PBS, stained with DAPI for 10min, and mounted with Prolong Gold. Slides were imaged with an inverted Wave FX spinning disc confocal microscope (Zeiss). For quantification purposes, high GSDMD expression (3X background MFI) was used as a surrogate marker for pyroptosis.

2.3.2 Experimental autoimmune encephalomyelitis (EAE) induction and monitoring

C57Bl/6 female mice (10–12 weeks old) were immunized with MOG_{35-55} peptide (1mg/mL) emulsified with complete Freund's adjuvant (CFA) (Hooke laboratories, EK-0115/EK-2110, Lawrence, MA, USA) and injected with pertussis toxin (200ng/mouse) at Day 0 and Day 2 according to the manufacturer's instructions [264]. For the duration of each experiment, animals were fed a Bio-Serv NutraGel diet (BioServ #F4798-KIT) instead of conventional chow to prevent dehydration after onset of disease.

Several different EAE experimental designs were utilized. To analyze the time-dependent induction of inflammasome-related genes, 6 CFA and 6 MOG animals were sacrificed at Day 8, 10, 15, and 20 respectively and hindbrains collected for PCR. To analyze the effect of VX-765 on neurobehavioural and neuropathological outcomes, EAE animals received daily intraperitoneal injections of VX-765 (50 mg/kg) diluted in PBS/DMSO after the onset of clinical signs (Day 12) until the end of the experiment. Vehicle-treated animals received daily injections of PBS/DMSO on the same schedule. CFA animals were untreated. EAE animals were assessed daily and scored for disease severity up to 24 days following EAE induction using an established 0-15 point scale[266]. As the observed disease severity was only moderate in these experiments, the neurobehavioural scale is shown only up to 5 points. Hindbrains and spinal cords were collected for PCR experiments, immunohistochemistry, histopathological, and immunofluorescence analysis.

2.3.2 Immunohistochemistry

Tissue sections were deparaffinized and hydrated using decreasing concentrations of ethanol. Antigen retrieval was performed by boiling the slides in 0.01M trisodium citrate buffer (pH 6.0) for 60 min. Endogenous peroxidases were inactivated by incubating sections in 0.3% hydrogen peroxide for 20 min. To prevent nonspecific binding, sections were pre-incubated with Odyssey buffer for 1hr at room temperature prior to overnight incubation with primary antibody. Biotinylated secondary antibodies were applied for two hours, and immunoreactivity detected using the Vectastain Avidin-Biotin Complex (ABC) kit (Vector Laboratories) with a 3,3'-diaminobenzidine

tetrachloride (DAB) peroxidase substrate kit (Vector Laboratories). All slides were imaged using an upright microscope (Axioskop2; Zeiss MicroImaging Inc.).

2.3.3 Immunohistochemistry quantification

For human autopsy samples, immunohistochemical quantification was performed using a minimum of three MS and three non-MS control autopsy samples per protein of interest, with a minimum of six non-overlapping fields of view (FOV) per patient. For *in vivo* experiments, EAE and CFA animals were sacrificed at peak disease and sections of the lumbar spinal cord labeled for proteins of interest as described above. The number of IL-1β$^+$, caspase-1$^+$, and GSDMD$^+$ cells in the ventral spinal column was quantified (cells per mm^2) for multiple spinal cord sections from 2-3 representative animals per condition, with a minimum of ten non-overlapping fields of view (FOV) per animal. Cells were counted manually using the particle counting feature of ImageJ.

2.3.4 Motor neuron quantification

EAE and CFA animals were sacrificed at peak disease and sections of the lumbar spinal cord stained with silver (Bielchowsky) staining. Spinal cords were imaged at 40X and motor neurons in the ventral horn counted using the particle counting feature of ImageJ. Motor neurons in the ventral horn were identified visually based upon the criteria of large triangular cell body and prominent nucleolus.

II.IV Statistical Analyses

2.4.1 Statistical tests

Chi-square test was used to compare distributions of microglia across the stages of pyroptosis. Comparisons between two groups were performed by unpaired Student's *t*-test or by ANOVA with Dunnett's post hoc tests, using GraphPad Instat 3.0 (GraphPad Software, San Diego, CA, USA).

CHAPTER III: PYROPTOSIS IN EAE/MS

This chapter has been published:

McKenzie, BA, Mamik MK, Saito LB, Boghozian R, Monaco MC, Major EO, Lu JQ, Branton WG, Power C. (2018) Caspase-1 inhibition prevents glial inflammasome activation and pyroptosis in models of multiple sclerosis. *PNAS*. 115 (26): E6065-E6074.

All figures were included in the published manuscript with the exception of the antibody validation shown in [Figure 3.1J]. GSDMD-deficient THP-1 clones for antibody validation were kindly provided by Dr. Vijay Rathinam, University of Connecticut.

All *in vivo* and *in vitro* experiments were performed by Brienne McKenzie with the following exceptions:

- Human autopsy tissue immunofluorescence [Figure 3.2] was performed and quantified with the assistance of technician William Branton.
- The EAE time course experiment [Figure 3.3] was performed by post-doctoral fellow Dr. Stacey Reinke, with molecular analysis [Figure 3.3, 3.4] performed by Brienne McKenzie.
- Bielchowsky silver stain [Figure 3.10E-G] was performed by NACTRC personnel, imaged and quantified by Brienne McKenzie.

III.I. Brief Introduction

CHAPTER III OBJECTIVE:

To evaluate the evidence for CNS inflammasome activation and pyroptosis in MS and EAE and determine whether caspase-1 modulation affected neuroinflammation and neurobehavioural outcomes using the EAE model

As outlined in Chapter I, inflammasome components have been identified in the serum, CSF, and lesions of MS patients, typically in microglia/macrophages. They have also been widely implicated in the immunopathogenesis of EAE, through a variety of mechanisms including the priming and recruitment of Th1 and Th17 cells, activation of CNS endothelial cells, and transmigration of monocytes into the CNS. Several of these mechanisms involve the activation and recruitment of circulating immune cells; however, evidence from the cuprizone literature suggests the CNS inflammasomes may also play a role in inflammatory demyelination independently of their effect on peripheral immunity. This is supported by evidence from other neurodegenerative and neuroinflammatory disease models whose pathogenesis lacks a peripheral immune component (e.g. AD, PD, epilepsy, and others), but in which CNS inflammasome activation plays a key role in the neurodegenerative pathology. Pyroptosis, however, has never been characterized in the CNS in either MS or EAE, despite widespread cell death in multiple cell types during inflammatory demyelination. Furthermore, since the discovery of GSDMD as the executioner of pyroptosis in 2015, no group has studied its role in any CNS pathology.

CHAPTER III Hypothesis:

Inflammasome activation and pyroptosis occur in the CNS during MS and EAE, which can be modulated with the caspase-1 inhibitor VX-765 to improve neurobehavioural outcomes and reduce neuroinflammation.

Within this chapter, I have provided evidence for CNS inflammasome activation and pyroptosis in multiple glial cell types in MS patient white matter. I delineated the inflammasome profile at the transcript level within the CNS over time during EAE, and provided evidence for pyroptosis in multiple CNS cell types at peak disease using confocal microscopy. I also demonstrated that inhibition of inflammasome activation and pyroptosis using VX-765 (a caspase-1 inhibitor currently in trials for epilepsy and psoriasis) improved outcomes in EAE, reducing both neuroinflammation and neurodegeneration. *In vitro* validation of this inhibitor is provided in Chapter IV.

III.II. Results

3.2.1 Inflammasome and pyroptosis-associated genes and proteins are up-regulated in the CNS of MS patients

Earlier studies have reported increased levels of inflammasome components, including IL-1β and caspase-1, in CNS tissues from patients with MS[244,245]. To examine CNS inflammasome expression in a systematic manner, a wider panel of inflammasome genes was assessed in post-mortem samples from frontal white matter of age- and sex-matched MS and non-MS patients [Table 3.1]. Transcript was detectable for all inflammasome-associated genes examined in human CNS tissue, with increased *IL1B*, *IL18*, *CASP1,* and *GSDMD* transcript levels in MS compared to non-MS samples [Figure 3.1A]. Similarly, transcripts were detectable for all inflammasome sensors examined, including *MEFV* (encoding pyrin), *NLRP3*, *NLRP1*, *AIM2*, and *NLRP2* in MS tissue. *NLRP3* expression was significantly elevated in MS white matter compared to non-MS controls [Figure 3.1B]. *AIM2* levels were significantly elevated when all patients were included in the dataset; however, upon exclusion

Table 3.1: Clinical and demographic features of MS and nonMS patients

	MS (*n*=14)	non-MS (*n*=10)	*p* value*
Mean age (range, years)	60 (25-80)	62 (36-77)	NS
Sex (M:F ratio)	6:8	5:5	NS
Disease phenotype	PPMS[1] (*n*=3) RRMS[2] (*n*=2) SPMS[3] (*n*=9)	stroke (*n*=1) drug overdose (*n*=1) cancer (*n*=2) sepsis (*n*=2) myocardial infarction (*n*=2) HIV/AIDS (*n*=2)	NA
Disease duration (range, years)	5-20	1-5	NA
Therapy	DMT (*n*=2)[4]	cancer chemotherapy (*n*=2) antibiotics (*n*=1)	NA
EDSS[5]	5.0-9.5	NA	NA

* non-significant (NS)
[1] Primary progressive MS
[2] Relapsing-remitting MS
[3] Secondary progressive MS
[4] Disease-modifying therapy (IFN-beta and glatiramer acetate)
[5] EDSS = expanded disability status scale

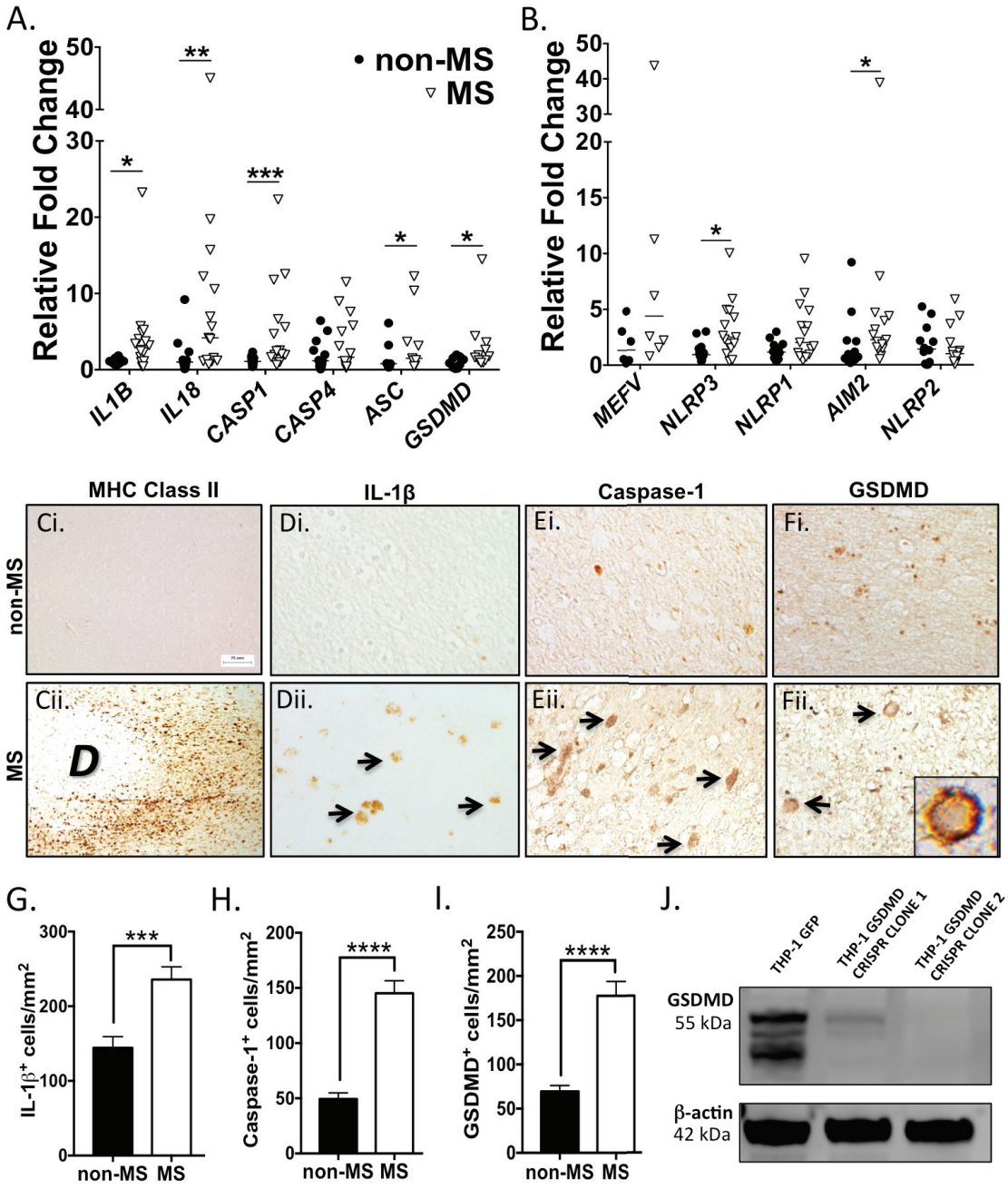

Figure 3.1 *(Figure legend on following page)*

FIGURE 3.1: ***Inflammasome components are up-regulated in the CNS of MS patients***.

(A-B) Transcript levels of inflammasome-associated genes were assessed using qRT-PCR in MS (*n*=14) and nonMS (*n*=10) white matter autopsy samples. Values represent relative fold change (RFC) compared to nonMS controls, with threshold cycles normalized to GAPDH (Mann Whitney U test, **p*<0.05, ***p*<0.01, ****p*<0.001). **(C-F)** Cerebral white matter from MS patients and nonMS controls was immunostained for proteins of interest, including MHC Class II [**(C)**, 10X magnification, demyelinated lesion indicated with "***D***"]; IL-1β [**(D)**, 40X magnification]; caspase-1 [**(E)**, 40X magnification], and GSDMD [**(F)**, 40X magnification]. GSDMD immunoreactivity was often localized to the periphery of cells within MS lesions (**Fii**, *inset*). Immunopositive cells indicated with *black arrows*. **(G-I)** The number of IL-1β$^+$, caspase-1$^+$, and GSDMD$^+$ cells in white matter from MS and non-MS controls was quantified (cells per mm^2). Immunohistochemical quantification was performed using a minimum of three MS and three nonMS autopsy samples per protein of interest, with a minimum of six non-overlapping fields of view (FOV) per patient. Data shown represent mean cell number per mm^2 +/- SEM and were tested for significance using Student's *t*-test (****p*<0.001, *****p*<0.0001). **(J)** Specificity of the GSDMD antibody was validated by immunoblot using lysates from untreated, previously validated wildtype or GSDMD knock-out THP-1 clones (provided by Vijay Rathinam, University of Connecticut).

of the highest outlier, *AIM2* transcript levels in MS patients only trended upwards compared to non-MS controls (p=0.059 with outlier excluded versus p=0.0365 with outlier included). *IL1B*, *IL18*, *CASP1*, *GSDMD*, and *NLRP3* retained significance when the high outlier was excluded [Figure 3.1A, B].

The above findings prompted further examination of inflammasome-associated proteins in the CNS. Comparison of non-MS white matter with MS lesions revealed increased MHC Class II immunoreactivity at the border of a demyelinated lesion [Figure 3.1Cii; demyelinated area indicated by "*D*"], indicating the robust recruitment of activated antigen-presenting cells in MS white matter, which was not observed in non-MS tissue [Figure 3.1Ci]. IL-1β immunoreactivity was minimal in non-MS white matter [Figure 3.1Di] while abundant IL-1β immunopositive cells were observed in MS tissues [Figure 3.1Dii]. Caspase-1 immunoreactivity was detected in occasional cells in the white matter of non-MS tissue [Figure 3.1Ei] but was markedly increased in MS tissues [Figure 3.1Eii]. To assess whether pyroptosis was occurring in MS lesions, expression of GSDMD was also investigated. Although limited GSDMD immunoreactivity was observed in non-MS white matter [Figure 3.1Fi], intense GSDMD immunostaining concentrated at the plasma membrane was observed in MS white matter [Fig. 3.1Fii, *inset*], forming a "ring of fire" that is consistent with GSDMD's role as a pore-forming membrane protein during pyroptosis. Quantification of the frequency of immunopositive cells verified a robust increase in the number of IL-1β^{+}, caspase-1^{+}, and GSDMD^{+} cells in the white matter of MS compared to non-MS patients [Figure 3.1G-I]. As the GSDMD antibody we utilized had not been validated in published manuscripts at the time, we confirmed that the antibody detected GSDMD at the correct

molecular weight (55kDa) in untreated THP-1 cells, and demonstrated that this band was not present in two previously validated THP-1 clones in which GSDMD had been knocked out using CRISPR/Cas9 technology (kindly provided by Dr. Vijay Rathinam, University of Connecticut) [Figure 3.1J].

3.2.2 GSDMD is expressed in multiple glial cell types in MS lesions

In MS lesions, GSDMD immunopositive cells and cellular debris was observed [Figure 3.2A], with only a few remaining intact nuclei, consistent with widespread death of GSDMD-positive cells within a demyelinated lesion. Among the intact cells, GSDMD was often expressed within microglia/macrophages expressing the myeloid marker Iba-1 [Figure 3.2A, *insets*: GSDMD, *red*; Iba-1, *green*; DAPI, *blue*]. GSDMD was also detected in GST-pi immunopositive ODCs in active lesions [Figure 3.2C, *insets*: GSDMD, *red*; GST-pi, *green*; DAPI, *blue*; *overlap appears yellow*]. To quantify co-expression of GSDMD with these cell markers of interest, the proportion of microglia/macrophages (Iba-1$^+$) and ODCs (GST-pi$^+$) that were also positive for GSDMD was calculated in a subset of representative patients [Figure 3.2B, D]. As indicated, the proportion of GSDMD-immunopositive Iba-1$^+$ microglia/macrophages in MS white matter (46%) is significantly higher than the proportion (24%) in other-disease control autopsy samples ($p<0.0001$). This was recapitulated in the GST-pi$^+$ ODCs, wherein 53% of ODCs in MS white matter express GSDMD, compared to 38% in other-disease controls ($p<0.0001$). The robust and significant increase in the proportion of microglia/macrophages and ODCs expressing GSDMD underscored the potential impact of inflammasome activation and pyroptosis on MS pathogenesis.

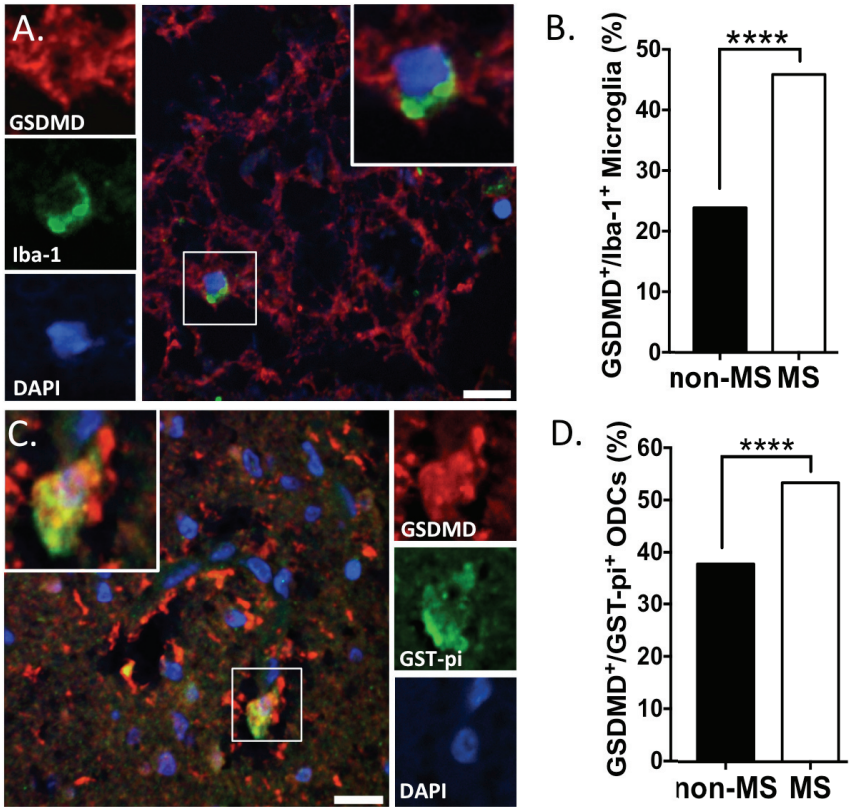

Figure 3.2: ***GSDMD is expressed in macrophages/microglia and ODCs in MS white matter.***

(A) Immunofluorescent labeling of macrophages/microglia in MS white matter for GSDMD (*red*), Iba-1 (*green*), and DAPI (*blue*; separate channels shown in insets). Scale bar represents 13μm. **(B)** The proportion of macrophages/microglia expressing GSDMD was quantified in white matter in non-MS and MS samples. Data shown represent the proportion of GSDMD$^+$ Iba-1$^+$ cells as a percent of the total number of Iba-1$^+$ cells. Proportions were calculated based on analysis of a minimum of 150 Iba-1$^+$ cells per group, using white matter sections from 2-3 representative autopsy samples. **(C)** Immunofluorescent labeling of ODCs in MS white matter for GSDMD (*red*), GST-pi (*green*), and DAPI (*blue*; separate channels shown in insets). Scale bar represents 13μm. **(D)** The proportion of ODCs expressing GSDMD was quantified in non-MS and MS samples. Data shown represent the proportion of GSDMD$^+$ GSTpi$^+$ ODCs as a percent of the total number of GSTpi$^+$ ODCs. Proportions were calculated based on analysis of a minimum of 400 GSTpi$^+$ cells per group, using white matter sections from 2-3 representative autopsy samples. Cells were considered "positive" when MFI exceeded triple the background levels in a given channel. Data were tested for significance using two-sided Chi-square test (****p<0.0001).

3.2.3 Inflammasome- and pyroptosis-related genes are up-regulated over time in the hindbrain in EAE

Although there is compelling evidence to suggest that inflammasome activation participates in the pathogenesis of EAE[252,267,268], the implicated genes and their temporal expression profiles within the CNS were uncertain. Furthermore, it was imperative to establish whether the up-regulation of inflammasome genes observed in MS brains was recapitulated in the EAE model before considering CNS-targeted therapies to attenuate inflammasome activation. To address this issue, EAE was induced in 10 week old C57/Bl6 female mice using CFA/MOG_{35-55} with pertussis toxin (PTX), as previously reported by our group[264,269], following which tissues were collected at Days 8 (pre-onset), 10 (onset), 15 (moderate disease), and 20 (peak disease) post-induction [Figure 3.3A]. Profiling hindbrain transcript levels by RT-PCR revealed a significant up-regulation of prototypical inflammatory genes with known contributions to EAE pathology, including the cytokines *ifng* and *tnfa* [Figure 3.3B, C], the macrophage marker *f4-80* [Figure 3.3D] and the T-lymphocyte marker *cd3e* [Figure 3.3E]. When inflammasome markers were examined [Figure 3.4], a significant increase in *nlrp3* gene expression was observed by Day 8, [Figure 3.4C] followed by *il1b*, *casp11*, and *pyrin* at the onset of disease (Day 10) [Figure 3.4A, G, I]. *Casp1* expression was significantly increased at Day 15 [Figure 3.4D] and both *gsdmd* and *asc* at Day 20 [Figure 3.4B, E]. *Nlrp1*, *nlrc4* and *aim2* were significantly up-regulated at different points in the disease course [Figure 3.4F, H, J] while *il18* was modestly up-regulated on Day 15 [Figure 3.4K]. *Nlrp6* was unchanged throughout the disease course [Figure 3.4L].

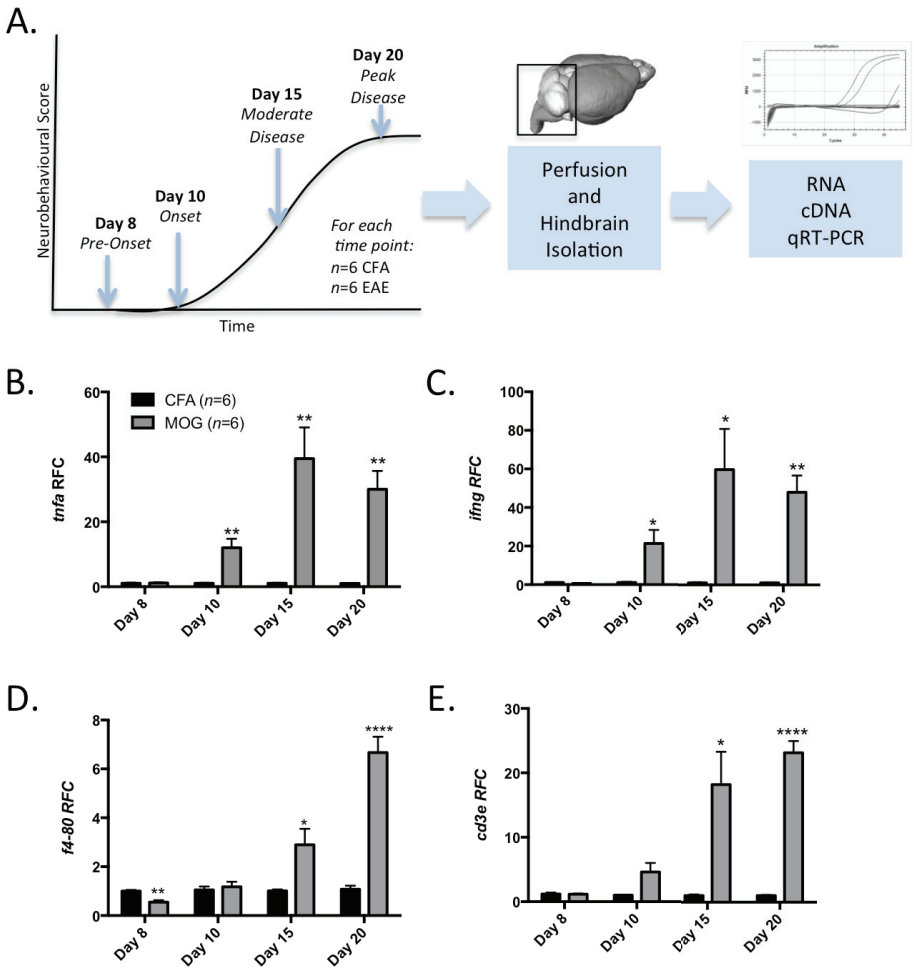

Figure 3.3: ***EAE time course experiment set-up and validation***

(A) Control (CFA) and EAE (MOG) female C57/Bl6 mice were induced on Day 0, and six mice from each group were sacrificed on Day 8 (pre-onset), Day 10 (onset of neurobehavioral symptoms), Day 15 (mid-disease), and Day 20 (peak disease). **(B)** Hindbrain transcript levels of EAE-associated proinflammatory cytokines **(B)** *tnfa* and **(C)** *ifng*, as well as **(D)** myeloid cell marker *f4-80*, and **(E)** T cell marker *cd3e* were assessed using RT-PCR. Levels of several transcripts were significantly increased at various times throughout the disease course (Student's *t*-test, **p*<0.05, ***p*<0.01, *****p*<0.0001). Data represent relative fold change (RFC) compared to CFA controls, normalized to the housekeeping gene *hprt* (mean +/- SEM).

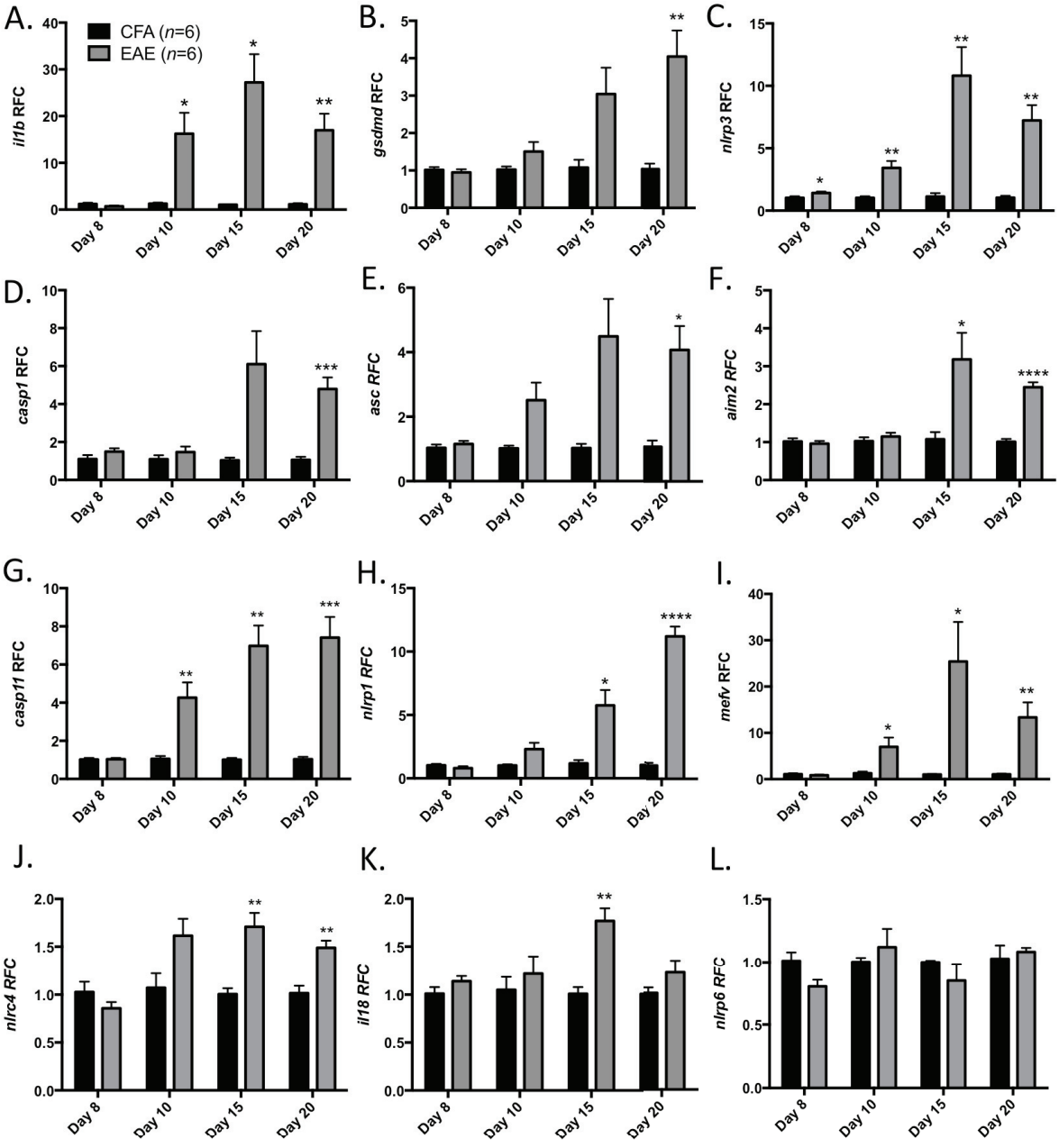

Figure 3.4: ***Inflammasome components are up-regulated in the hindbrain during EAE.***

Hindbrain transcript levels of inflammasome-associated genes were assessed by qRT-PCR. **(A)** *il1b* **(B)** *gsdmd* **(C)** *nlrp3* **(D)** *casp1* **(E)** *asc* **(F)** *aim2* **(G)** *casp11* **(H)** *nlrp1* **(I)** *mefv* **(J)** *nlrc4* **(K)** *il18* **(L)** *nlrp6*. Levels of several transcripts were significantly increased at various times throughout the disease course (Student's *t*-test, *p<0.05, ** p<0.01, ***p<0.001, ****p<0.0001). Data represent relative fold change (RFC) for EAE (n=6) compared to CFA controls (n=6) at each time point, normalized to the housekeeping gene *hprt* (mean +/- SEM).

3.2.4 GSDMD expression is evident in multiple glial cell types in the spinal cord in EAE

Spinal cords from CFA and EAE animals were examined for evidence of pyroptosis, revealing profound expression of both Iba-1 and GSDMD in spinal cord lesions [Figure 3.5Aii, Iba-1, *red*; GSDMD, *green, overlap appears yellow/orange*] compared to CFA-exposed controls [Figure 3.5Ai]. GSDMD immunoreactivity was clearly evident in a subset of Iba-1 immunopositive myeloid cells [Figure 3.5Aiii; Iba-1, *red*; GSDMD, *green*; *overlap appears yellow/orange*) as well as in cells that were not Iba-1 immunopositive [Figure 3.5Aiv, *white arrow*]. This suggested that pyroptosis might occur in both myeloid (Iba-1^{+}) and non-myeloid (Iba-1^{-}) CNS cells during EAE.

To investigate this finding further, lumbar spinal cord sections were co-labeled with antibodies to GSDMD and the ODC marker GST-pi, revealing GST-pi immunopositive cells (*purple*) with GSDMD immunoreactivity at the cell surface (*green*) in spinal cord lesions [Figure 3.5Bi-v]. These double immunopositive cells were often proximal to Iba-1-immunopositive myeloid cells within the lesion [Figure 3.5Bii, *red*], some of which were also GSDMD-immunopositive (Figure 3.5Biv, *green; overlap appears yellow*).

As neither inflammasome activation nor pyroptosis had been previously shown in ODCs, we next determined whether GSDMD was expressed in ODCs that co-expressed caspase-1, thus diminishing the likelihood that GSDMD was playing a non-inflammasome-related role in ODCs *in vivo*. To this end, immunofluorescent triple-labeling was performed to assess caspase-1, GSDMD, and GST-pi immunoreactivity simultaneously [Figure 3.5Ci-v], revealing multiple GST-pi immunopositive cells [Figure 3.5Ciii, *purple*] that were also

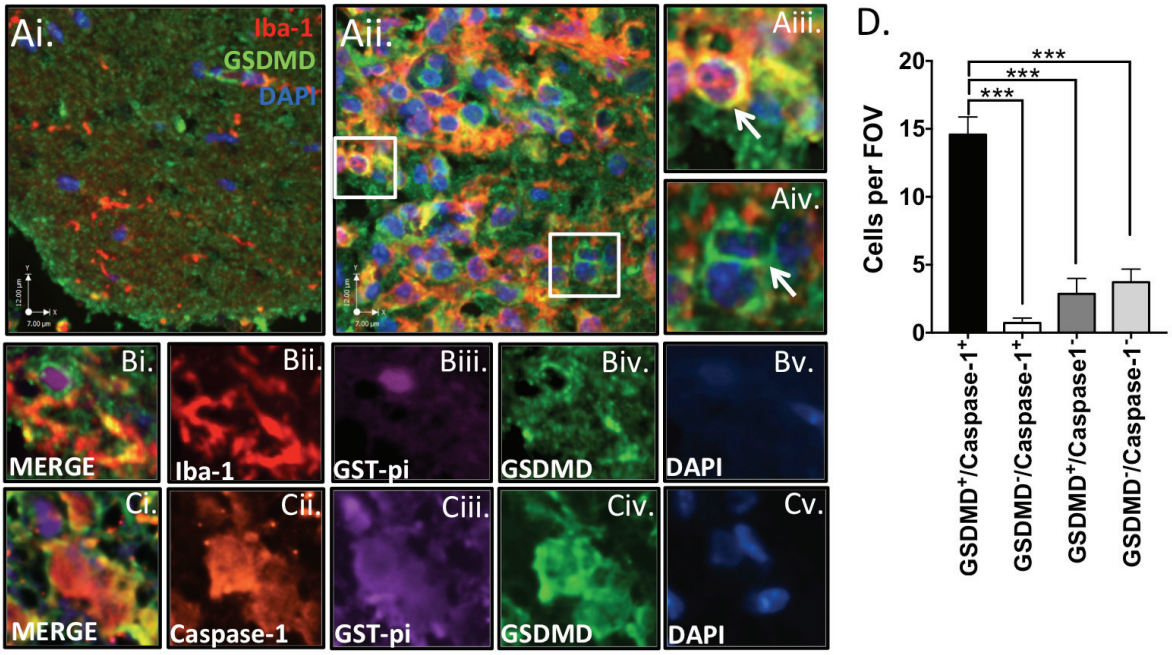

FIGURE 3.5: ***GSDMD is expressed in macrophages/microglia and ODCs in EAE spinal cord lesions.***

(A) IF of EAE lumbar spinal cord tissue at peak disease (Day 20) was performed to assess cellular localization of GSDMD (*green*) compared to Iba-1 (*red*) within active lesions. While CFA-exposed control animals demonstrated minimal immunostaining for GSDMD in the lumbar spinal cord white matter (**Ai**, *green*) and only trace numbers of Iba-1-positive cells (**Ai**, *red*), EAE peak disease animals (**Aii**) demonstrated intense GSDMD immunostaining and a profound increase in Iba-1-positive cells in spinal cord lesions. GSDMD immunoreactivity was observed in many Iba-1-positive cells (**Aiii**, overlap appears *yellow*) but other GSDMD-positive cells lacked Iba-1 immunostaining (**Aiv**). **(B)** IF of EAE spinal cords from peak disease animals with the ODC marker GST-pi (**Biii**, *purple*) revealed rings of GSDMD immunoreactivity (**Biv**, *green*) at the surface of ODCs within spinal cord lesions. These GSDMD$^+$ ODCs **(Bi)** were often found near activated macrophages/microglia. **(C)** IF triple-labeling of EAE spinal cords for GST-pi (**Ciii**, *purple*), GSDMD (**Civ**, *green*), and caspase-1 (**Cii**, *red*) demonstrated the presence of both pyroptosis markers within GST-pi-immunopositive cells. Scale bars represent 7μm (horizontal) and 12μm (vertical). **(D)** 150 GST-pi$^+$ ventral column ODCs from EAE animals at peak disease were classified as either double-positive (GSDMD$^+$ CASP1$^+$), single positive (GSDMD$^+$CASP1$^-$ or GSDMD$^-$ CASP1$^+$) or double-negative (GSDMD$^-$ CASP1$^-$). Cells were considered "positive" when MFI exceeded triple the background levels in a given channel. Data shown represent the mean number of double- or single-positive cells per FOV +/-SEM (1-way ANOVA with Dunnett's test for multiple comparisons, ***p<0.001).

positive for both GSDMD [Figure 3.5Civ, *green*] and caspase-1 [Figure 3.5Cii, *orange*]. We quantified the number of GSDMD$^+$/caspase-1$^+$/GST-pi$^+$ ODCs per field of view, and compared this to the number of single-positive or double-negative GST-pi$^+$ ODCs in EAE animals. We observed that the majority of GST-pi$^+$ ODCs in the ventral spinal cords from EAE animals were immunopositive for both GSDMD and caspase-1 [Figure 3.5D, $p<0.001$]. GSDMD expression was not observed in astrocytes (GFAP-labeled) or neurons (neurofilament-labeled) in the ventral columns of the lumbar spinal cord in EAE animals [Figure 3.6A, B]. Given that pyroptosis is highly proinflammatory, we hypothesized that this cell death modality would propagate the cycle of neuroinflammation in the CNS during inflammatory demyelination. This was supported by high magnification confocal microscopy [Figure 3.7A], during which we observed cells undergoing pyroptosis within spinal cord lesions (*red arrows*) that appeared to recruit and interact with GSDMD$^-$ Iba-1$^+$ reactive microglia (*green arrows*). This observation highlighted that unlike apoptosis, which has been well-characterized in MS and EAE lesions, pyroptosis is not immunologically silent.

To test the hypothesis that pyroptosis drives neuroinflammation and neuropathology in EAE, it would be ideal to target GSDMD individually; however, GSDMD knock-out mice are still not commercially available, and at the time these experiments were performed, no GSDMD inhibitors had been developed. Thus, it was not possible to selectively assess the contribution of pyroptosis to neuropathology in EAE. Instead, we sought to assess whether caspase-1 inhibition generally had a protective effect in the EAE model. Our strategy was to use the well-validated, clinically well-tolerated, BBB-permeable caspase-1 inhibitor, VX-765, and assess multiple endpoints, including neuroinflammation, neurobehavioural signs, and

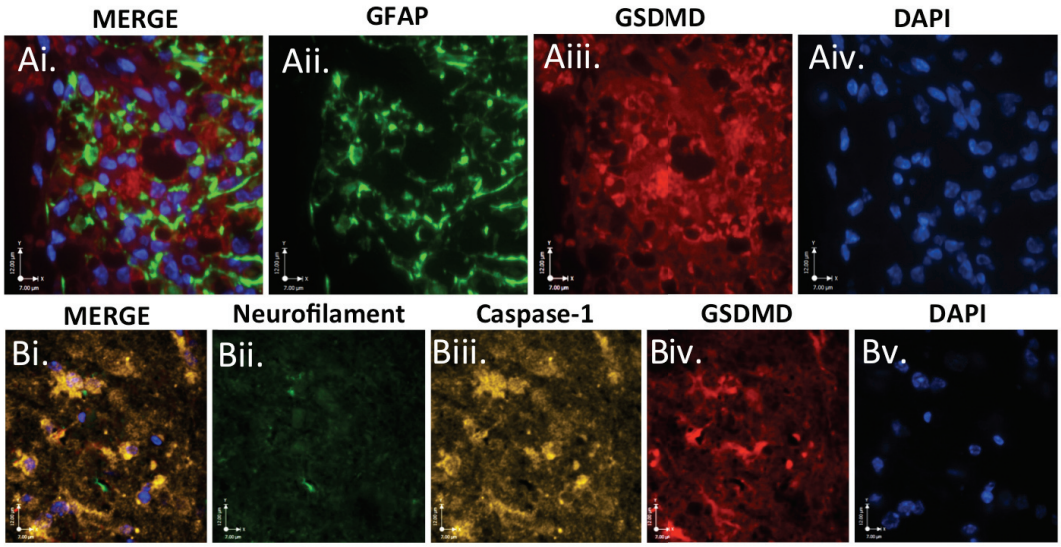

Figure 3.6: ***GSDMD is not highly expressed in astrocytes or neurons in EAE WM lesions.***

(A-B) Immunofluorescent labeling of white matter from EAE animals sacrificed at peak disease. Astrocyte marker GFAP (**Aii**, *green*) and pyroptosis marker GSDMD (**Aiii**, *red*) do not appear to co-localize within the same cells (**Ai,** *merge*). **(B)** Neuronal marker neurofilament (**Bii**, *green*) does not appear to colocalize with either caspase-1 (**Biii**, *amber*) or GSDMD (**Biv**, *red*). Horizontal scale axis represents 7μm and vertical scale axis represents 12μm.

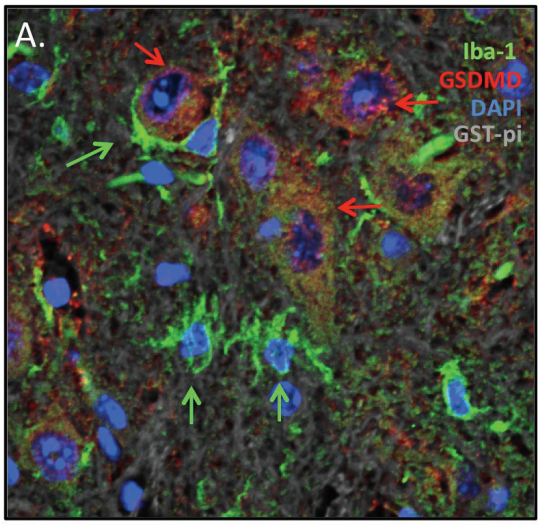

Figure 3.7: ***Macrophages/microglia detect cells undergoing pyroptosis.***

(A) High-magnification imaging of EAE lumbar spinal cord tissue at peak disease (Day 20) was performed to assess the cellular localization of GSDMD (*red*) compared to myeloid cell marker Iba-1 (*green*) and GST-pi (*grey-scale*) in the white matter. This representative image illustrates the interaction between healthy macrophages/microglia (*green arrows*; defined as strongly Iba-1^{+} with intact processes and nucleus) and cells undergoing pyroptosis (*red arrows*; defined by dysmorphic nuclei, GSDMD immunoreactivity, and moderate Iba-1 expression). Healthy intact microglia that are GSDMD^{-} are shown in close proximity to cells undergoing pyroptosis.

neurodegeneration in the CNS. Although we could not selectively inhibit GSDMD, this experimental design would allow us to determine whether upstream inhibition of caspase-1 was protective, and whether pyroptosis in the CNS could be reduced through pharmacological intervention.

This experimental design naturally comes with the caveat that caspase-1-mediated activation of other proteins, including IL-1β and IL-18, will also be inhibited by VX-765 in addition to GSDMD. While this is a clear limitation scientifically, we believe that it presents an advantage in the clinical scenario: both IL-1β and IL-18 have known pathological roles in MS/EAE, and a drug that could target these cytokines while simultaneously limiting proinflammatory cell death in the CNS would be potentially advantageous.

To recapitulate the clinical scenario as well as possible, rather than initiating VX-765 treatment at induction, treatment was delayed until after the onset of neurobehavioural signs. Thus, to determine whether VX-765 treatment influenced disease outcomes, animals with EAE were treated with VX-765 (50mg/kg IP) daily or vehicle-treated with PBS/DMSO after neurobehavioral deficits were observed (Day 12), and continued until sacrifice.

3.2.5 VX-765 reduces expression of inflammasome-associated and pyroptosis-associated proteins

Morphological analyses of spinal cords from CFA, solvent-treated EAE or VX-765-treated EAE animals at peak disease were performed by IHC and IF, concentrating on the ventral columns because they largely mediate motor functions. IHC studies revealed that

columns because they largely mediate motor functions. IHC studies revealed that parenchymal Iba-1 immunoreactivity was detected in ventral spinal cord white matter of CFA-exposed animals [Figure 3.8Ai] but was markedly increased in EAE animals [Figure 3.8Aii]. VX-765 treatment attenuated myeloid cell recruitment/activation as indicated by Iba-1 immunoreactivity [Figure 3.8Aiii]. IL-1β immunoreactivity was minimal in CFA-exposed animals [Figure 3.8Bi] and was significantly induced in EAE spinal cords [Figure 3.8Bii], compared to VX-765-treated animals [Figure 3.8Biii; $p<0.0001$, quantified in Figure 3.8E]. Caspase-1 immunoreactivity was also limited in CFA-exposed animals [Figure 3.8Ci] and increased in vehicle-treated EAE animals [Figure 3.8Cii], but again caspase-1 expression was reduced with VX-765 treatment [$p<0.0001$, quantified in Figure 3.8F]. GSDMD expression was minimal in the spinal cords of CFA-exposed animals [Figure 3.8Di] but was enhanced in the spinal cords of EAE animals. Notably, cells displayed a rim of GSDMD immunoreactivity at the plasma membrane [Figure 3.8Dii *inset*], consistent with pyroptosis. VX-765 treatment suppressed GSDMD immunoreactivity in spinal cords from EAE animals [Figure 3.8Diii; $p<0.0001$, quantified in Figure 3.8G].

3.2.6 VX-765 treatment diminishes pyroptosis in microglia/macrophages and ODCs during EAE

Next, the proportions of GSDMD$^+$ microglia/macrophages and ODCs in the ventral spinal column were assessed using confocal microscopy. Similar to MS patients, EAE animals displayed a significant increase in the proportion of both Iba-1$^+$ microglia/macrophages and GST-pi$^+$ ODCs that were immunopositive for GSDMD in the ventral spinal cord, compared to CFA controls [Figure 3.9Ai-iii, $p<0.0001$]. The proportion of GSDMD$^+$ microglia/macrophages decreased significantly upon treatment with VX-765 [Figure 3.9B,

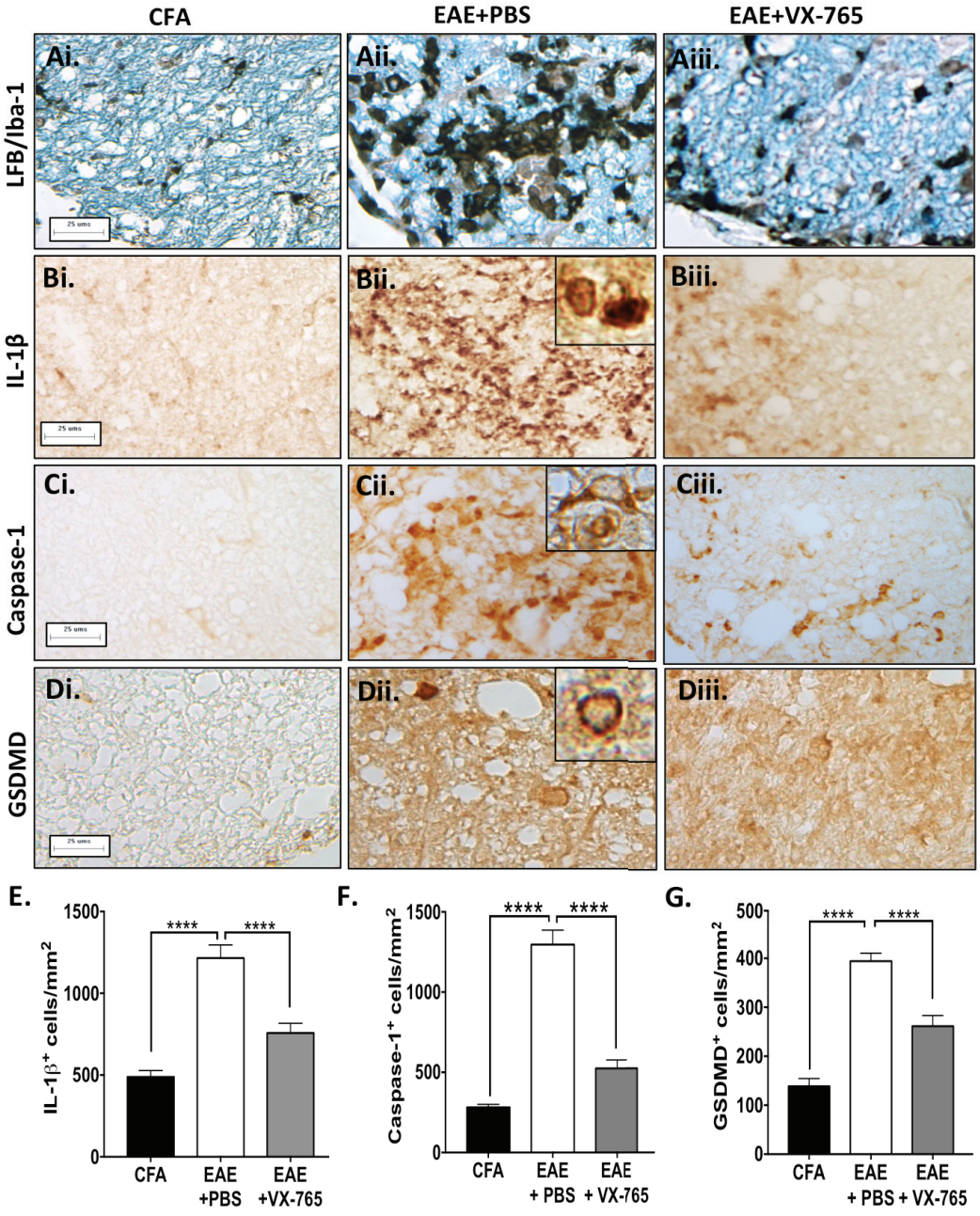

Figure 3.8 *(Figure legend on following page)*

FIGURE 3.8: ***Expression of inflammasome- and pyroptosis-associated proteins is diminished with VX-765 treatment.***

Lumbar spinal cords from control (CFA) and EAE mice treated with either vehicle (EAE+PBS) or VX-765 (EAE +VX-765) and sacrificed at peak disease were labelled with **(A)** LFB to stain myelin and Iba-1 to immunolabel macrophages/microglia **(B)** IL-1β **(C)** caspase-1 or **(D)** GSDMD. Localization of GSDMD to the plasma membrane was observed in PBS-treated animals, indicative of pyroptosis (**Dii,** *inset*). The number of **(E)** IL-1β$^+$, **(F)** caspase-1$^+$, and **(G)** GSDMD$^+$ cells in the ventral spinal column from CFA, EAE+PBS, and EAE+VX-765 animals was quantified (cells per mm^2). Immunohistochemical quantification was performed using multiple spinal cord sections from 2-3 representative animals per condition, with a minimum of ten non-overlapping fields of view (FOV) per animal. Data shown represent mean cell number per mm^2 +/- SEM (1-way ANOVA with Tukey's test for multiple comparisons, ****p<0.0001).

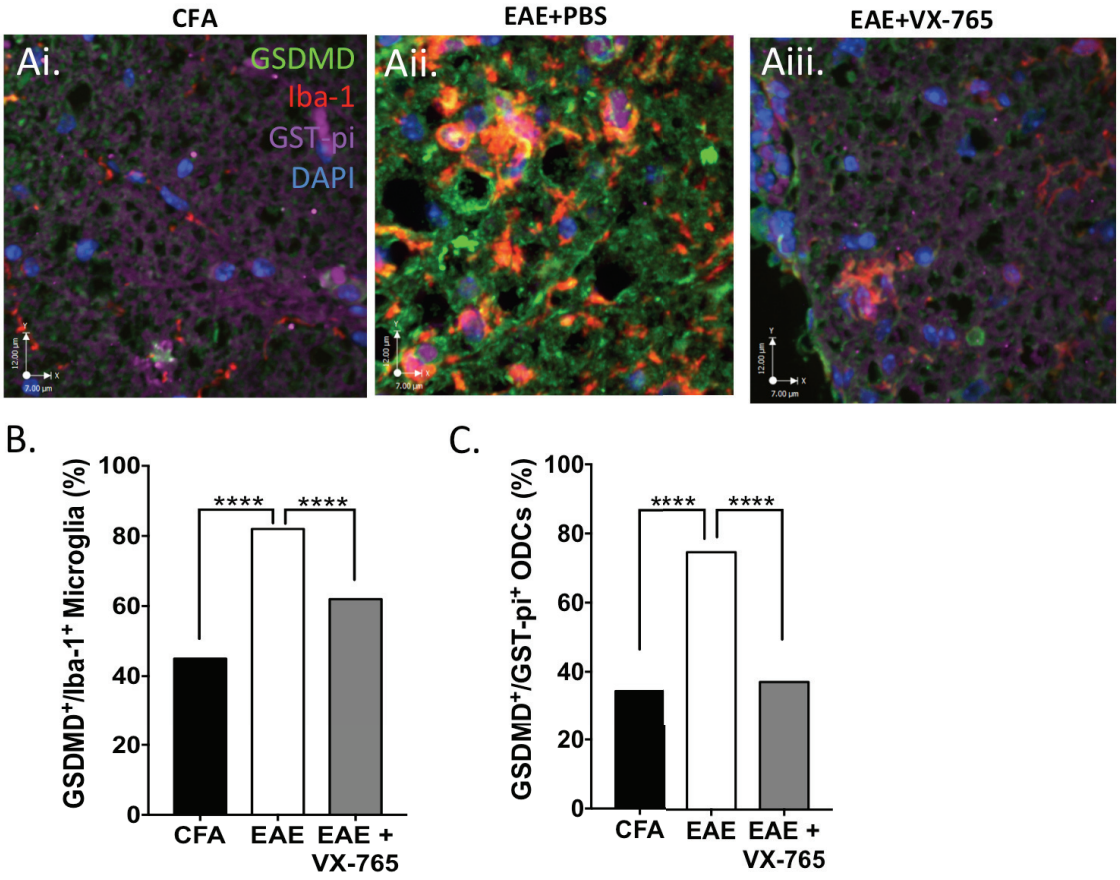

Figure 3.9: ***VX-765 treatment prevents pyroptosis in macrophages/microglia and ODCs.***

(A) Immunofluorescent triple-labeling of spinal cords from **(Ai)** CFA, **(Aii)** EAE+PBS, and **(Aiii)** EAE +VX-765 animals with the ODC marker GST-pi (*purple*), macrophage/microglia marker Iba-1 (*red*), and GSDMD (*green*). Scale bars represent 7μm (horizontal) and 12μm (vertical). **(B)** The proportion of microglia in the ventral column of the lumbar spinal cord expressing GSDMD was quantified in CFA controls, solvent-treated EAE animals, and VX-765-treated EAE animals at peak disease. Data represent the proportion of GSDMD$^+$ Iba-1$^+$ microglia (%) as a fraction of the total number of Iba-1$^+$ cells. Proportions were calculated based on analysis of up to 500 Iba-1$^+$ cells/condition, using multiple spinal cord sections from 2-3 representative animals per condition. **(C)** The proportion of ODCs in the ventral column of the lumbar spinal cord expressing GSDMD was quantified in CFA controls, solvent-treated EAE animals, and VX-765-treated EAE animals at peak disease. Data represent the proportion of GSDMD$^+$ GST-pi$^+$ ODCs (%) as a fraction of the total number of GST-pi$^+$ ODCs. Proportions were calculated based on analysis of up to 400 GSTpi$^+$ cells/condition, using multiple spinal cord sections from 2-3 representative animals per condition. Cells were considered "positive" when MFI exceeded triple the background levels in a given channel. Data were tested for significance using Chi-square test (****p<0.0001).

$p<0.0001$] while the proportion of $GSDMD^+$ ODCs fell to baseline levels [Figure 3.9C]. These data support the hypothesis that VX-765 treatment diminishes pyroptosis in multiple cell types in the CNS during EAE.

3.2.7 VX-765 treatment reduces neuroinflammation, diminishes neurodegeneration, and improves neurobehavioural outcomes

Evaluation of transcript levels in spinal cord at Day 20 post-induction revealed that *il1b* [Figure 3.10A], *nlrp3* [Figure 3.10B] and *casp1* [Figure 3.10C] were highly induced in the spinal cords of vehicle-treated EAE animals, but VX-765 treatment abrogated the induction of *nlrp3* and *casp1*. Additionally, other induced genes including *pyrin, ifng* and *tnfa* were also suppressed in VX-765-treated EAE animals [Figure 3.10D]. These data indicated that VX-765 treatment reduced the expression of several key inflammasome and inflammation-related genes in the CNS, pointing to an overall suppression of neuroinflammation.

Axonal integrity was assessed by Bielchowsky silver staining in ventral columns of spinal cords from CFA, EAE + PBS, and EAE + VX-765 treatment groups. Densely stained silver-positive axons were observed in the CFA-exposed animals [Figure 3.10E] while fewer silver-positive axons were detected in the EAE group [Figure 3.10F]; VX-765 treatment preserved axonal density [Figure 3.10G]. Quantification of axonal density demonstrated that vehicle-treated EAE animals had significantly fewer axons per unit area than CFA-exposed and VX-765-treated EAE animals [Figure 3.10H]. Collectively, these studies highlighted the contribution of inflammasome activation to axonal injury in EAE and highlighted a role for VX-765 in neuroprotection.

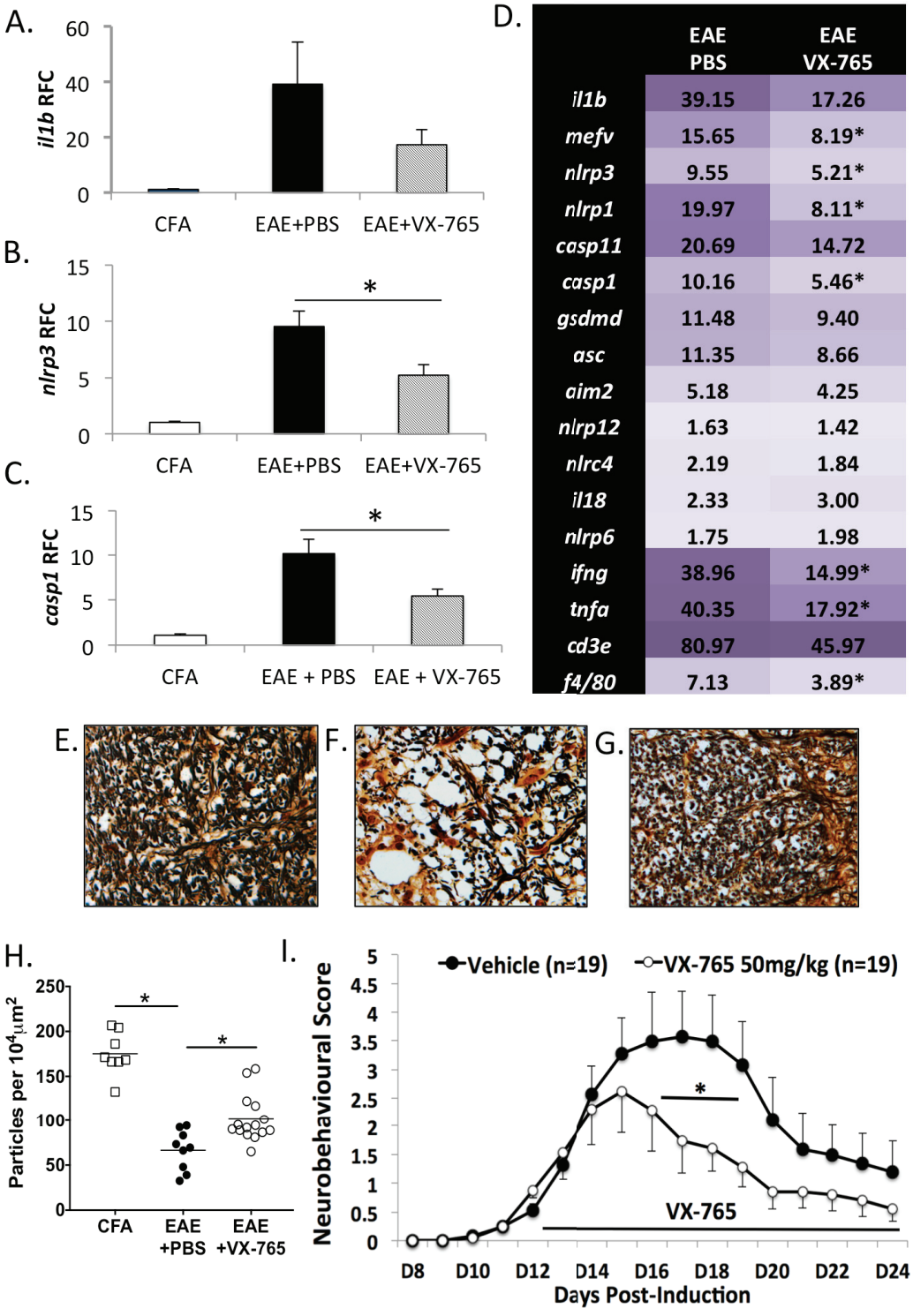

	EAE PBS	EAE VX-765
il1b	39.15	17.26
mefv	15.65	8.19*
nlrp3	9.55	5.21*
nlrp1	19.97	8.11*
casp11	20.69	14.72
casp1	10.16	5.46*
gsdmd	11.48	9.40
asc	11.35	8.66
aim2	5.18	4.25
nlrp12	1.63	1.42
nlrc4	2.19	1.84
il18	2.33	3.00
nlrp6	1.75	1.98
ifng	38.96	14.99*
tnfa	40.35	17.92*
cd3e	80.97	45.97
f4/80	7.13	3.89*

Figure 3.10 *(Figure legend on following page)*

FIGURE 3.10: ***VX-765 treatment reduces neuroinflammation, protects axons in the spinal cord, and improves neurobehavioral outcomes in EAE.***

(A) *il1b*, **(B)** *nlrp3* and **(C)** *casp1* gene expression was assessed by qRT-PCR at peak disease (Day 20 post-induction) in lumbar spinal cords of EAE animals treated with VX-765 (*n*=9) or vehicle control (*n*=9). **(D)** Heatmap of other inflammatory genes implicated in EAE pathogenesis. Values represent mean relative fold change compared to CFA controls, with threshold cycle normalized to the housekeeping gene *hprt* (*n*=6). * indicates a significant difference between VX-765- and vehicle-treated EAE animals (Student's *t*-test, *$p<0.05$). **(E-G)** Silver staining of lumbar spinal cord axons from CFA-exposed controls **(E)**, EAE+PBS mice **(F)**, and EAE+VX-765 mice **(G)** revealed a loss of axons in the ventral column of the spinal cord compared to CFA-treated controls at 24 days post-induction. VX-765 treatment resulted in the preservation of axons (*n*=2-3 animals per group, 4-5 discreet images per animal). **(H)** Quantification of axonal density was expressed as particles per 10,000μm^2 and showed axonal density was significantly reduced in PBS-treated EAE animals. This effect was partially rescued with VX-765 treatment. **(I)** Neurobehavioral signs were scored daily and VX-765 treatment was initiated after the onset of tail paralysis (Day 12). VX-765 treatment (*n*=19) reduced EAE-associated neurobehavioral deficits compared to vehicle-treated EAE animals (*n*=19) over time (one-way ANOVA; *$p<0.05$). Neurobehavioural data combines two independent EAE experiments.

In addition to the molecular and neuropathological findings indicating that inflammasome activation in EAE was suppressed by VX-765 treatment, neurobehavioral assessment permitted serial analyses of the effects of the therapeutic intervention. VX-765 treatment modestly reduced the severity of neurobehavioral deficits by Day 15 (after only 3 days of treatment) compared to vehicle-treated EAE animals, which was sustained over several time points [Figure 3.10I]. Thus, VX-765 treatment exerted some beneficial effects on EAE-associated neurobehavioral deficits, in conjunction with reduced CNS inflammasome activity. We also quantified the density of motor neurons in the ventral horn as indicated by large triangular cell bodies and prominent nucleoli [Figure 3.11B], and observed a loss of motor neurons in EAE animals at peak disease, which was prevented by VX-765 treatment [Figure 3.11C, $p<0.05$].

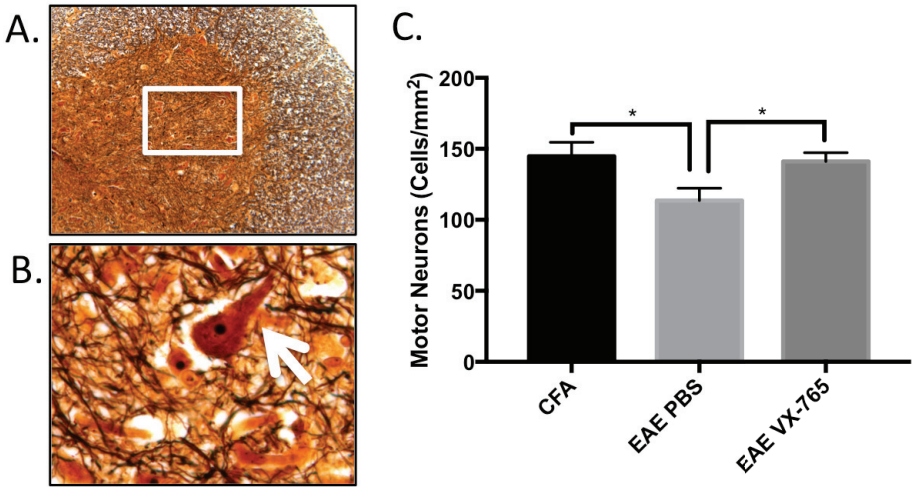

Figure 3.11: ***VX-765 rescues motor neuron loss in EAE.***

CFA and EAE animals treated with VX-765 or solvent control were sacrificed at peak disease and sections of the lumbar spinal cord stained with silver (Bielchowsky) staining. **(A-B)** Motor neurons in the ventral horn were identified visually based upon a criteria of large triangular cell body and prominent nucleolus. **(C)** Quantification of motor neuron density in different treatment groups. Data shown represent mean +/- SEM (1-way ANOVA with Tukey's test for multiple comparisons, *p<0.05).

III.III. Chapter Summary

In this chapter, multiple experimental platforms were utilized to investigate the previously unrecognized contributions of CNS inflammasome activation and pyroptosis to inflammatory demyelination. Morphological and molecular evidence of pyroptosis was observed in multiple glial cell types in both MS and EAE, indicated by GSDMD immunoreactivity and accumulation on the plasma membrane. Treatment of EAE animals with VX-765 improved multiple outcomes, including neurobehavioral performance, neuropathological severity, and molecular indicators of inflammation. Taken together, the present observations defined a distinctive CNS inflammasome profile for MS and EAE, yielded the discovery of pyroptosis in microglia/macrophages and ODCs during demyelination, and illustrated the potential therapeutic impact of caspase-1 inhibition using VX-765. Pyroptosis in myeloid cells and ODCs represents a therapeutically targetable and previously unrecognized mechanism driving neuroinflammation and neurodegeneration in MS.

Based on our findings of inflammasome activation in MS/EAE neuropathogenesis [Figure 3.12], we propose that dying ODCs release DAMPs that activate inflammasomes in resident microglia and infiltrating macrophages. These activated myeloid cells release both non-inflammasome-dependent cytokines (e.g. TNFα) and inflammasome-dependent cytokines (IL-1β and IL-18), which drive a persistent inflammatory cascade that activates infiltrating lymphocytes and also causes neuronal toxicity. A subset of microglia/macrophages also undergoes pyroptosis, which further amplifies pathology through the release of neurotoxic and inflammatory mediators (e.g. cytokines, ROS) and intracellular DAMPs, many of which have recognized off-target effects on neurons and ODCs. TNFα released from activated

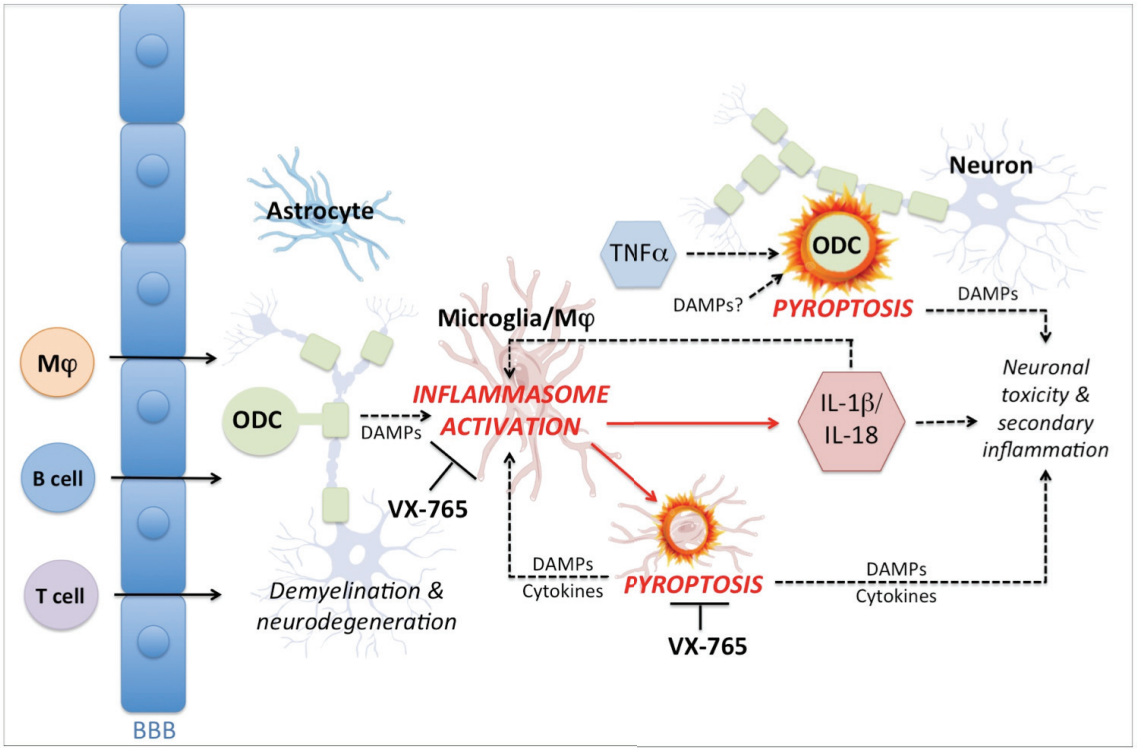

Figure 3.12: ***Schematic of inflammasome activation and pyroptosis in MS/EAE***

In MS and EAE, ODCs undergo an initial damaging event leading to demyelination/neurodegeneration, potentially driven by infiltrating peripheral immune cells, including T cells, B cells, and macrophages (Mϕ). Dying ODCs and neurons release damage-associated molecular patterns (DAMPs), putative drivers of inflammasome activation in resident microglia and infiltrating macrophages. Activated macrophages/microglia release both non-inflammasome-associated (e.g. TNFα) and inflammasome-associated cytokines (IL-1β and IL-18). Secreted IL-1β and IL-18 act in autocrine/paracrine loops to drive local inflammasome activation, activate infiltrating lymphocytes, and cause direct neuronal toxicity. Inflammasome activation drives GSDMD-mediated pyroptosis in brain myeloid cells. Pyroptosis leads to further release of DAMPs and inflammasome-associated cytokines, driving a secondary inflammatory cascade in the CNS. GSDMD upregulation and pyroptosis is also observed in ODCs, which may be driven by TNFα, putatively derived from activated microglia, or DAMPs in the local microenvironment. Although inflammasome-associated cytokines are not released from dying ODCs, pyroptosis may further exacerbate tissue damage and inflammation through direct loss of ODCs and release of proinflammatory DAMPs into the microenvironment. VX-765 directly blocks inflammasome activation through caspase-1 inhibition, thus reducing both the maturation/release of proinflammatory cytokines IL-1β and IL-18, and the maturation/activation of GSDMD. Through these actions, VX-765 reduces cytokine neurotoxicity, interrupts local inflammatory feedback loops, and prevents pyroptosis in multiple cell types, leading to tissue preservation and improved disease outcomes.

microglia/macrophages promotes GSDMD up-regulation and pyroptosis in ODCs, further exacerbating tissue loss and demyelination [TNFα-dependent pyroptosis of ODCs *in vitro* was demonstrated as part of the MSc thesis of Leina Saito in the Power lab]. We suggest that VX-765 blocks inflammasome signaling, reduces cytokine-associated neurotoxicity, and prevents GSDMD-mediated pyroptosis in both myeloid cells and mature ODC populations, leading to tissue preservation and improved disease outcome.

CHAPTER IV: MICROGLIAL PYROPTOSIS *IN VITRO*

Sections of this chapter have been published:

McKenzie, BA, Mamik MK, Saito LB, Boghozian R, Monaco MC, Major EO, Lu JQ, Branton WG, Power C. (2018) Caspase-1 inhibition prevents glial inflammasome activation and pyroptosis in models of multiple sclerosis. *PNAS*. 115 (26): E6065-E6074.

Sections of this chapter have been submitted:

McKenzie, BA, Fernandes J, Doan M, Branton WG, Power C. (2019). Caspase-3/7 drive pyroptosis in human microglia. *Submitted*.

All experiments in this chapter were designed, performed, and analyzed by Brienne McKenzie.

IV.I. Brief Introduction

CHAPTER IV OBJECTIVE:

To characterize primary human microglial pyroptosis ex vivo using well-characterized and disease-relevant NLRP3 inflammasome activating stimuli and to validate a clinically relevant inhibitor of caspase-1 in this system

In Chapter III, microglial CNS inflammasome activation and pyroptosis were established as key pathogenic features of MS/EAE, and caspase-1 inhibition with VX-765 was shown to be protective in the EAE model. In this chapter, I sought to further interrogate the mechanisms of pyroptosis in primary human microglia. Since the discovery of GSDMD (and prior to the publication of the results of this thesis[270]), no group had studied the role of GSDMD in pyroptosis in any CNS cell type in either human or mouse *in vitro* systems. Here, we used both molecular assays (LDH release, cytokine release, etc.) and semi-quantitative confocal microscopy to establish that primary human microglia undergo GSDMD-dependent, caspase-1-dependent pyroptosis in response to MS-relevant DAMPs. We validated the ability of the caspase-1 inhibitor VX-765 (used in Chapter III) to block inflammasome-associated cytokine release and pyroptosis, and used GSDMD-targeting siRNA to establish a crucial role for this protein in microglial pyroptosis. Based upon the progression of pyroptosis described in the literature, we also proposed a classification system for identifying the stages of pyroptosis in fixed populations of microglia by confocal microscopy. This allowed us to identify the stages of pyroptosis at which specific morphological and molecular changes occurred. Collectively, these observations provide a framework for a deeper investigation into previously undiscovered mechanisms driving pyroptosis in Chapter V.

CHAPTER IV Hypothesis:
Human microglia undergo inflammasome activation and pyroptosis in response to MS-relevant stimuli in vitro in a GSDMD- and caspase-1 dependent manner.

IV.II. Results

4.2.1 Human microglial pyroptosis is dependent upon caspase-1 and GSDMD

To investigate the mechanisms underpinning our *in vivo* findings, inflammasome activation and pyroptosis were assessed using cultured primary human microglia. First, microglia were exposed to the well-characterized NLRP3 inflammasome activator, nigericin, with or without the caspase-1 inhibitor, VX-765 [Figure 4.1]. Nigericin, a bacterial toxin that induces NLRP3 inflammasome activation downstream of K^+ efflux, was selected for initial characterization experiments for several reasons: (i) it has been shown to cause both inflammasome activation and pyroptosis in many cell types including microglia[261] (ii) nigericin is a specific inducer of the NLRP3 inflammasome, the major sensor for a diverse range of CNS-relevant and MS-relevant DAMPs upstream of inflammasome activation, and (iii) NLRP3 emerged in both MS and EAE as an inflammasome of interest (Chapter III).

Using semi-quantitative confocal microscopy, I characterized the molecular features of microglial pyroptosis following nigericin exposure (4hr, 5μM). Nigericin-exposed microglia demonstrated a distinctive pyroptotic phenotype [Figure 4.1Bi], defined by a rounded morphology, loss of processes, intracellular GSDMD and IL1β immunoreactivity, and localization of GSDMD to the plasma membrane, often within local protrusions (pyroptotic bodies) [Figure 4.1Bi, *white arrows*]. Upon nigericin

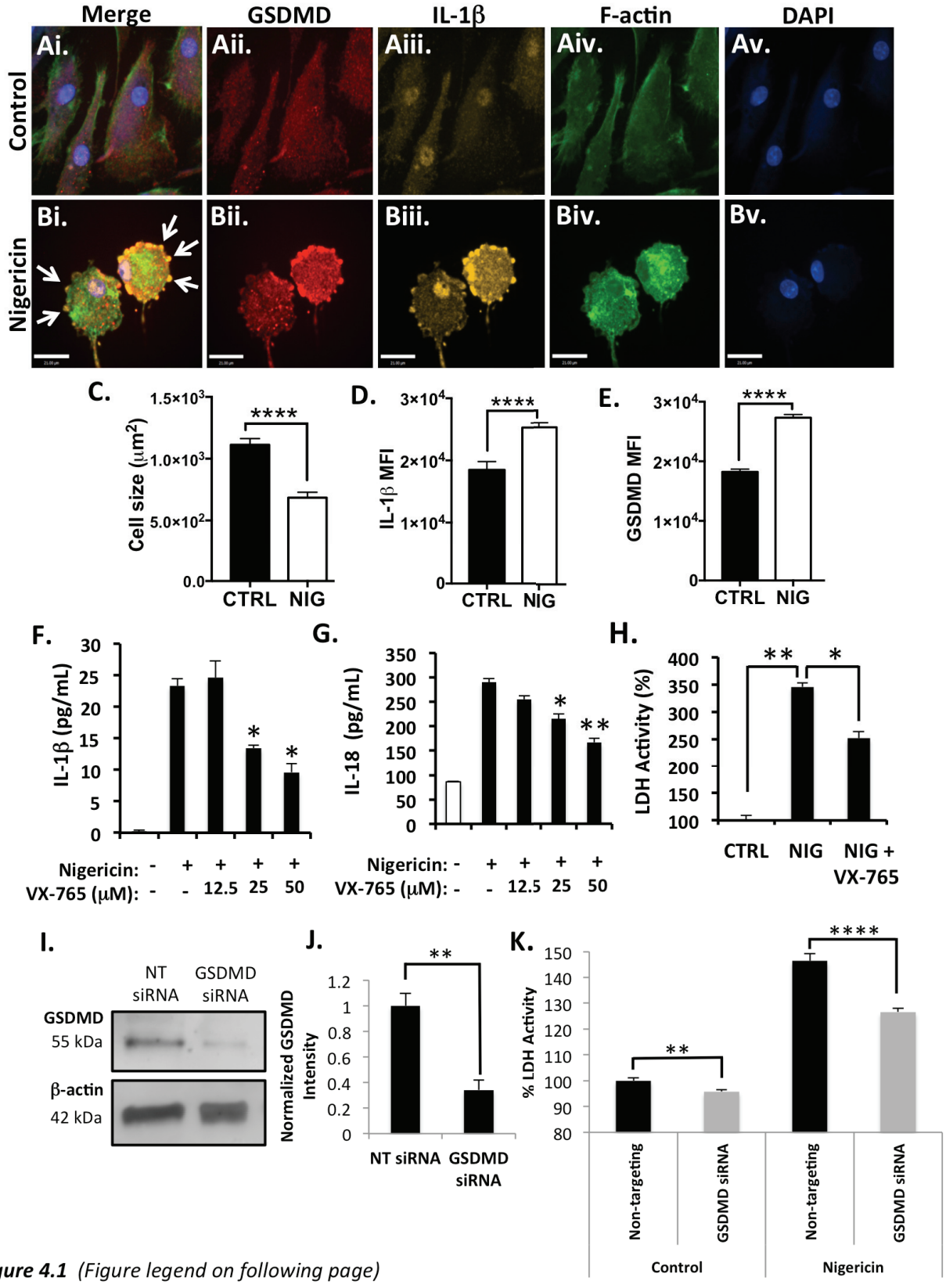

Figure 4.1 *(Figure legend on following page)*

FIGURE 4.1: ***Nigericin-induced pyroptosis in human microglia is both caspase-1- and GSDMD-dependent.***

Human microglia were exposed to nigericin (5μM, 4 hr), +/- VX-765 (50μM, 4hr pre-treatment) or solvent control. Control **(A)** and nigericin-treated **(B)** microglia were immunolabelled for GSDMD **(Aii, Bii)** and IL-1β **(Aiii, Biii)**, and labelled for F-actin **(Aiv, Biv)**. Nigericin-treated microglia undergoing pyroptosis display the prototypic phenotype, characterized by a rounded cell body, retraction of processes, high GSDMD and IL-1β expression, and formation of $GSDMD^+$ $IL\text{-}1\beta^+$ pyroptotic bodies on the cell membrane (*white arrows*, **Bi**). Scale bar represents 23μm. **(C)** Cell size (μm^2) was quantified for 100-150 individual microglia per condition. Data shown represent mean +/- SEM and incorporate measurements from two biological donors. To quantify induction of pyroptosis-associated proteins, IL-1β **(D)** and GSDMD **(E)** mean fluorescence intensity (MFI) was assessed for 100-150 microglia per condition. Data shown represent mean +/- SEM and incorporate measurements from two biological donors (****p<0.0001). **(F)** ELISA measurements of IL-1β **(F)** and IL-18 **(G)** in supernatant from nigericin-exposed microglia demonstrated a VX-765-concentration-dependent decrease in cytokine release 24hr post-exposure. Data represent mean cytokine levels +/- SEM, and were tested for significance using Student's *t*-test (*p<0.05, **p<0.01, ***p<0.001). ELISAs were performed with technical replicates of 4-6 wells/condition and data replicated in a minimum of three unique donor samples (representative microglial donor shown). **(H)** Loss of cell membrane integrity was assessed using an LDH activity assay. Nigericin-exposed microglia (5μM, 24hr) displayed a significant increase in supernatant LDH activity relative to control cells, while pre-treatment with VX-765 (50μM, 4hr) significantly reduced LDH activity (Student's *t*-test, (*p<0.05, **p<0.01). LDH assays were performed with technical replicates of 3-6 wells/condition and data replicated in a minimum of three unique donor samples (representative microglial donor shown). **(I)** Human microglia were transfected with either non-targeting siRNA (NT siRNA) or three pooled GSDMD-targeting siRNAs (GSDMD siRNA) for 48hrs. Protein was extracted, pooled, and GSDMD expression assessed by immunoblot. **(J)** Average GSDMD intensity from four unique donors was assessed by immunoblot, normalized to β-actin, and expressed relative to NT siRNA controls. Data shown represent mean +/- SEM, Student's *t*-test (**p<0.01). **(K)** Human microglia were transfected with either NT or GSDMD-targeting siRNAs for 48hrs then exposed to nigericin (5μM, 24hrs). Supernatant LDH activity (expressed as percent of untreated NT siRNA-transfected controls) was assessed (ANOVA with Tukey's test for multiple comparisons, **p<0.01, ****p<0.0001). Data were replicated in microglia derived from three independent donors, representative donor shown.

exposure, cell size also decreased significantly [Figure 4.1C, $p<0.0001$], which was accompanied by a significant increase in both IL-1β and GSDMD immunoreactivity [Figure 4.1D, E, $p<0.0001$]. Release of IL-1β [Figure 4.1F] and IL-18 [Figure 4.1G] was also quantified following exposure to nigericin, and release of both cytokines was significantly reduced by VX-765 pre-treatment in a concentration-dependent manner. To quantify the loss of plasma membrane integrity during pyroptosis, LDH activity was measured in cell culture supernatants, indicating extravasation of cellular contents caused by membrane rupture during pyroptosis. Nigericin exposure significantly increased LDH release from microglia, while VX-765 treatment significantly reduced its release in nigericin-exposed cells [Figure 4.1H]. To verify GSDMD involvement in pyroptotic cell death, microglia were transfected with a cocktail of three GSDMD-targeting siRNAs or a universal non-targeting siRNA (NT siRNA). An average knockdown of 70% was achieved over multiple biological replicates, as measured by Western blot of GSDMD immunoreactivity [Figure 4.1I, J]. This knockdown was sufficient to cause a robust and significant ($p<0.0001$) decrease in LDH release in nigericin-exposed GSDMD-knockdown microglia, compared to microglia transfected with non-targeting siRNA [Figure 4.1K], verifying the role of GSDMD in microglial pyroptosis.

4.2.2 Nigericin-induced pyroptosis does not up-regulate GSDMD transcript

Given the increase in GSDMD immunoreactivity during pyroptosis, we sought to assess whether transcriptional up-regulation of GSDMD was also associated with pyroptosis. Following nigericin exposure, microglial transcript levels of *GSDMD* and other

inflammasome genes were assessed by qRT-PCR [Figure 4.2A-H]. At 4hr post-exposure, transcript levels of *GSDMD* and *NLRP3* had decreased significantly, while transcript levels of *CASP1*, *ASC*, *CASP4*, and *AIM2* were unchanged. Of the inflammasome-associated cytokines, *IL1B* transcript was significantly up-regulated but *IL18* was unchanged. These data suggest that pyroptosis does not involve transcriptional up-regulation of GSDMD or other structural inflammasome components, with the caveat that transcriptional inhibition was not explicitly tested in this system.

4.2.3 Exogenous IL-1β alone does not cause pyroptosis

While nigericin is an excellent experimental tool for assessing pyroptosis, we also sought to assess the relevance of MS-relevant DAMPs and cytokines to microglial pyroptosis. As reported in the literature and confirmed in Chapter III, IL-1β is highly up-regulated in the CNS in MS and EAE, and also serves as a well-documented priming stimulus in inflammasome activation. However, no role in pyroptosis has been observed. As expected, exposure of human microglia to exogenous IL-1β did not cause rounding, loss of processes, GSDMD accumulation at the cell periphery, or pyroptotic bodies [Figure 4.3 A, B]. IL-1β exposure caused a modest decrease in cell size [Figure 4.3C], combined with a significant increase in intracellular IL-1β immunoreactivity [Figure 4.3D] and a modest but significant increase in intracellular GSDMD [Figure 4.3E]. However, these changes were not accompanied by an increase in supernatant LDH activity [Figure 4.3F] indicative of membrane rupture, or reduction in the metabolic activity/viability of the cell as indicated by Alamar Blue™ [Figure 4.3G]. Combined with the lack of GSDMD translocation to the cell membrane or formation of

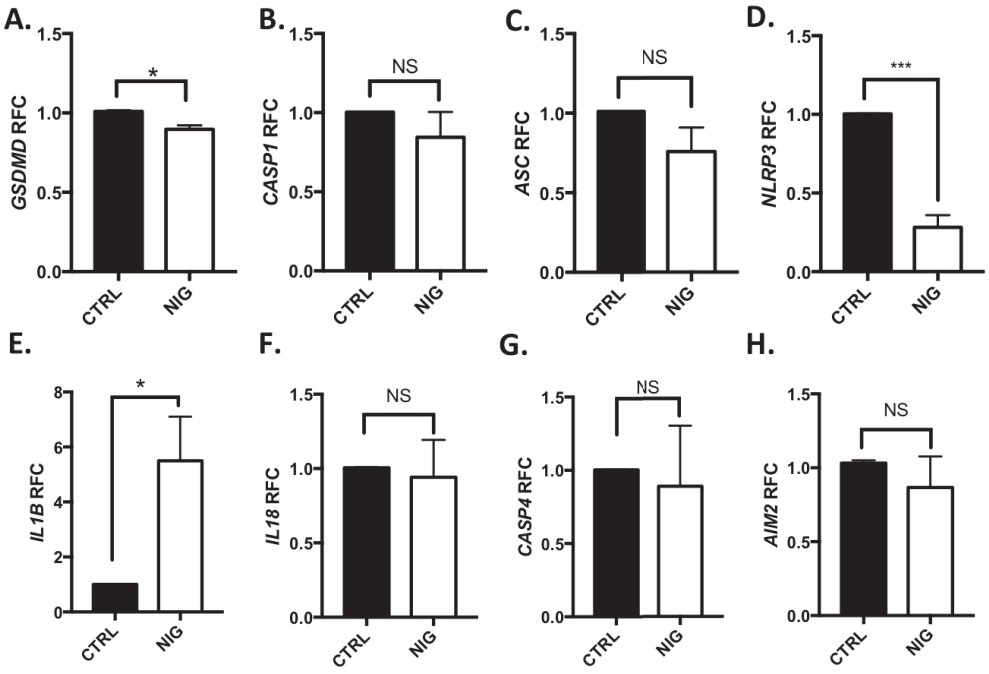

Figure 4.2: ***Microglial pyroptosis does not involve transcriptional up-regulation of GSDMD or structural inflammasome components.***

Microglia were treated with nigericin (5μM, 4hrs) or solvent and transcript levels of **(A)** *GSDMD* **(B)** *CASP1* **(C)** *ASC* **(D)** *NLRP3* **(E)** *IL1B* **(F)** *IL18* **(G)** *CASP4* and **(H)** *AIM2* were assessed by qRT-PCR. Values represent mean relative fold change (RFC) compared to solvent-treated controls, with threshold cycle normalized to the housekeeping gene *GAPDH.* Data shown are mean RFC +/- SEM for microglia derived from 3-4 separate donors (Student's *t*-test, **p*<0.05, ****p*<0.001, NS = not significant).

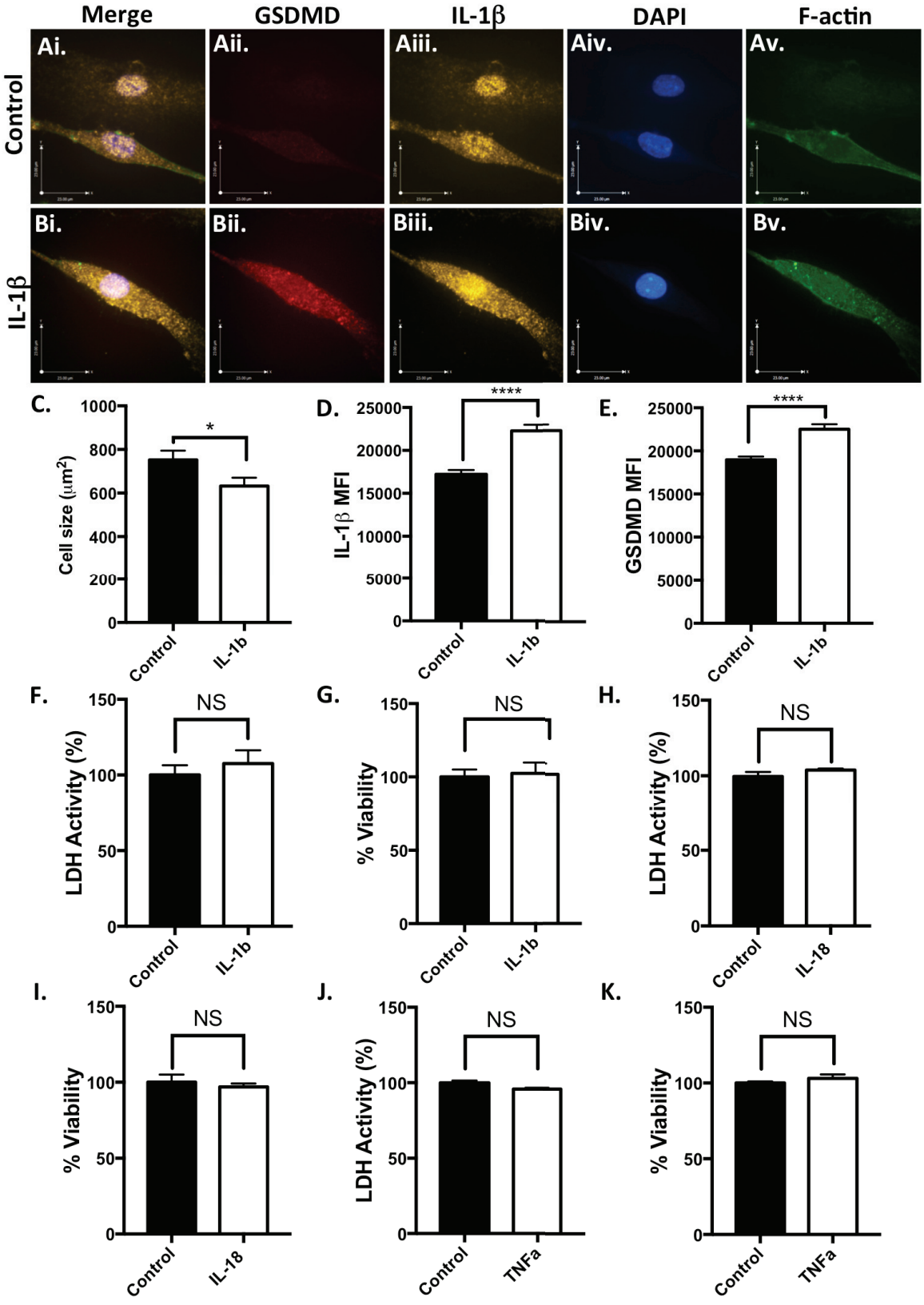

Figure 4.3 *(Figure legend on following page)*

FIGURE 4.3: ***Exogenous IL-1β does not cause pyroptosis.***

Human microglia were exposed to exogenous human IL-1β (25 ng/mL) for 24hr. Controls were treated with equivalent volumes of PBS. Control **(A)** and IL-1β-exposed **(B)** microglia were immunolabelled for GSDMD (*red*, **Aii**, **Bii**) and IL-1β (*amber*, **Aiii**, **Biii**), and labelled for F-actin (*green*, **Av**, **Bv**). IL-1β-treated microglia do not display a rounded pyroptotic phenotype or $GSDMD^+$ $IL\text{-}1\beta^+$ pyroptotic bodies on the cell membrane. Scale bar represents 23μm. **(C)** Cell size (μm^2) was quantified for 70-80 individual microglia per condition. Data shown represent mean +/- SEM. IL-1β **(D)** and GSDMD **(E)** mean fluorescence intensity was assessed for 70-80 individual microglia per condition. Data shown represent mean +/- SEM (**p*<0.05, *****p*<0.0001). **(F)** Loss of cell membrane integrity was assessed using an LDH activity assay. IL-1β-exposed microglia displayed no change in supernatant LDH activity (Student's *t*-test, NS = non-significant). **(G)** Cell viability/metabolic activity was measured using Alamar Blue™ assay. Microglia displayed no loss of viability in response to exogenous IL-1β (Student's *t*-test, NS = non-significant). LDH and Alamar Blue™ assays were performed with technical replicates of 8 wells/condition and data replicated in 2-3 unique donor samples, representative microglial donor shown. **(H-I)** Microglia were treated with exogenous human IL-18 (25 ng/mL) or solvent control and LDH activity **(H)** and cell viability **(I)** were assessed (NS = non-significant, Student's *t*-test). **(J-K)** Microglia were treated with exogenous TNFα (50ng/mL) or solvent control, and LDH activity **(J)** and cell viability **(K)** were assessed (Student's *t*-test, NS = non-significant). Data shown represent mean +/- SEM. LDH and Alamar Blue™ assays were performed with technical replicates of 4-8 wells/condition and data replicated in microglia derived from 2-3 independent donors, representative microglial donor shown.

pyroptotic bodies, these data confirm that pyroptosis does not occur in IL-1β-exposed microglia. Similar results were obtained when microglia were exposed to either exogenous IL-18 [Figure 4.3H, I] or TNFα [Figure 4.3J, K], suggesting that these cytokines individually are not major drivers of pyroptosis, despite being up-regulated in the CNS during MS and EAE.

4.2.4 Exogenous ATP drives pyroptosis in human microglia

Extracellular ATP has been shown to drive neuropathology in EAE through the P2X7 receptor, and is a well-documented driver of pyroptosis in multiple systems. Cultured microglia were exposed to extracellular phosphatase-resistant ATP (100μM, 24hr) and assessed for morphological and molecular indicators of pyroptosis. Like nigericin-exposed microglia, ATP-exposed microglia demonstrated a prototypic pyroptosis phenotype, including formation of pyroptotic bodies [Figure 4.4A, B, *white arrows*]. Exposure to ATP caused cellular rounding and shrinkage [Figure 4.4C, $p<0.0001$] as well as an increase in both IL-1β and GSDMD intracellular immunoreactivity [Figure 4.4D, E, $p<0.0001$]. ATP-induced IL-1β release and LDH release was significantly reduced by VX-765 pre-treatment [Figure 4.4F, G, $p<0.0001$]. These observations indicated that VX-765 was an effective inhibitor of inflammasome activation and pyroptosis in microglia in response to MS- and EAE-relevant stimuli. To assess whether GSDMD was important in ATP-induced microglial pyroptosis, microglia were transfected with a cocktail of three GSDMD-targeting siRNAs or a universal non-targeting (NT) siRNA and exposed to ATP. LDH release was significantly reduced in GSDMD siRNA-transfected ATP-exposed

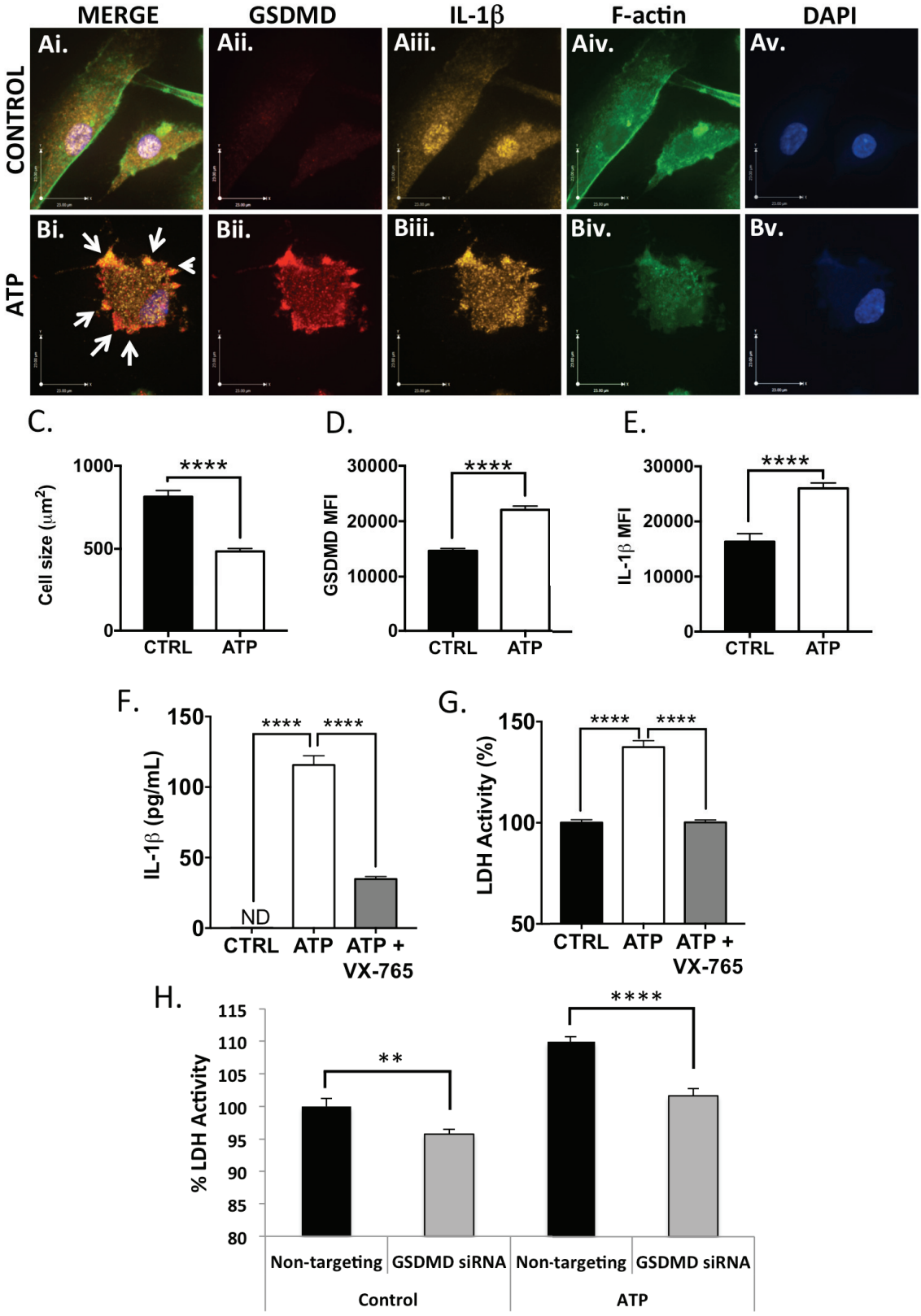

Figure 4.4 *(Figure legend on following page)*

FIGURE 4.4: ***ATP-induced pyroptosis in human microglia is caspase-1- and GSDMD-dependent.***

Human microglia were exposed to exogenous ATP (100μM, 24hrs) +/- VX-765 (50μM, 4hr pre-treatment) or solvent control. Control **(A)** and ATP-exposed **(B)** microglia were immunolabelled for GSDMD (*red*, **Aii, Bii**) and IL-1β (*amber*, **Aiii, Biii**), and labelled for F-actin (*green*, **Aiv, Biv**). ATP-treated microglia undergoing pyroptosis display the pyroptotic phenotype, characterized by a rounded cell body, retraction of processes, high levels of GSDMD and IL-1β immunoreactivity relative to controls, and the formation of $GSDMD^+$ $IL\text{-}1\beta^+$ pyroptotic bodies on the cell membrane (*white arrows*, **Bi**). Scale bar represents 23μm. **(C)** Cell size (μm^2) was quantified for 80-150 individual microglia per condition. Data shown represent mean +/- SEM. To quantify the induction of pyroptosis-associated proteins, GSDMD **(D)** and IL-1β **(E)** mean fluorescence intensity was assessed for 80-150 individual microglia per condition. Data shown represent mean +/- SEM (****p<0.0001). **(F)** ELISA measurements of IL-1β in supernatant from ATP-exposed microglia (100μM ATP, 24hr) demonstrated a significant increase in cytokine release following ATP exposure, which is rescued by VX-765 treatment. Data represent mean cytokine levels +/- SEM, and were tested for significance using 1-way ANOVA (****p<0.0001). ELISAs were performed with technical replicates of 4-6 wells/condition and data replicated in a minimum of three unique donor samples. **(G)** Loss of cell membrane integrity was assessed using an LDH activity assay (1-way ANOVA, ****p<0.0001). LDH assays were performed with technical replicates of 6-12 wells/condition and data replicated in microglia derived from a minimum of three independent donors. **(H)** GSDMD siRNA or non-targeting (NT) siRNA-transfected cells were exposed to ATP (100μM, 24hr) and supernatant LDH activity assessed (1-way ANOVA with Tukey's test for multiple comparisons, **p<0.01, ****p<0.0001).

microglia [Figure 4.4H, $p<0.0001$], indicating a functional role for GSDMD in ATP-induced microglial pyroptosis.

4.2.5 The morphological and molecular characteristics of nigericin-exposed microglia recapitulate the stages of pyroptosis identified in the literature

As discussed in Chapter I, different stages of pyroptosis have been identified in the literature using a combination of scanning electron microscopy and live cell imaging. Exposure of macrophages to pyroptosis-inducing stimuli has been shown to cause a distinctive enrichment of GSDMD immunoreactivity at the plasma membrane prior to the formation of pyroptotic bodies[167]. In the later stages of pyroptosis, the cell membrane ruptures, leaving a relatively intact nucleus and diffuse GSDMD-immunopositive cellular debris[167]. Live cell imaging has recapitulated these findings, demonstrating that diffuse cytoplasmic GSDMD immunoreactivity gives way to localized aggregates of GSDMD at the plasma membrane, and this plasma membrane localization corresponds to the appearance of pyroptotic bodies[177]. Examples of nigericin-treated microglia that recapitulate these features can be observed, including GSDMD enrichment along the membrane [Figure 4.5Bi-Bv], formation of pyroptotic bodies [Figure 4.5Ci-Cv, *white arrows*], and GSDMD$^+$ cellular debris [Figure 4.5Di-Dv].

4.2.6 Development of a classification paradigm for the stages of pyroptosis

Based upon the known mechanisms and features of GSDMD-dependent cell death described above, I proposed a classification paradigm involving distinctive stages of pyroptosis that allowed us to profile a population of fixed cells at a given time point

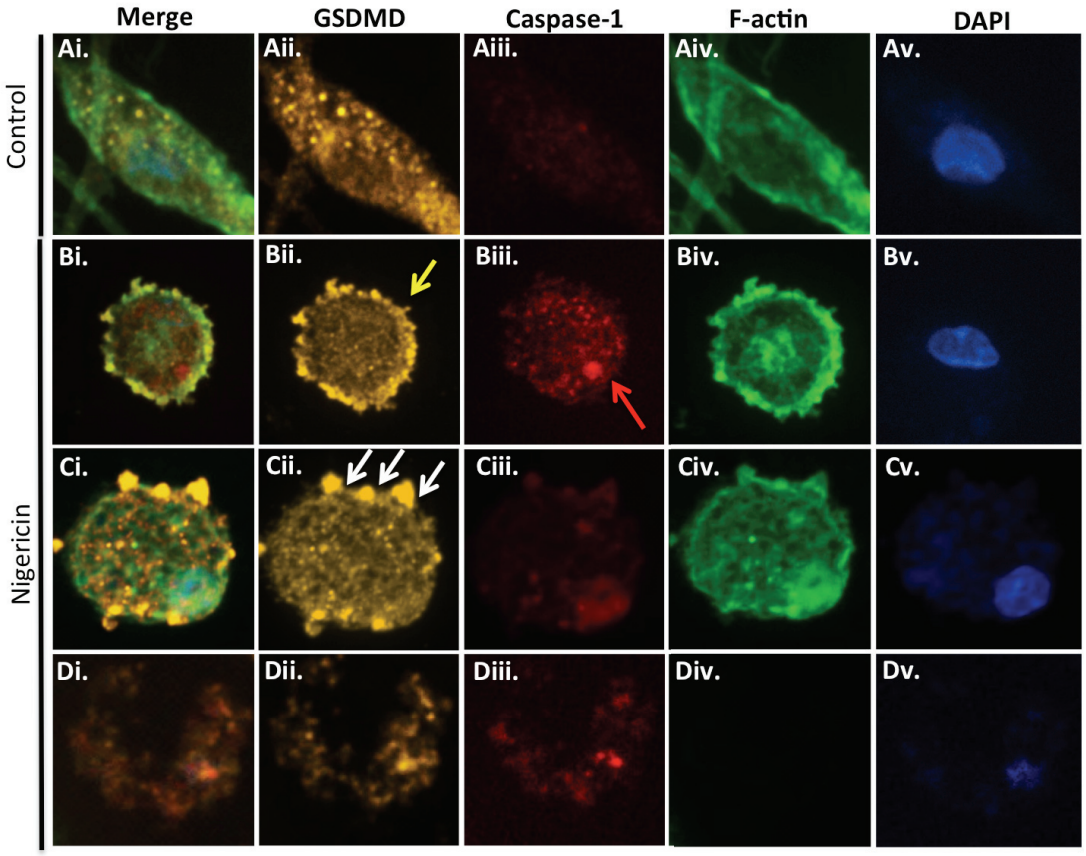

FIGURE 4.5: ***Different stages of pyroptosis in fixed human microglia in vitro***

Human microglia were exposed to PBS **(A)** or nigericin (5μM, 24hr) **(B-D)**. Control and nigericin-treated microglia were immunolabelled for GSDMD (*amber*) and caspase-1 (*red*), and labelled for F-actin (*green*) and DAPI (*blue*). Nigericin-treated microglia undergoing pyroptosis display the pyroptotic phenotype, characterized by a rounded phenotype, retraction of processes, and high levels of GSDMD immunoreactivity at the cell periphery (**Bii**, *yellow arrow*) and in pyroptotic bodies (**Cii**, *white arrows*) accompanied by caspase-1 immunopositive foci (**Biii**, *red arrow*). A proportion of nigericin-exposed microglia **(D)** reach a lytic stage, characterized by loss of F-actin staining, diffuse GSDMD immunopositive cellular debris, and nuclear disintegration. Sample cells from a representative microglial donor shown.

[Figure 4.6A]. The stages were: STAGE 0: “intact” (adherent cell with elongated processes, baseline GSDMD expression); STAGE 1: “rounding” (rounded cell, loss of processes, high GSDMD expression); STAGE 2: “ring of fire” (translocation of GSDMD to the cell membrane); STAGE 3: “pyroptotic bodies” (formation of $GSDMD^+$ membrane blebs); STAGE 4: “lysis” (rupture of the cell, nucleus intact), and finally STAGE 5: “ghost cells” (nucleus disintegrated, some $GSDMD^+$ cell contents remain).

Because the population of microglia is fixed at a given time point, and thus no single microglia is tracked longitudinally in real time, a few caveats are worth mentioning. Stage 1 microglia are rounded and lose their processes, a morphology that is consistent with microglial activation; although it has been observed prior to pyroptosis by live cell imaging, this rounded morphology is not unique to pyroptosis and thus it is conceptualized in this framework as a pre-pyroptotic activation stage. By contrast, Stages 2 and 3 display unequivocal morphological features of GSDMD-dependent pyroptosis, including the accumulation of GSDMD at the cell membrane and the formation of highly GSDMD immunopositive pyroptotic bodies. No other cell death sub-routine documented to date includes these features. Thus, by studying the molecular features of Stage 2 and 3 cells, we can make conclusions about individual cells that are unequivocally undergoing pyroptosis. Stage 4 is a lytic phenotype, which again has been observed following pyroptotic body rupture by live cell imaging; nonetheless, other lytic cell death sub-routines exist and thus it is not possible to ascertain that a given cell at Stage 4 died by pyroptosis. Stage 5, which is simply the cellular corpse, likewise is not unique to pyroptosis and may include necrotic cells as well.

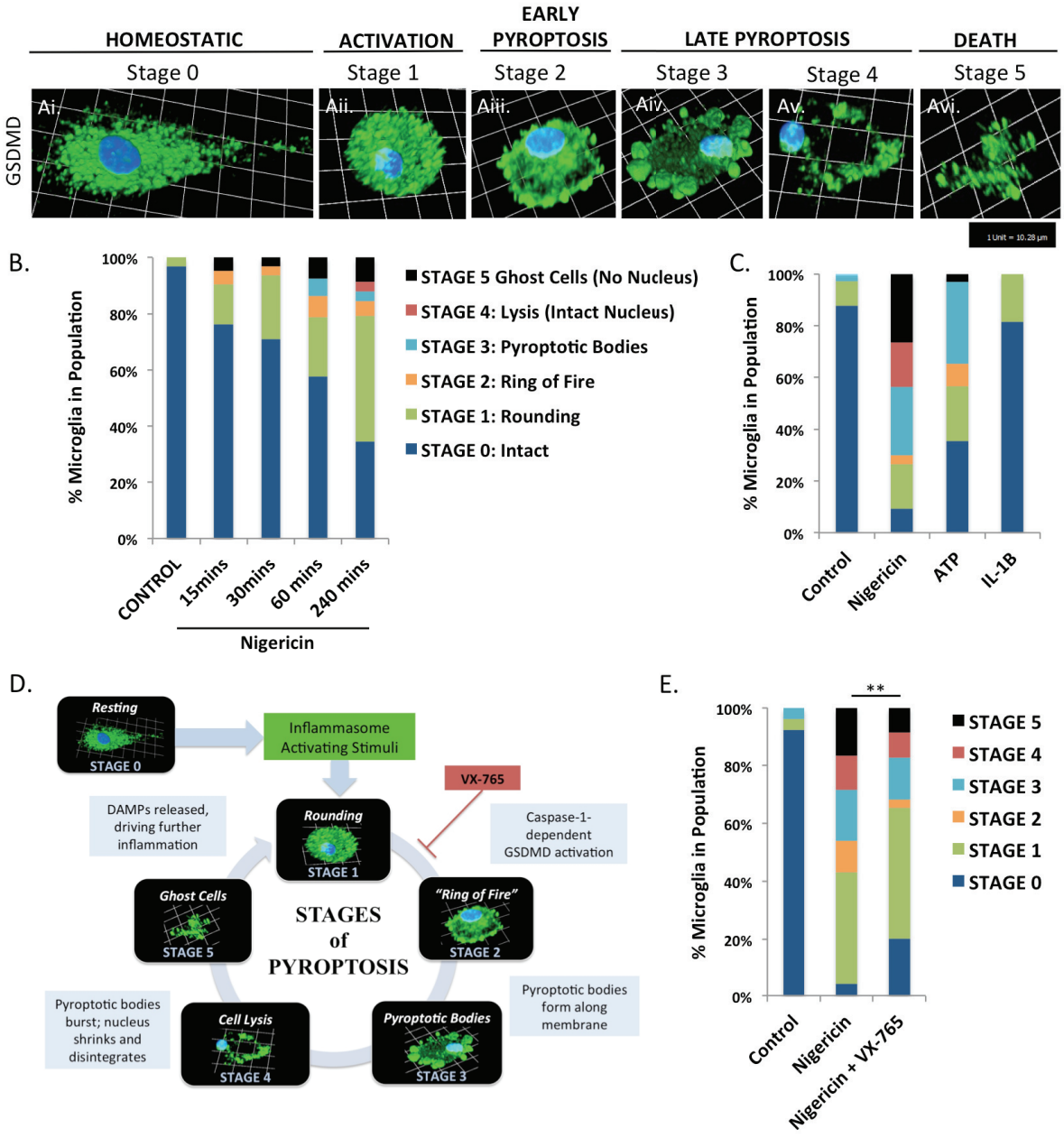

Figure 4.6 *(Figure legend on following page)*

Figure 4.6: ***Classification paradigm for quantifying stages of pyroptosis by confocal microscopy using morphological and molecular criteria***

(A) Microglia were exposed to nigericin (5μM, 4hrs), fixed, and immunolabelled for GSDMD (**Ai-vi,** *green*) and visualized using confocal microscopy. Based upon morphological and molecular characteristics, five stages of pyroptosis were defined, including **STAGE 0: "***Intact"* (adherent cell with elongated processes, baseline GSDMD expression); **STAGE 1: "***Rounding"* (rounded cell, loss of processes, increased GSDMD expression throughout the cell); **STAGE 2*: "****Ring of fire"* (translocation of GSDMD to the cell periphery); **STAGE 3**: "*Pyroptotic bodies*" (formation of $GSDMD^+$ membrane blebs); **STAGE 4**: "*Lysis"* (rupture of the cell, nucleus still intact), and finally **STAGE 5: "***Ghost cells"* (nucleus disintegrated, residual $GSDMD^+$ cell debris). Images shown for each stage are representative 3-dimensional z-stacks incorporating 15 XY planes over a vertical distance of 4-6 μm. 1 square unit represents 10.28μm. **(B)** Human microglia were exposed to nigericin (5μM, 15, 30, 60, 240 mins), fixed, and immunolabelled for GSDMD. Each cell was classified by stage (0-5) of pyroptosis. Proportion of microglia at each stage of pyroptosis is shown, with a minimum of *n*=30 cells per time point. **(C)** Human microglia were exposed to nigericin (5μM, 24hrs), ATP (1μm, 24hrs), or IL-1β (25ng/mL, 24hrs), fixed, and immunolabelled for GSDMD. Each cell was classified by stage (0-5) of pyroptosis. Proportion of microglia at each stage is shown, with a minimum of *n*=50 cells per condition. **(D)** Schematic showing stages of pyroptosis and predicted action of VX-765 **(E)** Human microglia were exposed to nigericin (5μM, 4hrs) +/- VX-765 (50μM, 4 hrs pre-treatment), fixed, and immunolabelled for GSDMD. Each cell was classified by stage (0-5) of pyroptosis. Proportion of microglia at each stage of pyroptosis is shown, with a minimum of *n*=20 cells for controls and *n*=100 cells per treatment condition. Distribution of cells across the stages was significantly different in VX-765-pre-treated microglia using Chi-square test. All results shown are from a representative human donor and were replicated in microglia derived from 2-4 independent donors (**p<0.01).

To further characterize microglia at different stages of pyroptosis, we profiled populations of fixed microglia following nigericin exposure [Figure 4.6B] and illustrated the sequential appearance first of "rounded" (STAGE 1) and "ring of fire" (STAGE 2) phenotypes starting at 15min post-exposure, followed by "pyroptotic bodies" (STAGE 3) and "lysis" (STAGE 4) at 1hr post-exposure. The proportion of cells in mid- and late-stage pyroptosis increased progressively over time. As expected, at 24hrs post-exposure, both ATP and nigericin-treated populations contained a substantial number of cells in early- and late-stage pyroptosis [Figure 4.6C]. Conversely, microglia exposed to IL-1β remained at Stage 0 [Figure 4.6C].

Based upon known mechanisms of GSDMD activation, only the activated N-terminal of GSDMD is believed to translocate to the cell membrane. As caspase-1 activation is upstream of GSDMD activation, we hypothesized that VX-765 treatment would prevent GSDMD activation and thus prevent the accumulation of active GSDMD at the cell's periphery [Figure 4.6D]. This would be apparent as a decrease in the number of cells in Stage 2 and thereafter. As expected, caspase-1 inhibition by VX-765 significantly changed the distribution of cells within the stages of pyroptosis, and reduced progression into Stage 2 [Figure 4.6E].

With the development of this classification system, we were able to quantify the molecular and morphological properties of cells at different stages of pyroptosis. For instance, we observed that progression through the stages of pyroptosis was associated with an increase in intracellular GSDMD MFI, until the lytic stage of pyroptosis (STAGE

4), at which time GSDMD intensity decreased substantially [Figure 4.7A, B]. Cross-sectional area of nigericin-exposed cells dropped significantly during the rounding phase (STAGE 1) and remained stable thereafter [Figure 4.7C, D]. By contrast, nuclear cross-sectional area decreased modestly in the early stages of pyroptosis [Figure 4.7E, F] but decreased dramatically as cells transitioned into the lytic phase (STAGE 4), recapitulating the observation of nuclear disintegration often reported during late stage pyroptosis.

4.2.7 Pyroptotic bodies observed during STAGE 3 are highly immunopositive for GSDMD and morphologically distinct from apoptotic bodies

Using semi-quantitative confocal microscopy [Figure 4.8Ai-Biv], I demonstrated that microglia at STAGE 3 of pyroptosis had an average of 7.2 ± 1.7 membrane protrusions/cell [Figure 4.8C, D]. These pyroptotic bodies were an average of 8.2 ± 0.9μm^2 in size but could extend up to >30μm^2 [Figure 4.8E]. Furthermore, the ratio of GSDMD immunoreactivity in membrane protrusions compared to the cytoplasm was significantly higher in microglia undergoing pyroptosis compared to that observed in control cells, which have occasional membrane protrusions [Figure 4.8F; $p<0.05$]. These pyroptotic bodies were morphologically distinct from apoptotic bodies, which formed following exposure of microglia to staurosporine [Figure 4.8G]. As outlined with F-actin staining, apoptotic bodies formed in a beads-on-a-string pattern [Figure 4.8Gii, *white arrows*], which was phenotypically distinct from the pattern of pyroptotic bodies observed following nigericin exposure [Figure 4.8Biii].

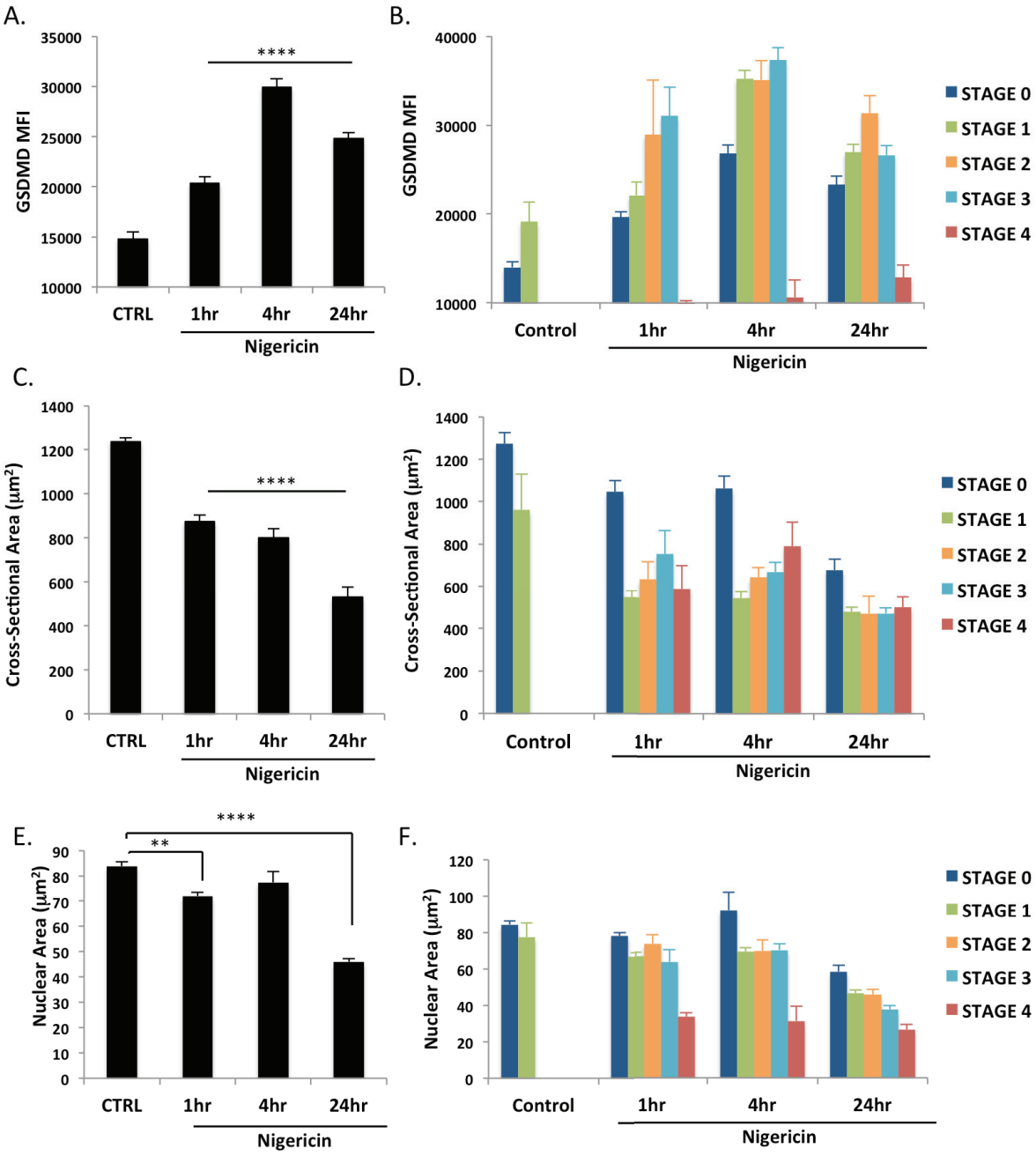

Figure 4.7 *(Figure legend on following page)*

Figure 4.7: ***Molecular features of pyroptosis by time and stage***

(A-D) Human microglia were exposed to nigericin (5μM, 1hr, 4hr, 24hr), fixed, immunolabelled for GSDMD, and visualized using confocal microscopy. **(A)** Mean fluorescence intensity (MFI) of GSDMD was assessed for a minimum of *n*=150 microglia per condition. Data shown represent mean MFI +/- SEM for a representative human donor. Results were independently recapitulated in microglia from 2-3 separate human donors. **(B)** Each cell from **(A)** was classified by stage of pyroptosis and MFI expressed separately for each stage of pyroptosis at the indicated timepoints. **(C)** Cross-sectional area of each cell from **(A)** was determined and expressed separately for each stage of pyroptosis at the indicated time points **(D)**. Data shown represent mean cross sectional area +/- SEM for a representative human donor. Results were independently recapitulated in microglia from 2-3 separate human donors (1-way ANOVA with Dunnett's test for multiple comparisons, ** $p<0.01$, **** $p<0.0001$).

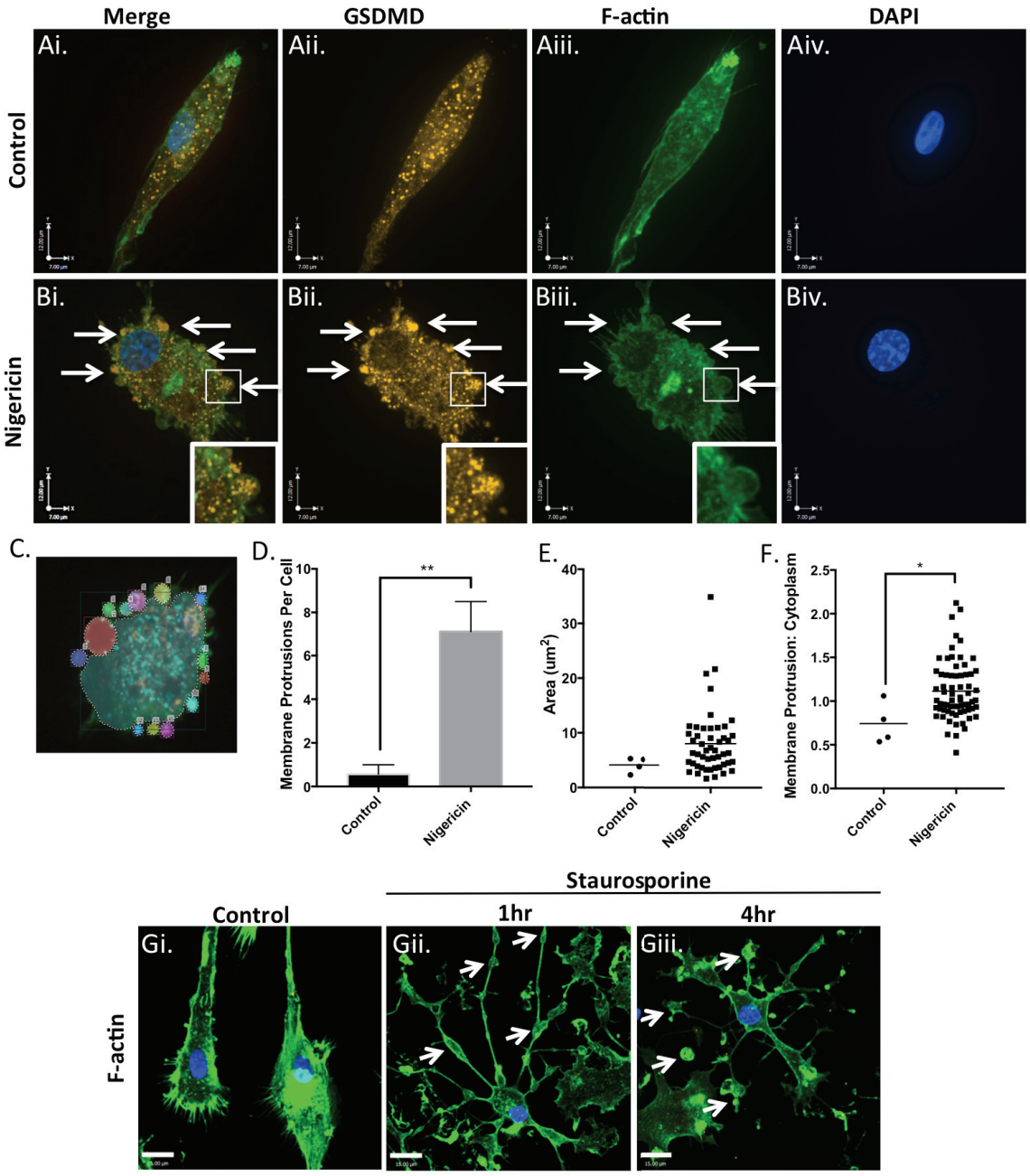

Figure 4.8 *(Figure legend on following page)*

Figure 4.8: ***Characterization of pyroptotic bodies in nigericin-treated microglia***

(A) Human microglia were exposed to nigericin (5μM, 4hr), fixed, immunolabelled for GSDMD (*amber*), stained for F-actin (*green*), and visualized using confocal microscopy. Immunofluorescent imaging reveal intact processes **(Aiii)** and diffuse GSDMD staining **(Aii)**. Nigericin exposure causes the loss of processes and formation of GSDMD-immunopositive pyroptotic bodies (**Bi-Biii**, *white arrows,* **Bi-iii** *insets*). All images were taken with a 60X objective lens; horizontal scale axis represents 7μm and vertical scale axis represents 12μm. **(C)** Screenshot from Volocity 6.3 analysis software demonstrating quantification procedure for pyroptotic bodies on nigericin-treated microglia. Quantification of pyroptotic bodies was performed by selecting a circular ROI overlaying each membrane protrusion and measuring MFI and area (μm^2) of each pyroptotic body. MFI of cytoplasm was calculated by selecting an ROI within the cell body that excluded pyroptotic bodies. **(D)** The number of membrane protrusions (i.e. pyroptotic bodies) identified on Stage 3 nigericin-treated microglia was compared to control microglia. Data represent mean +/- SEM and were tested for significance using Student's *t*-test. **(E)** Size of membrane protrusions was calculated for nigericin-treated microglia and compared to the small number of membrane protrusions normally visible on untreated control cells. The area of pyroptotic bodies on microglia was observed to be 8.1+/- 0.9 mm^2. Each data point corresponds to an individual pyroptotic body. **(F)** The ratio of GSDMD immunoreactivity in each pyroptotic body compared to the cytoplasm was calculated by dividing the MFI of each pyroptotic body by the MFI of the cytoplasm. Each data point corresponds to an individual pyroptotic body. Data were tested for significance using Student's *t*-test (**p*<0.05, ***p*<0.01). **(G)** Microglia treated with the apoptosis inducer staurosporine (5μM, 1 and 4hr) and stained for F-actin (*green*) reveal a distinctive beads-on-a-string apoptotic morphology, with individual apoptotic bodies attached to the cell body with long tethers (*white arrows*, scale bar 15μm).

4.2.8 Rupturing pyroptotic bodies can be observed by confocal microscopy

The rupture of a pyroptotic body has been shown to cause rapid and catastrophic lysis of a cell; as such, it is rare to capture images of bursting pyroptotic bodies in a population of fixed cells by confocal microscopy. We were nonetheless able to identify cells with what appeared to be rupturing pyroptotic bodies in the course of quantification experiments [Figure 4.9]. Unlike in control cells [Figure 4.9Ai-iv], pyroptotic bodies with a typical morphology were visible on nigericin-exposed cells [Figure 4.9Bi-iv], characterized by GSDMD immunoreactivity within the bounds of a large membrane protrusion, as delineated by F-actin staining [Figure 4.9Ci-Ciii]. Examples of rupturing pyroptotic bodies, wherein the F-actin signal became less clearly defined and GSDMD immunoreactivity significantly over-reached the boundaries of the membrane protrusion, were also visible [Figure 4.9Di-iii].

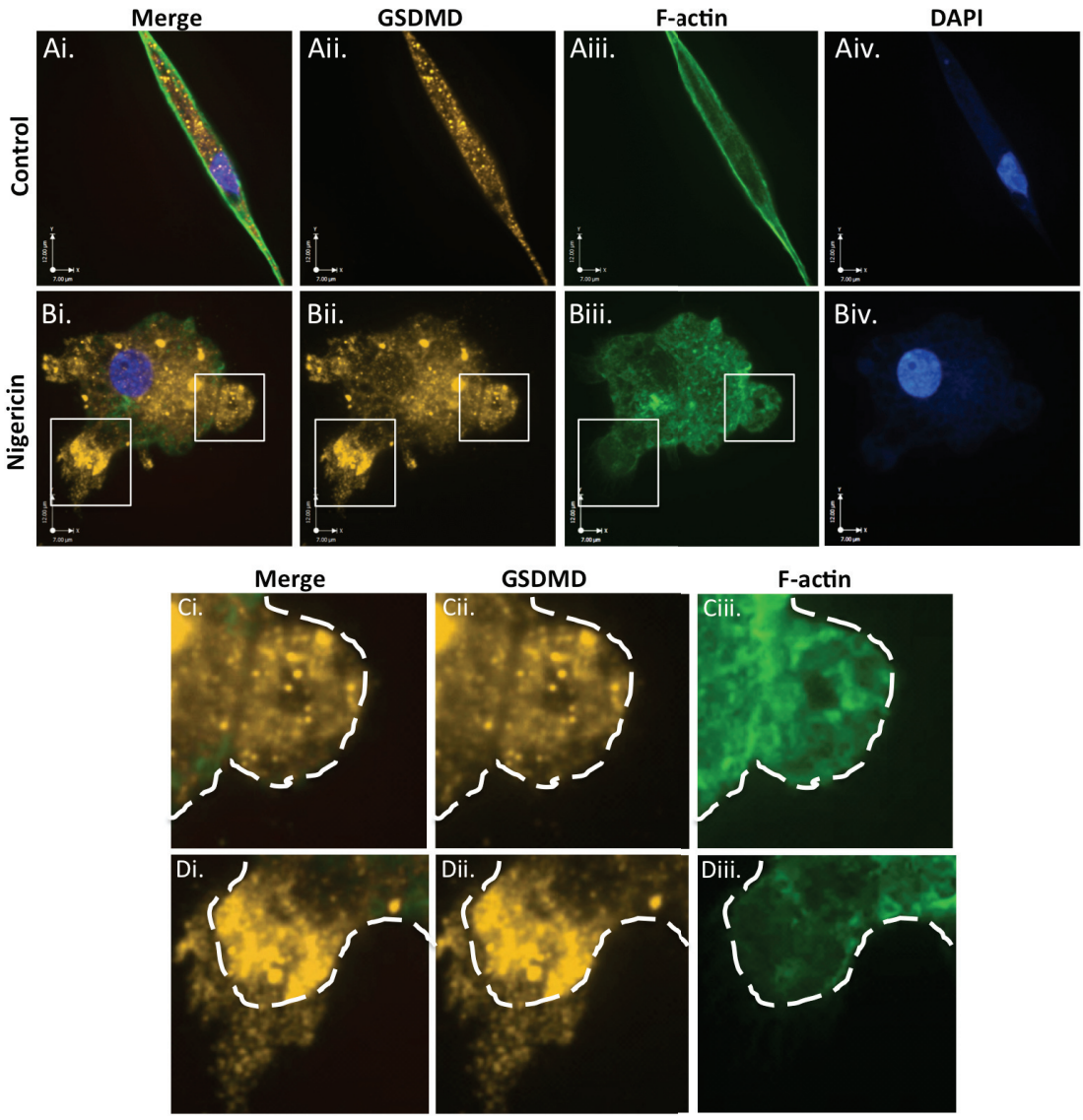

Figure 4.9: ***Bursting pyroptotic bodies can be observed during human microglial pyroptosis.***

(A) Immunofluorescent imaging of healthy human microglia reveal an elongated morphology **(Aiii)** and diffuse GSDMD staining (**Aii**, *amber*). Nigericin exposure (4hrs, 5μM) causes the formation of highly GSDMD-immunopositive pyroptotic bodies (**Bi-iii**, *white boxes*). Most pyroptotic bodies observed at the time of imaging are intact **(Ci-iii)**, with the boundary of the cell (*white dashed line*) as indicated by F-actin staining (*green*) closely corresponding to the boundary of GSDMD immunopositive signal (*amber*). **(D)** Pyroptotic bodies that appear to be in the process of bursting can be observed, in which GSDMD immunopositive cell contents (*amber*) appear to spill past the boundary of the cell (*white dashed line*) as indicated by F-actin staining (*green*).

IV.III. Chapter Summary

In this chapter, I established that primary human microglia undergo GSDMD- and caspase-1-dependent pyroptosis in response to MS-relevant DAMPs, but not in response to any of the individual proinflammatory cytokines tested. We validated the ability of the caspase-1 inhibitor VX-765 to rescue inflammasome-associated cytokine release and inhibit pyroptosis, and used GSDMD-targeting siRNA to establish a crucial role for GSDMD in microglial pyroptosis. We also proposed a classification system for identifying the stages of pyroptosis in fixed populations of microglia by confocal microscopy, and used it to characterize the unique morphological and molecular changes associated with pyroptosis, including the formation of pyroptotic bodies. Collectively, these observations provide a framework for a deeper investigation into previously undiscovered mechanisms driving pyroptosis, which will be described in Chapter V.

CHAPTER V: CASPASE-3/7 IN MICROGLIAL PYROPTOSIS

Sections of this chapter have been submitted:

McKenzie, BA, Fernandes J, Doan M, Branton WG, Power C. (2019). Caspase-3/7 drive pyroptosis in human microglia. *Submitted*.

All experiments in this chapter were designed, performed, and analyzed by Brienne McKenzie with the following exceptions:

- Western blots and quantification in Figure 5.3B, Figure 5.9B,C, Figure 5.11A-C, and Figure 5.13H-I were performed by Jason Fernandes, a technician in the Power lab, using lysates provided by Brienne McKenzie.

- Human autopsy sample immunofluorescence in Figure 5.15A-C was performed by William Branton, a technician in the Power lab.

V.I. Brief Introduction

OBJECTIVE III:

To interrogate whether a functional role exists for apoptotic caspases-3/7 in pyroptosis using human microglia as a model system

Recent evidence suggests the occurrence of subcellular changes, such as loss of mitochondrial function and cell motility, prior to GSDMD-mediated membrane rupture during pyroptosis[189,190]. These changes indicate a broader disruption of cellular function during pyroptosis, reminiscent of that observed in apoptosis. Caspase-1 has been shown to activate apoptotic executioner caspases, mediating cleavage of caspase-3/7 either directly through proteolysis or indirectly through activation of upstream caspases[75,78-80]. In some systems, but not all[78], caspase-1-mediated cleavage of caspase-3/7 downstream of inflammasome activation is only unmasked in GSDMD-deficient conditions[181]. PARP, the prototypic marker of caspase-3/7 activation in apoptosis, is also cleaved during pyroptosis downstream of caspase-3/7 activation[79,195], although GSDMD deficiency can increase PARP cleavage and promote an apoptotic cell death program[79]. Many groups attribute the caspase-3/7 activation and/or PARP cleavage observed during pyroptosis to a subset of apoptotic cells[79], but this conclusion is often drawn in the absence of supporting data at the single-cell level.

In Chapter IV, I established a framework to investigate the molecular characteristics of pyroptosis at the single-cell level using semi-quantitative confocal microscopy. This approach allows for simultaneous assessment of both the morphological features of pyroptosis (such as pyroptotic body formation and nuclear disintegration) concurrently

with molecular features (such as intracellular GSDMD and cleaved caspase-3 expression) at the single-cell level. These tools, among others, enabled me to investigate the hypothesis that caspase-3/7 activation drives GSDMD-mediated pyroptosis.

Within this chapter, evidence is provided for caspase-3/7 cleavage and activation in cells actively undergoing pyroptosis downstream of caspase-1 activation, but not in cells exposed to exogenous inflammasome-associated cytokines. Cleaved caspase-3/7 and their activated substrates were shown to accumulate in the nucleus (which is rescued by caspase-3/7 inhibition), and siRNA inhibition of caspase-3/7 was shown to prevent nuclear disintegration. Furthermore, I utilized semi-quantitative confocal microscopy to show that caspase-3/7 accumulated in pyroptotic bodies and that inhibition of caspase-3/7 blocked pyroptotic body formation. ROCK1, the caspase-3 substrate responsible for apoptotic body formation during apoptosis, was also cleaved and activated during pyroptosis, supporting the hypothesis that caspase-3/7 may facilitate pyroptotic body formation through the cleavage of substrates such as ROCK1. Finally, I demonstrated that inhibition of caspase-3/7 reduced membrane rupture, illuminating a previously undiscovered role for caspase-3/7 in pyroptosis.

To demonstrate that these findings were applicable *in vivo,* we demonstrated that cleaved caspase-3 was co-expressed with GSDMD in white matter lesions in MS and EAE. Collectively, these data provide the first evidence for an executioner role for caspase-3/7 in GSDMD-mediated pyroptosis, and challenge the practice of using cleaved caspase-3/7 and their substrates as biomarkers for apoptosis.

V.II. Results

5.2.1 Total caspase-3 expression is increased during pyroptosis in a non-caspase-1-dependent manner

Microglia exposed to nigericin demonstrated a significant increase in intracellular total caspase-3 MFI [Figure 5.1A, B, D, $p<0.0001$], combined with an increase in intracellular total caspase-1 [Figure 5.1C] and GSDMD MFI [Figure 5.1E]. Like GSDMD, caspase-3 immunoreactivity was particularly concentrated in the pyroptotic bodies [Figure 5.1Bii, *white arrows*]. Nigericin-induced caspase-3 expression was not affected by VX-765 pre-treatment [Figure 5.1F], suggesting that caspase-1 activation is not required for this phenomenon.

5.2.2 Caspase-3/7 activity is increased during pyroptosis

Using a FAM-FLICA activation assay for caspase-3/7 in combination with semi-quantitative confocal microscopy, a significant increase in intracellular caspase-3/7 activity was observed during pyroptosis [Figure 5.2A, B]. These results were validated at the population level by microplate reader [Figure 5.2C, D], which demonstrated that nigericin-, ATP-, and staurosporine-exposed microglia all display increased caspase-3/7 activity of a comparable magnitude to the increase in caspase-1 activity during pyroptosis [Figure 5.2E]. However, to optimize sensitivity and specificity, further experiments were conducted using antibodies specific for cleaved caspases instead.

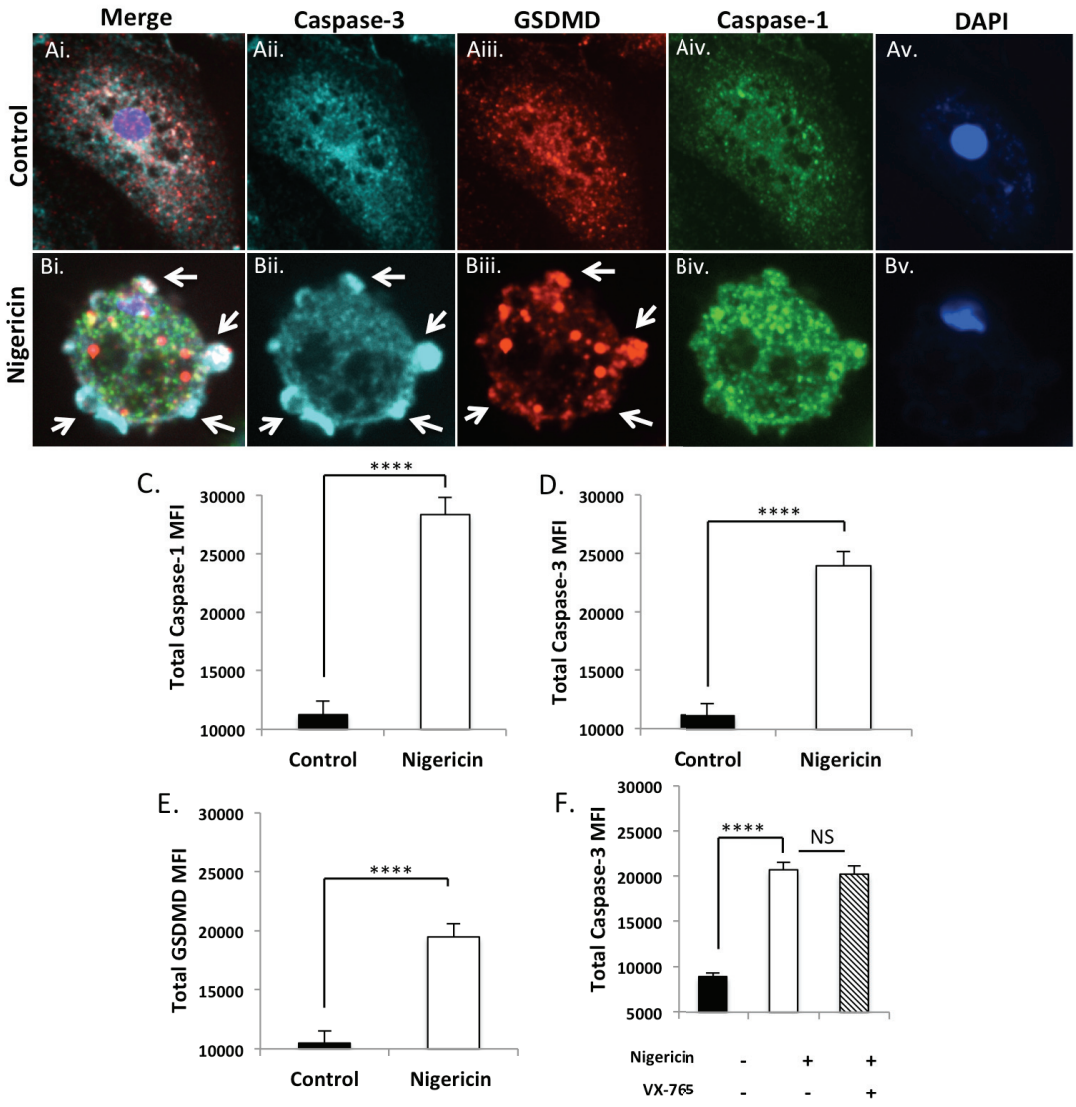

Figure 5.1: ***Total caspase-3 is up-regulated during pyroptosis in a non-caspase-1-dependent manner.***

(A,B) Human microglia were exposed to nigericin (5μM, 4hrs) or solvent control, fixed, immunolabelled for total caspase-3 (**Aii, Bii**, *cyan*), total caspase-1 (**Aiv, Biv,** *green*), and total GSDMD (**Aiii, Biii,** *red*), and visualized using confocal microscopy (40X objective). **(C-E)** Mean fluorescence intensity (MFI) of each protein was assessed for *n*=20 control microglia and *n*=40 nigericin-treated microglia. Data shown represent mean MFI +/- SEM for a representative human donor with background MFI subtracted (Student's *t*-test, ****$p<0.0001$). **(F)** Microglia were exposed to nigericin (5μm, 4hrs) +/- pre-treatment with VX-765 (50μM, 4hrs), fixed, and immunolabelled for total caspase-3. MFI was assessed for *n*=30-50 microglia per condition. Data shown represent mean caspase-3 MFI +/- SEM for a representative human donor with background subtracted. Results were independently recapitulated in microglia from 2-3 separate human donors (ANOVA with Tukey's test for multiple comparisons, ****$p<0.0001$, NS = not significant).

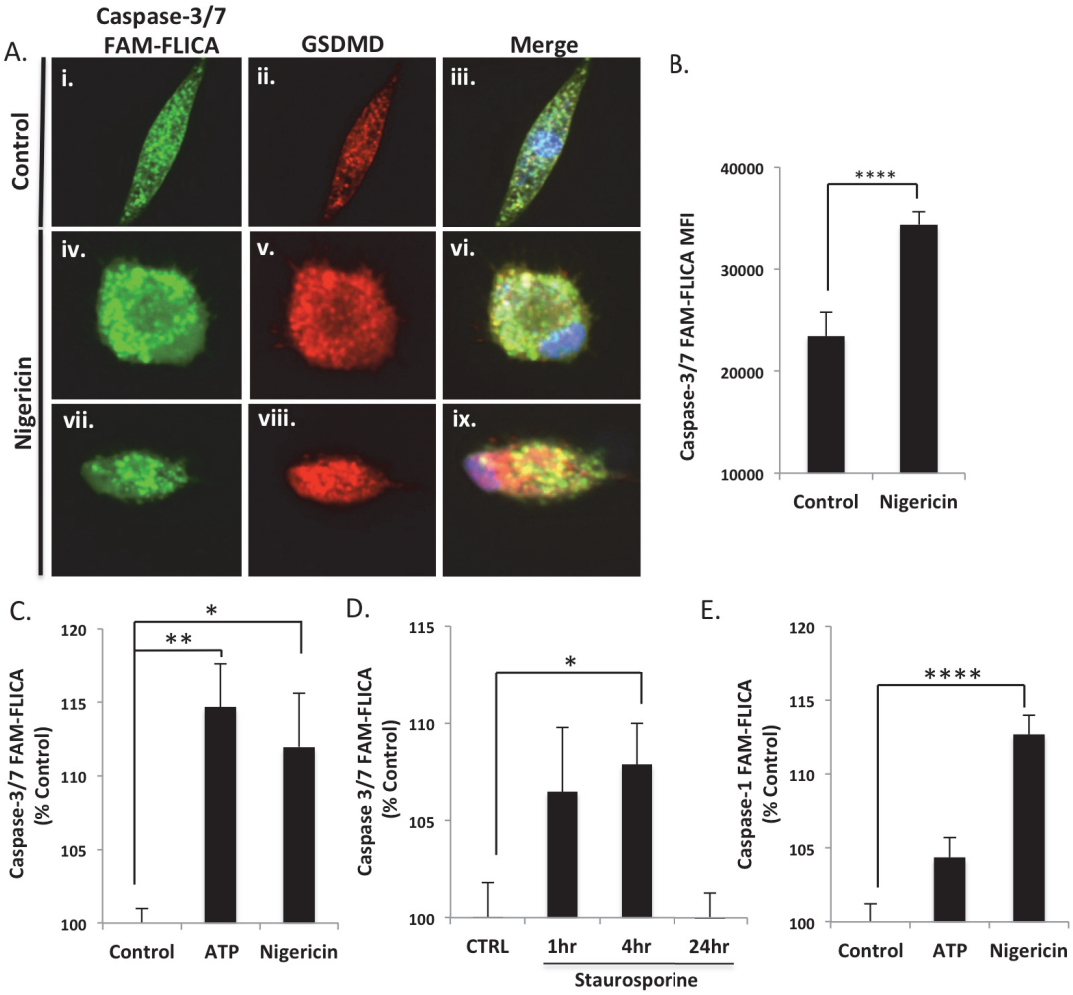

Figure 5.2: ***Caspase-3/7 activity is detectable during pyroptosis.***

(A) Human microglia were exposed to nigericin (5μM, 4hrs) or solvent control and probed with fluorescent FAM-FLICA caspase-3/7 reagent (*green*), fixed, co-labelled with GSDMD (*red*), and imaged (40X objective). Two examples of nigercin-treated microglia are shown (**Aiv-ix**). **(B)** Mean fluorescence intensity (MFI) of FAM-FLICA signal was assessed for *n*=30 control microglia and *n*=50 nigericin-treated microglia. Data shown represent mean MFI +/- SEM for a representative human donor (Student's *t*-test, ****$p<0.0001$). **(C-D)** Microglia in 96-well plates were treated with nigericin (5μM, 4hrs), ATP (100μM, 24hrs), or staurosporine (5μM, 1, 4, 24 hrs), probed with FAM-FLICA caspase-3/7 reagent, and fluorescence measured (*n*=8 technical replicates/condition) with a microplate reader. Data shown represent mean fluorescent signal (MFI) normalized to untreated controls +/- SEM for a representative human donor. **(E)** Microglia in 96-well plates were treated with nigericin (5μM, 4hrs), ATP (100μM, 24hrs) and probed with FAM-FLICA caspase-1 reagent, and fluorescence measured (*n*=8 technical replicates/ condition). Data shown represent mean fluorescent signal normalized to untreated controls +/- SEM for a representative human donor (ANOVA with Dunnett's test for multiple comparisons, *$p<0.05$, **$p<0.01$, ****$p<0.0001$).

5.2.3 Caspase-3/7 are cleaved during pyroptosis in a caspase-1-dependent manner

To quantify the presence of active caspase-3/7 during pyroptosis, cleaved caspase-3 p17/19 and GSDMD immunoreactivity in pyroptotic microglia was assessed, with the apoptotic stimulus, staurosporine, as a control [Figure 5.3Ai-xii: p17/p19 *amber*; GSDMD *green*]. Cleaved caspase-3 immunoreactivity was evident in staurosporine-, nigericin- and ATP-exposed microglia [Figure 5.3Avii-viii], particularly in the nucleus (*blue*), apoptotic bodies (*grey arrow*), and pyroptotic bodies (*white arrows*). While ATP- and nigericin-exposed microglia demonstrated a signature pyroptotic morphology, staurosporine-exposed apoptotic microglia displayed long protruding apoptopodia (*grey arrows*) and lacked the prototypic pattern of GSDMD immunoreactivity in pyroptotic bodies observed during pyroptosis[270]. Cleaved caspase-3 immunoreactivity was also detectable by immunoblot in cell lysates from pyroptotic (nigericin-exposed) and apoptotic (staurosporine-exposed) microglia, with the p19 fragment dominating in nigericin-exposed conditions [Figure 5.3B]. Detection of cleaved caspase-3 in ATP-exposed microglia by immunoblot was not consistent, potentially due to the higher proportion of resting (Stage 0) microglia following ATP exposure compared to nigericin exposure [Figure 4.6C]. It is worth noting that in cell-free assays, initiator caspases (-8/-9/-10) predominantly generate a p17 caspase-3 fragment (observed after staurosporine exposure); conversely, caspase-1-mediated cleavage predominantly generates a p19 fragment, which is also bioactive[80]. Our observation of the p19 fragment in nigericin-exposed cell lysates is consistent with a caspase-1-mediated cleavage of caspase-3.

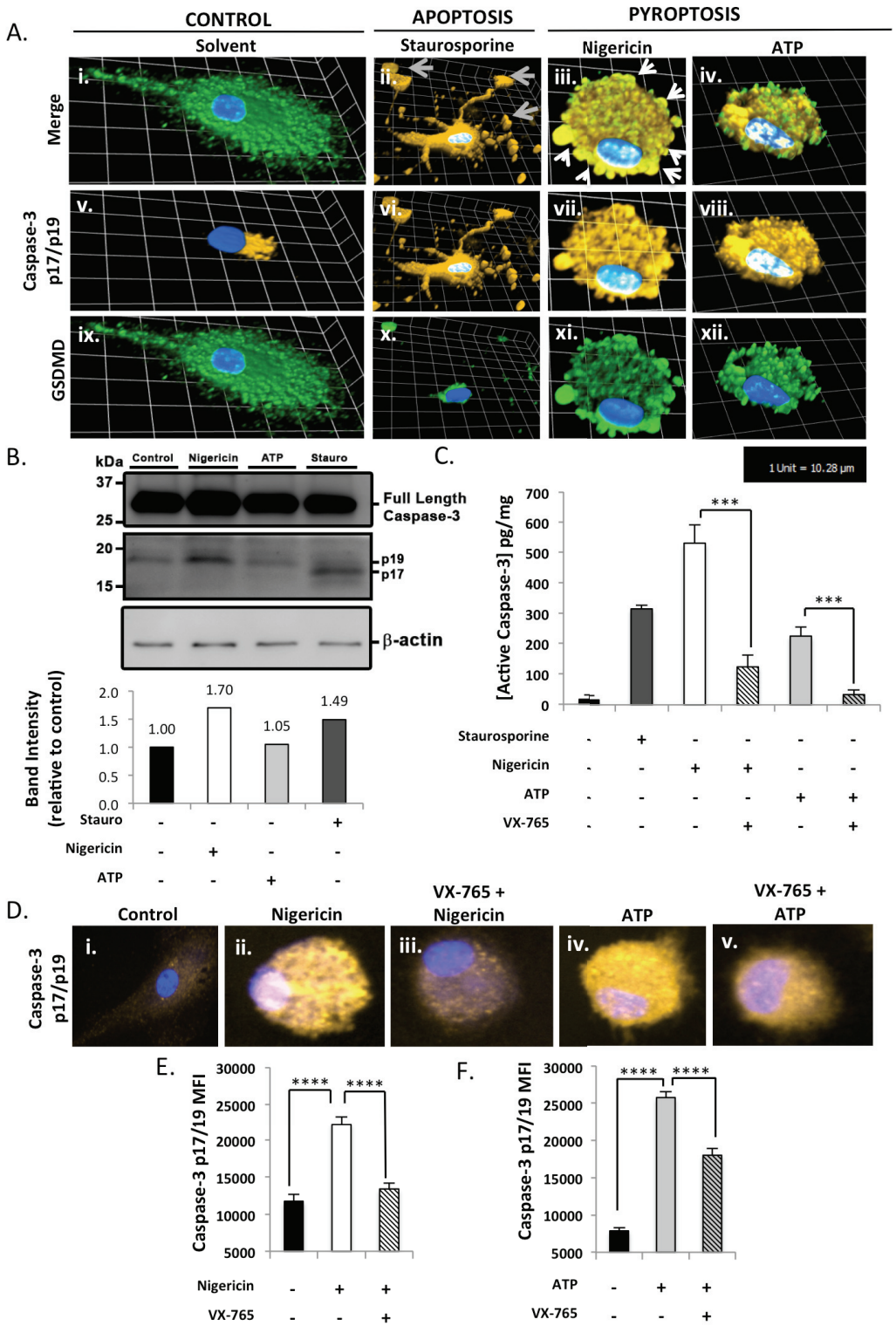

Figure 5.3 *(Figure legend on following page)*

FIGURE 5.3: ***Caspase-3 is cleaved during pyroptosis in a caspase-1-dependent manner.***

Primary human microglia were exposed to pyroptotic stimuli [ATP (100μM, 24hrs) or nigericin (5μM, 4hrs)], apoptotic stimuli [staurosporine (5μM, 4hrs)], or solvent [equivalent volume PBS (4hrs)]. Cells were fixed and immunolabelled for cleaved caspase-3 p17/p19 (**Av-viii**, *amber*) and GSDMD (**Aix-xii**, *green*), merge shown in **(Ai-iv)** and visualized using confocal microscopy. Images shown are representative 3-dimensional z-stacks incorporating 15 XY planes over a vertical distance of 4-6μm (40X objective). 1 square unit represents 10.28μm. *Grey arrows*: apoptopodia; *white arrows*: pyroptotic bodies **(B)** Cells lysates were harvested at the indicated timepoints post-exposure and immunoblotted for both full-length and cleaved caspase-3 as well as β-actin. Data shown are immunoreactive bands normalized to β-actin and expressed relative to solvent-treated controls. **(C)** Nigericin- or ATP-exposed microglia were pre-treated with VX-765 (50μM, 4hrs), from which lysates were harvested and cleaved caspase-3 levels assessed by ELISA. Data shown represent mean cleaved caspase-3 levels +/- SEM (*n*=6 technical replicates) from a representative human donor. Results were independently confirmed in microglia from 3-5 separate human donors. **(D)** Microglia were treated as in **(C)** and immunolabelled for cleaved caspase-3 p17/p19 (*amber*). Representative 2-dimensional images shown (40X objective). **(E-F)** Mean fluorescence intensity (MFI) of cleaved caspase-3 was assessed for *n*=20 control microglia and a minimum of *n*=100 nigericin- or ATP-exposed microglia +/- VX-765. Data shown represent mean cleaved caspase-3 MFI +/- SEM for a representative human donor with background subtracted. Results were independently verified in microglia from 2-3 separate donors (ANOVA with Tukey's test for multiple comparisons, ***$p<0.001$, ****$p<0.0001$).

To quantify cleaved caspase-3 in lysates from pyroptotic microglia, a highly sensitive ELISA specific for activated (Ser29) caspase-3 was utilized. Cleaved caspase-3 was consistently detected in staurosporine-, nigericin-, and ATP-exposed microglial lysates [Figure 5.3C]. Pre-treatment with VX-765[113,270,271] reduced cleaved caspase-3 in lysates following nigericin or ATP exposure, positioning caspase-1 activation upstream of caspase-3 cleavage [Figure 5.3C]. Using semi-quantitative confocal microscopy, I demonstrated that intracellular caspase-3 p17/19 MFI was increased following nigericin or ATP exposure, which was prevented by caspase-1 inhibition [Figure 5.3D-F]. To address potential off-target effects on caspase-3, I demonstrated that VX-765 did not reduce caspase-3 activation induced by staurosporine (a well-validated pan-caspase inhibitor that induces apoptosis) [Figure 5.4A, B].

5.2.4 Inflammasome-associated cytokines do not cause pyroptosis and do not cause caspase-3 activation

As a negative control, I assessed whether proinflammatory cytokines that did not cause pyroptosis affected caspase-3 cleavage. Exogenous IL-1β- and IL-18-exposed microglia remained in Stage 0 and did not progress through pyroptosis [Figure 5.5A, B], consistent with the observations from Chapter IV that exposure to these cytokines caused no change in cell viability or membrane permeability [Figure 4.3]. Neither GSDMD nor cleaved caspase-3 MFI increased significantly upon exposure to these cytokines, unlike in microglia exposed to nigericin [Figure 5.5B, C], suggesting that caspase-3 cleavage is unique to cell death, and not a conserved phenomenon following exposure to proinflammatory stimuli.

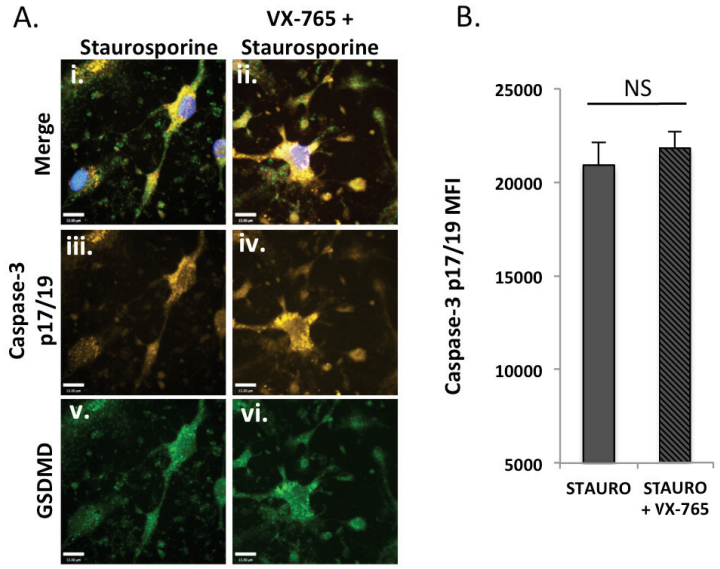

Figure 5.4: ***VX-765 does not reduce staurosporine-induced caspase-3 cleavage.***

(A) Human microglia were exposed to staurosporine (5μM, 4hrs) +/- VX-765 (50μM, 4 hrs pre-treatment), fixed, immunolabelled for cleaved caspase-3 (*amber*) and GSDMD (*green*), and visualized using confocal microscopy. Scale bar represents 13μm (40X objective). **(B)** Mean fluorescence intensity (MFI) was assessed in cell bodies (not detaching apoptopodia) for a minimum of *n*=40 microglia per group. Data shown represent mean MFI +/- SEM for a representative human donor with background subtracted (Student's *t*-test, NS = not significant).

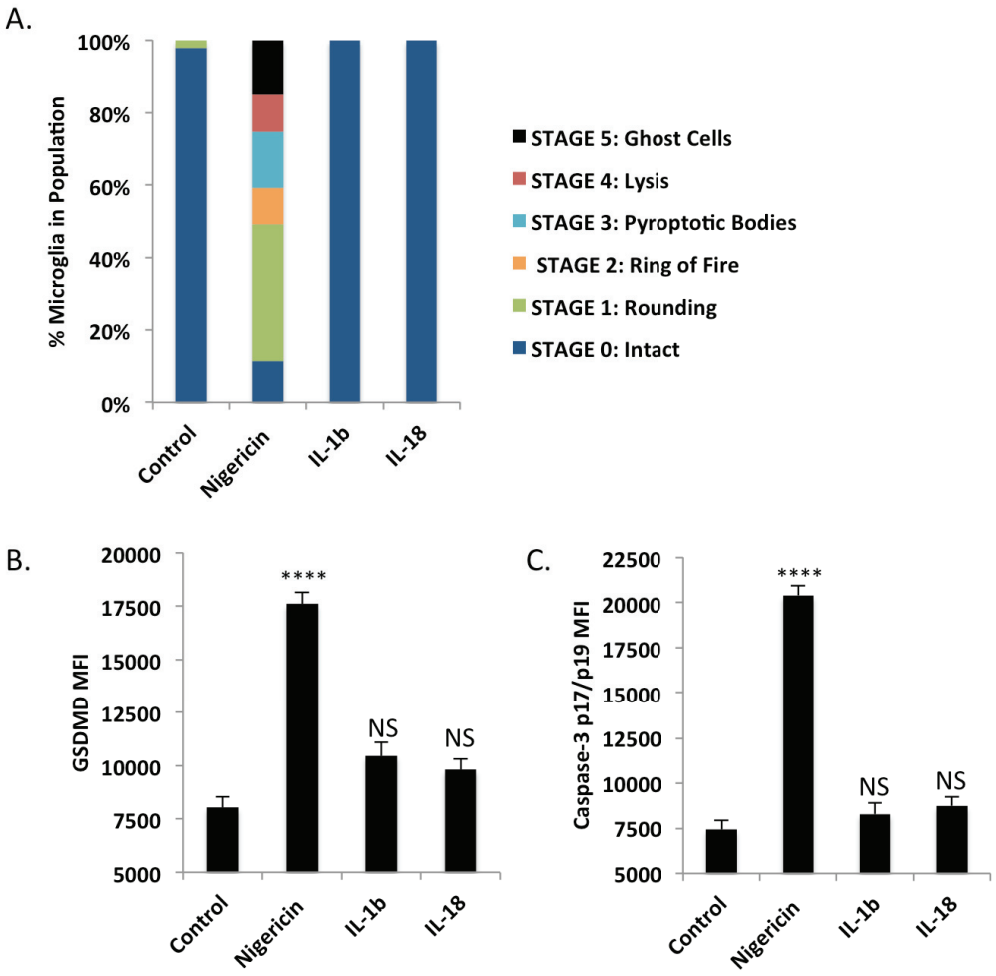

Figure 5.5: ***Inflammatory cytokines do not cause pyroptosis or caspase-3 activation.***

(A) Microglia were exposed to nigericin (5μM, 24hrs), IL-1β (25ng/mL, 24hr) or IL-18 (25ng/mL, 24hr), fixed, immunolabelled for GSDMD, and visualized using confocal microscopy. Cells were classified into one of the five stages of pyroptosis. The proportion of cells at each stage was quantified at 24hr post-exposure to each stimuli, using a minimum of *n*=25 microglia per condition. GSDMD **(B)** and cleaved caspase-3 **(C)** MFI was quantified for each microglia classified in **(A)**. Data shown represent mean cleaved MFI +/- SEM for a representative human donor (1-way ANOVA with Dunnett's test for multiple comparisons, ****p<0.0001, NS = not significant).

5.2.5 Caspase-7 is also cleaved during pyroptosis downstream of caspase-1

Using semi-quantitative confocal microscopy, I assessed whether cleaved caspase-7 was detected intracellularly following ATP or nigericin exposure. Caspase-7 p20 MFI was significantly increased following nigericin or ATP exposure, and like cleaved caspase-3 MFI, this effect was significantly reduced with VX-765 pre-treatment [Figure 5.6A, B]. These data highlighted that both caspase-3 and-7 activation occurred downstream of caspase-1 activation during pyroptosis.

5.2.6 Caspase-3/7 cleavage is observed in multiple stages of pyroptosis

Using the classification framework developed in Chapter IV, I assessed the stage-dependent cleavage of caspase-3/7 and demonstrated at the single-cell level that cleaved caspase-3/7 were detectable in cells actively undergoing pyroptosis. Caspase-3 p17/p19 is expressed at very low levels in Stage 0 microglia, but abundantly expressed during activation (Stage 1) and pyroptosis (Stage 2 onwards), with particularly abundant expression in the nucleus and in pyroptotic bodies [Figure 5.7Ai-Cvi]. To quantify changes in cleaved caspase-3 MFI over time and through the stages of pyroptosis, three time points post-nigericin exposure were examined (1, 4, and 24hrs post-exposure). Recapitulating our results from Chapter IV, the proportion of intact (Stage 0) microglia decreased with time, while the proportion of cells at early and late stages of pyroptosis increased [Figure 5.7D], paralleling an increase in supernatant LDH activity that indicated a time-dependent loss of plasma membrane integrity [Figure 5.7E]. Cleaved caspases-3 and -7 MFI were significantly increased at all time points

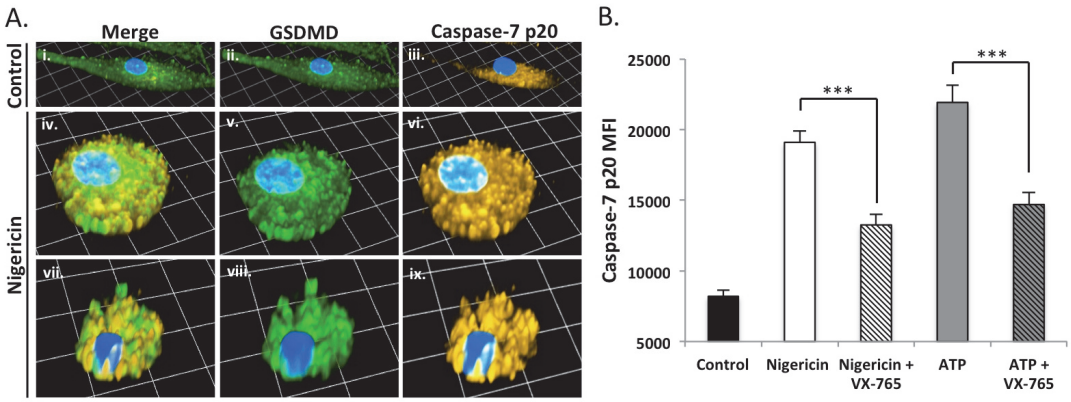

Figure 5.6: A*ctivated caspase-7 is observed in pyroptosis downstream of caspase-1.*

(A) Human microglia were exposed to nigericin (5μM, 4hrs) or solvent control, fixed, and immunolabelled for GSDMD (*green*) and cleaved caspase-7 (*amber*). Images shown are representative 3-dimensional z-stacks incorporating 15 XY planes over a vertical distance of 4-6μm. 1 square unit represents 10.28μm (40X objective, two representative nigericin-treated microglia shown). **(B)** Human microglia were exposed to nigericin (5μM, 4hrs) or ATP (100μm, 24hrs) +/- VX-765 (50μM, 4 hrs pre-treatment), fixed, and immunolabelled for GSDMD (*green*) and cleaved caspase-7 (*amber*). MFI of cleaved caspase-7 was assessed in a minimum of *n*=30 cells per condition. Data shown represent mean MFI +/- SEM with background subtracted for a representative human donor (1-way ANOVA with Tukey's test for multiple comparisons, ***$p<0.001$).

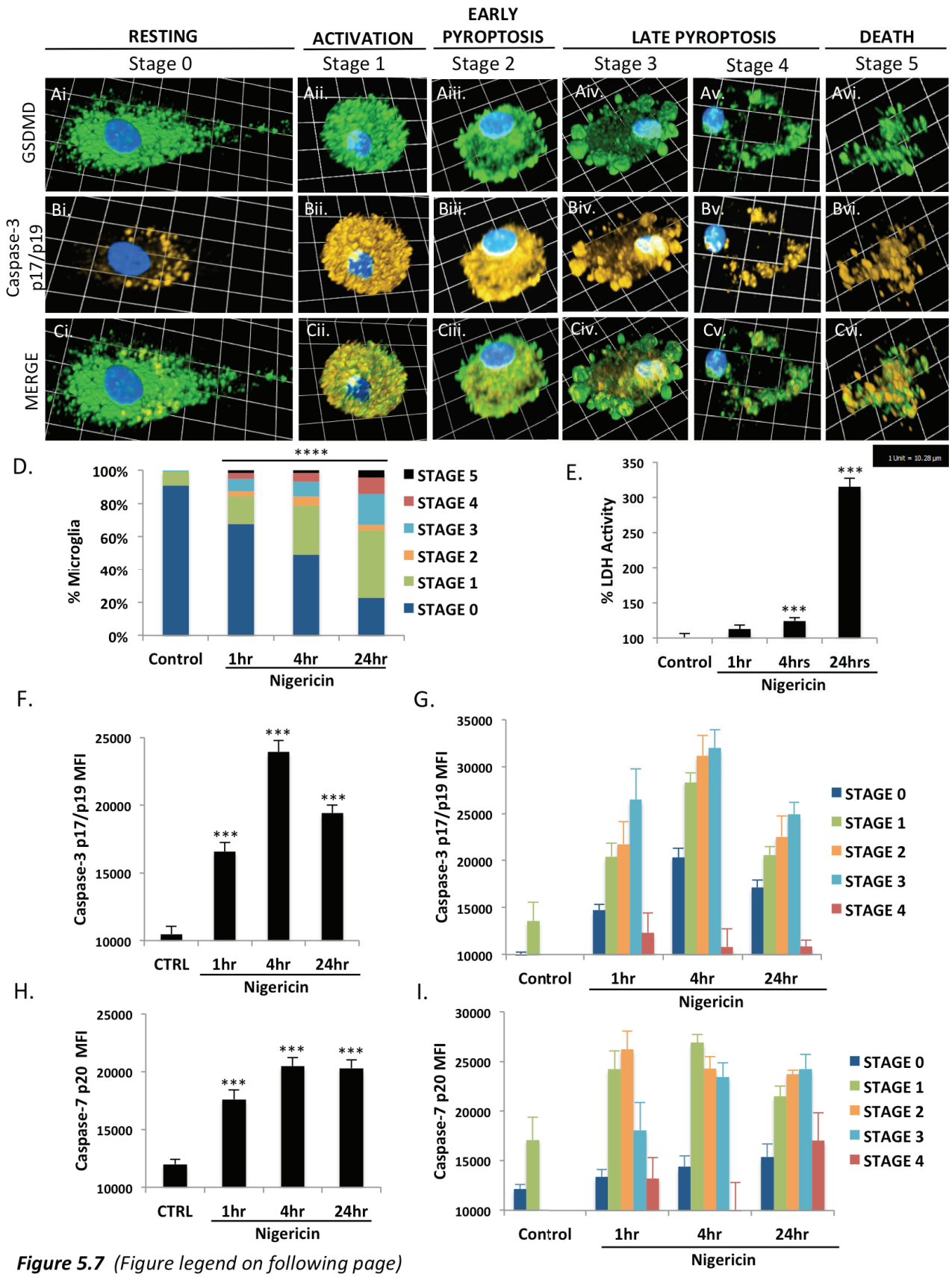

Figure 5.7 *(Figure legend on following page)*

FIGURE 5.7: ***Activation of caspase-3 and -7 depends on time and stage of pyroptosis.***

Microglia were exposed to nigericin (5μM, 4hrs), fixed, and immunolabelled for GSDMD (**Ai-vi**, *green*) and cleaved caspase-3 p17/p19 (**Bi-vi**, *amber*), merge shown in **(Ci-vi)** and visualized using confocal microscopy. Microglia were classified into one of the five stages of pyroptosis, including **STAGE 0: "***Intact"* (adherent cell with elongated processes, baseline GSDMD expression); **STAGE 1: "***Rounding"* (rounded cell, loss of processes, increased GSDMD expression throughout the cell); **STAGE 2***: "Ring of fire"* (translocation of GSDMD to the cell periphery); **STAGE 3**: *"Pyroptotic bodies"* (formation of $GSDMD^+$ membrane blebs); **STAGE 4**: *"Lysis"* (rupture of the cell, nucleus still intact), and finally **STAGE 5: "***Ghost cells"* (nucleus disintegrated, residual $GSDMD^+$ cell debris). Images shown for each stage are representative 3-dimensional z-stacks incorporating 15 XY planes over a vertical distance of 4-6 μm. **(D)** The proportion of cells at each stage was quantified at 0,1,4, and 24hr post-exposure to nigericin, using *n*=60 microglia for unexposed microglia and a minimum of *n*=100 microglia at each time point post-exposure. Time course data represent the proportion of cells at each stage for a representative sample. Distribution of the cells across the stages was assessed using a Chi-squared test (*****p*<0.0001). **(E)** Loss of plasma membrane integrity over time was assessed using an LDH activity assay. Data shown are mean +/- SEM for a representative human donor (1-way ANOVA with Dunnett's test for multiple comparisons). LDH assays were performed with technical replicates of *n*=6-8 wells/condition and data replicated in multiple donor samples. Cleaved caspase-3 **(F)** or -7 **(H)** MFI was quantified at each time point for the microglia classified in **(D)**. Data shown represent mean cleaved caspase-3/7 MFI +/- SEM for a representative human donor. **(G)** Microglia were classified according to the stage of pyroptosis and cleaved caspase-3 **(G)** or cleaved caspase-7 **(I)** MFI expressed for each stage of pyroptosis. All time course data were independently replicated using microglia derived from a minimum of two human donors. Data in **(E)**, **(F)**, and **(H)** were tested for significance using 1-way ANOVA with Dunnett's test for multiple comparisons (****p*<0.001).

tested post-nigericin exposure [Figure 5.7F, H], peaking in Stages 1-3 of pyroptosis before dropping significantly during lysis [Figure 5.7G, I]. The confirmation of cleaved caspase-3/7 at Stages 2 and 3 is particularly vital, because these stages display unequivocal morphological indicators of pyroptosis that are not shared with any other cell death sub-routine.

5.2.7 The majority of nigericin-exposed microglia are double-immunopositive for GSDMD and cleaved caspase-3

To assess whether GSDMD and cleaved caspase-3 were co-expressed in the same cells during pyroptosis, a threshold of 3X background fluorescence was established as the threshold for being "immunopositive" and every microglia was classified as single-immunopositive, double-immunopositive, or double-negative based on cleaved caspase-3 and GSDMD MFI. GSDMD and cleaved caspase-3 double-immunopositive cells predominated at all time points tested following nigericin exposure [Figure 5.8A]. Most control microglia [Figure 5.8B] were double-negative, but a subset did meet the threshold for being GSDMD immunopositive while in a resting state, which is not unexpected since untreated microglia express some GSDMD at rest. At 1hr post-exposure to nigericin [Figure 5.8C], microglia were observed at several stages of pyroptosis, all of which included sizeable double-immunopositive populations (with the exception of the lytic stage, which loses immunoreactivity for all proteins tested to date). By 4hrs post-exposure [Figure 5.8D], most cells at all stages (except lysis) were double-immunopositive for GSDMD and cleaved caspase-3, with a small double-negative population reappearing at 24hrs post-treatment [Figure 5.8E]. The cleaved

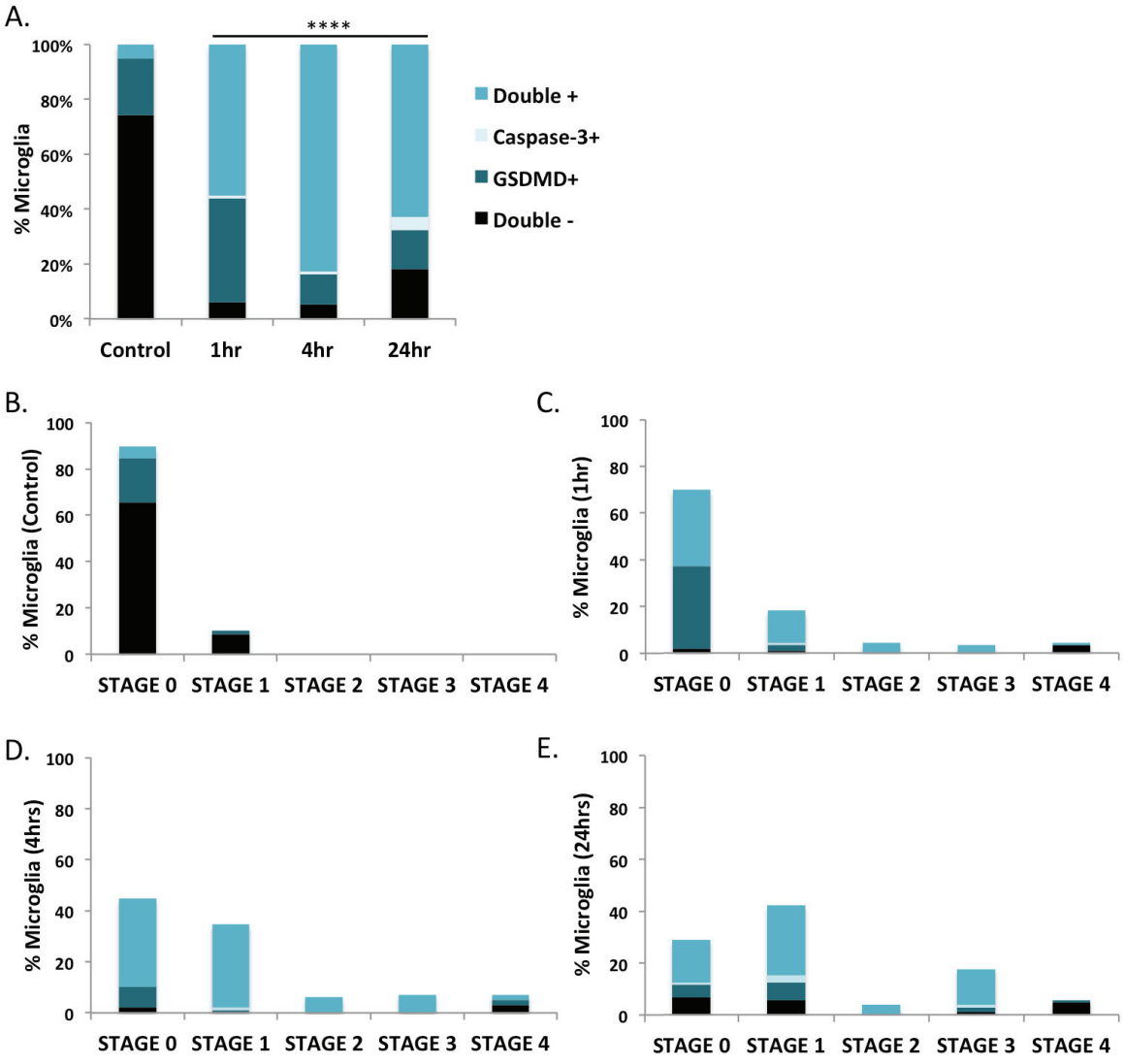

Figure 5.8: ***Most nigericin-exposed microglia are double-immunopositive for GSDMD and cleaved caspase-3.***

(A) Human microglia were exposed to nigericin (5μM, 1hr, 4hr, 24hr), fixed, immunolabelled for GSDMD and cleaved caspase-3, and visualized using confocal microscopy. Mean fluorescence intensity (MFI) of each protein was assessed, and each cell categorized as single-immunopositive, double-immunopositive, or double-immunonegative for GSDMD and cleaved caspase-3 using a threshold of 3X background fluorescence. A minimum of n=40 microglia were classified per time point. Distribution of cells at each timepoint post-nigericin exposure was significantly different from controls using Chi-square test (****p<0.0001). **(B-E)** Microglia from **(A)** that were either untreated **(B)**, or exposed to nigericin for 1hr **(C)**, 4hr **(D)**, or 24hr **(E)** were categorized by stage and expressed as a percentage of total microglia at that time point. Data shown are from a representative human donor.

caspase-3 single-immunopositive population was minimal or not present at all time points and in all stages tested post-nigericin exposure. Cells at Stage 2 and 3, which display unique features of pyroptosis, are almost exclusively double-immunopositive for GSDMD and cleaved caspase-3. Collectively, these data support the presence of cleaved caspase-3 in cells undergoing pyroptosis.

5.2.8 GSDMD but not GSDME suppression inhibits microglial pyroptosis

As chemotherapy can activate GSDME-dependent pyroptosis downstream of caspase-3[171], I next assessed whether the caspase-3-GSDME axis underpinned pyroptosis in this model. GSDMD knockdown using the GSDMD-targeting siRNAs validated in Chapter IV recapitulated our previous results, and significantly reduced nigericin-induced pyroptosis as indicated by supernatant LDH activity [Figure 5.9A]. However, siRNA-mediated GSDME knockdown did not reduce supernatant LDH activity [Figure 5.9A-C]. This finding implicated GSDMD, not GSDME, as the major executioner of pyroptosis in this system and eliminated the caspase-3-GSDME axis as a major driver of cell death.

5.2.9 Nuclear disintegration during pyroptosis is caspase-3/7 dependent

Following nigericin exposure, intense cleaved caspase-3/7 immunoreactivity was apparent in the nucleus [Figure 5.10A-C], which prompted the exploration of caspase-3/7 participation in nuclear disintegration [Figure 4.7E, F]. Transfection of siRNAs targeting caspase-3/7 prior to nigericin exposure partially inhibited nuclear disintegration compared to non-coding siRNA controls [Figure 5.10D, E], illustrating a

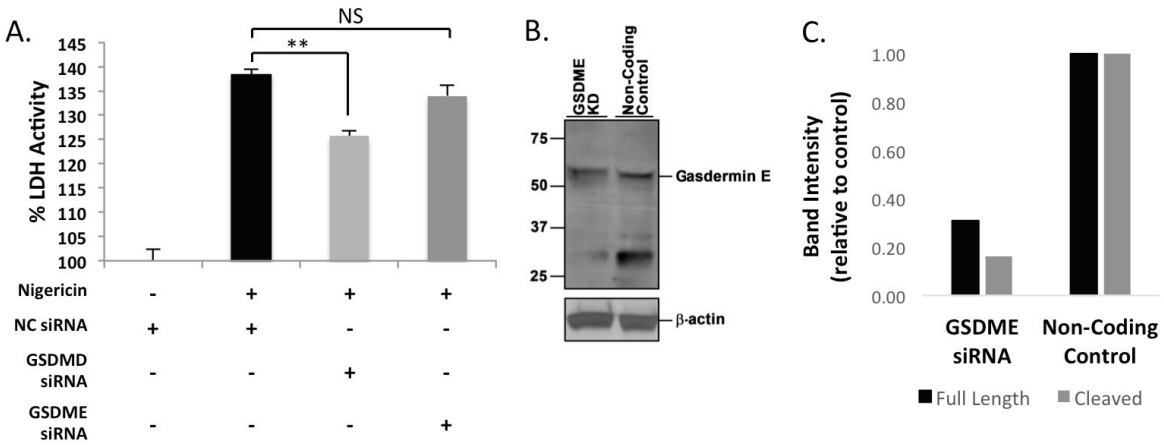

Figure 5.9: ***GSDMD but not GSDME suppression inhibits microglial pyroptosis.***

(A) Microglia were transfected with non-coding (NC) siRNA, GSDMD-targeting siRNAs, or GSDME-targeting siRNAs prior to nigericin exposure (5μM, 24hrs) and supernatant LDH activity assessed. Data shown are mean LDH activity +/- SEM for a representative human donor, analyzed using 1-way ANOVA with Tukey's test for multiple comparisons (NS = not significant, $^{**}p<0.01$). LDH assays were performed with n=6-12 technical replicates per condition and independently replicated in 3-4 biologically unique donors. **(B)** To validate the GSDME siRNA knockdown, microglia were transfected with either NC siRNA or GSDME-targeting siRNA. Transfected cells were harvested and GSDME levels assessed by immunoblot. **(C)** Band intensity was calculated for each condition by normalizing to NC siRNA controls.

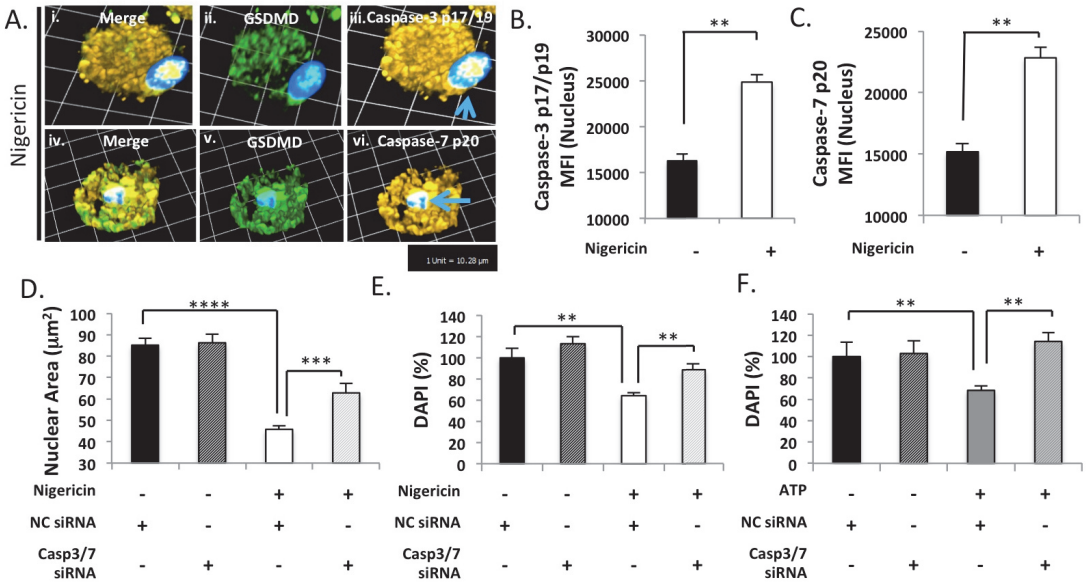

FIGURE 5.10: ***Nuclear disintegration during pyroptosis is caspase-3/7-dependent.***

(A) Human microglia were exposed to nigericin (5μM, 4hrs), fixed, and immunolabelled for GSDMD (*green*) and either cleaved caspase-3 or -7 (*amber*). *Blue arrows* indicate cleaved caspase-3/7 accumulation in the nucleus. Images shown are representative 3-dimensional z-stacks incorporating 15 XY planes over a vertical distance of 4-6μm. 1 square unit represents 10.28μm. (40X objective, representative nigericin-treated microglia shown). **(B-C)** Mean fluorescence intensity (MFI) of cleaved caspase-3/7 in the nucleus was assessed for *n*=50 control microglia and a minimum of *n*=150 nigericin-exposed cells. Data shown represent mean nuclear cleaved caspase-3/7 MFI +/- SEM for a representative human donor with background subtracted (Student's *t*-test, $^{**}p<0.01$). **(D)** Microglia were transfected with either universal non-targeting siRNA (NT siRNA) or a cocktail of different siRNAs targeting caspases-3 and -7 (Casp-3/7 siRNA) prior to nigericin exposure (5μM, 24hrs). Cells were fixed, DAPI stained to label nuclei, and assessed by confocal microscopy. Cross-sectional area (μm²) of DAPI-stained nuclei were measured for a minimum of *n*=20 solvent-treated cells and a minimum of *n*=50 nigericin-treated cells. Data shown represent mean nuclear area +/- SEM for a representative human donor. **(E)** Microglia in 96-well plate were transfected with either NT siRNA or Casp-3/7 siRNA prior to **(E)** nigericin (5μM, 24hrs) or **(F)** ATP (100μM, 24hrs) exposure. Total DAPI levels within each population were assessed fluorometrically by microplate reader, with a minimum of *n*=8 technical replicates per condition. Results were independently recapitulated in microglia from 2-3 separate human donors (1-way ANOVA with Tukey's test for multiple comparisons, $^{**}p<0.01$, $^{***}p<0.001$, $^{****}p<0.0001$).

potential role for caspase-3/7 activation upstream of nuclear disintegration during pyroptosis. The siRNA-mediated knockdown of caspase-3/7 was validated by immunoblot in [Figure 5.11A-C]. Nuclear caspase-3/7 increased over time [Figure 5.12A, C] and peaked in Stages 2-3, prior to the decrease in nuclear cross-sectional area that is observed during Stage 4 [Figure 4.7F]. Overall DAPI signal in the population (measured by microplate reader) is an indicator of the number and size of nuclei within a population of cells; DAPI signal was also shown to decrease significantly during pyroptosis in response to exposure to either nigericin or ATP [Figure 5.10E, F], which was rescued by caspase-3/7 inhibition. Collectively, these data verify an active executioner role for caspase-3/7 in pyroptosis.

5.2.10 Cleaved caspase-3/7 substrates are detected in the nucleus during pyroptosis

Caspase-3/7 proteolytic activity was verified by quantifying the accumulation of their prototypic substrates, PARP and DFF45, in the nucleus following exposure to nigericin or ATP, with staurosporine as a positive control. Cleaved PARP and DFF45 immunoreactivity were detected in the nucleus during pyroptosis at levels comparable to staurosporine exposure [Figure 5.13A-D], with a concomitant decrease in nuclear size [Figure 5.13E]. Nigericin-induced nuclear accumulation of cleaved DFF45 was significantly reduced with caspase-3/7 inhibition [Figure 5.13F, G], illustrating that DFF45 was likely not being cleaved by a different caspase upstream. Likewise, siRNA knockdown of caspase-3/7 prevented PARP cleavage by immunoblot [Figure 5.13H, I]. These observations provided further evidence for the proteolytic activity of caspase-3/7 during pyroptosis.

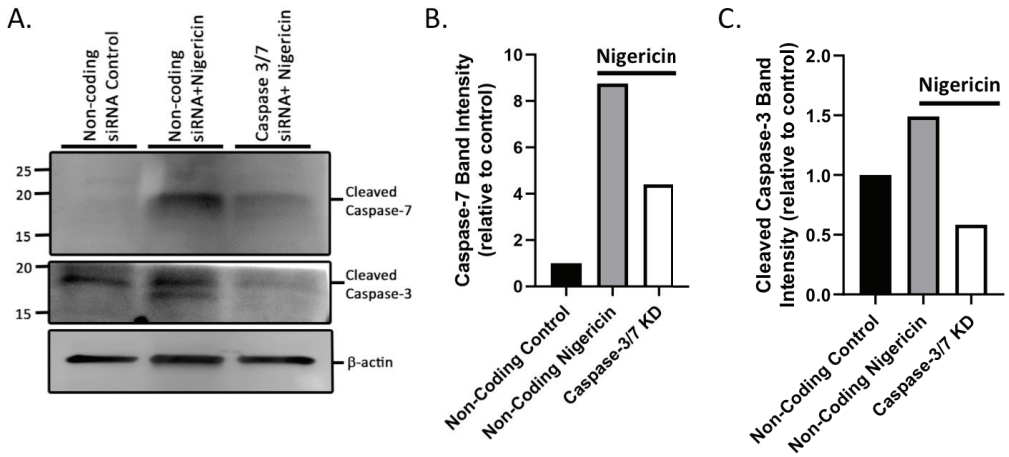

Figure 5.11: ***Validation of caspase-3/7 siRNA knockdown***

(A-B) Microglia were transfected with either universal non-targeting siRNA (NT siRNA) or a cocktail of siRNAs targeting caspase-3 and -7 (Casp-3/7 siRNA; KD = knock-down) prior to nigericin exposure (5μM, 4hrs). Lysates were harvested at the indicated timepoints post-exposure, and immunoblotted for cleaved caspase-7, cleaved caspase-3, and β-actin. **(B-C)** Data shown are protein band intensities of cleaved caspase-7 **(B)** and cleaved caspase-3 **(C)**, normalized to β-actin and expressed relative to untreated non-coding siRNA control.

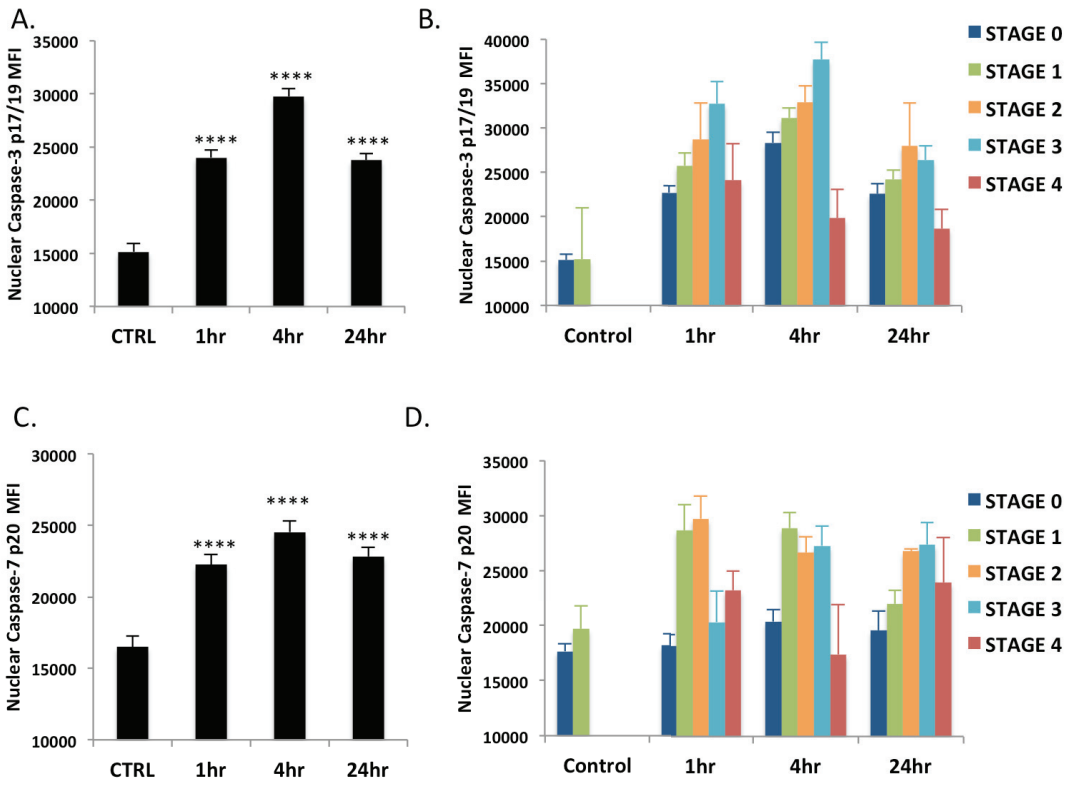

Figure 5.12: ***Nuclear mean fluorescence intensity of cleaved caspsae-3 and -7 peaks prior to cell lysis.***

(A-D) Human microglia were exposed to nigericin (5μM, 1hr, 4hr, 24hr), fixed, immunolabelled for cleaved caspase-3 or cleaved caspase-7, and visualized using confocal microscopy. Mean fluorescence intensity (MFI) of cleaved caspase-3 **(A,B)** or cleaved caspase-7 **(C,D)** in the nucleus was assessed for a minimum of *n*=60 control microglia and *n*=80 microglia per time point post-nigericin exposure. Each cell was classified by stage of pyroptosis and nuclear cleaved caspase-3 **(B)** or cleaved caspase-7 **(D)** MFI was expressed separately for each stage of pyroptosis at the indicated timepoints. Data shown represent mean MFI +/- SEM for a representative human donor with background subtracted. Results were independently recapitulated in microglia from 2 separate human donors (1-way ANOVA with Dunnett's test for multiple comparisons, ****p<0.0001).

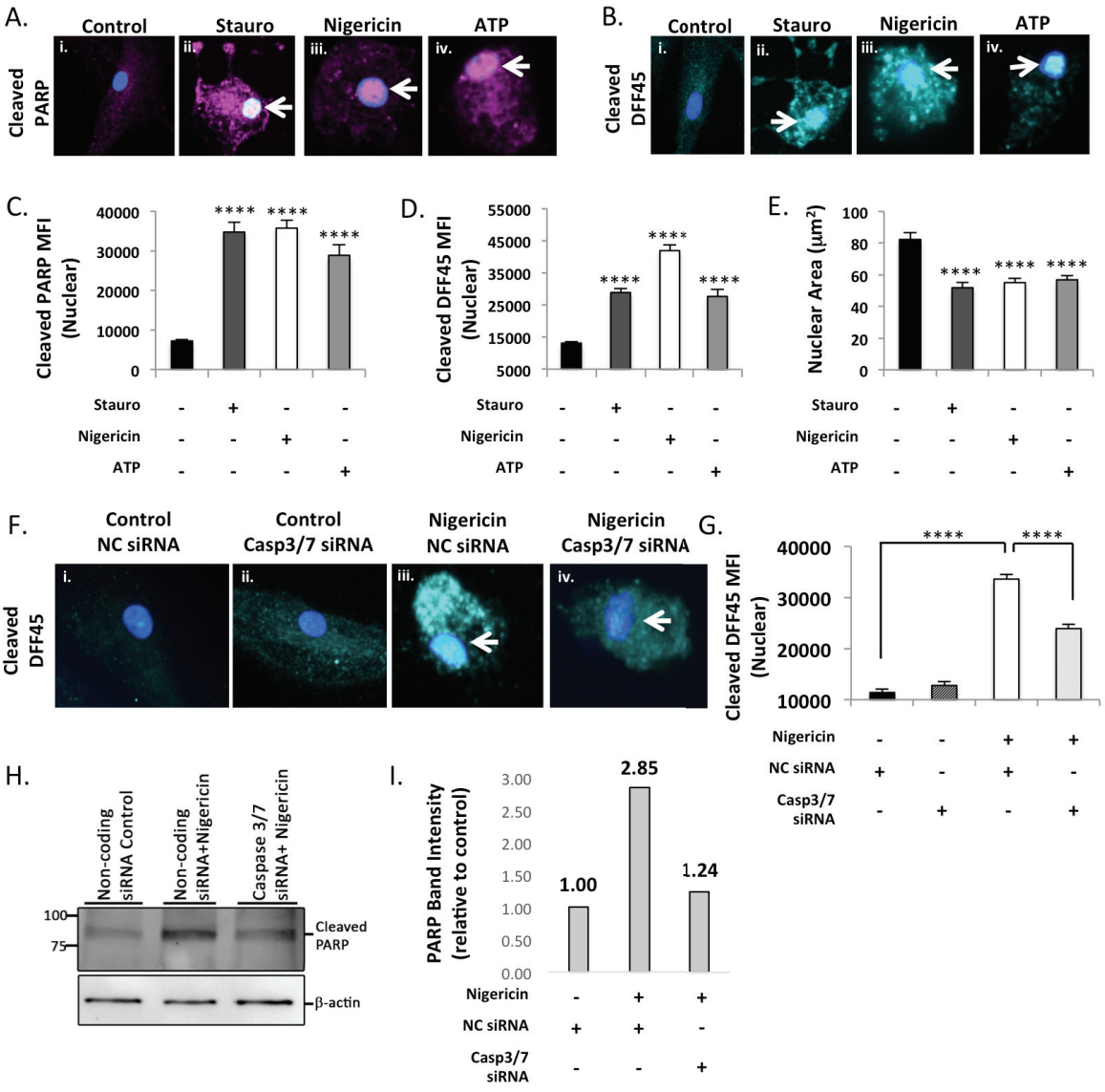

Figure 5.13 *(Figure legend on following page)*

Figure 5.13: ***Caspase-3/7 substrates are cleaved in the nucleus during pyroptosis.***

(A) Human microglia were exposed to nigericin (5μM, 4hrs), ATP (100μM, 24hrs) or staurosporine (5μM, 4hrs), fixed, and immunolabelled for cleaved PARP (**A**, *magenta*) or cleaved DFF45 (**B**, *cyan*). Representative 2-dimensional images shown (nuclei indicated by *white arrows*). **(C-D)** Nuclear mean fluorescence intensity (MFI) of cleaved PARP **(C)** and cleaved DFF45 **(B)** was assessed for 10-20 cells per condition. Microglia in Stage 0 were excluded from analysis. Data shown represent mean nuclear MFI +/- SEM for a representative human donor. **(E)** Cross-sectional area (μm^2) of DAPI-stained nuclei were measured for 10-20 cells per condition. Data shown represent mean nuclear area +/- SEM for a representative human donor. **(F)** Microglia were transfected with either universal non-targeting siRNA (NT siRNA) or a cocktail of different siRNAs targeting caspase-3 and -7 (Casp-3/7 siRNA) prior to nigericin exposure (5μM, 4hrs). Cells were fixed, immunolabelled for cleaved DFF45 (*cyan*), and assessed by confocal microscopy (nuclei indicated by *white arrows*). Representative 2-dimensional images shown. **(G)** Nuclear mean fluorescence intensity (MFI) of cleaved DFF45 was assessed for a minimum of n=20 untreated and n=50 nigericin-exposed cells. Microglia in Stage 0 were excluded from analysis. Data shown represent mean MFI +/- SEM for a representative human donor (1-way ANOVA with Tukey's test for multiple comparisons, ****p<0.0001). All results were independently recapitulated using microglia derived from 2-3 separate human donors. **(H-I)** Microglia were transfected with either NT siRNA or Casp-3/7 siRNA prior to nigericin exposure (5μM, 4hrs). Lysates were harvested and immunoblotted for cleaved PARP and β-actin. Data shown are protein band intensities normalized β-actin and expressed relative to untreated non-coding siRNA control.

5.2.11 Activation of caspase-3/7 mediates pyroptotic body formation and plasma membrane rupture during pyroptosis

Active caspase-3/7 immunoreactivity could also be observed localized to the plasma membrane and within pyroptotic bodies following nigericin exposure [Figure 5.14A]. Given that caspase-3 substrates such as ROCK1 are vital in the formation of apoptotic bodies during apoptosis, we hypothesized that caspase-3/7 and/or their substrates mediate pyroptotic body formation during pyroptosis [Figure 5.14B]. Using semi-quantitative confocal microscopy, I demonstrated that caspase-3/7 suppression led to an accumulation of cells at Stage 2 [Figure 5.14B-C, *orange*], in which GSDMD has translocated to the membrane but pyroptotic bodies have not yet formed, suggesting caspase-3/7 or their substrates might facilitate pyroptotic body formation. Stage 2 cells from the nigericin-treated caspase-3/7 siRNA condition displayed a clear "ring of fire" pattern of GSDMD immunoreactivity, but very low cleaved caspase-3 signal compared to their non-targeting siRNA transfected counterparts [Figure 5.14D].

Next, we tested the effect of caspase-3/7 inhibition on cell membrane rupture during pyroptosis. Both nigericin- and ATP-induced LDH activity in microglial supernatants decreased with caspase-3/7 inhibition, compared to non-targeting controls [Figure 5.14E, F] despite the fact the GSDMD MFI was not affected by caspase-3/7 inhibition [Figure 5.14G]. As LDH is only released upon rupture of the cell membrane, and pyroptotic bodies are believed to be the sites of membrane rupture during pyroptosis, our data would suggest that caspase-3/7 inhibition prevents LDH release [Figure 5.14E, F] through inhibition of pyroptotic body formation [Figure 5.14C]. In apoptosis, the

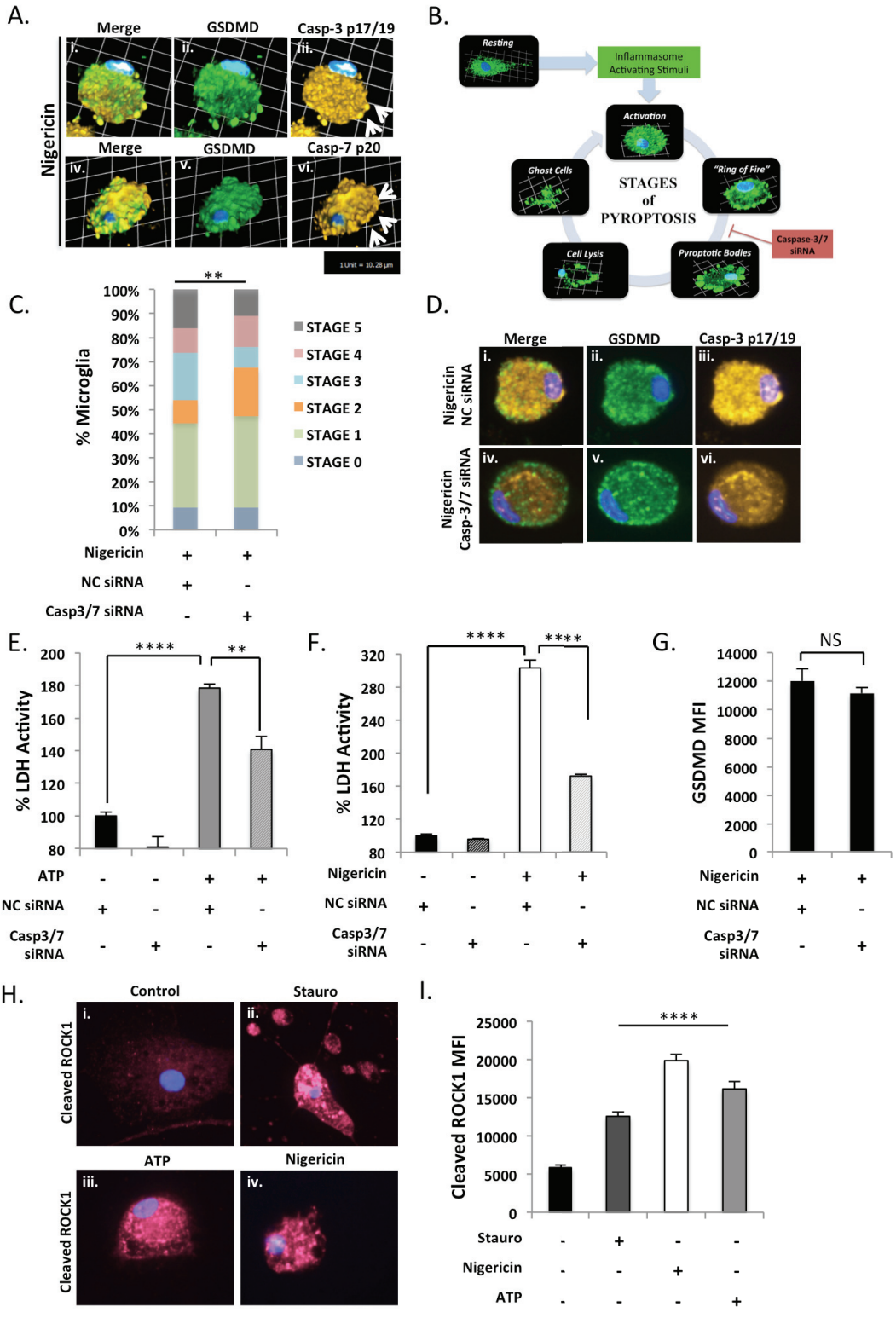

Figure 5.14 *(Figure legend on following page)*

FIGURE 5.14: ***Activation of caspase-3/7 mediates pyroptotic body formation and plasma membrane rupture during pyroptosis.***

(A) Human microglia were exposed to nigericin (5μM, 4hrs), fixed, and immunolabelled for GSDMD (*green*) and either cleaved caspase-3 or -7 (*amber*). *White arrows* indicate cleaved caspase-3/7 accumulation at the cell membrane and in pyroptotic bodies. Images shown are representative 3-dimensional z-stacks incorporating 15 XY planes over a vertical distance of 4-6μm. 1 square unit represents 10.28μm. **(B)** Schematic illustrating the hypothesized role for caspase-3/7 in pyroptotic body formation **(C-D)** Microglia were transfected with either universal non-targeting siRNA (NT siRNA) or a cocktail of different siRNAs targeting caspase-3 and -7 (Casp-3/7 siRNA) prior to nigericin exposure (5μM, 24hrs). Cells were fixed, immunolabelled for GSDMD (*green*) and cleaved caspase-3 (*amber*) and categorized by stage of pyroptosis (Stages 0-5) using confocal microscopy. Distribution of the cells across the stages was assessed using a Chi-squared test (pooled data from two donors shown, $**p<0.01$). **(D)** Representative images illustrating a Stage 2 ("*Ring of fire*") microglia from non-coding (NC) versus caspase-3/7 siRNA-transfected, nigericin-exposed cells. **(E-F)** Loss of cell membrane integrity following exposure of non-coding (NC) or caspase-3/7 siRNA-transfected microglia to nigericin or ATP was assessed by supernatant LDH activity. Data shown are mean +/- SEM for a representative human donor, analyzed using 1-way ANOVA with Dunnett's test for multiple comparisons. LDH assays were performed with technical replicates of n=6-8 wells/condition and results confirmed in multiple donor samples. **(G)** MFI of GSDMD was assessed in nigericin-exposed microglia transfected with either non-coding (NC) or caspase-3/7 siRNA-transfected. Data shown represent mean MFI+/- SEM for a representative human donor (NS = not significant, Student's t-test). **(H-I)** Human microglia were exposed to nigericin (5μM, 4hrs), ATP (100μM, 24hrs) or staurosporine (5μM, 4hrs), fixed, and immunolabelled for cleaved ROCK1. Representative 2-dimensional images shown. **(I)** Mean fluorescence intensity (MFI) of cleaved ROCK1 was assessed (n=20-30 cells per condition). Microglia in Stage 0 were excluded from analysis. Data shown represent mean MFI +/- SEM for a representative human donor (1-way ANOVA with Tukey's test for multiple comparisons, $**p<0.01$, $****p<0.0001$). All results were independently confirmed in microglia derived from 2-3 separate human donors.

caspase-3/7 substrate ROCK1 is key to forming apoptotic bodies through cytoskeletal reorganization[158]. We also assessed whether ROCK1 was proteolytically activated during pyroptosis. Cleaved ROCK1 MFI was significantly increased in microglia exposed to nigericin, ATP, or staurosporine [Figure 5.14H, I], suggesting a potential mechanism linking caspase-3/7 activation with pyroptotic body formation. Collectively, these observations denote a functional role for caspase-3/7 activation upstream of plasma membrane rupture during pyroptosis.

5.2.12 Cleaved caspase-3 is co-expressed with pyroptosis markers in the CNS during MS/EAE

In Chapter III, I demonstrated microglial pyroptosis in white matter of MS autopsy samples and EAE spinal cord lesions, using high levels of GSDMD expression as a biomarker for pyroptosis. Based upon the data in this chapter, we hypothesized that cleaved caspase-3 would be co-expressed with GSDMD during microglial pyroptosis *in vivo*. To assess this, brain tissues from MS and non-MS patients were examined. In control WM, expression of cleaved caspase-3 and GSDMD was low and co-expression was not observed; by contrast, inflammatory MS lesions contained cells co-expressing GSDMD and cleaved caspase-3 [Figure 5.15A, B]. Co-expression was observed in MHC Class II immunopositive cells within MS lesions [Figure 5.15C]. Similarly, GSDMD and cleaved caspase-3 were co-expressed in multiple cells within spinal cord lesions of EAE animals but not in CFA controls [*white arrows*, Figure 5.15D]. Cleaved caspase-3 and GSDMD appeared to be co-expressed within pyroptotic bodies [Figure 5.15D, *inset*].

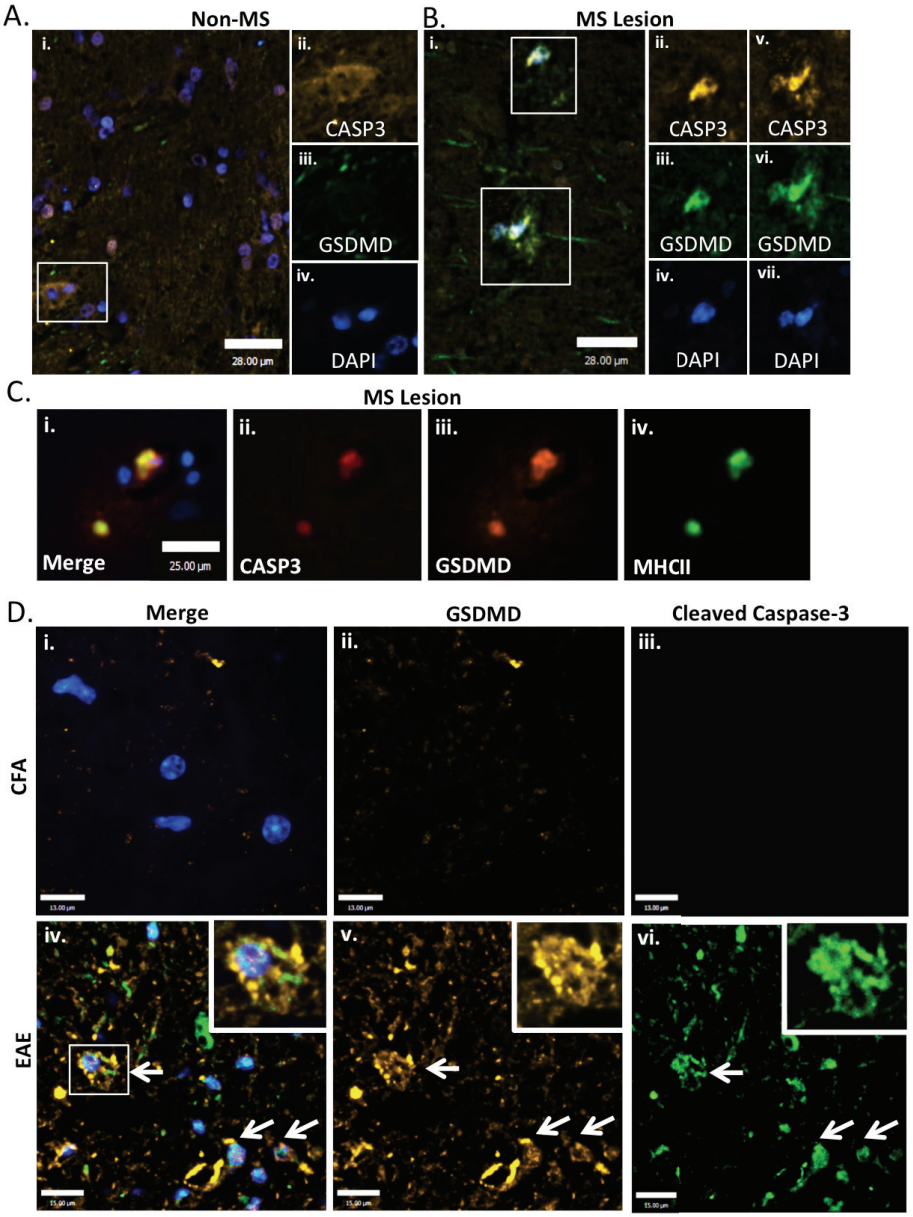

Figure 5.15: ***Co-expression of cleaved caspase-3 and GSDMD during MS/EAE***

(A-B) Autopsy tissue sections from non-MS controls **(A)** or MS patient WM **(B)** were immunolabelled for GSDMD (*green*) and cleaved caspase-3 (*amber*) to assess co-expression within MS lesions. While single immunopositive cells expressing low levels of cleaved caspase-3 are visible in control WM **(Aii-iv)**, multiple double immunopositive cells are visible in MS WM **(Bii-vii). (C)** Triple labeling shows GSDMD$^+$ (*orange*) / cleaved caspase-3$^+$ (*red*) / MHC Class II$^+$ (*green*) triple immunopositive cells in MS WM lesions, indicative of myeloid cells undergoing pyroptosis in conjunction with caspase-3 activation. Scale bar is 25µm. **(D)** Spinal cord lesions from CFA controls and EAE animals at peak disease were immunolabelled for GSDMD (*amber*) and cleaved caspase-3 (*green*) to assess co-expression within EAE lesions. Double-immunopositive cells are indicated with *white arrows*. Both cleaved caspase-3 and GSDMD can be found in pyroptotic bodies of a double-labeled cell (*inset*). Scale bar is 13µm.

V. III. Chapter Summary

As depicted in [Figure 5.16], I have illustrated that upon activation of caspase-1 and the inflammasome with a pyroptotic stimulus such as ATP or nigericin, GSDMD is cleaved and activated by caspase-1, leading to formation of membrane pores and pyroptotic bodies. In parallel, caspase-3/7 are cleaved and activated (either directly or indirectly) downstream of caspase-1, which is inhibited by VX-765. Activation of caspase-3/7 leads to cleavage of caspase-3/7 substrates, which results in the systematic dismantling of cellular structures, including the nucleus. Caspase-3/7 also contribute to the formation of pyroptotic bodies, either directly or indirectly through their proteolytic substrates. Inhibition of caspase-3/7 interrupts pyroptosis, reduces membrane rupture, and prevents nuclear degradation during pyroptosis. Lastly, cleaved caspase-3^{+}/GSDMD^{+} cells putatively undergoing pyroptosis can be found *in vivo* in both MS and EAE.

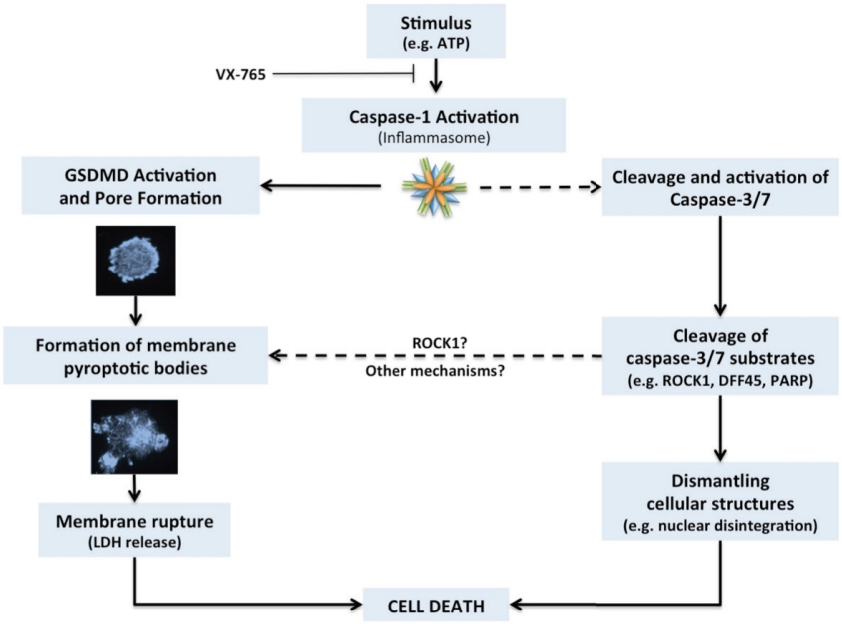

Figure 5.16: ***Schematic representation of caspase-3/7 functions in pyroptosis***

Upon activation of caspase-1 and the inflammasome with a pyroptotic stimulus (such as ATP or nigericin), GSDMD is cleaved and activated, leading to formation of membrane pores and pyroptotic bodies. In parallel, caspase-3/7 are cleaved and activated either directly or indirectly by caspase-1. This leads to widespread cleavage of caspase-3/7 substrates, which results in dismantling of cellular structures, including the nucleus. Caspase-3/7 also contribute to the formation of pyroptotic bodies either directly or indirectly through a cleaved substrate. These two pathways converge to mediate pyroptotic cell death. Inhibition of caspase-3/7, either directly with siRNA or upstream with the caspase-1 inhibitor VX-765, interrupts pyroptosis, reduces membrane permeability, and prevents nuclear degradation during pyroptosis. Dotted lines indicate pathways that may contain intermediates.

CHAPTER VI: DISCUSSION

VI.I. Overall Remarks

In this thesis, I have provided evidence for inflammasome activation and pyroptosis in primary human microglia/macrophages and ODCs in MS/EAE, investigated the molecular mechanisms underlying microglial pyroptosis, and discovered a novel signaling pathway that drives pyroptosis upstream of membrane rupture. Collectively, these results are important for several reasons. Our group was the first to interrogate the role of GSDMD in the CNS and the first to identify evidence for pyroptosis during MS or EAE. These observations are coupled with a therapeutic intervention strategy – namely the well-tolerated, BBB-permeable caspase-1 inhibitor VX-765, which reduces CNS inflammasome activation and pyroptosis (likely through several over-lapping mechanisms – detailed below). Furthermore, I have provided insight into the molecular mechanisms of human microglial pyroptosis *in vitro* in response to MS-relevant stimuli using semi-quantitative confocal microscopy. This platform enabled me to demonstrate conclusively that cells displaying the iconic morphological and molecular features of pyroptosis activate the apoptotic executioner caspases-3/7 as well as their substrates downstream of caspase-1. Although caspase-3/7 activation has occasionally been observed in response to inflammasome-activating stimuli, a functional role for caspase-3/7 has never been shown; moreover, evidence for caspase-3/7 activation has widely been dismissed as indicating a sub-population of apoptotic cells, often without the crucial single-cell analysis that would support this interpretation. In this thesis, I show caspase-1-dependent caspase-3/7 activation at the single-cell level during pyroptosis, and demonstrate that blocking caspase-3/7 prevents cardinal features of pyroptosis, including membrane rupture, pyroptotic body formation, and nuclear disintegration.

This constitutes the first demonstration of a functional role for caspase-3/7 in non-apoptotic cell death, and directly challenges the use of cleaved caspase-3/7 and their substrates as biomarkers of apoptosis. These findings are discussed individually in the sections below.

VI.II. Discussion

OBJECTIVE I:

To evaluate the evidence for CNS inflammasome activation and pyroptosis in MS and EAE and determine whether caspase-1 modulation affects neuroinflammation and neurobehavioural outcomes using the EAE model

Within this objective, I provided evidence for CNS inflammasome activation and pyroptosis in the white matter during both MS and EAE, using high GSDMD expression as a biomarker of pyroptosis [Figures 3.1, 3.2, 3.5, 3.8, 3.9]. While total GSDMD expression in response to non-lethal stimuli (such as IL-1β) is relatively modest and often comparable to untreated microglia [e.g. Figure 5.5B], high intra-cellular expression of GSDMD is a consistent feature of pyroptosis [Figures 4.1, 4.4]. Nonetheless, as discussed in Chapter I, detection of the activated N-terminal of GSDMD is the gold-standard for detecting pyroptosis; however, at the time of writing, no antibodies specific for activated human GSDMD were commercially available and antibodies specific for activated mouse GSDMD only become available after publication of my results[270]. I anticipate that confirmation of these findings, which utilized a monoclonal antibody raised against (but not specific for) the N-terminal domain of GSDMD, will be necessary as the appropriate reagents become available. In the meantime, my observation of the "ring of fire" aggregation of GSDMD immunoreactivity

along the cell membrane in both MS and EAE [Figures 3.1Fii, 3.8Dii] is consistent with known subcellular localization patterns of activated GSDMD.

6.2.1 Discovery of pyroptosis in ODCs

In addition to providing the first evidence of pyroptosis in MS and EAE, we are also the first group to provide evidence of GSDMD expression and pyroptosis in ODC-lineage cells. Hints of caspase-1/11 involvement in ODC cell death under inflammatory conditions have been observed historically, including following TNFα and IFNγ exposure, although these publications preceded the discovery of inflammasomes/pyroptosis and their findings were often conceptualized as a unique caspase-1/11-dependent form of apoptosis[125,126,211,272]. Nonetheless, these studies lend credence to the conclusion that ODCs can undergo pyroptosis *in vitro* and *in vivo,* and in fact demonstrate remarkable concordance with my *in vivo* findings. For instance, I demonstrated in EAE spinal cords that approximately 70% of GSTpi$^+$ ODCs express high levels of GSDMD [Figure 3.9]; this is remarkably similar to early studies quantifying caspase-1/11 expression in spinal cord lesions during EAE, which demonstrated that approximately 50% of GSTpi$^+$ ODCs were immunopositive for caspase-1, while over 70% of ODCs were immunopositive for caspase-11[125].

These findings highlight another limitation of this thesis, wherein caspase-1 but not caspase-4/11 was specifically investigated for its role in pyroptosis. The above study, as well as transcriptional data from this thesis demonstrating up-regulation of human caspase-4 [Figure 3.1] and murine caspase-11 [Figure 3.4] during MS and EAE respectively, highlights that other caspase-1-family proteases may play a role in CNS

inflammasome activation during MS/EAE. Interestingly, caspase-4/11-dependent non-canonical inflammasome activation is best characterized in the context of LPS stimulation and bacterial infection[273,274], raising the possibility that either (i) CNS microbiome components are triggering inflammasome activation during demyelination[275] or (ii) additional activators of the caspase-11 inflammasome exist but have yet to be characterized. Considering the role for caspase-11 in ODC death previously established in the literature, this warrants further investigation.

As demonstrated in the schematic [Figure 3.12], proinflammatory cytokines (including TNFα) released from activated microglia during MS/EAE are one potential mechanism driving ODC pyroptosis. A role for TNFα in MS/EAE is well-documented and high levels of TNFα expression were confirmed at the transcript level during my time course experiments [Figure 3.3B]. Our group has also verified that exogenous TNFα can induce pyroptosis in ODC lineage cells *in vitro* [MSc thesis of Leina Saito, *in progress*], which is coupled with high expression of GSDMD and caspase-1, cellular rounding, and loss of processes; ODC pyroptosis is rescued with caspase-1 inhibition using VX-765. Although TNFα has also been shown to cause ODC apoptosis[276] and necroptosis[232], these observations highlight that cell death modality is likely context-dependent, and different responses to the same stimuli may be observed depending on variables such as the maturation state, surface marker expression profile, and species of the ODCs being studied. At the same time, it bears consideration that biomarkers used for decades as indicators of apoptosis (including membrane blebs, nuclear disintegration, TUNEL positivity, caspase-3/7 cleavage, PARP cleavage, and Annexin V staining) are shared

with pyroptosis; likewise, experimental approaches that have historically been used to validate apoptosis (such as pan-caspase blockade using Z-VAD-FMK) likewise block pyroptosis through inhibition of caspase-1/11. Thus, early studies must be interpreted with the caveat that many of the techniques used therein would not have adequately distinguished between apoptosis and pyroptosis. Although TNFα was utilized as a proof-of-principle cytotoxic agent to induce ODC pyroptosis *in vitro* in our lab [Leina Saito, MSc thesis, *in progress*], extracellular DAMPs might also cause ODC pyroptosis during MS/EAE. For instance, ODCs express P2X7R, and ATP can cause ODC cell death through what was deemed to be P2X7R-dependent excitotoxicity[277] and thus DAMPs merit further investigation as potential triggers of ODC pyroptosis. Importantly, my studies herein do not necessarily implicate pyroptosis as the primary form of ODC cell death in MS/EAE, nor as the initiating event in demyelination, since various other mechanisms driving ODC loss have been well documented (including both antigen-dependent and antigen-independent T-cell toxicity, as well as auto-antibodies against myelin components[90]). Nonetheless, my findings demonstrate a potential mechanism linking robust microglia/macrophage activation to ODC death in the context of inflammatory demyelination.

6.2.2 Pyroptosis in other demyelination models

To further interrogate the hypothesis that ODC pyroptosis plays a role in demyelination, our lab has also investigated GSDMD expression in the cuprizone model of demyelination, which involves chronic demyelination coupled with local microglial and astrocyte activation. These experiments suggest a significant increase in the number of $GSDMD^+$ ODCs in the corpus callosum of mice receiving cuprizone compared to control

mice, and rescue experiments with VX-765 are in progress at the time of writing [Leina Saito, MSc thesis, *in progress*]. These results support a potential role for ODC pyroptosis in a demyelination model that lacks an autoimmune component and reduces the likelihood that my observations in EAE were unique to that model. It would be informative in the future to expand these studies to other models of inflammatory demyelination that recapitulate different aspects of MS pathogenesis. In the current studies, female MOG_{35-55} C57/Bl6 EAE mice were used to study white matter lesions in the spinal cord and demonstrate evidence for ODC pyroptosis in white matter lesions at peak disease. This model involves an acute monophasic disease course, with disease activity occurring predominantly in the spinal cord, and does not recapitulate the progressive stage of MS, which involves total brain atrophy, profound axonal loss in both lesions and NAWM, an abundance of subpial/cortical lesions, and permanent neurological deficits corresponding with axonal loss[212]. To that end, it warrants exploring whether pyroptosis contributes to neurodegeneration in the progressive stage of MS using mouse models that recapitulate this phenotype. Examples of this include MOG_{35-55} immunization on the non-obese diabetic (NOD) mouse background[278] or spinal cord homogenate or the neuronal antigen neurofilament light chain (NF-L) immunization on the Biozzi ABH mouse background[279,280]. Likewise, the current studies were largely confined to white matter lesions of the spinal cord, since this is the primary site of disease activity in the MOG_{35-55} C57/Bl6 EAE model. Cortical lesions are not well recapitulated in this experimental system, and thus merit further investigation in a different model, such as the EAE/cuprizone model wherein demyelination is induced using pre-intoxication with cuprizone prior to immunization with MOG_{35-55}; profound

cortical and subcortical grey matter lesion formation is apparent in this system[281]. In our current model, neuronal pyroptosis was not a major consideration since neuronal cell bodies are not located within the white matter lesions under investigation; nonetheless, it would be fascinating to interrogate whether neuronal pyroptosis plays a role in cortical lesions using the appropriate animal models. All animal models have the potential to be confounded by the method of inducing demyelination, and thus histological examination of cortical lesions from MS autopsy samples would be the most direct way of answering this question.

6.2.3 GSDMD-deficient mouse models

Regardless of the demyelination model under investigation, one current limitation is the lack of a commercially available GSDMD knock-out mouse (anticipated to be available from Jackson labs July 2019). Clearly, as these mice become available, it will be necessary to repeat the pertinent experiments in a GSDMD-deficient background. While such experiments are certainly necessary, an important caveat is that GSDMD also likely plays a role in unconventional cytokine release[180]. This may confound the ability to interpret the pathogenic role of pyroptosis as distinct from IL-1β and IL-18 (both of which have clearly defined pathogenic roles in EAE) in a GSDMD-deficient mouse model, as GSDMD-deficient macrophages have been shown to have deficient cytokine release pathways[81,282]. One future strategy to circumvent these issues would be to examine the disease course of GSDMD single-knockout animals compared to IL-1β/IL-18 double knockout animals, and triple knockout animals deficient in GSDMD, IL-1β, and IL-18. Although such triple knockout animals are not currently available, one could anticipate

a growing need for them within the field of pyroptosis research. GSDMD inhibitors that are tolerated *in vivo* have recently been reported[175,176], and these could be used in conjunction with existing IL-1β/IL-18 double knockout transgenic mice to determine whether blocking GSDMD pore formation confers additional therapeutic benefit in the context of IL-1β and IL-18 deficiency in an EAE model.

6.2.4 Pyroptosis as a mechanism of primary demyelination

One clear future direction that emerges from these observations is the determination of whether the induction of pyroptosis in ODCs *in vivo* can drive primary demyelination. A number of interesting approaches could be considered to interrogate this hypothesis, with varying degrees of feasibility. One approach would be the inducible expression of the pore-forming N-terminal fragment of GSDMD in an ODC-specific manner; such approaches have already been developed to induce caspase-9-mediated apoptosis in ODCs and these models could inform a comparable strategy using GSDMD as the driver of ODC death[231,283]. Although extremely informative, such models have yet to be developed. Studies using TNFα-transgenic mice (Tg6074) that constitutively over-express murine TNFα in a CNS-specific manner demonstrated demyelination, microglial activation, and ODC apoptosis in patterns that histologically resembled chronic MS lesions[276]; however, the primary indicators of apoptosis utilized in the paper (nuclear morphology and TUNEL staining) are not specific to apoptosis[276]. Such experiments would be worth revisiting to determine whether constitutive TNFα expression in the CNS induces ODC pyroptosis, either instead of or in parallel to ODC apoptosis, using activated GSDMD as a read-out for pyroptotic cell death.

6.2.5 Pyroptosis as a driver of CNS autoimmunity

Studies in which GSDMD-mediated pyroptosis could be specifically induced in ODCs would also provide the fascinating opportunity to assess whether pyroptosis of ODCs can induce an adaptive response against CNS antigen. As might be predicted, models that induce widespread ODC apoptosis through ODC-specific caspase-9 activation do not seem to generate an autoimmune response despite generating microglial activation[231]. By contrast, diphtheria toxin-induced depletion of ODCs in the DTA mouse model induces a fatal T-cell-mediated demyelinating disease several months after recovery from the initial insult, which is characterized by temporary demyelination and microglial activation/proliferation[284,285]. In these studies, ODC cell death in response to diphtheria toxin was interpreted as apoptotic, based upon TUNEL staining and cleaved caspase-3 immunopositivity, but the conclusions of this thesis suggest that diphtheria toxin-mediated ODC ablation might be pyroptotic instead. By using a model in which the pore-forming N-terminal domain of GSDMD was uniquely over-expressed in ODCs, one could drive pyroptosis unequivocally and determine specifically whether pyroptotic death of ODCs could drive CNS-targeted autoimmunity. Given the various functional roles of inflammasome-associated cytokines in adaptive immunity[286], and the likelihood that pyroptosis would liberate greater quantities of myelin antigen, this seems a worthy and interesting hypothesis to investigate.

6.2.6 Microglial/macrophage pyroptosis in the CNS

In this thesis, evidence is also provided for microglial/macrophage pyroptosis in the context of MS/EAE. While death of ODCs is clearly a major component of MS/EAE

pathology, death of myeloid cells has not been well-studied. Despite well-documented toxicity towards ODCs, TNFα activates but does not cause pyroptosis in primary human microglia [Figure 4.3K,L]. Nonetheless, a precedent for myeloid cell death does exist in the literature in MS/EAE, where it was hypothesized to result from activity-induced cell death[206] or iron overload[287]. It is conceivable that the extent of myeloid cell death in MS/EAE has been under-estimated due to the massive recruitment of macrophages/microglia to sites of demyelination. Further evidence that these GSDMD high-expressing macrophages/microglia are indeed dying in the context of these MS/EAE studies could be provided by co-staining with TUNEL, a non-specific indicator of DNA damage and cell death. Multiple reports have indicated that TUNEL-positive macrophage and microglial populations are detectable during EAE[206,235], but cell death was attributed to apoptosis based upon TUNEL staining alone. Importantly, although high-throughput RNA sequencing and mass cytometry studies have been performed to characterize myeloid cells in the context of inflammatory demyelination, the parameters of such studies may exclude dying cells from analysis; thus the population of dying myeloid cells likely remains incompletely characterized.

6.2.7 The nature of DAMPs driving pyroptosis in MS/EAE

In these studies, it was hypothesized that the high concentration of extracellular DAMPs (such as ATP) released by ODC death and/or axonal degeneration might be a trigger for microglial/macrophage pyroptosis. ATP was chosen for further investigation because of the pathogenic role of its receptor P2X7R in EAE[39]; P2X7R is also known to be up-regulated on activated microglia/macrophages within spinal cords of MS patients[37] and gain-of-function mutations in the P2X7R are associated with increased risk of MS[38].

Proof-of-principle evidence is provided *in vitro* that extracellular ATP can trigger microglial pyroptosis [Chapter IV]. To test this hypothesis *in vivo*, a number of experimental strategies are possible, including (i) depletion of extracellular ATP through systematic administration of apyrase[288] during EAE (ii) blocking of ATP signaling using a broad-spectrum antagonist of the P2 purinergic receptors[288] or (iii) induction of EAE in a P2X7R-deficient background, using $GSDMD^{+}$ macrophages/microglia as a readout. Several of these strategies have been tested in EAE and are associated with improvements in neurobehavioural outcomes, but a link with pyroptosis has never been established. A different approach would be to investigate primary ODC depletion models (such as the diptheria toxin ODC ablation model[285]) to determine whether acute ODC loss causes sufficient extracellular DAMP release to induce microglial pyroptosis. This strategy could be used in combination with ATP/P2X7R blocking strategies to determine whether this effect was mediated specifically by extracellular ATP. Microglial pyroptosis in the cuprizone model is currently being evaluated [Leina Saito, MSc thesis, *in progress*], but it is possible that the gradual nature of ODC loss during cuprizone-induced demyelination prevents the large-scale accumulation of extra-cellular DAMPs sufficient to trigger microglial/macrophage pyroptosis.

6.2.8 Macrophages versus microglia

In these studies, pyroptosis was demonstrated in both ODCs and microglia/macrophages based upon the expression of GST-pi and Iba-1 respectively. Unfortunately, this paradigm did not distinguish between infiltrating macrophages and resident microglia. Although infiltrating macrophages and microglia share many

morphological, molecular, and functional features, recent studies have begun to highlight heterogeneity between the two groups, particularly in the context of inflammatory demyelination. Evidence exists in the literature for the expression of inflammasome-associated genes in both cell types within the context of EAE; Yamasaki and colleagues investigated differential roles for the two cell types in EAE using transgenic mice expressing GFP under the Cx3CR1 promoter (microglia) and RFP under the CCR2 promoter (monocyte-derived macrophages) across four different stages of EAE (naïve, onset, peak disease, and recovery)[289]. The authors showed enrichment of inflammasome-associated genes in both macrophage and microglial populations, with microglia showing enriched *il18* expression compared to monocyte-derived macrophages, and macrophages showing enriched *il1b* compared to microglia, when cells from all time points in EAE were analyzed collectively[289]. When compared to naïve mice, microglia showed a profound up-regulation of genes involved in acute inflammation, including *il1b*. Other studies have also demonstrated that disease-associated choroid plexus macrophages highly up-regulate *il1b* at peak disease compared to naïve mice[235]. Thus, one cannot infer from the literature whether inflammasome activation and/or pyroptosis is preferentially induced in microglia, CNS-resident macrophages, or monocyte-derived macrophages. Yamasaki et al and other groups have indicated that infiltrating macrophages tend to predominate in the early stages of disease, while microglia predominate later in the disease course of EAE[289]. Although GSDMD was not profiled over time at the protein level in this study, GSDMD was induced at the transcript level in the mid-late stages of EAE. This may be a function of GSDMD being more prominently expressed in microglia, which accumulate

preferentially in peak disease rather than at onset, or may simply be a function of cell death occurring later in the disease course. To definitely address the macrophages versus microglia question, high throughput cytometry experiments would be very helpful. Likewise, the current study did not screen other immune cells (e.g. neutrophils, T cells, etc.) for evidence of pyroptosis; a precedent exists in the literature for pyroptosis in T cells, DCs, neutrophils, and other cell types that are known to accumulate during demyelination, although these have predominantly been characterized in infection models[271,290,291].

6.2.9 Inflammasome sensors in EAE

Within these EAE studies, expression of inflammasome components was also profiled in the hindbrain of animals at various stages of disease [Figure 3.4]. In addition to verifying the up-regulation of *gsdmd* and various other inflammasome components such as *casp1* and *asc*, these studies revealed a number of different inflammasome sensors whose expression was up-regulated, including *nlrp3* (detects various DAMPs), *aim2* (detects double-stranded DNA), *mefv* (encodes pyrin; detects bacterial toxins), *nlrp1* (detects bacterial proteases), and *nlrc4* (detects flagellin). Of these, only the NLRP3 and pyrin inflammasomes have previously been implicated in the pathology of EAE[250,252,258], although polymorphisms in *NLRP3* and *NLRC4* that decrease their expression levels have been associated with decreased MS risk[292]. Several possibilities may be considered for the interpretation of the data. Firstly, tissue-wide up-regulation at the transcript level does not necessarily indicate that these sensor proteins are engaging their ligand at the protein level. Different sensors are expressed at baseline in different cell types, and thus changes in inflammasome sensor expression at the tissue level may simply

reflect an influx of immune cells and the resultant changes in the cellular composition of the tissue. Secondly, it is possible that sensors with bacterial ligands are being engaged during EAE as a result of the bacterial components used during active EAE induction (e.g. PTX) as has previously been illustrated with the pyrin inflammasome[252]. However, *NLRP1*, *MEFV (*pyrin*)*, and *AIM2* also demonstrated trends towards up-regulation in MS white matter [Figure 3.1], suggesting that this phenomenon may not be unique to the EAE model. Thirdly, it is possible that these inflammasome sensors engage with less well-characterized ligands, potentially DAMPs in addition to their well-characterized PAMP ligands. For instance, NLRP1, AIM2, and NLRC4 inflammasomes contribute to the pathology of TBI, which is generally considered a sterile-injury model, and have been proposed to detect DAMPs during neuroinflammation, although definitive ligands have not yet been identified[293,294]. Likewise NLRP1 has been repeatedly implicated in AD, in which amyloid-beta aggregates trigger NLRP1 inflammasome activation[138]. I did not test which sensor proteins are involved in the pathology of EAE in this thesis; genetic studies using knock-out mice will be required to determine which of these inflammasomes, in addition to NLRP3 and pyrin, might contribute to the pathogenesis of EAE.

6.2.10 Strengths and limitations of VX-765

In this study, the BBB-permeable, clinically tested caspase-1 inhibitor VX-765 was used as a therapeutic in EAE. This approach generated partial improvements in neurobehavioural outcomes [Figure 3.10I], reduced neuroinflammation and preservation of axons/motor neurons [Figure 3.8, 3.10, 3.11]. These observations were

associated with a significant reduction in the proportion of GSDMD$^+$ ODCs and microglia/macrophages, suggesting a decrease in pyroptosis associated with improved disease outcomes [Figure 3.9]. VX-765 may be protective through several mechanisms, including: (i) inhibition of T cell priming and extravasation into the CNS (ii) inhibition of CNS endothelial cell priming and monocyte extravasation into the CNS (iii) inhibition of microglial/macrophage IL-1β and IL-18 release within the CNS, and (iv) inhibition of pyroptosis in multiple cell types. Dissecting the mechanism at play would be challenging, since inhibiting pyroptosis *in vivo* without affecting cytokine release is not currently feasible. While multiple mechanisms of action complicate the scientific interpretation of my data, they are advantageous clinically, in that the same compound would putatively provide clinical benefit through immunomodulatory and neuroprotective mechanisms. While VX-765 is considered specific for caspase-1, it likely retains some off-target activity against other caspases, e.g. caspase-4/11[113]. Testing VX-765 in a caspase-1-deficient background would determine whether it retains therapeutic efficacy. Although the protective effect of VX-765 suggests a pathological role for inflammasome activation/pyroptosis, protection from EAE is only partial; early treatment may improve the magnitude of this effect. Nonetheless, the diversity of pathological mechanisms that ultimately contribute to MS/EAE suggests that a combinatorial approach, using VX-765 with other DMTs, will ultimately be a more viable approach than VX-765 alone.

OBJECTIVE II:

To characterize primary human microglial pyroptosis ex vivo using well-characterized and disease-relevant NLRP3 inflammasome activating stimuli and to validate a clinically relevant inhibitor of caspase-1 in this system

Within this objective, primary human microglia were established as a model for both inflammasome activation and pyroptosis *in vitro* and a classification paradigm was proposed for profiling the molecular and morphological features of pyroptosis using semi-quantitative confocal microscopy. The caspase-1 inhibitor VX-765 as a modulator of inflammasome activation and pyroptosis was also validated *in vitro* and both nigericin and ATP were shown to induce pyroptosis in a GSDMD-dependent fashion.

6.2.11 Considerations for human fetal microglia

One consideration is the use of human fetal microglia for our *in vitro* studies. As has been extensively reviewed[34], embryonic and early postnatal murine microglia have unique transcriptional signatures compared to adult homeostatic microglia, and likewise cultured microglia have distinct transcriptional signatures compared to their *in vivo* counterparts[20,295]. Our lab has not yet performed transcriptomics studies on human fetal microglia compared to adult human microglia, although this would certainly be a valuable study. Nonetheless, sources of adult human microglia are limited (e.g. epilepsy surgical resections and very rapid autopsies) and have their own confounding factors. For instance, microglia can be successfully cultured from surgical samples from epilepsy and GBM patients[296], but both of these diseases have persistent microglial activation, and specifically increased inflammasome activation, as part of their disease pathology[122]. Likewise, autopsy samples are a viable source of adult microglia[296], but may be confounded by factors such as "inflammaging", the donor-specific microbiome (gut and other organs), and cause of death. When studying human microglia in a disease-specific context (e.g. MS), microglia derived from human autopsy samples for

the disease of interest would be ideal, using age- and sex-matched controls where possible, though the practical feasibility of this approach is an ongoing consideration.

Another consideration that pertains to our microglial studies is the possible presence of other CNS macrophage populations, including perivascular, meningeal, and choroid plexus macrophages, within our microglial preparations. Although we have previously demonstrated that cells within these cultures are immunopositive for Iba-1[263], we have not yet attempted to discriminate between the contributions of different CNS macrophage populations to this myeloid population.

6.2.12 Activators of pyroptosis in human microglia

Many of the experiments in this chapter were performed using nigericin, an extremely well-characterized NLRP3 inflammasome activator. Since NLRP3 emerged as a sensor protein of interest in both MS and EAE, this was considered a useful approach to characterize microglial pyroptosis. Nigericin was an excellent tool to establish that microglia display the prototypic signs of pyroptosis, including the "ring of fire", pyroptotic bodies, and nuclear disintegration [Figure 4.1, 4.7], and for demonstrating that VX-765 inhibited inflammasome-associated cytokine release and pyroptosis as predicted. However, as a bacterial pore-forming toxin, nigericin does not represent an MS-relevant inducer of pyroptosis. To this end, several cytokines released from activated microglia in MS/EAE, including IL-1β, IL-18, and TNFα, were tested for the ability to induce pyroptosis; none of them were found to induce LDH release or loss of cell viability [Figure 4.3]. By contrast, ATP-exposed microglia release inflammasome-associated cytokines and readily undergo pyroptosis [Figure 4.4]. Extracellular ATP has

been shown to be a relevant DAMP in MS/EAE; its primary receptor (the P2X7 receptor, a ligand-gated ion channel) is widely expressed in the nervous system[297], and blocking P2X7R is protective in EAE[277]. The P2X7 receptor is also elevated in MS in various cell types including macrophages/microglia[37,277], highlighting a potential role for extracellular ATP in the disease pathogenesis. As suggested by qRT-PCR [Figure 4.2], transcriptional up-regulation of inflammasome-associated genes is not required for microglial pyroptosis; although the LPS+ATP two-signal paradigm is well-validated, human microglia did not require transcriptional priming to undergo pyroptosis. This provided an opportunity to interrogate mechanisms of pyroptosis independently of a TLR-ligation step. As many neurological conditions do not have a clear microbial component, the absence of LPS may more accurately recapitulate "sterile" disease. For ATP and nigericin-induced pyroptosis, both siRNA-mediated knock-down of GSDMD and caspase-1 inhibition with VX-765 only partially rescued cell death (measured by LDH release). This may result from incomplete target inhibition, or may indicate a degree of functional redundancy with related caspase or gasdermin family members.

6.2.13 Classification of the stages of pyroptosis

Within this objective, a paradigm for classifying the stages of pyroptosis in fixed populations of microglia was proposed. As discussed in Chapter I, different stages of pyroptosis have been identified in the literature using a combination of scanning electron microscopy and live cell imaging. Exposure of macrophages to pyroptosis-inducing stimuli has been shown to cause a distinctive enrichment of GSDMD immunoreactivity at the plasma membrane early in pyroptosis, followed by the

formation of pyroptotic bodies[167]. In the later stages of pyroptosis, the cell membrane ruptures, leaving a relatively intact nucleus and diffuse GSDMD-immunopositive cellular debris[167]. Live cell imaging has recapitulated these findings, illustrating that diffuse cytoplasmic GSDMD immunoreactivity gives way to localized aggregates of GSDMD immunoreactivity at the plasma membrane, and this plasma membrane localization corresponds to the appearance of pyroptotic bodies[177]. Based upon this literature, the stages proposed for classification of fixed microglia were: STAGE 0: "Intact" (adherent cell with elongated processes, baseline GSDMD expression); STAGE 1: "Rounding" (rounded cell, loss of processes, high GSDMD expression); STAGE 2: "Ring of fire" (translocation of GSDMD to the cell membrane); STAGE 3: "Pyroptotic bodies" (formation of $GSDMD^+$ membrane blebs); STAGE 4: "Lysis" (rupture of the cell, nucleus intact), and finally STAGE 5: "Ghost cells" (nucleus disintegrated, some $GSDMD^+$ cell contents remain). Because the population of microglia is fixed and microglia are not tracked longitudinally, several important caveats inform the use of this classification method. First, Stage 1 microglia are rounded and lose their processes, a morphology that is consistent with microglial activation, and although it has been observed prior to pyroptosis by live cell imaging, this rounded morphology is not unique to pyroptosis and thus it is conceptualized as a pre-pyroptotic activation stage. By contrast, Stages 2 and 3 display unequivocal morphological features of GSDMD-dependent pyroptosis, including the accumulation of GSDMD at the cell membrane and the formation of highly GSDMD immunopositive pyroptotic bodies. No other cell death sub-routine documented to date includes these features. This became particularly important in Chapter V, during which I sought to prove that cleaved caspase-3/7 were present in cells unequivocally

undergoing pyroptosis. Although I did not capture pyroptotic bodies bursting in real time with live cell imaging, I was able to find examples in which the cell had been fixed immediately following the rupture of one of its pyroptotic bodies [Figure 4.9], representing the transition stage between Stage 3 and 4. Stage 4 is a lytic phenotype, which has been observed following pyroptotic body rupture by live cell imaging; nonetheless, other lytic cell death sub-routines exist and thus it is not possible to ascertain that a given cell at Stage 4 died by pyroptosis. Stage 5, which consists of a cellular corpse that has not yet disintegrated, likewise is not unique to pyroptosis and may include necrotic cells as well. With those caveats considered, the classification paradigm was validating by showing the sequential appearance of the different stages of pyroptosis over time. Notably, a few cellular corpses were apparent at very early time points post-treatment with nigericin, suggesting that at least a small fraction of cells succumbed to a much faster lytic process, such as necrosis.

The development of this classification paradigm enabled us to investigate the unique morphological features of pyroptosis by stage. This is important because pyroptosis in response to nigericin or ATP is neither instantaneous nor synchronized, and the first wave of cell death in response to the stimulus itself may trigger secondary and tertiary rounds of pyroptosis within the population. Because pyroptosis is not synchronized across the population, dramatic molecular differences may be minimized or disguised, either by the resting non-pyroptotic (Stage 0) cells or lytic cells (Stage 4) within that population; both of these groups have vastly different molecular properties than cells actively undergoing pyroptosis. For instance, cells in Stage 2 and 3 (which are

unequivocally undergoing pyroptosis) have the highest GSDMD levels at all time points tested; however, Stage 4 lytic cells have GSDMD expression that is on par with untreated controls. The classification paradigm was also used to demonstrate that nuclear cross-sectional area decreases over time, with the most profound decrease corresponding to the lytic stage of pyroptosis [Figure 4.7]. This is important, because nuclear shrinkage/condensation has been used historically as a histological indicator of apoptosis, despite evidence that it is not unique for non-inflammatory cell death[298].

Most importantly, the classification paradigm permitted the development of two experimental strategies that would prove critical for the final objective of this thesis. Firstly, it allowed the identification and analysis of a population of cells that were unequivocally undergoing pyroptosis. Given the propensity of researchers to dismiss caspase-3/7 activation during pyroptosis as a sub-population of apoptotic cells, the ability to unequivocally identify pyroptotic cells was essential. Secondly, it enabled us to determine whether inhibition of caspase-3/7 affected progression through pyroptosis. This approach was validated using VX-765, which caused cells to accumulate in Stage 1 rather than progressing to Stage 2 [Figure 4.6]. Thus, the classification paradigm would enable us to test whether the distribution of cells across the stages of pyroptosis at a given time point was affected by caspase-3/7 inhibition in Chapter V.

Nonetheless, validation of our classification paradigm by tracking single cells longitudinally in culture using two-photon microscopy would be important for validating our results.

OBJECTIVE III:

To interrogate whether a functional role exists for apoptotic caspases-3/7 in pyroptosis using human microglia as a model system

In this objective, a ground-breaking functional role for the apoptotic executioner caspase-3/7 in pyroptosis was discovered. Caspase-3/7 were shown to be activated downstream of canonical NLRP3 inflammasome activation, as inhibition of caspase-1 with VX-765 blocked caspase-3/7 activation induced by either ATP or nigericin [Figure 5.3, 5.6]. As an extra measure, it was demonstrated that while VX-765 does inhibit nigericin- and ATP-induced caspase-3 activation, it does not inhibit staurosporine-induced caspase-3 activation, reducing the likelihood that VX-765 exerts off-target effects on caspase-3 itself. Validation of these results using caspase-1-targeting siRNAs is currently underway in the lab. Nonetheless, an important limitation of this work is that it has not yet been shown whether caspase-1 cleaves caspase-3/7 directly or through an intermediate caspase. Direct cleavage and activation of caspase-3/7 by caspase-1 has been repeatedly shown in the literature[78,80], so this mechanism is plausible. The p19 caspase-3 fragment was shown to accumulate preferentially in response to pyroptotic but not apoptotic stimuli, which is a cleavage signature associated with caspase-1-mediated rather than caspase-8/9-mediated cleavage of caspase-3[80]. Nonetheless, this evidence is far from definitive, and future studies will be required to determine whether caspase-3/7 are activated by inflammasome-associated caspase-1 or by a different initiator caspase downstream of caspase-1. Inhibition of the initiator caspases-8/9, with activated caspase-3 as a read-out, would be an important first step in addressing this question.

6.2.14 GSDMD and mitochondrial depolarization

One alternative pathway that has not been excluded is whether caspase-3 is activated downstream of GSDMD-mediated mitochondrial damage during pyroptosis. GSDMD has been postulated to interact with a variety of membranes in the cell and has been shown to accumulate in the mitochondria following non-canonical inflammasome activation[188]. In this case, one could hypothesize that caspase-1 activates GSDMD, which permeabilizes the mitochondrial membrane, leading to cytochrome C release, caspase-9 activation and apoptotsome formation, and subsequent activation of caspase-3/7 by caspase-9. Studies are in progress in the lab to determine whether GSDMD deficiency reduces caspase-3 cleavage and whether GSDMD localizes to the mitochondria in response to canonical NLRP3 inflammasome activation.

6.2.15 Role for caspase-3/7 in pyroptotic body formation

Although cleavage of caspase-3/7 and their substrate PARP downstream of caspase-1 has been shown previously in the literature[78-80,181], this is generally either (i) only unmasked in the context of GSDMD deficiency or (ii) interpreted to occur in a subset of apoptotic rather than pyroptotic cells. To our knowledge, prior to this thesis, no group has demonstrated caspase-3/7 activation at the single cell level in cells undergoing GSDMD-dependent pyroptosis. Using the classification paradigm developed in Chapter IV, we were able to demonstrate and quantify cleaved caspase-3/7 immunoreactivity in cells that were unequivocally undergoing pyroptosis, identified by either the ring of GSDMD immunoreactivity (Stage 2) or GSDMD$^+$ pyroptotic bodies (Stage 3). Evidence was also provided for a functional contribution of caspase-3/7 to pyroptosis. These

proteins facilitate the formation of pyroptotic bodies, as caspase-3/7 inhibition with siRNA caused cells to accumulate in Stage 2 ("ring of fire") rather than progress to Stage 3 ("pyroptotic bodies"), suggesting that either caspase-3/7 or their substrates facilitated pyroptotic body formation [Figure 5.14 B,C]. Importantly, GSDMD expression levels were not reduced in the context of caspase-3/7 suppression, thus ruling out the possibility that caspase-3/7 affected pyroptotic body formation through disruption of GSDMD expression [Figure 5.14G]. It is currently believed that pyroptotic bodies form when GSDMD pores disrupt the ion gradient across the cell membrane, leading to a net influx of Na^+ and water, which leads to localized swelling, separation of the plasma membrane from the cortical cytoskeleton, formation of swollen fluid-filled pyroptotic bodies, and subsequent membrane rupture[168]. However, although mechanistically elegant, this concept is not entirely consistent with my observations. In apoptosis, membrane-associated apoptotic bodies are formed with the assistance of caspase-3/7 substrates such as ROCK1 that regulate the actin-myosin cytoskeleton, enabling the separation of the plasma membrane from the cortical cytoskeleton. Herein, cleaved ROCK1 is detectable during pyroptosis [Figure 5.14 H, I], and although a causal role for ROCK1 in pyroptotic body formation is not verified in this thesis, ROCK1 represents a conceptual link between caspase-3/7 activation and pyroptotic body formation that merits future investigation. Rupture of the pyroptotic bodies is typically considered the point-of-no-return in pyroptosis, and as described above, is considered to be driven by the passive process of osmotic swelling. However, this thesis demonstrates that caspase-3/7 inhibition rescues membrane rupture as measured by supernatant LDH activity, one of the key read-outs for pyroptosis. This constituted the first evidence of a

functional role for caspase-3/7 in GSDMD-dependent pyroptosis, using well-validated endpoints within the pyroptosis literature.

6.2.16 Caspase-3/7 in the nucleus

Within this objective, cleaved caspase-3/7 were also shown to accumulate in the nucleus, to cleave nuclear substrates (including DFF45 and PARP), and to facilitate nuclear degradation during both nigericin-induced and ATP-induced pyroptosis [Figures 5.10, 5.12, 5.13]. Inhibition of caspase-3/7 with siRNA inhibited nuclear disintegration, rescued total DAPI expression within the population, and prevented the accumulation of cleaved caspase-3/7 substrates. These findings verified that activation of these substrates was indeed driven by caspase-3/7 and not by another caspase with an overlapping substrate profile. Collectively, these findings identify a previously unrecognized role for executioner caspases-3/7 in proinflammatory cell death and reposition these proteins as central drivers of pyroptosis.

6.2.17 Other interactions between caspase-3 and gasdermins

Nonetheless, this is not the first report of an interaction between GSDMD and caspase-3. Interestingly, GSDMD does contain a caspase-3 cleavage site; cleavage of GSDMD at this site inactivates the pore-forming capacity of the protein and generates a non-functional GSDMD N-terminal domain (p43)[79]. This enables a cell to silence the proinflammatory GSDMD pyroptotic pathway in response to pro-apoptotic stimuli. This report begs the question of whether caspase-3-dependent GSDMD cleavage is occurring in our model of nigericin- and ATP-induced pyroptosis. Given that the caspase-3-dependent cleavage event identified in the literature is inactivating, and GSDMD is highly active within this

system, it is unlikely that caspase-3 cleaves and inactivates GSDMD in this system. Others in our lab have identified the presence of the inactive p43 in response to stimuli that do not induce pyroptosis (e.g. HIV infection of microglia) but I have not identified this fragment in nigericin- or ATP-treated microglia.

Another consideration addressed in this thesis was the possibility that caspase-3 was directing pyroptosis through a GSDME-dependent pathway, which has been demonstrated in the literature[171]. siRNA-mediated knockdown of GSDME in this system did not affect pyroptosis (measured by LDH activity), whereas knock-down of GSDMD rescued LDH activity in response to both nigericin and ATP [Figure 5.9].

6.2.18 GSDMD and cleaved caspase-3 co-expression *in vivo*

To eliminate the possibility that these observations were an artifact of the *in vitro* experimental system, tissue from MS and EAE white matter was also examined to assess whether GSDMD$^+$ cells co-expressed cleaved caspase-3 [Figure 5.15]. In both MS and EAE, GSDMD and cleaved caspase-3 co-expression were observed. In EAE, cells that contained prototypic GSDMD$^+$ pyroptotic bodies were observed, and cleaved caspase-3 was readily detectable in these cells. Although these experiments are preliminary, they provide two important pieces of evidence: (i) cleaved caspase-3 and GSDMD were co-expressed *in vivo* as well as *in vitro*, in cells that appear to be undergoing pyroptosis, and (ii) mouse cleaved caspase-3 and GSDMD were co-expressed *in vivo*, suggesting that this phenomenon is not unique to the human system.

As described previously in this chapter, loss of ODCs is a defining feature of MS/EAE pathogenesis, and thus the mechanisms driving their death merit intensive investigation. Having demonstrated that myeloid cells in MS autopsy samples can co-express activated caspase-3 and GSDMD, it would be logical to next interrogate whether caspase-3/7 contribute to pyroptosis in ODCs during MS/EAE. An abundance of evidence exists in the literature to suggest that ODC cell death in response to inflammatory stimuli involves both apoptotic and inflammatory caspases. For instance, TNFα and IFNγ have been shown to induce caspase-3 activation in ODCs in a caspase-11-dependent manner; cell death and caspase-3 activation were both decreased in caspase-11-deficient cells[125]. In the EAE model, investigators have demonstrated that ~40% of cleaved caspase-3-immunopositive ODCs also expressed caspase-1, while ~50% co-expressed caspase-11. Such data establish a clear precedent that inflammatory and apoptotic caspases are not mutually exclusive in ODCs, and as such I would expect to find comparable results using GSDMD as the prototypic marker for pyroptosis in combination with caspase-3.

6.2.19 Cytokine secretion versus pyroptosis

As discussed in Chapter I, it is not yet clear which mechanisms direct a cell to either undergo nonlethal cytokine secretion through GSDMD pores (referred to by some researchers as "hyper-activation"[180]) or to undergo pyroptosis. Caspase-3/7 activation could represent one mechanism by which a cell is directed down one of these two pathways. As such, one could anticipate that viral and bacterial pathogens might actively modulate the executioner caspases in order to stall cells in a hyperactive state

and prevent progression to pyroptosis. Consistent with this hypothesis, our lab has preliminary data to suggest that HIV-infected microglia, which release IL-1β but do not undergo pyroptosis, likewise lack caspase-3 activation.

6.2.20 Experimental design considerations

When considering the important role identified in this thesis for caspase-3/7 in pyroptosis, it warrants consideration why other experimental paradigms may have failed to reveal this mechanism. Several possibilities initially present themselves. The first possibility is that the cell types utilized in other experimental models do not activate the same pathway identified in this thesis. The experiments herein utilized primary human fetal microglia, a unique experimental strategy within the pyroptosis field, which tends to rely heavily on immortalized cell lines (e.g. THP-1, RAW 264.7 cells) and primary mouse BMDMs. Primary, non-transformed human cell lines have notable limitations, including limited availability and extensive sample-to-sample variability, making them challenging to work with and thus, not as widely studied. Cancer cell lines on the other hand are easily available, can be passaged over the long-term, and are clonal, eliminating sample-to-sample variability. However, dysregulated cell death pathways are one of the fundamental hallmarks of cancer[299], making cancer cell lines potentially misleading models for studying cell death in contexts other than cancer biology. We have not yet tested whether caspase-3/7 activation is required for pyroptosis in cancer cell lines, but given that cancer cells evolve to resist apoptosis, pyroptotic pathways may also be quite different than in primary cells. Likewise, murine cells do not have identical inflammasome activation and regulatory pathways compared to human cells, and it remains to be determined whether a functional role for caspase-

3/7 is upheld in the murine context. In the mouse macrophage cancer cell line RAW 264.7 for example, caspase-3/7 activation in response to inflammasome-activating stimuli is only unmasked in the context of GSDMD inactivation[79], which is not the case in our system; whether this is due to the species, the transformed nature of the cells, or the stimulus remains to be seen. While it is possible that the caspase-3/7 functional role in pyroptosis is unique to microglia, early reports in the literature of a joint involvement for caspase-1 and -3 in ODC "apoptotic" death suggests this phenomenon is not unique. Nonetheless, future studies must confirm these findings using additional (non-CNS) cell types.

The second possibility for why caspase-3/7 involvement in pyroptosis has not been identified to date is that the experimental design strategies camouflaged caspase-3/7 activation pathways. Caspases are notoriously redundant and plastic in their substrate profiles, and inhibition of either caspase-3 or -7 individually may not have been sufficient to affect pyroptosis. Likewise, many experimental strategies for assessing pyroptosis lack single cell resolution. Some studies that had identified cleavage of caspase-3/7 or their substrates dismissed this as evidence of a sub-population of apoptotic cells without undertaking characterization of this population at the single-cell level[79]. Finally, experimental strategies that use live pathogens to induce pyroptosis must take into account that many pathogens actively modulate cell death pathways (through encoding of anti-apoptotic proteins for example); that such mechanisms may camouflage the role that caspase-3/7 may otherwise have played in pyroptosis.

Considering the spectrum of biomarkers that are known to be shared between apoptosis and pyroptosis (including caspase-3/7 activation, PARP cleavage, TUNEL positivity, Annexin V staining, membrane bleb formation, and nuclear disintegration), it is worth re-examining biological paradigms whereby the existing dogma has historically implicated apoptosis as the sole or primary mechanism of cell death. Such studies have already been successfully undertaken in the context of HIV[271] and sepsis[175], wherein pyroptosis was shown to play a major role in disease pathogenesis. Other inflammatory cell death scenarios, such as granzyme B-mediated cytotoxicity, have also historically been considered apoptotic in nature, which may merit re-evaluation in the context of pyroptosis. While the experiments in this thesis were performed using microglia, these findings demonstrate a previously unknown functional role for caspase-3/7 in pyroptosis, and suggest that the use of caspase-3/7 and their substrates as unequivocal biomarkers of apoptosis is conceptually obsolete.

The findings in this thesis, and others in the literature, highlight the conceptual possibility that cell death modalities are not necessarily as discrete as previously assumed. Apoptosis and pyroptosis can both be initiated under conditions of microbial or viral infection, disruptions in homeostasis, or exposure to noxious stimuli. One could conceive of a scenario wherein common programmed cell death pathways are engaged, with the final modality being determined by factors such as the specific caspases activated, the expression profile of their substrates, and the additional regulatory mechanisms at play post-activation in the cell, as has previously been postulated[72].

VI.III. Overall Conclusions

This thesis provides robust evidence for inflammasome activation and pyroptosis in multiple CNS cell types (including microglia/macrophages and ODCs) during MS/EAE. Inhibition of caspase-1 upstream of GSDMD is shown to be neuroprotective in the EAE model, likely through multiple mechanisms including inhibition of pyroptosis. These findings offer a mechanism that unifies the concepts of smoldering inflammation and cell death during inflammatory demyelination. I have also characterized microglial pyroptosis *in vitro* and suggested a provocative new pathway wherein caspase-3/7 drive pyroptosis upstream of GSDMD-mediated cell membrane rupture. These findings provide novel perspectives on cell death in the inflamed CNS, offer valuable and clinically relevant therapeutic strategies for MS, and represent a substantial conceptual advance in our understanding of the molecular mechanisms underlying pyroptosis.

VI.IV. Future Directions

In this section, I outline an experimental strategy going forward that unifies the findings within this thesis, and proposes four aims to direct future research, centered around the following hypothesis:

Hypothesis: Caspase-3/7 activation drives GSDMD-mediated pyroptosis during inflammation and neurodegeneration.

AIM I: *To interrogate the molecular pathways by which caspase-3/7 promote pyroptosis in human myeloid cells*

In this aim, human microglia and donor-matched bone marrow-derived macrophages (BMDMs) would be used to elucidate the pathways involved in caspase-3/7-mediated

pyroptosis. To establish the caspase substrate cleavage profile downstream of canonical inflammasome activation, high throughput proteomics methods, which have been widely used to study caspase substrate profiles during apoptotic cell death, would be utilized in combination with established datasets of caspase substrates[72]. Using a forward-approach, microglia and BMDMs would be exposed to an inducer of pyroptosis (such as nigericin or exogenous ATP), the cell lysates collected, the cleavage fragments isolated/digested, and the corresponding peptides subjected to tandem mass spectrometry[72]. This method would enable the generation of a comprehensive list of protein substrates that are cleaved during pyroptosis, which can then be interpreted within the context of known cleavage signatures associated with individual caspases. Based upon the results of this thesis, which demonstrate that multiple caspase-3/7 substrates are cleaved during pyroptosis, I hypothesize that this unbiased approach would unveil a robust caspase-3/7 cleavage signature in addition to a caspase-1 signature during pyroptotic cell death.

Following this, it would likewise be important to determine which caspase is immediately upstream of caspase-3/7 activation. The above proteomics experiment would likely reveal whether there was evidence for activation of other caspases (particularly the initiator caspases-8 and-9) during pyroptosis, but this hypothesis could be more directly tested by inhibiting caspase-1/8/9 individually (using siRNA or CRISPR-Cas9 knockout). In this thesis, pharmacological inhibition of caspase-1 (with VX-765) demonstrated that caspase-1 is upstream of caspase-3/7 cleavage and activation. While direct cleavage of caspase-3/7 by caspase-1 has been repeatedly

shown in the literature, it is also possible that caspase-3/7 is cleaved by a more complex pathway, such as GSDMD-mediated mitochondrial permeability and apoptosome formation. This second pathway would be ruled out if GSDMD deficiency was shown not to affect cleaved caspase-3/7 levels during pyroptosis. However, if GSDMD deficiency was shown to decrease caspase-3/7 activation, then the role for mitochondrial permeabilization, cytochrome C release, and apoptosome formation upstream of caspase-3/7 activation could be assessed. Confocal microscopy could be utilized to determine the subcellular localization of activated GSDMD and whether GSDMD accumulation at the mitochondria is associated with loss of mitochondrial membrane potential (using potential-dependent mitochondrial probes) and/or cytochrome C release into the cytoplasm prior to or concurrent with the detection of activated caspase-3/7. Pharmacological inhibition of mitochondrial depolarization (e.g. PKF220-384 or NIM811)[300] would provide evidence to support or refute the role for this process in caspase-3/7 activation during pyroptosis, and help to delineate the specific mechanisms driving caspase-3/7 activation.

AIM II: *To determine the mechanism by which caspase-3/7 activation drives pyroptosis*

In addition to determining the upstream signals that initiate caspase-3/7 activation, it would also be interesting and informative to elucidate how caspase-3/7 drive pyroptosis. Substrate cleavage profiles are not identical in response to different stimuli[72], and to this end, profiling the specific substrates of caspase-3/7 that are involved in pyroptosis compared to apoptosis would be a useful first step in determining which substrates might play a role in pyroptosis. Given that caspase-3/7 inhibition specifically prevented the formation of pyroptotic bodies and membrane

rupture, caspase-3/7 substrates that are functionally involved in cytoskeletal rearrangement and membrane changes during apoptosis would be rational candidates to investigate functionally in pyroptosis. Strategies to assess these substrates include both pharmacological and genetic inhibition approaches. In this thesis, ROCK1 (which mediates membrane bleb formation during apoptosis) was shown to be present in its active cleaved form during both pyroptosis and apoptosis, which suggested this caspase-3 substrate as a potential link between caspase-3/7 activation and pyroptotic body formation during pyroptosis. Inhibition of ROCK1 directly would enable assessment of its functional role in pyroptotic body formation and membrane rupture. Should this hypothesis be supported, it would position ROCK1 as a novel therapeutic target to prevent pyroptosis; all other strategies to target pyroptosis to date (e.g. inhibition of NLRP3, caspase-1, GSDMD, etc.) also have effects on unconventional cytokine release, but preventing pyroptotic body formation would theoretically prevent membrane rupture and pyroptosis without affecting IL-1β and IL-18 release. Over 170 different ROCK inhibitors are under development, particularly for neurodegenerative conditions; several of these, including fasudil, have proven well-tolerated in the clinic and are known to cross the BBB[301].

AIM III: *To determine whether caspase-3/7 activation drives pyroptosis during neuroinflammation and neurodegeneration*

Pyroptosis, apoptosis, and necroptosis have all been observed in different CNS cell types during neuroinflammation and neurodegeneration, but the relative contribution of these cell death modalities to human neurological disease has not been assessed in a

high-throughput, unbiased manner. It would thus be reasonable to establish a large-scale screening protocol for biopsy and autopsy samples from a broad range of neurological conditions, with the aim of quantifying the cell-type specific expression of programmed cell death markers. Automated IF tissue-screening systems (e.g. the Nikon large-view Ti2E system) are now available to minimize bias and quantify co-expression of different markers over large tissue sections. This initial strategy would (i) permit the quantification of pyroptotic cell death markers compared to other types of cell death across a panel of neurological diseases, and (ii) reveal whether cleaved caspase-3/GSDMD/TUNEL co-expression was a conserved feature of pyroptosis in multiple disease scenarios and in multiple cell types.

This strategy would inform the use of animal models (including EAE and others), in which the clinical data indicates caspase-3 involvement in GSDMD-dependent pyroptosis. Because caspase-3-deficient mice have neurodevelopmental abnormalities ranging from mild to severe[302], as might be expected, pharmacological caspase-3 inhibition is a more rational strategy in studying the contribution of caspase-3 to pyroptosis to neurological disease[303]. I hypothesize that caspase-3 inhibition would be neuroprotective through the prevention of GSDMD-dependent pyroptosis in the CNS during neuroinflammation and neurodegeneration. Such animal models would also provide a useful avenue to examine whether inhibition of caspase-1, presumably the apical caspase upstream of both GSDMD and caspase-3, would reduce caspase-3 expression and pyroptosis during neurodegeneration.

AIM IV: *To determine whether caspase-3/7 drive pyroptosis in models of systemic inflammation*

Neurodegeneration and neuroinflammation are complex scenarios in which a multitude of cell death modalities contribute to neuropathology. Considering that caspase-3 plays a crucial role in intrinsic apoptosis, caspase-3 inhibition will naturally affect both pyroptosis and apoptosis, which may confound the interpretation of any improved neurobehavioural outcomes. As such, the role of caspase-3/7 as drivers of GSDMD-dependent pyroptosis is most elegantly evaluated in systems wherein pyroptosis is the primary form of cell death. In such models, the improvements in disease outcome can be attributed directly to an inhibition of pyroptosis. One example is the mouse model of NOMID (neonatal-onset multisystem inflammatory disease), a severe autoinflammatory condition driven by NLRP3 mutations that lead to hyperactivity of the inflammasome and systemic inflammation, stunted growth, and organ damage (including skin, spleen, liver, and others). Recent studies have demonstrated that virtually all inflammatory signs of NOMID are exquisitely GSDMD-dependent and that pyroptosis is a major driver of disease pathology[111]. Inhibition of caspase-3/7 in this context would enable us to evaluate whether caspase-3/7 is indeed necessary for GSDMD-dependent pyroptosis and whether this observation was organ-, tissue-, or cell-type-dependent.

Collectively, experiments outlined here would (i) enable the elucidation of signaling pathways both upstream and downstream of activated executioner caspases-3/7 during pyroptosis (ii) demonstrate whether caspase-3/7 activation in pyroptosis was a conserved feature of neuroinflammation, and (iii) provide *in vivo* evidence for the role of caspase-3/7 in a pyroptosis-driven pathology.

References

1 Gadani, S. P., Walsh, J. T., Lukens, J. R. & Kipnis, J. Dealing with Danger in the CNS: The Response of the Immune System to Injury. *Neuron* **87**, 47-62, doi:10.1016/j.neuron.2015.05.019 (2015).

2 Wilson, E. H., Weninger, W. & Hunter, C. A. Trafficking of immune cells in the central nervous system. *The Journal of Clinical Investigation* **120**, 1368-1379, doi:10.1172/JCI41911 (2010).

3 Waisman, A., Liblau, R. S. & Becher, B. Innate and adaptive immune responses in the CNS. *The Lancet. Neurology* **14**, 945-955, doi:10.1016/S1474-4422(15)00141-6 (2015).

4 Marin, I. A. & Kipnis, J. Central Nervous System: (Immunological) Ivory Tower or Not? *Neuropsychopharmacology* **42**, 28-35, doi:10.1038/npp.2016.122 (2017).

5 Ousman, S. S. & Kubes, P. Immune surveillance in the central nervous system. *Nature Neuroscience* **15**, 1096-1101, doi:10.1038/nn.3161 (2012).

6 Louveau, A. *et al.* CNS lymphatic drainage and neuroinflammation are regulated by meningeal lymphatic vasculature. *Nature Neuroscience* **21**, 1380-1391, doi:10.1038/s41593-018-0227-9 (2018).

7 Louveau, A. *et al.* Structural and functional features of central nervous system lymphatic vessels. *Nature* **523**, 337-341, doi:10.1038/nature14432 (2015).

8 Korn, T. & Kallies, A. T cell responses in the central nervous system. *Nature Reviews. Immunology* **17**, 179-194, doi:10.1038/nri.2016.144 (2017).

9 Galea, I., Bechmann, I. & Perry, V. H. What is immune privilege (not)? *Trends in Immunology* **28**, 12-18, doi:10.1016/j.it.2006.11.004 (2007).

10 Mrdjen, D. *et al.* High-Dimensional Single-Cell Mapping of Central Nervous System Immune Cells Reveals Distinct Myeloid Subsets in Health, Aging, and Disease. *Immunity* **48**, 599, doi:10.1016/j.immuni.2018.02.014 (2018).

11 Korin, B. *et al.* High-dimensional, single-cell characterization of the brain's immune compartment. *Nature Neuroscience* **20**, 1300-1309, doi:10.1038/nn.4610 (2017).

12 Voet, S., Prinz, M. & van Loo, G. Microglia in Central Nervous System Inflammation and Multiple Sclerosis Pathology. *Trends in Molecular Medicine*, doi:10.1016/j.molmed.2018.11.005 (2018).

13 Daneman, R. & Prat, A. The blood-brain barrier. *Cold Spring Harbor Perspectives in Biology* **7**, a020412, doi:10.1101/cshperspect.a020412 (2015).

14 Daneman, R. The blood-brain barrier in health and disease. *Annals of Neurology* **72**, 648-672, doi:10.1002/ana.23648 (2012).

15 Audoy-Remus, J. *et al.* Rod-Shaped monocytes patrol the brain vasculature and give rise to perivascular macrophages under the influence of proinflammatory cytokines and angiopoietin-2. *The Journal of Neuroscience* **28**, 10187-10199, doi:10.1523/JNEUROSCI.3510-08.2008 (2008).

16 Andersson, P. B., Perry, V. H. & Gordon, S. The acute inflammatory response to lipopolysaccharide in CNS parenchyma differs from that in other body tissues. *Neuroscience* **48**, 169-186 (1992).

17 Galea, I. & Perry, V. H. The blood-brain interface: a culture change. *Brain, Behavior, and Immunity* **68**, 11-16, doi:10.1016/j.bbi.2017.10.014 (2018).
18 Frost, J. L. & Schafer, D. P. Microglia: Architects of the Developing Nervous System. *Trends in Cell Biology* **26**, 587-597, doi:10.1016/j.tcb.2016.02.006 (2016).
19 Lawson, L. J., Perry, V. H., Dri, P. & Gordon, S. Heterogeneity in the distribution and morphology of microglia in the normal adult mouse brain. *Neuroscience* **39**, 151-170 (1990).
20 Li, Q. *et al.* Developmental Heterogeneity of Microglia and Brain Myeloid Cells Revealed by Deep Single-Cell RNA Sequencing. *Neuron* **101**, 207-223 e210, doi:10.1016/j.neuron.2018.12.006 (2019).
21 Alboni, S., Cervia, D., Sugama, S. & Conti, B. Interleukin 18 in the CNS. *Journal of Neuroinflammation* **7**, 9, doi:10.1186/1742-2094-7-9 (2010).
22 Bennett, M. L. *et al.* New tools for studying microglia in the mouse and human CNS. *Proceedings of the National Academy of Sciences of the United States of America* **113**, E1738-1746, doi:10.1073/pnas.1525528113 (2016).
23 Ginhoux, F. *et al.* Fate mapping analysis reveals that adult microglia derive from primitive macrophages. *Science* **330**, 841-845, doi:10.1126/science.1194637 (2010).
24 Gomez Perdiguero, E. *et al.* Tissue-resident macrophages originate from yolk-sac-derived erythro-myeloid progenitors. *Nature* **518**, 547-551, doi:10.1038/nature13989 (2015).
25 Ajami, B., Bennett, J. L., Krieger, C., Tetzlaff, W. & Rossi, F. M. Local self-renewal can sustain CNS microglia maintenance and function throughout adult life. *Nature Neuroscience* **10**, 1538-1543, doi:10.1038/nn2014 (2007).
26 Reu, P. *et al.* The Lifespan and Turnover of Microglia in the Human Brain. *Cell reports* **20**, 779-784, doi:10.1016/j.celrep.2017.07.004 (2017).
27 Askew, K. *et al.* Coupled Proliferation and Apoptosis Maintain the Rapid Turnover of Microglia in the Adult Brain. *Cell Reports* **18**, 391-405, doi:10.1016/j.celrep.2016.12.041 (2017).
28 Bruttger, J. *et al.* Genetic Cell Ablation Reveals Clusters of Local Self-Renewing Microglia in the Mammalian Central Nervous System. *Immunity* **43**, 92-106, doi:10.1016/j.immuni.2015.06.012 (2015).
29 Elmore, M. R. *et al.* Colony-stimulating factor 1 receptor signaling is necessary for microglia viability, unmasking a microglia progenitor cell in the adult brain. *Neuron* **82**, 380-397, doi:10.1016/j.neuron.2014.02.040 (2014).
30 Tay, T. L. *et al.* A new fate mapping system reveals context-dependent random or clonal expansion of microglia. *Nature Neuroscience* **20**, 793-803, doi:10.1038/nn.4547 (2017).
31 Kierdorf, K. & Prinz, M. Microglia in steady state. *The Journal of Clinical Investigation* **127**, 3201-3209, doi:10.1172/JCI90602 (2017).
32 Nimmerjahn, A., Kirchhoff, F. & Helmchen, F. Resting microglial cells are highly dynamic surveillants of brain parenchyma in vivo. *Science* **308**, 1314-1318, doi:10.1126/science.1110647 (2005).
33 Hickman, S. E. *et al.* The microglial sensome revealed by direct RNA sequencing. *Nature Neuroscience* **16**, 1896-1905, doi:10.1038/nn.3554 (2013).

34 Dubbelaar, M. L., Kracht, L., Eggen, B. J. L. & Boddeke, E. The Kaleidoscope of Microglial Phenotypes. *Frontiers in Immunology* **9**, 1753, doi:10.3389/fimmu.2018.01753 (2018).
35 Matzinger, P. The danger model: a renewed sense of self. *Science* **296**, 301-305, doi:10.1126/science.1071059 (2002).
36 Amarante-Mendes, G. P. *et al.* Pattern Recognition Receptors and the Host Cell Death Molecular Machinery. *Frontiers in Immunology* **9**, 2379, doi:10.3389/fimmu.2018.02379 (2018).
37 Yiangou, Y. *et al.* COX-2, CB2 and P2X7-immunoreactivities are increased in activated microglial cells/macrophages of multiple sclerosis and amyotrophic lateral sclerosis spinal cord. *BMC Neurology* **6**, 12, doi:10.1186/1471-2377-6-12 (2006).
38 Oyanguren-Desez, O. *et al.* Gain-of-function of P2X7 receptor gene variants in multiple sclerosis. *Cell Calcium* **50**, 468-472, doi:10.1016/j.ceca.2011.08.002 (2011).
39 Matute, C. *et al.* P2X(7) receptor blockade prevents ATP excitotoxicity in oligodendrocytes and ameliorates experimental autoimmune encephalomyelitis. *The Journal of Neuroscience* **27**, 9525-9533, doi:10.1523/JNEUROSCI.0579-07.2007 (2007).
40 Sharp, A. J. *et al.* P2x7 deficiency suppresses development of experimental autoimmune encephalomyelitis. *Journal of Neuroinflammation* **5**, 33, doi:10.1186/1742-2094-5-33 (2008).
41 Gaidt, M. M. & Hornung, V. Alternative inflammasome activation enables IL-1beta release from living cells. *Current Opinion in Immunology* **44**, 7-13, doi:10.1016/j.coi.2016.10.007 (2017).
42 Holtman, I. R., Skola, D. & Glass, C. K. Transcriptional control of microglia phenotypes in health and disease. *The Journal of Clinical Investigation* **127**, 3220-3229, doi:10.1172/JCI90604 (2017).
43 Gordon, S. Alternative activation of macrophages. *Nature Reviews. Immunology* **3**, 23-35, doi:10.1038/nri978 (2003).
44 Mantovani, A., Sica, A. & Locati, M. Macrophage polarization comes of age. *Immunity* **23**, 344-346, doi:10.1016/j.immuni.2005.10.001 (2005).
45 Tang, Y. & Le, W. Differential Roles of M1 and M2 Microglia in Neurodegenerative Diseases. *Molecular Neurobiology* **53**, 1181-1194, doi:10.1007/s12035-014-9070-5 (2016).
46 Orihuela, R., McPherson, C. A. & Harry, G. J. Microglial M1/M2 polarization and metabolic states. *British Journal of Pharmacology* **173**, 649-665, doi:10.1111/bph.13139 (2016).
47 Ransohoff, R. M. A polarizing question: do M1 and M2 microglia exist? *Nature neuroscience* **19**, 987-991, doi:10.1038/nn.4338 (2016).
48 Jassam, Y. N., Izzy, S., Whalen, M., McGavern, D. B. & El Khoury, J. Neuroimmunology of Traumatic Brain Injury: Time for a Paradigm Shift. *Neuron* **95**, 1246-1265, doi:10.1016/j.neuron.2017.07.010 (2017).
49 Butovsky, O. & Weiner, H. L. Microglial signatures and their role in health and disease. *Nature Reviews. Neuroscience* **19**, 622-635, doi:10.1038/s41583-018-0057-5 (2018).

50 Mathys, H. *et al.* Temporal Tracking of Microglia Activation in Neurodegeneration at Single-Cell Resolution. *Cell Reports* **21**, 366-380, doi:10.1016/j.celrep.2017.09.039 (2017).
51 Keren-Shaul, H. *et al.* A Unique Microglia Type Associated with Restricting Development of Alzheimer's Disease. *Cell* **169**, 1276-1290 e1217, doi:10.1016/j.cell.2017.05.018 (2017).
52 Ajami, B. *et al.* Single-cell mass cytometry reveals distinct populations of brain myeloid cells in mouse neuroinflammation and neurodegeneration models. *Nature Neuroscience* **21**, 541-551, doi:10.1038/s41593-018-0100-x (2018).
53 Mrdjen, D. *et al.* High-Dimensional Single-Cell Mapping of Central Nervous System Immune Cells Reveals Distinct Myeloid Subsets in Health, Aging, and Disease. *Immunity* **48**, 380-395 e386, doi:10.1016/j.immuni.2018.01.011 (2018).
54 Locatelli, G. *et al.* Mononuclear phagocytes locally specify and adapt their phenotype in a multiple sclerosis model. *Nature Neuroscience* **21**, 1196-1208, doi:10.1038/s41593-018-0212-3 (2018).
55 Perry, V. H., Nicoll, J. A. & Holmes, C. Microglia in neurodegenerative disease. *Nature reviews. Neurology* **6**, 193-201, doi:10.1038/nrneurol.2010.17 (2010).
56 Hutchinson, M. Natalizumab: A new treatment for relapsing remitting multiple sclerosis. *Therapeutics and Clinical Risk Management* **3**, 259-268 (2007).
57 Lund, H. *et al.* Competitive repopulation of an empty microglial niche yields functionally distinct subsets of microglia-like cells. *Nature Communications* **9**, 4845, doi:10.1038/s41467-018-07295-7 (2018).
58 Bartholomaus, I. *et al.* Effector T cell interactions with meningeal vascular structures in nascent autoimmune CNS lesions. *Nature* **462**, 94-98, doi:10.1038/nature08478 (2009).
59 Perez-de-Puig, I. *et al.* Neutrophil recruitment to the brain in mouse and human ischemic stroke. *Acta Neuropathologica* **129**, 239-257, doi:10.1007/s00401-014-1381-0 (2015).
60 Zenaro, E. *et al.* Neutrophils promote Alzheimer's disease-like pathology and cognitive decline via LFA-1 integrin. *Nature Medicine* **21**, 880-886, doi:10.1038/nm.3913 (2015).
61 Pierson, E. R., Wagner, C. A. & Goverman, J. M. The contribution of neutrophils to CNS autoimmunity. *Clinical Immunology* **189**, 23-28, doi:10.1016/j.clim.2016.06.017 (2018).
62 Ransohoff, R. M. & Brown, M. A. Innate immunity in the central nervous system. *The Journal of Clinical Investigation* **122**, 1164-1171, doi:10.1172/JCI58644 (2012).
63 Michel, L. *et al.* B Cells in the Multiple Sclerosis Central Nervous System: Trafficking and Contribution to CNS-Compartmentalized Inflammation. *Frontiers in Immunology* **6**, 636, doi:10.3389/fimmu.2015.00636 (2015).
64 Martinon, F., Burns, K. & Tschopp, J. The inflammasome: a molecular platform triggering activation of inflammatory caspases and processing of proIL-beta. *Molecular Cell* **10**, 417-426 (2002).
65 Guo, H., Callaway, J. B. & Ting, J. P. Inflammasomes: mechanism of action, role in disease, and therapeutics. *Nature Medicine* **21**, 677-687, doi:10.1038/nm.3893 (2015).

66 Rathinam, V. A. & Fitzgerald, K. A. Inflammasome Complexes: Emerging Mechanisms and Effector Functions. *Cell* **165**, 792-800, doi:10.1016/j.cell.2016.03.046 (2016).
67 Franklin, B. S., Latz, E. & Schmidt, F. I. The intra- and extracellular functions of ASC specks. *Immunological Reviews* **281**, 74-87, doi:10.1111/imr.12611 (2018).
68 Dick, M. S., Sborgi, L., Ruhl, S., Hiller, S. & Broz, P. ASC filament formation serves as a signal amplification mechanism for inflammasomes. *Nature Communications* **7**, 11929, doi:10.1038/ncomms11929 (2016).
69 Martinon, F. & Tschopp, J. Inflammatory caspases: linking an intracellular innate immune system to autoinflammatory diseases. *Cell* **117**, 561-574, doi:10.1016/j.cell.2004.05.004 (2004).
70 McIlwain, D. R., Berger, T. & Mak, T. W. Caspase functions in cell death and disease. *Cold Spring Harbor Perspectives in Biology* **5**, a008656, doi:10.1101/cshperspect.a008656 (2013).
71 Lamkanfi, M., Declercq, W., Kalai, M., Saelens, X. & Vandenabeele, P. Alice in caspase land. A phylogenetic analysis of caspases from worm to man. *Cell Death and Differentiation* **9**, 358-361, doi:10.1038/sj/cdd/4400989 (2002).
72 Julien, O. & Wells, J. A. Caspases and their substrates. *Cell Death and Differentiation* **24**, 1380-1389, doi:10.1038/cdd.2017.44 (2017).
73 Walsh, J. G., Logue, S. E., Luthi, A. U. & Martin, S. J. Caspase-1 promiscuity is counterbalanced by rapid inactivation of processed enzyme. *The Journal of Biological Chemistry* **286**, 32513-32524, doi:10.1074/jbc.M111.225862 (2011).
74 Boucher, D. *et al.* Caspase-1 self-cleavage is an intrinsic mechanism to terminate inflammasome activity. *The Journal of Experimental Medicine* **215**, 827-840, doi:10.1084/jem.20172222 (2018).
75 Denes, A., Lopez-Castejon, G. & Brough, D. Caspase-1: is IL-1 just the tip of the ICEberg? *Cell Death & Disease* **3**, e338, doi:10.1038/cddis.2012.86 (2012).
76 Shao, W., Yeretssian, G., Doiron, K., Hussain, S. N. & Saleh, M. The caspase-1 digestome identifies the glycolysis pathway as a target during infection and septic shock. *The Journal of Biological Chemistry* **282**, 36321-36329, doi:10.1074/jbc.M708182200 (2007).
77 Agard, N. J., Maltby, D. & Wells, J. A. Inflammatory stimuli regulate caspase substrate profiles. *Molecular & Cellular Proteomics : MCP* **9**, 880-893, doi:10.1074/mcp.M900528-MCP200 (2010).
78 Lamkanfi, M. *et al.* Targeted peptidecentric proteomics reveals caspase-7 as a substrate of the caspase-1 inflammasomes. *Molecular & Cellular Proteomics : MCP* **7**, 2350-2363, doi:10.1074/mcp.M800132-MCP200 (2008).
79 Taabazuing, C. Y., Okondo, M. C. & Bachovchin, D. A. Pyroptosis and Apoptosis Pathways Engage in Bidirectional Crosstalk in Monocytes and Macrophages. *Cell chemical biology* **24**, 507-514 e504, doi:10.1016/j.chembiol.2017.03.009 (2017).
80 Van de Craen, M., Declercq, W., Van den brande, I., Fiers, W. & Vandenabeele, P. The proteolytic procaspase activation network: an in vitro analysis. *Cell Death and Differentiation* **6**, 1117-1124, doi:10.1038/sj.cdd.4400589 (1999).
81 Shi, J. *et al.* Cleavage of GSDMD by inflammatory caspases determines pyroptotic cell death. *Nature* **526**, 660-665, doi:10.1038/nature15514 (2015).

82 Kayagaki, N. *et al.* Caspase-11 cleaves gasdermin D for non-canonical inflammasome signalling. *Nature* **526**, 666-671, doi:10.1038/nature15541 (2015).
83 Ding, J. & Shao, F. SnapShot: The Noncanonical Inflammasome. *Cell* **168**, 544-544 e541, doi:10.1016/j.cell.2017.01.008 (2017).
84 Allan, S. M., Tyrrell, P. J. & Rothwell, N. J. Interleukin-1 and neuronal injury. *Nature Reviews. Immunology* **5**, 629-640, doi:10.1038/nri1664 (2005).
85 Boutin, H., Kimber, I., Rothwell, N. J. & Pinteaux, E. The expanding interleukin-1 family and its receptors: do alternative IL-1 receptor/signaling pathways exist in the brain? *Molecular Neurobiology* **27**, 239-248, doi:10.1385/MN:27:3:239 (2003).
86 Dinarello, C. A. Overview of the IL-1 family in innate inflammation and acquired immunity. *Immunological Reviews* **281**, 8-27, doi:10.1111/imr.12621 (2018).
87 Lopez-Castejon, G. & Brough, D. Understanding the mechanism of IL-1beta secretion. *Cytokine & Growth Factor Reviews* **22**, 189-195, doi:10.1016/j.cytogfr.2011.10.001 (2011).
88 Keller, M., Ruegg, A., Werner, S. & Beer, H. D. Active caspase-1 is a regulator of unconventional protein secretion. *Cell* **132**, 818-831, doi:10.1016/j.cell.2007.12.040 (2008).
89 Weber, A., Wasiliew, P. & Kracht, M. Interleukin-1 (IL-1) pathway. *Science Signaling* **3**, cm1, doi:10.1126/scisignal.3105cm1 (2010).
90 Chitnis, T. & Weiner, H. L. CNS inflammation and neurodegeneration. *The Journal of Clinical Investigation* **127**, 3577-3587, doi:10.1172/JCI90609 (2017).
91 Lamkanfi, M. & Dixit, V. M. Mechanisms and functions of inflammasomes. *Cell* **157**, 1013-1022, doi:10.1016/j.cell.2014.04.007 (2014).
92 Walsh, J. G., Muruve, D. A. & Power, C. Inflammasomes in the CNS. *Nature Reviews. Neuroscience* **15**, 84-97, doi:10.1038/nrn3638 (2014).
93 Chavarria-Smith, J., Mitchell, P. S., Ho, A. M., Daugherty, M. D. & Vance, R. E. Functional and Evolutionary Analyses Identify Proteolysis as a General Mechanism for NLRP1 Inflammasome Activation. *PLoS Pathogens* **12**, e1006052, doi:10.1371/journal.ppat.1006052 (2016).
94 Mangan, M. S. J. *et al.* Targeting the NLRP3 inflammasome in inflammatory diseases. *Nature Reviews. Drug Discovery* **17**, 688, doi:10.1038/nrd.2018.149 (2018).
95 Liston, A. & Masters, S. L. Homeostasis-altering molecular processes as mechanisms of inflammasome activation. *Nature Reviews. Immunology* **17**, 208-214, doi:10.1038/nri.2016.151 (2017).
96 He, Y., Hara, H. & Nunez, G. Mechanism and Regulation of NLRP3 Inflammasome Activation. *Trends in Biochemical Sciences* **41**, 1012-1021, doi:10.1016/j.tibs.2016.09.002 (2016).
97 Bauernfeind, F. G. *et al.* Cutting edge: NF-kappaB activating pattern recognition and cytokine receptors license NLRP3 inflammasome activation by regulating NLRP3 expression. *Journal of Immunology* **183**, 787-791, doi:10.4049/jimmunol.0901363 (2009).

98 Dinarello, C. A., Simon, A. & van der Meer, J. W. Treating inflammation by blocking interleukin-1 in a broad spectrum of diseases. *Nature Reviews. Drug Discovery* **11**, 633-652, doi:10.1038/nrd3800 (2012).
99 Lin, K. M. *et al.* IRAK-1 bypasses priming and directly links TLRs to rapid NLRP3 inflammasome activation. *Proceedings of the National Academy of Sciences of the United States of America* **111**, 775-780, doi:10.1073/pnas.1320294111 (2014).
100 Schmid-Burgk, J. L. *et al.* A Genome-wide CRISPR (Clustered Regularly Interspaced Short Palindromic Repeats) Screen Identifies NEK7 as an Essential Component of NLRP3 Inflammasome Activation. *The Journal of Biological Chemistry* **291**, 103-109, doi:10.1074/jbc.C115.700492 (2016).
101 Shi, H. *et al.* NLRP3 activation and mitosis are mutually exclusive events coordinated by NEK7, a new inflammasome component. *Nature Immunology* **17**, 250-258, doi:10.1038/ni.3333 (2016).
102 He, Y., Zeng, M. Y., Yang, D., Motro, B. & Nunez, G. NEK7 is an essential mediator of NLRP3 activation downstream of potassium efflux. *Nature* **530**, 354-357, doi:10.1038/nature16959 (2016).
103 Gaidt, M. M. *et al.* Human Monocytes Engage an Alternative Inflammasome Pathway. *Immunity* **44**, 833-846, doi:10.1016/j.immuni.2016.01.012 (2016).
104 Petrilli, V. *et al.* Activation of the NALP3 inflammasome is triggered by low intracellular potassium concentration. *Cell Death and Differentiation* **14**, 1583-1589, doi:10.1038/sj.cdd.4402195 (2007).
105 Munoz-Planillo, R. *et al.* K(+) efflux is the common trigger of NLRP3 inflammasome activation by bacterial toxins and particulate matter. *Immunity* **38**, 1142-1153, doi:10.1016/j.immuni.2013.05.016 (2013).
106 Subramanian, N., Natarajan, K., Clatworthy, M. R., Wang, Z. & Germain, R. N. The adaptor MAVS promotes NLRP3 mitochondrial localization and inflammasome activation. *Cell* **153**, 348-361, doi:10.1016/j.cell.2013.02.054 (2013).
107 Manthiram, K., Zhou, Q., Aksentijevich, I. & Kastner, D. L. The monogenic autoinflammatory diseases define new pathways in human innate immunity and inflammation. *Nature Immunology* **18**, 832-842, doi:10.1038/ni.3777 (2017).
108 Brydges, S. D. *et al.* Divergence of IL-1, IL-18, and cell death in NLRP3 inflammasomopathies. *The Journal of Clinical Investigation* **123**, 4695-4705, doi:10.1172/JCI71543 (2013).
109 Amin, J., Boche, D. & Rakic, S. What do we know about the inflammasome in humans? *Brain Pathology* **27**, 192-204, doi:10.1111/bpa.12479 (2017).
110 Keddie, S., Parker, T., Lachmann, H. J. & Ginsberg, L. Cryopyrin-Associated Periodic Fever Syndrome and the Nervous System. *Current Treatment Options in Neurology* **20**, 43, doi:10.1007/s11940-018-0526-1 (2018).
111 Xiao, J. *et al.* Gasdermin D mediates the pathogenesis of neonatal-onset multisystem inflammatory disease in mice. *PLoS Biology* **16**, e3000047, doi:10.1371/journal.pbio.3000047 (2018).
112 Wannamaker, W. *et al.* (S)-1-((S)-2-{[1-(4-amino-3-chloro-phenyl)-methanoyl]-amino}-3,3-dimethyl-butanoy l)-pyrrolidine-2-carboxylic acid ((2R,3S)-2-ethoxy-5-oxo-tetrahydro-furan-3-yl)-amide (VX-765), an orally available selective interleukin (IL)-converting enzyme/caspase-1 inhibitor, exhibits potent anti-inflammatory activities by inhibiting the release of IL-1beta and IL-18. *The*

Journal of Pharmacology and Experimental Therapeutics **321**, 509-516, doi:10.1124/jpet.106.111344 (2007).
113 Flores, J. *et al.* Caspase-1 inhibition alleviates cognitive impairment and neuropathology in an Alzheimer's disease mouse model. *Nature Communications* **9**, 3916, doi:10.1038/s41467-018-06449-x (2018).
114 Noe, F. M. *et al.* Pharmacological blockade of IL-1beta/IL-1 receptor type 1 axis during epileptogenesis provides neuroprotection in two rat models of temporal lobe epilepsy. *Neurobiology of Disease* **59**, 183-193, doi:10.1016/j.nbd.2013.07.015 (2013).
115 Xu, Y. *et al.* NLRP3 inflammasome activation mediates estrogen deficiency-induced depression- and anxiety-like behavior and hippocampal inflammation in mice. *Brain, Behavior, and Immunity* **56**, 175-186, doi:10.1016/j.bbi.2016.02.022 (2016).
116 Wang, W. *et al.* Caspase-1 causes truncation and aggregation of the Parkinson's disease-associated protein alpha-synuclein. *Proceedings of the National Academy of Sciences of the United States of America* **113**, 9587-9592, doi:10.1073/pnas.1610099113 (2016).
117 Bassil, F. *et al.* Reducing C-terminal truncation mitigates synucleinopathy and neurodegeneration in a transgenic model of multiple system atrophy. *Proceedings of the National Academy of Sciences of the United States of America* **113**, 9593-9598, doi:10.1073/pnas.1609291113 (2016).
118 Ravizza, T. *et al.* Interleukin Converting Enzyme inhibition impairs kindling epileptogenesis in rats by blocking astrocytic IL-1beta production. *Neurobiology of Disease* **31**, 327-333, doi:10.1016/j.nbd.2008.05.007 (2008).
119 Church, J. A. Cell Death by Pyroptosis Drives CD4 T-Cell Depletion in HIV-1 Infection. *Pediatrics* **134 Suppl 3**, S184, doi:10.1542/peds.2014-1817JJJJ (2014).
120 Yang, X. M. *et al.* The Highly Selective Caspase-1 Inhibitor VX-765 Provides Additive Protection Against Myocardial Infarction in Rat Hearts When Combined With a Platelet Inhibitor. *Journal of Cardiovascular Pharmacology and Therapeutics*, 1074248417702890, doi:10.1177/1074248417702890 (2017).
121 Mangan, M. S. J. *et al.* Targeting the NLRP3 inflammasome in inflammatory diseases. *Nature Reviews. Drug discovery* **17**, 588-606, doi:10.1038/nrd.2018.97 (2018).
122 Mamik, M. K. & Power, C. Inflammasomes in neurological diseases: emerging pathogenic and therapeutic concepts. *Brain* **awx133** (2017).
123 Tsai, S. J. Effects of interleukin-1beta polymorphisms on brain function and behavior in healthy and psychiatric disease conditions. *Cytokine & Growth Factor Reviews* **37**, 89-97, doi:10.1016/j.cytogfr.2017.06.001 (2017).
124 Heneka, M. T., McManus, R. M. & Latz, E. Inflammasome signalling in brain function and neurodegenerative disease. *Nature Reviews. Neuroscience* **19**, 610-621, doi:10.1038/s41583-018-0055-7 (2018).
125 Hisahara, S., Yuan, J., Momoi, T., Okano, H. & Miura, M. Caspase-11 mediates oligodendrocyte cell death and pathogenesis of autoimmune-mediated demyelination. *The Journal of Experimental Medicine* **193**, 111-122 (2001).

126 Shibata, M. *et al.* Caspases determine the vulnerability of oligodendrocytes in the ischemic brain. *The Journal of Clinical Investigation* **106**, 643-653, doi:10.1172/JCI10203 (2000).
127 Minkiewicz, J., de Rivero Vaccari, J. P. & Keane, R. W. Human astrocytes express a novel NLRP2 inflammasome. *Glia* **61**, 1113-1121, doi:10.1002/glia.22499 (2013).
128 Tarassishin, L., Suh, H. S. & Lee, S. C. LPS and IL-1 differentially activate mouse and human astrocytes: role of CD14. *Glia* **62**, 999-1013, doi:10.1002/glia.22657 (2014).
129 Didier, N. *et al.* Secretion of interleukin-1beta by astrocytes mediates endothelin-1 and tumour necrosis factor-alpha effects on human brain microvascular endothelial cell permeability. *Journal of Neurochemistry* **86**, 246-254 (2003).
130 Stroemer, R. P. & Rothwell, N. J. Exacerbation of ischemic brain damage by localized striatal injection of interleukin-1beta in the rat. *Journal of Cerebral Blood Flow and Metabolism* **18**, 833-839, doi:10.1097/00004647-199808000-00003 (1998).
131 Yang, G. Y., Zhao, Y. J., Davidson, B. L. & Betz, A. L. Overexpression of interleukin-1 receptor antagonist in the mouse brain reduces ischemic brain injury. *Brain Research* **751**, 181-188 (1997).
132 Downen, M., Amaral, T. D., Hua, L. L., Zhao, M. L. & Lee, S. C. Neuronal death in cytokine-activated primary human brain cell culture: role of tumor necrosis factor-alpha. *Glia* **28**, 114-127 (1999).
133 Chao, C. C., Lokensgard, J. R., Sheng, W. S., Hu, S. & Peterson, P. K. IL-1-induced iNOS expression in human astrocytes via NF-kappa B. *Neuroreport* **8**, 3163-3166 (1997).
134 Vezzani, A. & Baram, T. Z. New roles for interleukin-1 Beta in the mechanisms of epilepsy. *Epilepsy Currents* **7**, 45-50, doi:10.1111/j.1535-7511.2007.00165.x (2007).
135 Freeman, L. C. & Ting, J. P. The pathogenic role of the inflammasome in neurodegenerative diseases. *Journal of Neurochemistry* **136 Suppl 1**, 29-38, doi:10.1111/jnc.13217 (2016).
136 LaFerla, F. M., Green, K. N. & Oddo, S. Intracellular amyloid-beta in Alzheimer's disease. *Nature Reviews. Neuroscience* **8**, 499-509, doi:10.1038/nrn2168 (2007).
137 Kaushal, V. *et al.* Neuronal NLRP1 inflammasome activation of Caspase-1 coordinately regulates inflammatory interleukin-1-beta production and axonal degeneration-associated Caspase-6 activation. *Cell Death and Differentiation* **22**, 1676-1686, doi:10.1038/cdd.2015.16 (2015).
138 Tan, M. S. *et al.* Amyloid-beta induces NLRP1-dependent neuronal pyroptosis in models of Alzheimer's disease. *Cell Death & Disease* **5**, e1382, doi:10.1038/cddis.2014.348 (2014).
139 Heneka, M. T. *et al.* NLRP3 is activated in Alzheimer's disease and contributes to pathology in APP/PS1 mice. *Nature* **493**, 674-678, doi:10.1038/nature11729 (2013).
140 Dempsey, C. *et al.* Inhibiting the NLRP3 inflammasome with MCC950 promotes non-phlogistic clearance of amyloid-beta and cognitive function in APP/PS1

mice. *Brain, Behavior, and Immunity* **61**, 306-316, doi:10.1016/j.bbi.2016.12.014 (2017).
141 Daniels, M. J. *et al.* Fenamate NSAIDs inhibit the NLRP3 inflammasome and protect against Alzheimer's disease in rodent models. *Nature Communications* **7**, 12504, doi:10.1038/ncomms12504 (2016).
142 Venegas, C. *et al.* Microglia-derived ASC specks cross-seed amyloid-beta in Alzheimer's disease. *Nature* **552**, 355-361, doi:10.1038/nature25158 (2017).
143 Gordon, R. *et al.* Inflammasome inhibition prevents alpha-synuclein pathology and dopaminergic neurodegeneration in mice. *Science Translational Medicine* **10**, doi:10.1126/scitranslmed.aah4066 (2018).
144 Lee, E. *et al.* MPTP-driven NLRP3 inflammasome activation in microglia plays a central role in dopaminergic neurodegeneration. *Cell Death and Differentiation* **26**, 213-228, doi:10.1038/s41418-018-0124-5 (2019).
145 Vertex Pharmaceuticals Incorporated (2007) Phase 2 clinical study in psoriasis with oral investigational drug VX-765. Clinical trial. Available at https://clinicaltrials.gov/ct2/show/NCT00205465?id=NCT00205465&rank=1.

146 Vertex Pharmaceuticals Incorporated (2010) Study of VX-765 in subjects with treat- ment-resistant partial epilepsy. Clinical trial. Available at https://clinicaltrials.gov/ct2/ show/NCT01048255?id=NCT01048255&rank=1.

147 Chiavegato, A., Zurolo, E., Losi, G., Aronica, E. & Carmignoto, G. The inflammatory molecules IL-1beta and HMGB1 can rapidly enhance focal seizure generation in a brain slice model of temporal lobe epilepsy. *Frontiers in Cellular Neuroscience* **8**, 155, doi:10.3389/fncel.2014.00155 (2014).
148 Morin-Brureau, M. *et al.* Microglial phenotypes in the human epileptic temporal lobe. *Brain* **141**, 3343-3360, doi:10.1093/brain/awy276 (2018).
149 Adamczak, S. *et al.* Inflammasome proteins in cerebrospinal fluid of brain-injured patients as biomarkers of functional outcome: clinical article. *Journal of Neurosurgery* **117**, 1119-1125, doi:10.3171/2012.9.JNS12815 (2012).
150 Irrera, N. *et al.* Lack of the Nlrp3 Inflammasome Improves Mice Recovery Following Traumatic Brain Injury. *Frontiers in Pharmacology* **8**, 459, doi:10.3389/fphar.2017.00459 (2017).
151 Adamczak, S. E. *et al.* Pyroptotic neuronal cell death mediated by the AIM2 inflammasome. *Journal of Cerebral Blood Flow and Metabolism* **34**, 621-629, doi:10.1038/jcbfm.2013.236 (2014).
152 Yin, X. F. *et al.* NLRP3 in human glioma is correlated with increased WHO grade, and regulates cellular proliferation, apoptosis and metastasis via epithelial-mesenchymal transition and the PTEN/AKT signaling pathway. *International Journal of Oncology* **53**, 973-986, doi:10.3892/ijo.2018.4480 (2018).
153 Tarassishin, L., Casper, D. & Lee, S. C. Aberrant expression of interleukin-1beta and inflammasome activation in human malignant gliomas. *PloS one* **9**, e103432, doi:10.1371/journal.pone.0103432 (2014).
154 Burm, S. M., Zuiderwijk-Sick, E. A., Weert, P. M. & Bajramovic, J. J. ATP-induced IL-1beta secretion is selectively impaired in microglia as compared to

hematopoietic macrophages. *Glia* **64**, 2231-2246, doi:10.1002/glia.23059 (2016).
155 Burm, S. M. *et al.* Inflammasome-induced IL-1beta secretion in microglia is characterized by delayed kinetics and is only partially dependent on inflammatory caspases. *The Journal of Neuroscience* **35**, 678-687, doi:10.1523/JNEUROSCI.2510-14.2015 (2015).
156 Galluzzi, L. *et al.* Molecular mechanisms of cell death: recommendations of the Nomenclature Committee on Cell Death 2018. *Cell Death and Differentiation* **25**, 486-541, doi:10.1038/s41418-017-0012-4 (2018).
157 Taylor, R. C., Cullen, S. P. & Martin, S. J. Apoptosis: controlled demolition at the cellular level. *Nature Reviews. Molecular Cell Biology* **9**, 231-241, doi:10.1038/nrm2312 (2008).
158 Zhang, Y., Chen, X., Gueydan, C. & Han, J. Plasma membrane changes during programmed cell deaths. *Cell research* **28**, 9-21, doi:10.1038/cr.2017.133 (2018).
159 Earnshaw, W. C., Martins, L. M. & Kaufmann, S. H. Mammalian caspases: structure, activation, substrates, and functions during apoptosis. *Annual Review of Biochemistry* **68**, 383-424, doi:10.1146/annurev.biochem.68.1.383 (1999).
160 Rogers, C. *et al.* Cleavage of DFNA5 by caspase-3 during apoptosis mediates progression to secondary necrotic/pyroptotic cell death. *Nature Communications* **8**, 14128, doi:10.1038/ncomms14128 (2017).
161 Galluzzi, L. *et al.* Molecular definitions of cell death subroutines: recommendations of the Nomenclature Committee on Cell Death 2012. *Cell Death and Differentiation* **19**, 107-120, doi:10.1038/cdd.2011.96 (2012).
162 Man, S. M., Karki, R. & Kanneganti, T. D. Molecular mechanisms and functions of pyroptosis, inflammatory caspases and inflammasomes in infectious diseases. *Immunological Reviews* **277**, 61-75, doi:10.1111/imr.12534 (2017).
163 Ding, J. *et al.* Pore-forming activity and structural autoinhibition of the gasdermin family. *Nature* **535**, 111-116, doi:10.1038/nature18590 (2016).
164 Liu, X. *et al.* Inflammasome-activated gasdermin D causes pyroptosis by forming membrane pores. *Nature* **535**, 153-158, doi:10.1038/nature18629 (2016).
165 Aglietti, R. A. *et al.* GsdmD p30 elicited by caspase-11 during pyroptosis forms pores in membranes. *Proceedings of the National Academy of Sciences of the United States of America* **113**, 7858-7863, doi:10.1073/pnas.1607769113 (2016).
166 Sborgi, L. *et al.* GSDMD membrane pore formation constitutes the mechanism of pyroptotic cell death. *The EMBO Journal* **35**, 1766-1778, doi:10.15252/embj.201694696 (2016).
167 Chen, X. *et al.* Pyroptosis is driven by non-selective gasdermin-D pore and its morphology is different from MLKL channel-mediated necroptosis. *Cell Research* **26**, 1007-1020, doi:10.1038/cr.2016.100 (2016).
168 Kovacs, S. B. & Miao, E. A. Gasdermins: Effectors of Pyroptosis. *Trends in Cell Biology*, doi:10.1016/j.tcb.2017.05.005 (2017).
169 Zhou, B. *et al.* Tom20 senses iron-activated ROS signaling to promote melanoma cell pyroptosis. *Cell Research*, doi:10.1038/s41422-018-0090-y (2018).

170 Lu, H. *et al.* Molecular Targeted Therapies Elicit Concurrent Apoptotic and GSDME-Dependent Pyroptotic Tumor Cell Death. *Clinical Cancer Research* **24**, 6066-6077, doi:10.1158/1078-0432.CCR-18-1478 (2018).
171 Wang, Y. *et al.* Chemotherapy drugs induce pyroptosis through caspase-3 cleavage of a gasdermin. *Nature* **547**, 99-103, doi:10.1038/nature22393 (2017).
172 Wang, Y. *et al.* GSDME mediates caspase-3-dependent pyroptosis in gastric cancer. *Biochemical and Biophysical Research Communications* **495**, 1418-1425, doi:10.1016/j.bbrc.2017.11.156 (2018).
173 Liu, Z. *et al.* Structures of the Gasdermin D C-Terminal Domains Reveal Mechanisms of Autoinhibition. *Structure* **26**, 778-784 e773, doi:10.1016/j.str.2018.03.002 (2018).
174 Shi, J., Gao, W. & Shao, F. Pyroptosis: Gasdermin-Mediated Programmed Necrotic Cell Death. *Trends in Biochemical Sciences* **42**, 245-254, doi:10.1016/j.tibs.2016.10.004 (2017).
175 Rathkey, J. K. *et al.* Chemical disruption of the pyroptotic pore-forming protein gasdermin D inhibits inflammatory cell death and sepsis. *Science Immunology* **3**, doi:10.1126/sciimmunol.aat2738 (2018).
176 Sollberger, G. *et al.* Gasdermin D plays a vital role in the generation of neutrophil extracellular traps. *Science Immunology* **3**, doi:10.1126/sciimmunol.aar6689 (2018).
177 Rathkey, J. K. *et al.* Live-cell visualization of gasdermin D-driven pyroptotic cell death. *The Journal of Biological Chemistry* **292**, 14649-14658, doi:10.1074/jbc.M117.797217 (2017).
178 Jorgensen, I., Zhang, Y., Krantz, B. A. & Miao, E. A. Pyroptosis triggers pore-induced intracellular traps (PITs) that capture bacteria and lead to their clearance by efferocytosis. *The Journal of Experimental Medicine* **213**, 2113-2128, doi:10.1084/jem.20151613 (2016).
179 Semino, C., Carta, S., Gattorno, M., Sitia, R. & Rubartelli, A. Progressive waves of IL-1beta release by primary human monocytes via sequential activation of vesicular and gasdermin D-mediated secretory pathways. *Cell Death & Disease* **9**, 1088, doi:10.1038/s41419-018-1121-9 (2018).
180 Evavold, C. L. *et al.* The Pore-Forming Protein Gasdermin D Regulates Interleukin-1 Secretion from Living Macrophages. *Immunity* **48**, 35-44 e36, doi:10.1016/j.immuni.2017.11.013 (2018).
181 He, W. T. *et al.* Gasdermin D is an executor of pyroptosis and required for interleukin-1beta secretion. *Cell Research* **25**, 1285-1298, doi:10.1038/cr.2015.139 (2015).
182 Monteleone, M. *et al.* Interleukin-1beta Maturation Triggers Its Relocation to the Plasma Membrane for Gasdermin-D-Dependent and -Independent Secretion. *Cell Reports* **24**, 1425-1433, doi:10.1016/j.celrep.2018.07.027 (2018).
183 Heilig, R. *et al.* The Gasdermin-D pore acts as a conduit for IL-1beta secretion in mice. *European Journal of Immunology* **48**, 584-592, doi:10.1002/eji.201747404 (2018).
184 Ruhl, S. *et al.* ESCRT-dependent membrane repair negatively regulates pyroptosis downstream of GSDMD activation. *Science* **362**, 956-960, doi:10.1126/science.aar7607 (2018).

185 Orning, P. *et al.* Pathogen blockade of TAK1 triggers caspase-8-dependent cleavage of gasdermin D and cell death. *Science*, doi:10.1126/science.aau2818 (2018).
186 Lei, X. *et al.* Enterovirus 71 Inhibits Pyroptosis through Cleavage of Gasdermin D. *Journal of Virology* **91**, doi:10.1128/JVI.01069-17 (2017).
187 Zhu, Q., Zheng, M., Balakrishnan, A., Karki, R. & Kanneganti, T. D. Gasdermin D Promotes AIM2 Inflammasome Activation and Is Required for Host Protection against Francisella novicida. *Journal of Immunology*, doi:10.4049/jimmunol.1800788 (2018).
188 Platnich, J. M. *et al.* Shiga Toxin/Lipopolysaccharide Activates Caspase-4 and Gasdermin D to Trigger Mitochondrial Reactive Oxygen Species Upstream of the NLRP3 Inflammasome. *Cell Reports* **25**, 1525-1536 e1527, doi:10.1016/j.celrep.2018.09.071 (2018).
189 de Vasconcelos, N. M., Van Opdenbosch, N., Van Gorp, H., Parthoens, E. & Lamkanfi, M. Single-cell analysis of pyroptosis dynamics reveals conserved GSDMD-mediated subcellular events that precede plasma membrane rupture. *Cell Death and Differentiation*, doi:10.1038/s41418-018-0106-7 (2018).
190 DiPeso, L., Ji, D. X., Vance, R. E. & Price, J. V. Cell death and cell lysis are separable events during pyroptosis. *Cell Death Discovery* **3**, 17070, doi:10.1038/cddiscovery.2017.70 (2017).
191 Yu, J. *et al.* Inflammasome activation leads to Caspase-1-dependent mitochondrial damage and block of mitophagy. *Proceedings of the National Academy of Sciences of the United States of America* **111**, 15514-15519, doi:10.1073/pnas.1414859111 (2014).
192 Bergsbaken, T., Fink, S. L. & Cookson, B. T. Pyroptosis: host cell death and inflammation. *Nature Reviews. Microbiology* **7**, 99-109, doi:10.1038/nrmicro2070 (2009).
193 Jorgensen, I. & Miao, E. A. Pyroptotic cell death defends against intracellular pathogens. *Immunological Reviews* **265**, 130-142, doi:10.1111/imr.12287 (2015).
194 Sagulenko, V. *et al.* AIM2 and NLRP3 inflammasomes activate both apoptotic and pyroptotic death pathways via ASC. *Cell Death and Differentiation* **20**, 1149-1160, doi:10.1038/cdd.2013.37 (2013).
195 Malireddi, R. K., Ippagunta, S., Lamkanfi, M. & Kanneganti, T. D. Cutting edge: proteolytic inactivation of poly(ADP-ribose) polymerase 1 by the Nlrp3 and Nlrc4 inflammasomes. *Journal of Immunology* **185**, 3127-3130, doi:10.4049/jimmunol.1001512 (2010).
196 Erener, S. *et al.* Inflammasome-activated caspase 7 cleaves PARP1 to enhance the expression of a subset of NF-kappaB target genes. *Molecular Cell* **46**, 200-211, doi:10.1016/j.molcel.2012.02.016 (2012).
197 Lee, S. W. *et al.* Microglial Inflammasome Activation in Penetrating Ballistic-Like Brain Injury. *Journal of Neurotrauma* **35**, 1681-1693, doi:10.1089/neu.2017.5530 (2018).
198 Lee, S. W., de Rivero Vaccari, J. P., Truettner, J. S., Dietrich, W. D. & Keane, R. W. The role of microglial inflammasome activation in pyroptotic cell death following

penetrating traumatic brain injury. *Journal of Neuroinflammation* **16**, 27, doi:10.1186/s12974-019-1423-6 (2019).
199 Poh, L. *et al.* Evidence that NLRC4 inflammasome mediates apoptotic and pyroptotic microglial death following ischemic stroke. *Brain, Behavior, and Immunity* **75**, 34-47, doi:10.1016/j.bbi.2018.09.001 (2019).
200 Rashad, S. *et al.* Early BBB breakdown and subacute inflammasome activation and pyroptosis as a result of cerebral venous thrombosis. *Brain Research* **1699**, 54-68, doi:10.1016/j.brainres.2018.06.029 (2018).
201 Liu, B. *et al.* Molecular consequences of activated microglia in the brain: overactivation induces apoptosis. *Journal of Neurochemistry* **77**, 182-189 (2001).
202 Mayo, L. *et al.* Dual role of CD38 in microglial activation and activation-induced cell death. *Journal of Immunology* **181**, 92-103 (2008).
203 Yun, H. J. *et al.* Daxx mediates activation-induced cell death in microglia by triggering MST1 signalling. *The EMBO Journal* **30**, 2465-2476, doi:10.1038/emboj.2011.152 (2011).
204 Lee, P. *et al.* NO as an autocrine mediator in the apoptosis of activated microglial cells: correlation between activation and apoptosis of microglial cells. *Brain Research* **892**, 380-385 (2001).
205 Lee, J. *et al.* Dual role of inflammatory stimuli in activation-induced cell death of mouse microglial cells. Initiation of two separate apoptotic pathways via induction of interferon regulatory factor-1 and caspase-11. *The Journal of Biological Chemistry* **276**, 32956-32965, doi:10.1074/jbc.M104700200 (2001).
206 Takeuchi, H. *et al.* Interferon-gamma induces microglial-activation-induced cell death: a hypothetical mechanism of relapse and remission in multiple sclerosis. *Neurobiology of Disease* **22**, 33-39, doi:10.1016/j.nbd.2005.09.014 (2006).
207 Tan, C. C. *et al.* NLRP1 inflammasome is activated in patients with medial temporal lobe epilepsy and contributes to neuronal pyroptosis in amygdala kindling-induced rat model. *Journal of Neuroinflammation* **12**, 18, doi:10.1186/s12974-014-0233-0 (2015).
208 Ge, X. *et al.* The pathological role of NLRs and AIM2 inflammasome-mediated pyroptosis in damaged blood-brain barrier after traumatic brain injury. *Brain Research* **1697**, 10-20, doi:10.1016/j.brainres.2018.06.008 (2018).
209 Feng, J. *et al.* Unconjugated bilirubin induces pyroptosis in cultured rat cortical astrocytes. *Journal of Neuroinflammation* **15**, 23, doi:10.1186/s12974-018-1064-1 (2018).
210 Alfonso-Loeches, S., Urena-Peralta, J. R., Morillo-Bargues, M. J., Oliver-De La Cruz, J. & Guerri, C. Role of mitochondria ROS generation in ethanol-induced NLRP3 inflammasome activation and cell death in astroglial cells. *Frontiers in Cellular Neuroscience* **8**, 216, doi:10.3389/fncel.2014.00216 (2014).
211 Hisahara, S., Takano, R., Shoji, S., Okano, H. & Miura, M. Role of caspase-1 subfamily in cytotoxic cytokine-induced oligodendrocyte cell death. *Journal of Neural Transmission. Supplementum*, 135-142 (2000).
212 Lassmann, H. Pathogenic Mechanisms Associated With Different Clinical Courses of Multiple Sclerosis. *Frontiers in Immunology* **9**, 3116, doi:10.3389/fimmu.2018.03116 (2018).

213 Lassmann, H. & van Horssen, J. The molecular basis of neurodegeneration in multiple sclerosis. *FEBS Letters* **585**, 3715-3723, doi:10.1016/j.febslet.2011.08.004 (2011).
214 Vargas, D. L. & Tyor, W. R. Update on disease-modifying therapies for multiple sclerosis. *Journal of Investigative Medicine* **65**, 883-891, doi:10.1136/jim-2016-000339 (2017).
215 Hemmer, B., Kerschensteiner, M. & Korn, T. Role of the innate and adaptive immune responses in the course of multiple sclerosis. *The Lancet. Neurology* **14**, 406-419, doi:10.1016/S1474-4422(14)70305-9 (2015).
216 Weiner, H. L. A shift from adaptive to innate immunity: a potential mechanism of disease progression in multiple sclerosis. *Journal of Neurology* **255 Suppl 1**, 3-11, doi:10.1007/s00415-008-1002-8 (2008).
217 Kuhlmann, T. *et al.* An updated histological classification system for multiple sclerosis lesions. *Acta Neuropathologica* **133**, 13-24, doi:10.1007/s00401-016-1653-y (2017).
218 Trapp, B. D. *et al.* Axonal transection in the lesions of multiple sclerosis. *The New England Journal of Medicine* **338**, 278-285, doi:10.1056/NEJM199801293380502 (1998).
219 Bjartmar, C., Wujek, J. R. & Trapp, B. D. Axonal loss in the pathology of MS: consequences for understanding the progressive phase of the disease. *Journal of the Neurological Sciences* **206**, 165-171 (2003).
220 Bjartmar, C., Kidd, G., Mork, S., Rudick, R. & Trapp, B. D. Neurological disability correlates with spinal cord axonal loss and reduced N-acetyl aspartate in chronic multiple sclerosis patients. *Annals of Neurology* **48**, 893-901 (2000).
221 Skulina, C. *et al.* Multiple sclerosis: brain-infiltrating CD8+ T cells persist as clonal expansions in the cerebrospinal fluid and blood. *Proceedings of the National Academy of Sciences of the United States of America* **101**, 2428-2433 (2004).
222 Jacobsen, M. *et al.* Oligoclonal expansion of memory CD8+ T cells in cerebrospinal fluid from multiple sclerosis patients. *Brain* **125**, 538-550 (2002).
223 Bieganowski, P., Bieganowska, K., Zaborski, J. & Czlonkowska, A. Oligoclonal expansion of gamma delta T cells in cerebrospinal fluid of multiple sclerosis patients. *Multiple Sclerosis* **2**, 78-82, doi:10.1177/135245859600200203 (1996).
224 Salou, M., Nicol, B., Garcia, A. & Laplaud, D. A. Involvement of CD8(+) T Cells in Multiple Sclerosis. *Frontiers in Immunology* **6**, 604, doi:10.3389/fimmu.2015.00604 (2015).
225 Zrzavy, T. *et al.* Loss of 'homeostatic' microglia and patterns of their activation in active multiple sclerosis. *Brain* **140**, 1900-1913, doi:10.1093/brain/awx113 (2017).
226 Giuliani, F., Hader, W. & Yong, V. W. Minocycline attenuates T cell and microglia activity to impair cytokine production in T cell-microglia interaction. *Journal of Leukocyte Biology* **78**, 135-143, doi:10.1189/jlb.0804477 (2005).
227 Metz, L. M. *et al.* Trial of Minocycline in a Clinically Isolated Syndrome of Multiple Sclerosis. *The New England Journal of Medicine* **376**, 2122-2133, doi:10.1056/NEJMoa1608889 (2017).
228 Dunham, J. *et al.* Oxidative Injury and Iron Redistribution Are Pathological Hallmarks of Marmoset Experimental Autoimmune Encephalomyelitis. *Journal of*

Neuropathology and Experimental Neurology **76**, 467-478, doi:10.1093/jnen/nlx034 (2017).
229 Barnett, M. H. & Prineas, J. W. Relapsing and remitting multiple sclerosis: pathology of the newly forming lesion. *Annals of Neurology* **55**, 458-468, doi:10.1002/ana.20016 (2004).
230 Lucchinetti, C. *et al.* Heterogeneity of multiple sclerosis lesions: implications for the pathogenesis of demyelination. *Annals of Neurology* **47**, 707-717 (2000).
231 Caprariello, A. V., Mangla, S., Miller, R. H. & Selkirk, S. M. Apoptosis of oligodendrocytes in the central nervous system results in rapid focal demyelination. *Annals of Neurology* **72**, 395-405, doi:10.1002/ana.23606 (2012).
232 Ofengeim, D. *et al.* Activation of necroptosis in multiple sclerosis. *Cell Reports* **10**, 1836-1849, doi:10.1016/j.celrep.2015.02.051 (2015).
233 Stromnes, I. M. & Goverman, J. M. Active induction of experimental allergic encephalomyelitis. *Nature Protocols* **1**, 1810-1819, doi:10.1038/nprot.2006.285 (2006).
234 Lin, C. C. & Edelson, B. T. New Insights into the Role of IL-1beta in Experimental Autoimmune Encephalomyelitis and Multiple Sclerosis. *Journal of Immunology* **198**, 4553-4560, doi:10.4049/jimmunol.1700263 (2017).
235 Jordao, M. J. C. *et al.* Single-cell profiling identifies myeloid cell subsets with distinct fates during neuroinflammation. *Science* **363**, doi:10.1126/science.aat7554 (2019).
236 Ajami, B., Bennett, J. L., Krieger, C., McNagny, K. M. & Rossi, F. M. Infiltrating monocytes trigger EAE progression, but do not contribute to the resident microglia pool. *Nature Neuroscience* **14**, 1142-1149, doi:10.1038/nn.2887 (2011).
237 White, C. A., McCombe, P. A. & Pender, M. P. Microglia are more susceptible than macrophages to apoptosis in the central nervous system in experimental autoimmune encephalomyelitis through a mechanism not involving Fas (CD95). *International Immunology* **10**, 935-941 (1998).
238 Matsushima, G. K. & Morell, P. The neurotoxicant, cuprizone, as a model to study demyelination and remyelination in the central nervous system. *Brain Pathology* **11**, 107-116 (2001).
239 Huang, W. X., Huang, P. & Hillert, J. Increased expression of caspase-1 and interleukin-18 in peripheral blood mononuclear cells in patients with multiple sclerosis. *Multiple Sclerosis* **10**, 482-487, doi:10.1191/1352458504ms1071oa (2004).
240 Furlan, R. *et al.* Peripheral levels of caspase-1 mRNA correlate with disease activity in patients with multiple sclerosis; a preliminary study. *Journal of Neurology, Neurosurgery, and Psychiatry* **67**, 785-788 (1999).
241 Seppi, D. *et al.* Cerebrospinal fluid IL-1beta correlates with cortical pathology load in multiple sclerosis at clinical onset. *Journal of Neuroimmunology* **270**, 56-60, doi:10.1016/j.jneuroim.2014.02.014 (2014).
242 Rossi, S. *et al.* Cerebrospinal fluid detection of interleukin-1beta in phase of remission predicts disease progression in multiple sclerosis. *Journal of Neuroinflammation* **11**, 32, doi:10.1186/1742-2094-11-32 (2014).

243 Peelen, E. *et al.* Increased inflammasome related gene expression profile in PBMC may facilitate T helper 17 cell induction in multiple sclerosis. *Molecular Immunology* **63**, 521-529, doi:10.1016/j.molimm.2014.10.008 (2015).
244 Ming, X. *et al.* Caspase-1 expression in multiple sclerosis plaques and cultured glial cells. *Journal of the Neurological Sciences* **197**, 9-18 (2002).
245 Burm, S. M. *et al.* Expression of IL-1beta in rhesus EAE and MS lesions is mainly induced in the CNS itself. *Journal of Neuroinflammation* **13**, 138, doi:10.1186/s12974-016-0605-8 (2016).
246 Keane, R. W., Dietrich, W. D. & de Rivero Vaccari, J. P. Inflammasome Proteins As Biomarkers of Multiple Sclerosis. *Frontiers in Neurology* **9**, 135, doi:10.3389/fneur.2018.00135 (2018).
247 Levesque, S. A. *et al.* Myeloid cell transmigration across the CNS vasculature triggers IL-1beta-driven neuroinflammation during autoimmune encephalomyelitis in mice. *The Journal of Experimental Medicine* **213**, 929-949, doi:10.1084/jem.20151437 (2016).
248 Ronchi, F. *et al.* Experimental priming of encephalitogenic Th1/Th17 cells requires pertussis toxin-driven IL-1beta production by myeloid cells. *Nature Communications* **7**, 11541, doi:10.1038/ncomms11541 (2016).
249 Pare, A. *et al.* IL-1beta enables CNS access to CCR2(hi) monocytes and the generation of pathogenic cells through GM-CSF released by CNS endothelial cells. *Proceedings of the National Academy of Sciences of the United States of America* **115**, E1194-E1203, doi:10.1073/pnas.1714948115 (2018).
250 Gris, D. *et al.* NLRP3 plays a critical role in the development of experimental autoimmune encephalomyelitis by mediating Th1 and Th17 responses. *Journal of Immunology* **185**, 974-981, doi:10.4049/jimmunol.0904145 (2010).
251 Jha, S. *et al.* The inflammasome sensor, NLRP3, regulates CNS inflammation and demyelination via caspase-1 and interleukin-18. *The Journal of Neuroscience* **30**, 15811-15820, doi:10.1523/JNEUROSCI.4088-10.2010 (2010).
252 Dumas, A. *et al.* The inflammasome pyrin contributes to pertussis toxin-induced IL-1beta synthesis, neutrophil intravascular crawling and autoimmune encephalomyelitis. *PLoS Pathogens* **10**, e1004150, doi:10.1371/journal.ppat.1004150 (2014).
253 Lalor, S. J. *et al.* Caspase-1-processed cytokines IL-1beta and IL-18 promote IL-17 production by gammadelta and CD4 T cells that mediate autoimmunity. *Journal of Immunology* **186**, 5738-5748, doi:10.4049/jimmunol.1003597 (2011).
254 Inoue, M., Williams, K. L., Gunn, M. D. & Shinohara, M. L. NLRP3 inflammasome induces chemotactic immune cell migration to the CNS in experimental autoimmune encephalomyelitis. *Proceedings of the National Academy of Sciences of the United States of America* **109**, 10480-10485, doi:10.1073/pnas.1201836109 (2012).
255 Coll, R. C. *et al.* A small-molecule inhibitor of the NLRP3 inflammasome for the treatment of inflammatory diseases. *Nature Medicine* **21**, 248-255, doi:10.1038/nm.3806 (2015).
256 Martin, D. & Near, S. L. Protective effect of the interleukin-1 receptor antagonist (IL-1ra) on experimental allergic encephalomyelitis in rats. *Journal of Neuroimmunology* **61**, 241-245 (1995).

257 Badovinac, V., Mostarica-Stojkovic, M., Dinarello, C. A. & Stosic-Grujicic, S. Interleukin-1 receptor antagonist suppresses experimental autoimmune encephalomyelitis (EAE) in rats by influencing the activation and proliferation of encephalitogenic cells. *Journal of Neuroimmunology* **85**, 87-95 (1998).
258 Inoue, M. *et al.* Interferon-beta therapy against EAE is effective only when development of the disease depends on the NLRP3 inflammasome. *Science Signaling* **5**, ra38, doi:10.1126/scisignal.2002767 (2012).
259 Inoue, M. *et al.* An interferon-beta-resistant and NLRP3 inflammasome-independent subtype of EAE with neuronal damage. *Nature Neuroscience* **19**, 1599-1609, doi:10.1038/nn.4421 (2016).
260 D'Angelo, C. *et al.* Profiling of Canonical and Non-Traditional Cytokine Levels in Interferon-beta-Treated Relapsing-Remitting-Multiple Sclerosis Patients. *Frontiers in Immunology* **9**, 1240, doi:10.3389/fimmu.2018.01240 (2018).
261 Mamik, M. K. *et al.* HIV-1 Viral Protein R Activates NLRP3 Inflammasome in Microglia: implications for HIV-1 Associated Neuroinflammation. *Journal of Neuroimmune Pharmacology* **12**, 233-248, doi:10.1007/s11481-016-9708-3 (2017).
262 Mamik, M. K. *et al.* Insulin Treatment Prevents Neuroinflammation and Neuronal Injury with Restored Neurobehavioral Function in Models of HIV/AIDS Neurodegeneration. *The Journal of Neuroscience* **36**, 10683-10695, doi:10.1523/JNEUROSCI.1287-16.2016 (2016).
263 Walsh, J. G. *et al.* Rapid inflammasome activation in microglia contributes to brain disease in HIV/AIDS. *Retrovirology* **11**, 35, doi:10.1186/1742-4690-11-35 (2014).
264 Boghozian, R. *et al.* Suppressed oligodendrocyte steroidogenesis in multiple sclerosis: Implications for regulation of neuroinflammation. *Glia*, doi:10.1002/glia.23179 (2017).
265 Ramaswamy, V. *et al.* Inflammasome induction in Rasmussen's encephalitis: cortical and associated white matter pathogenesis. *Journal of Neuroinflammation* **10**, 152, doi:10.1186/1742-2094-10-152 (2013).
266 Goncalves DaSilva, A. & Yong, V. W. Matrix metalloproteinase-12 deficiency worsens relapsing-remitting experimental autoimmune encephalomyelitis in association with cytokine and chemokine dysregulation. *The American Journal of Pathology* **174**, 898-909, doi:10.2353/ajpath.2009.080952 (2009).
267 Inoue, M. & Shinohara, M. L. NLRP3 Inflammasome and MS/EAE. *Autoimmune Diseases* **2013**, 859145, doi:10.1155/2013/859145 (2013).
268 Barclay, W. & Shinohara, M. L. Inflammasome activation in multiple sclerosis and experimental autoimmune encephalomyelitis (EAE). *Brain Pathology* **27**, 213-219, doi:10.1111/bpa.12477 (2017).
269 Ellestad, K. K. *et al.* Early life exposure to lipopolysaccharide suppresses experimental autoimmune encephalomyelitis by promoting tolerogenic dendritic cells and regulatory T cells. *Journal of Immunology* **183**, 298-309, doi:10.4049/jimmunol.0803576 (2009).
270 McKenzie, B. A. *et al.* Caspase-1 inhibition prevents glial inflammasome activation and pyroptosis in models of multiple sclerosis. *Proceedings of the*

National Academy of Sciences of the United States of America **115**, E6065-E6074, doi:10.1073/pnas.1722041115 (2018).
271 Doitsh, G. *et al.* Cell death by pyroptosis drives CD4 T-cell depletion in HIV-1 infection. *Nature* **505**, 509-514, doi:10.1038/nature12940 (2014).
272 Hisahara, S., Shoji, S., Okano, H. & Miura, M. ICE/CED-3 family executes oligodendrocyte apoptosis by tumor necrosis factor. *Journal of Neurochemistry* **69**, 10-20 (1997).
273 Kayagaki, N. *et al.* Non-canonical inflammasome activation targets caspase-11. *Nature* **479**, 117-121, doi:10.1038/nature10558 (2011).
274 Schmid-Burgk, J. L. *et al.* Caspase-4 mediates non-canonical activation of the NLRP3 inflammasome in human myeloid cells. *European Journal of Immunology* **45**, 2911-2917, doi:10.1002/eji.201545523 (2015).
275 Branton, W. G. *et al.* Brain microbiota disruption within inflammatory demyelinating lesions in multiple sclerosis. *Scientific Reports* **6**, 37344, doi:10.1038/srep37344 (2016).
276 Akassoglou, K. *et al.* Oligodendrocyte apoptosis and primary demyelination induced by local TNF/p55TNF receptor signaling in the central nervous system of transgenic mice: models for multiple sclerosis with primary oligodendrogliopathy. *The American Journal of Pathology* **153**, 801-813, doi:10.1016/S0002-9440(10)65622-2 (1998).
277 Arbeloa, J., Perez-Samartin, A., Gottlieb, M. & Matute, C. P2X7 receptor blockade prevents ATP excitotoxicity in neurons and reduces brain damage after ischemia. *Neurobiology of disease* **45**, 954-961, doi:10.1016/j.nbd.2011.12.014 (2012).
278 Levy, H., Assaf, Y. & Frenkel, D. Characterization of brain lesions in a mouse model of progressive multiple sclerosis. *Experimental Neurology* **226**, 148-158, doi:10.1016/j.expneurol.2010.08.017 (2010).
279 Peferoen, L. A. *et al.* Ageing and recurrent episodes of neuroinflammation promote progressive experimental autoimmune encephalomyelitis in Biozzi ABH mice. *Immunology* **149**, 146-156, doi:10.1111/imm.12644 (2016).
280 Huizinga, R. *et al.* Immunization with neurofilament light protein induces spastic paresis and axonal degeneration in Biozzi ABH mice. *Journal of Neuropathology and Experimental Neurology* **66**, 295-304, doi:10.1097/nen.0b013e318040ad5c (2007).
281 Ruther, B. J. *et al.* Combination of cuprizone and experimental autoimmune encephalomyelitis to study inflammatory brain lesion formation and progression. *Glia* **65**, 1900-1913, doi:10.1002/glia.23202 (2017).
282 Xu, T. Z. *et al.* Ginsenoside Rg1 protects against H2O2induced neuronal damage due to inhibition of the NLRP1 inflammasome signalling pathway in hippocampal neurons in vitro. *International Journal of Molecular Medicine*, doi:10.3892/ijmm.2018.4005 (2018).
283 Pajoohesh-Ganji, A. & Miller, R. H. Oligodendrocyte ablation as a tool to study demyelinating diseases. *Neural Regeneration Research* **11**, 886-889, doi:10.4103/1673-5374.184451 (2016).
284 Traka, M. *et al.* A genetic mouse model of adult-onset, pervasive central nervous system demyelination with robust remyelination. *Brain* **133**, 3017-3029, doi:10.1093/brain/awq247 (2010).

285 Traka, M., Podojil, J. R., McCarthy, D. P., Miller, S. D. & Popko, B. Oligodendrocyte death results in immune-mediated CNS demyelination. *Nature Neuroscience* **19**, 65-74, doi:10.1038/nn.4193 (2016).
286 Evavold, C. L. & Kagan, J. C. How Inflammasomes Inform Adaptive Immunity. *Journal of Molecular Biology* **430**, 217-237, doi:10.1016/j.jmb.2017.09.019 (2018).
287 Hametner, S. *et al.* Iron and neurodegeneration in the multiple sclerosis brain. *Annals of Neurology* **74**, 848-861, doi:10.1002/ana.23974 (2013).
288 Cauwels, A., Rogge, E., Vandendriessche, B., Shiva, S. & Brouckaert, P. Extracellular ATP drives systemic inflammation, tissue damage and mortality. *Cell Death & Disease* **5**, e1102, doi:10.1038/cddis.2014.70 (2014).
289 Yamasaki, R. *et al.* Differential roles of microglia and monocytes in the inflamed central nervous system. *The Journal of Experimental Medicine* **211**, 1533-1549, doi:10.1084/jem.20132477 (2014).
290 Ryu, J. C. *et al.* Neutrophil pyroptosis mediates pathology of P. aeruginosa lung infection in the absence of the NADPH oxidase NOX2. *Mucosal Immunology* **10**, 757-774, doi:10.1038/mi.2016.73 (2017).
291 Eichholz, K. *et al.* Immune-Complexed Adenovirus Induce AIM2-Mediated Pyroptosis in Human Dendritic Cells. *PLoS Pathogens* **12**, e1005871, doi:10.1371/journal.ppat.1005871 (2016).
292 Soares, J. L., Oliveira, E. M. & Pontillo, A. Variants in NLRP3 and NLRC4 inflammasome associate with susceptibility and severity of multiple sclerosis. *Multiple Sclerosis and Related Disorders* **29**, 26-34, doi:10.1016/j.msard.2019.01.023 (2019).
293 Denes, A. *et al.* AIM2 and NLRC4 inflammasomes contribute with ASC to acute brain injury independently of NLRP3. *Proceedings of the National Academy of Sciences of the United States of America* **112**, 4050-4055, doi:10.1073/pnas.1419090112 (2015).
294 de Rivero Vaccari, J. P. *et al.* Therapeutic neutralization of the NLRP1 inflammasome reduces the innate immune response and improves histopathology after traumatic brain injury. *Journal of Cerebral Blood Flow and Metabolism* **29**, 1251-1261, doi:10.1038/jcbfm.2009.46 (2009).
295 Gosselin, D. *et al.* An environment-dependent transcriptional network specifies human microglia identity. *Science* **356**, doi:10.1126/science.aal3222 (2017).
296 Rustenhoven, J. *et al.* Isolation of highly enriched primary human microglia for functional studies. *Scientific Reports* **6**, 19371, doi:10.1038/srep19371 (2016).
297 Sperlagh, B., Vizi, E. S., Wirkner, K. & Illes, P. P2X7 receptors in the nervous system. *Progress in Neurobiology* **78**, 327-346, doi:10.1016/j.pneurobio.2006.03.007 (2006).
298 Hou, L. *et al.* Necrotic pyknosis is a morphologically and biochemically distinct event from apoptotic pyknosis. *Journal of Cell Science* **129**, 3084-3090, doi:10.1242/jcs.184374 (2016).
299 Hanahan, D. & Weinberg, R. A. Hallmarks of cancer: the next generation. *Cell* **144**, 646-674, doi:10.1016/j.cell.2011.02.013 (2011).

300 Waldmeier, P. C., Feldtrauer, J. J., Qian, T. & Lemasters, J. J. Inhibition of the mitochondrial permeability transition by the nonimmunosuppressive cyclosporin derivative NIM811. *Molecular Pharmacology* **62**, 22-29 (2002).
301 Koch, J. C. *et al.* ROCK inhibition in models of neurodegeneration and its potential for clinical translation. *Pharmacology & Therapeutics* **189**, 1-21, doi:10.1016/j.pharmthera.2018.03.008 (2018).
302 Leonard, J. R., Klocke, B. J., D'Sa, C., Flavell, R. A. & Roth, K. A. Strain-dependent neurodevelopmental abnormalities in caspase-3-deficient mice. *Journal of Neuropathology and Experimental Neurology* **61**, 673-677 (2002).
303 Han, B. H. *et al.* Selective, reversible caspase-3 inhibitor is neuroprotective and reveals distinct pathways of cell death after neonatal hypoxic-ischemic brain injury. *The Journal of Biological Chemistry* **277**, 30128-30136, doi:10.1074/jbc.M202931200 (2002).